Synthesis and Characterization of Polyfunctional Polyhedral Silsesquioxane Cages

by

Santy Sulaiman

A dissertation submitted in partial fulfillment
Of the requirements for the degree of
Doctor of Philosophy
(Macromolecular Science and Engineering)
In the University of Michigan
2011

Doctoral Committee:

Professor Richard M. Laine, Chair
Professor Mark M. Banaszak Holl
Professor Emeritus Paul G. Rasmussen
Associate Professor Jinsang Kim

2011

This dissertation is dedicated to the loves of my life:

Ben, Luke, Millie, and Tali.

Life is not worth living without them.

Acknowledgement

I would like to thank the following people for their kindness, assistance, stubbornness, and friendship, without all of which this dissertation would not have been finished:

My husband Ben and cats Luke, Millie, and Tali
My Parents, Sisters, and Brother
My Cousins, In-laws, and Relatives

My advisor, Professor Richard M. Laine
And the entire Laine research group, past and present

My committee:
Professor Mark M. Banaszak Holl
Professor Paul G. Rasmussen (Emeritus)
Professor Jinsang Kim

For their contributions in two-photon absorption spectroscopy:
Ms. Jin Zhang and Professor Theodore Goodson, III

For their support and assistance:
Dr. Jose Azurdia, Dr. Chad Brick, Dr. Mark Roll, Dr. Michael Asuncion, and Dr. Marco Ronchi

The undergraduate students who have contributed to this dissertation:
Mr. Chris De Sana, Ms. Shana Kramer, Mr. Josh Katzenstein, Ms. Stephanie Snoblen, Ms. Erica VanNortwick, Mr. Nick Boston, Mr. Matt Schwartz, and numerous other undergraduate students who worked for me

For their friendship and times spent commiserating:
Dr. Sarah Spanninga and Ms. Anne Juggernauth

Special thanks to:
Ms. Nonna Hamilton
Mr. James Windak

Last but not least,
The cats and rabbits at the Humane Society of Huron Valley and Great Lakes Rabbit Sanctuary for putting a smile on my face every week during the dissertation writing process

Table of Contents

Dedication ii
Acknowledgements iii
List of Figures vii
List of Schemes x
List of Tables xii
List of Appendices xiii
Abstract xiv
Chapter 1 – Introduction 1
1.1 Project Goals and Objectives 1
1.2 Nanocomposite Materials 2
1.3 Silsesquioxanes 3
1.3.1 Definitions, Structures, and Nomenclatures 3
1.3.2 Formation of Silsesquioxane Cages and Networks 5
1.3.3 Silsesquioxanes as Nanobuilding Blocks 7
1.3.4 Octaphenylsilsesquioxane (OPS): Synthesis and Derivatives 9
1.3.4.1 Octa(nitrophenyl)silsesquioxane (ONPS) and Octa(aminophenyl) silsesquioxane 10
1.3.4.2 Brominated OPS (Br_xOPS) 12
1.3.4.3 Octa(*p*-iodophenyl)silsesquioxane (*p*-I_8OPS) 16
1.3.5 Octavinylsilsesquioxane (OVS): Synthesis and Functionalization 16
1.3.6 Electrophilicity of Silsesquioxane Core 19
1.3.6.1 Electron Delocalization Involving the Silsesquioxane Core 22
1.4 Olefin Metathesis Reactions 30
1.5 The Heck Reactions 33
1.6 Two-Photon Absorption (TPA) 35

Chapter 2 – Experimental Techniques and Syntheses 51
2.1 Materials 51
2.2 Analytical Techniques 52
2.3 Syntheses 55
2.3.1 Elaboration of Octavinylsilsesquioxane 55
2.3.2 Synthesis, Characterization, and Photophysical Properties of Poly-functional Phenylsilsesquioxanes 59
2.3.3 Fluoride Ion-Catalyzed Rearrangement of PVSQ and PMSQ 63
2.3.4 Silsesquioxane-based Epoxy Resins 66
Chapter 3 – Elaboration of Octavinylsilsesquioxane via Cross-Metathesis and Heck Reactions to Form Luminescent Star Molecules 71
3.1 Introduction 72
3.2 Experimental Procedures 74
3.3 Results and Discussions 74
3.3.1 Synthetic Methods 74
3.3.2 Solubilities 75
3.3.3 Molecular Characterization of RStyrenylOS, R'VinylStilbeneOS, and R"$_2$BenzamideOS 75
3.3.4 Thermal Behavior of HStyrenylOS 79
3.3.5 Photophysical Properties 82
3.3.6 Two Photon Cross-Section Studies 84
3.3.6.1 Steady-State Measurements 85
3.3.6.2 Two-Photon Absorption Measurements 85
3.3.7 Solvent-Dependence of Emission Spectra 86
3.4 Conclusions 90
Chapter 4 – Synthesis, Characterization, and Photophysical Properties of Polyfunctional Phenylsilsesquioxanes: [*o*-RPhSiO$_{1.5}$]$_8$, [2,5-R$_2$PhSiO$_{1.5}$]$_8$, and [R$_3$PhSiO$_{1.5}$]$_8$ 98
4.1 Introduction 99
4.2 Experimental Procedures 101
4.3 Results and Discussion 101

4.3.1 Synthetic Methods 104
4.3.2 Solubilities 105
4.3.3 Molecular Characterization of RStyr$_x$OPS 106
4.3.4 Photophysical Properties....110
4.3.5 Two-photon Excited Fluorescence Measurements 117
4.4 Conclusions....119
Chapter 5 – Fluoride-Catalyzed Rearrangements of Polysilsesquioxanes. Mixed Methyl,Vinyl-T$_8$, -T$_{10}$ and -T$_{12}$ Cages....124
5.1 Introduction....125
5.2 Experimental Procedures 127
5.3 Results and Discussions....127
5.4 Conclusions....134
Chapter 6 – Silsesquioxane-based Epoxy Resins with Very Low Coefficients of Thermal Expansion....139
5.1 Introduction....139
5.2 Experimental Procedures 141
5.3 Results and Discussions....141
5.4 Conclusions....144
Chapter 7 – Future Work....149
Appendices....158

List of Figures

Figure

1.1 Some schematic structures of silsesquioxanes 4

1.2 Silsesquioxane nomenclature 5

1.3 Completely condensed polyhedral silsesquioxane cage structures 5

1.4 (a) Typical sizes/volume of a silsesquioxane molecule. (b) 3-D schematic drawing of octamethylsilsesquioxane showing the functional groups in different octants in three-dimensional space 8

1.5 Linear (a) and bifurcated (b) tethers 12

1.6 Proposed complexation of Br_2 with OPS cage face 14

1.7 ORTEP plot of (a) $R_7T_7(OH)_3$ and (b) idealized β-cristobalite. For clarity, only C atoms attached to Si are shown 19

1.8 HOMO and LUMO of H_8T_8 20

1.9 Absorption and photoluminescence spectra of *para*-substituted vinylbiphenyl silsesquioxane 23

1.10 Normalized absorbance (empty symbols) and photoluminescence (full symbols) spectra of the dialdehyde (a) and dialcohol (b) compounds – small molecule analog (■) and silsesquioxane-tethered (▲). Solvent: THF-methanol 24

1.11 Silsesquioxane molecule with electron-donating 4-carbazolephenyl group and electron-withdrawing 4-cyanophenyl group 25

1.12 UV-Vis absorption and photoluminescence spectra of $StiI_8OS$ 26

1.13 Dimethylaminostilbene-functionalized (a) "corner", (b) "half", and (c) "cubic" silsesquioxane molecules 27

1.14 General structure of silsesquioxane-based BoC oligomers 29

1.15 Model compounds of silsesquioxane-based BoC oligomers with $–Si(OEt)_3$ endcaps 29

1.16 Absorption and emission spectra of silsesquioxane BoC oligomers and model compounds (λ_{ex} = 265 nm) 30

1.17 Mechanism of olefin metathesis reactions 31

1.18 Metal-alkylidene catalysts for metathesis reactions. a. Schrock catalyst. b. Grubbs 1st generation. c. Grubbs 2nd generation 32

1.19 General mechanism for Heck reactions 34

1.20 Schematic diagrams of one- and two photon-induced electron transition processes 36

3.1 Grubbs catalyst, 1st generation 73

3.2 MALDI-TOF spectra for RStyrenylOS. Octasubstitution was observed for all RStyrenylOS except a. MeStyrenylOS, b. BrStyrenylOS shown for comparison 76

3.3 TGA data in air (10°C/min) for RStyrenylOS 78

3.4 TGA data in air (10°C/min) for R'VinylStilbeneOS 78

3.5 TGA data in air (10°C/min) for R"$_2$BenzamideOS 79

3.6 DSC thermogram of HStyrenylOS. Red trace indicates second heating cycle 80

3.7 X-ray diffraction pattern of HStyrenylOS before and after heating to 300°C 80

3.8 FTIR spectra of HStyrenylOS before and after heating to 300°C 81

3.9 Decomposition of HStyrenylOS and polystyrene (TGA in air, 10°C/min) 81

3.10 UV absorption and PL emission of RStyrenylOS in THF 82

3.11 UV-Vis and PL spectra of R'VinylStilbeneOS in THF 83

3.12 UV-Vis and PL spectra of HStyrenylOS and HVinylStilbeneOS 83

3.13 Two photon cross-section of R'VinylStilbeneOS where R' = -H (SOVS), -MeO (OSOVS), -NH_2 (NSOVS) 85

3.14 UV-Vis and emission data for MeVinylStilbeneOS in three solvents 86

3.15 UV-Vis and emission data for NH_2VinylStilbeneOS in two good solvents 87

3.16 HOMO and LUMO of $[XSiO_{1.5}]_8$ 89

4.1 3-D symmetrical T_8 and Q_8 compounds 99

4.2 UV-Vis absorption (top) and PL emission (bottom) of *trans*-stilbene and *p*-Me(H)Stil$_8$OS in THF 100

4.3 *o*-RStyr$_x$OPS with exaggerated bond lengths and angles for clarity 104

4.4 TGA data in air (10°C/min) for (a) MeStyr$_x$OPS and (b) AceStyr$_x$OPS 108

4.5 TGA data in air (10°C/min) for NBocStyr$_x$OPS 109

4.6 Absorption and emission spectra for MeStyr$_x$OPS 110

4.7 Absorption and emission spectra for NBocStyr$_x$OPS 112

4.8 Absorption and emission spectra for AceStyr$_x$OS 112

4.9 Two possible configurations of RStilbene$_{24}$OS corner 115

4.10 Interactions of "fragments" of tristyrenylphenyl groups on each corner of $RStyr_{24}OS$ 116

4.11 TPA cross section measurements of the investigated chromophores 118

5.1 Types of silsesquioxanes. Only oligomeric rather than polymeric ladders have been made to date....125

5.2 MALDI-TOF spectrum of nBu$_4$NF-catalyzed PVSQ dissolution quenched with $CaCl_2$ 130

5.3 GPC analysis of ambient nBu$_4$NF-catalyzed PVSQ dissolution. Note that on precipitation it returns to a high MW albeit soluble polymer. OPS is $[PhSiO_{1.5}]_8$ used as an internal standard, TBAF = nBu$_4$NF 131

5.4 Room temperature nBu$_4$NF-catalyzed dissolution of 1:1 PMSQ:PVSQ 132

5.5 Room temperature nBu$_4$NF-catalyzed dissolution of 5:1 PMSQ:PVSQ....132

5.6 nBu$_4$NF-catalyzed dissolution of 5:1 PMSQ:PVSQ in THF at reflux....133

6.1 Sets of epoxies tested in OAPS resins....142

7.1 Simplified structures of T_{10} and T_{12} molecules 152

7.2 Schematic drawings of current silsesquioxane-based polymer materials....153

7.3 Silsesquioxane-based ball-on-chain (BoC) polymer....153

List of Schemes

Scheme

1.1 Hydrolysis and condensation of silsesquioxanes 6

1.2 General pathways for the synthesis of OPS 9

1.3 Synthesis of ONPS and OAPS 11

1.4 OAPS/epoxy nanocomposite 12

1.5 Functionalization of $Br_{5.3}$OPS via (a) Heck, (b) Suzuki, (c) Sonogashira, and (d) Buchwald-Hartwig amination reactions 13

1.6 Bromination of OPS 15

1.7 Iodination of OPS 16

1.8 Reactions across the vinyl groups in OVS: (a) thioether, (b) phosphonation, (c) hydrosilylation, (d) epoxidation 17

1.9 Heck coupling reaction of OVS 18

1.10 Cross-metathesis of OVS 19

1.11 Encapsulation of F^- ions inside silsesquioxane cage 21

1.12 Reduction of octa(4'-vinylbiphenyl-3,5-dicarbaldehyde)silsesquioxane to its dialcohol derivative 24

1.13 General schematic of olefin metathesis 30

1.14 Phillips triolefin process 31

1.15 General schematic of Heck reactions 33

3.1 Synthesis of OVS (30-40 % yield) and RStyrenylOS 73

3.2 Synthesis of R'VinylStilbeneOS from BrStyrenylOS 73

3.3 Synthesis of R"$_2$BenzamideOS from NH_2VinylStilbeneOS 74

4.1 Heck coupling reaction of $Br_{5.3}$OPS with RStyrenes 102

4.2 Heck coupling reaction of *p*-I_8OPS with RStyrenes 102

4.3 Heck coupling studies on *o*-Br_8OPS, 2,5-Br_{16}OPS and Br_{24}OPS. Preparation of selected functionalized stilbenes for comparison of photophysical properties 103

5.1 General concept of fluoride catalyzed rearrangement of polysilsesquioxanes to mixed T_{10} and T_{12} isomers with varying vinyl and methyl contents. Note that some T_8 isomers are seen. 126

5.2 Synthesis of $[RSiO_{1.5}]_8$ cages from alkoxysilanes....127

5.3 Synthesis of fluoride ion encapsulation within silsesquioxane cages....128

5.4 Treatment of $[iBu_7(styrene)T_8]$ with stoichiometric Me_4NF 128

5.5 Treatment of equimolar $F^-@[PhSiO_{1.5}]_8$ and $F^-@[ViSiO_{1.5}]_8$....129

5.6 Treatment of equimolar $[PhSiO_{1.5}]_8$ and $[ViSiO_{1.5}]_8$ with 2 equivalent Me_4NF....129

5.7 Treatment of PVSQ with catalytic nBu$_4$NF....130

7.1 Synthesis of BrStyrenyl$T_{10,12}$ and R'VinylStilbene$T_{10\text{-}12}$....152

7.2 Synthesis of $Vi_2Ph_{8,10}T_{10,12}$ from polyphenylsilsesquioxane (PPSQ) and polyvinyl-silsesquioxane (PVSQ) 154

7.3 Hydrosilylation of $Vi_2Ph_{8,10}T_{10,12}$ with 1,2-ethanediylbis(methylsilane) to form silsesquioxane-based BoC polymer with flexible organic linkers 154

7.4 Synthesis of $(NH_2Ph)_2Ph_{8,10}T_{10,12}$ from octaphenylsilsesquioxane (OPS) and octa(aminophenyl)silsesquioxane (OAPS) 155

7.5 Reaction of $(NH_2Ph)_2Ph_{8,10}T_{10,12}$ with DGEBA to form silsesquioxane-based BoC polymer with rigid organic linkers 155

List of Tables

Table

1.1 DFT HOMO-LUMO calculations for select silsesquioxane molecules. All values in eV 28

3.1 MALDI-ToF and GPC data for RStyrenylOS 76

3.2 MALDI-ToF and GPC data for R'VinylStilbeneOS 76

3.3 TGA and melting point data for RStyrenylOS....77

3.4 TGA data for R'VinylStilbeneOS....77

3.5 Characterization data for R"$_2$BenzamideOS 77

3.6 Spectral data of RStyrenylOS and R'VinylStilbeneOS 86

3.7 Spectral data of RStyrenylOS and R'VinylStilbeneOS as a function of solvent and two photon cross-sections of selected compounds 88

4.1 TPA properties of silsesquioxane derivatives....100

4.2 Physical characteristics of PAMAM dendrimers....101

4.3 Molecular species present in MeStyr$_x$OPS 106

4.4 Molecular species present in NH_2Styr$_x$OPS....106

4.5 Molecular species present in AceStyr$_x$OPS 106

4.6 MALDI-ToF and GPC data for RStyr$_x$OPS....107

4.7 TGA data for MeStyr$_x$OS and AceStyr$_x$OS 109

4.8 TGA data for NBocStyr$_x$OPS 110

4.9 Photophysical data for RStyr$_x$OPS (THF, CH_2Cl_2 peak positions are identical)....111

5.1 Synthesis of cage compounds from the alkoxysilanes using *n*Bu$_4$NF....127

6.1 CTEs of selected epoxy resins where N = number of NH_2s/epoxy group....142

6.2 Published CTEs of selected epoxy resins where N = NH_2s/epoxy group = 0.5 143

List of Appendices

Appendix

1 Characterization Data for RStyrenylOS, R'VinylStilbeneOS, and R"$_2$BenzamideOS 158

2 Characterization Data for [*o*-RPhSiO$_{1.5}$]$_8$, [2,5-R$_2$PhSiO$_{1.5}$]$_8$, and [R$_3$PhSiO$_{1.5}$]$_8$ 166

3 MALDI-ToF Data for Mixed Methyl,Vinyl-T$_8$, -T$_{10}$ and -T$_{12}$ cages 171

4 Synthesis and Hydrolysis of AceStyrenylOS 174

Abstract

Recent studies on octameric polyhedral silsesquioxanes, $(RSiO_{1.5})_8$, indicate that the silsesquioxane cage is not just a passive component but appears to be involved in electron delocalization with conjugated organic tethers in the excited state. This dissertation presents the synthesis and characterization of $(RSiO_{1.5})_8$ molecules with unique photophysical properties that provide support for the existence of conjugation that involves the $(RSiO_{1.5})_8$ cage.

The dissertation first discusses the elaboration of octavinylsilsesquioxane via cross-metathesis to form styrenyl-functionalized octasilsesquioxane molecules. Subsequent Heck coupling reactions of *p*-bromostyrenyl derivative provides vinylstilbene-functionalized octasilsesquioxane. The amino derivative, NH_2VinylStilbeneOS, show highly red-shifted emission spectrum (100 nm from the simple organic analog *p*-vinylstilbene) and high two-photon absorption (TPA) cross-section value (100 GM/moiety), indicating charge-transfer processes involving the silsesquioxane cage as the electron acceptor.

The unique photophysical properties of polyfunctional luminescent cubic silsesquioxanes synthesized from *ortho*-8-, (2,5)-16-, and 24-brominated octaphenylsilsesquioxane (OPS) via Heck coupling show how the steric interactions of the organic tethers at the silsesquioxane cage corner affect conjugation with the silsesquioxane cage. Furthermore, the high TPA cross-section (10 GM/moiety) and photoluminescence quantum yield (20%) of OPS functionalized with 24 acetoxystyrenyl groups suggest that the existence excited states in these molecules with similar energies and decay rates: normal radiative π- π^* transition and charge transfer involving the silsesquioxane cage.

The fluoride ion-catalyzed rearrangement reactions of cage and polymeric silsesquioxanes provide a convenient route to a mixture of deca- and dodecameric silsesquioxane molecules in high yields, giving us the opportunity to investigate the effect of silsesqui-

oxane cage geometry on their photophysical properties. The ability to recycle polymeric silsesquioxane resins, byproducts from cubic silsesquioxane syntheses, into useful cage silsesquioxane molecules adds another advantage.

Lastly, we present the synthesis of octa(aminophenyl)silsesquioxane-based epoxy resins with coefficient of thermal expansion (CTE) as low as 25^{o}C/ppm without ceramic fillers. The CTEs of these resins can be tailored over an order of magnitude by choosing epoxy crosslinking agents having different flexibilities.

Chapter 1
Introduction

This dissertation describes our work on the syntheses and characterization of polyhedral silsesquioxane cages along with investigations of their unique properties. This chapter provides background information on topics discussed in this dissertation. Section **1.1** gives an overview of the objectives and motivations for this work. Section **1.2** provides a brief discussion on the subject of organic/inorganic hybrid nanocomposites. Section **1.3** offers a brief review of silsesquioxanes, particularly previous work related to studies described in this dissertation. Sections **1.4** and **1.5** describe in general the chemical reactions used in this work, while section **1.6** describes the basic concepts of two-photon absorption.

1.1 Project Goals and Objectives

Polyhedral oligosilsesquioxanes comprise a group of nanometer-scaled organosilicon compounds with well-defined and highly symmetrical structures. These compounds embody the hybrid organic-inorganic architectures, with inner inorganic frameworks consisting of silicon and oxygen atoms surrounded by organic substituents in three-dimensional arrangements. With diameters between 1 and 3 nm, polyhedral silsesquioxanes can be considered the smallest possible particles of silica with surface organic groups. The properties of these hybrid compounds are combinations of those of the two components, making them really nanocomposite materials.[1-13]

The objectives of the work described in this dissertation are to develop facile and effective routes for the syntheses of polyfunctionalized silsesquioxanes with unique properties that can be easily tailored by simple modifications of the organic substituents. In Chapter **3**, we discuss the elaboration of octavinylsilsesquioxane to produce three generations of compounds via cross-metathesis, Heck coupling, and benzoylation reactions.

Chapter **4** details the synthesis and photophysical properties of luminescent polyfunctional cubic silsesquioxanes from crystalline Br_xOPS (x = 8, 16, 24). In Chapter **5**, we discuss the fluoride ion-catalyzed rearrangement reactions of cubic or polymeric silsesquioxanes to form mixed functionalized cage silsesquioxanes. Chapter **6** gives a brief discussion on silsesquioxane-based epoxy composites with low coefficients of thermal expansion. In Chapter **7**, we present an outline of potential future work based on results discussed in this dissertation.

1.2 Nanocomposite Materials

Composite materials are defined as a mixture of two or more constituent materials with different properties that remain in distinct phases while in intimate contact with each other. Composites have become significant in the field of materials science and engineering because they provide the opportunity to design materials with properties that are not available from conventional materials (i.e. metals, ceramics, and polymers) alone.

The properties of macroscale composites can be predicted by the "Rule of Mixtures,"[14,15] which describes the composites' properties as the sum of the properties of the individual components weighted by the volume fractions of that component in the composite.[14,15] For a composite material having two components (e.g. matrix and reinforcement), the equation for "Rule of Mixtures" becomes:

$$X_c = X_m v_m + X_f v_f$$

where X is a property of interest, v is the volume fraction, and the subscripts c, m, and f refer to the composite, matrix, and reinforcement, respectively.[15]

Organic/inorganic hybrid composites can be divided into two classes based on the nature of the bonds between their components. In hybrid composites of Class 1, the organic and inorganic components are embedded and held together by weak bonds such as van der Waals, hydrogen, and ionic bonds. In Class 2 composites, the components are linked together through strong chemical bonds such as covalent and iono-covalent bonds. [16]

To be called nanocomposite materials, one or more of the individual phases in the composites has to be less than 100 nm in scale. These materials have garnered a lot of attention in the past several decades because the ability to assemble materials at nanometer length scales should provide the opportunity to produce high homogeneity in the mi-

cro- and macrostructure of the composite. The macroscale properties of the product can be predicted with high accuracy and easily fine-tuned, leading to high reproducibility.[17-20]

At these nanometer length scales, as the sizes of the individual components decrease, the interfacial areas between the two components (termed "interphase") increase considerably to the point that they may become the primary component in the composite. This interphase can lead to a breakdown of the "Rule of Mixtures"[15,21-25] when predicting the properties of nanocomposites simply because they are not accounted for in the formula. The interphase is the major cause for nanocomposites having novel properties not generally observed in their macroscale or bulk counterparts.

1.3 Silsesquioxanes

The term silsesquioxanes refer to a group of compounds with the general formula $(RSiO_{1.5})_n$, where R can be hydrogen or a wide range of alkyl, alkenyl, aryl, or siloxy groups. This general formula places silsesquioxanes as an intermediate between the inorganic ceramic material silica, SiO_2, and the more organic silicone polymers, $(R_2SiO)_n$. Silsesquioxanes can therefore be considered hybrids, with inert and thermally stable Si-O-Si frameworks and potentially reactive and easily modified R groups on the silicon atoms. Silsesquioxane-based materials have found uses in a variety of applications, including as a component in polymer nanocomposites,[26-31] catalysts,[32-35] models for silica surfaces[36-38] and heterogeneous catalysts,[39-41] low-k dielectrics,[42-44] antimicrobial agents,[45-46] emitting layers in organic light-emitting diodes (OLEDs),[11] and coatings.[47,48]

1.3.1 Definitions, Structures, and Nomenclatures

The name "silsesquioxane" can be split into three terms: "sil-" (silicon), "-sesqui-" (one-and-a-half), and "-oxane" (oxygen), which refer to the 1.5 ratio between the silicon and oxygen atoms. Silsesquioxanes are the product of hydrolytic condensation reactions of trifunctional silicon monomers, $RSiX_3$, where X is normally a halide or alkoxide group. Different structures of silsesquioxanes can be formed depending on the reaction conditions. There are four basic structures of silsesquioxanes: random structures with no long-range order (Figure **1.1a**), ladder polymers with no polyhedra structures (Figure **1.1b**), incompletely condensed polyhedra species (Figure **1.1c**), and completely condensed

polyhedra species (Figure **1.1d**). In general, formation of discrete molecular species is favored under high dilution, which results in slower hydrolysis and higher possibility of intramolecular reactions. On the other hand, polymer formation occurs more readily under higher concentrations of reagents.

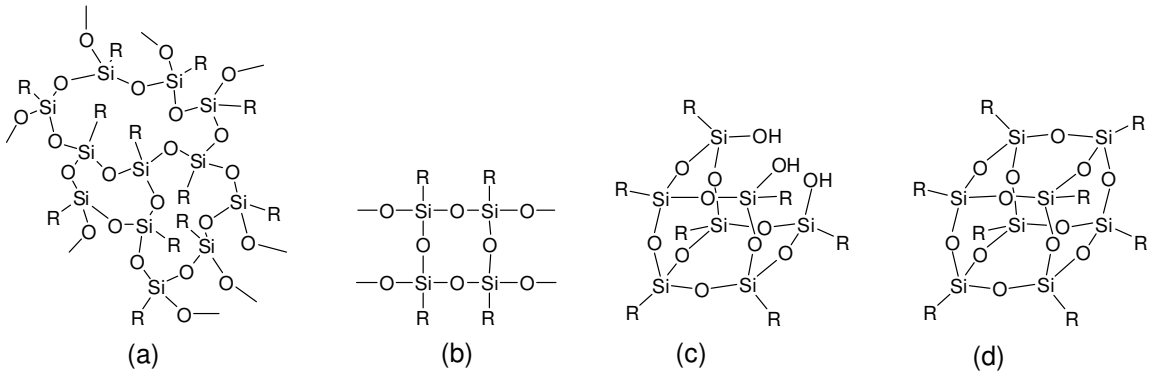

Figure 1.1. Some schematic structures of silsesquioxanes.[10]

The full IUPAC rules for silsesquioxane nomenclature are complicated and burdensome, and therefore the compounds are more conveniently named using systematic nomenclature that gives the number of silsesquioxane units ($SiO_{1.5}$) in the molecule and the substituents on the silicon atoms.[1] As an example is $(CH_3SiO_{1.5})_8$ or octamethylsilsesquioxane, having an octameric cage structure with methyl groups on the silicon atoms.

An alternative in naming silsesquioxane molecules is to use shorthand notations commonly used in siloxane chemistry.[10] These notations use letters to describe the type of silicon atom in the silicon-oxygen frameworks followed by numerical subscripts denoting the number of silicon atoms in the molecule and optional superscripts denoting the type of functional groups attached to the silicon atoms. There are four types of silicon atoms under this shorthand notation (see Figure **1.2**): an "M" unit has a silicon atom bound to one oxygen atom, a "D"-unit silicon atom is bound to two oxygen atoms, a "T" unit has three oxygen atoms bound on the silicon atom, and a "Q" unit consists of a silicon atom bound to four oxygen atoms.[49] With the example earlier, octamethylsilsesquioxane, is denoted as T_8^{Me} or Me_8T_8, having an octameric cage structure with each silicon atom connected to three oxygen atoms and a methyl group.

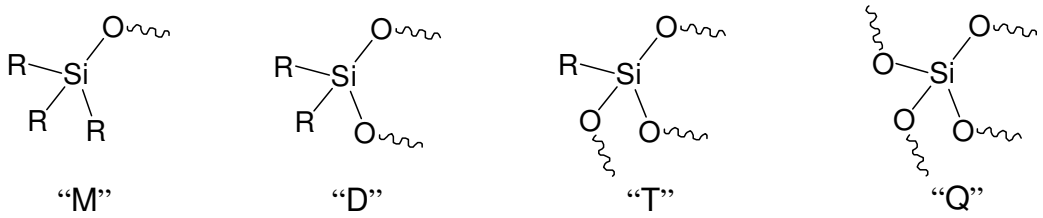

Figure 1.2. Silsesquioxane nomenclature.

There are multiple cage structures in the completely condensed polyhedral silsesquioxane category, although the majority of molecules synthesized and studied are octameric in structure, $(RSiO_{1.5})_8$ or T_8. Some researchers speculate that this is caused by the preference to form molecules containing all Si_4O_4 rings, which are the most stable of Si-O cyclic structures.[10] There are very limited examples of hexameric silsesquioxanes, $(RSiO_{1.5})_6$ or T_6,[10] and decameric silsesquioxanes, $(RSiO_{1.5})_{10}$ or T_{10},[10] but there have been an increasing number of works on dodecameric silsesquioxanes, $(RSiO_{1.5})_{12}$ or T_{12}.[10-13]

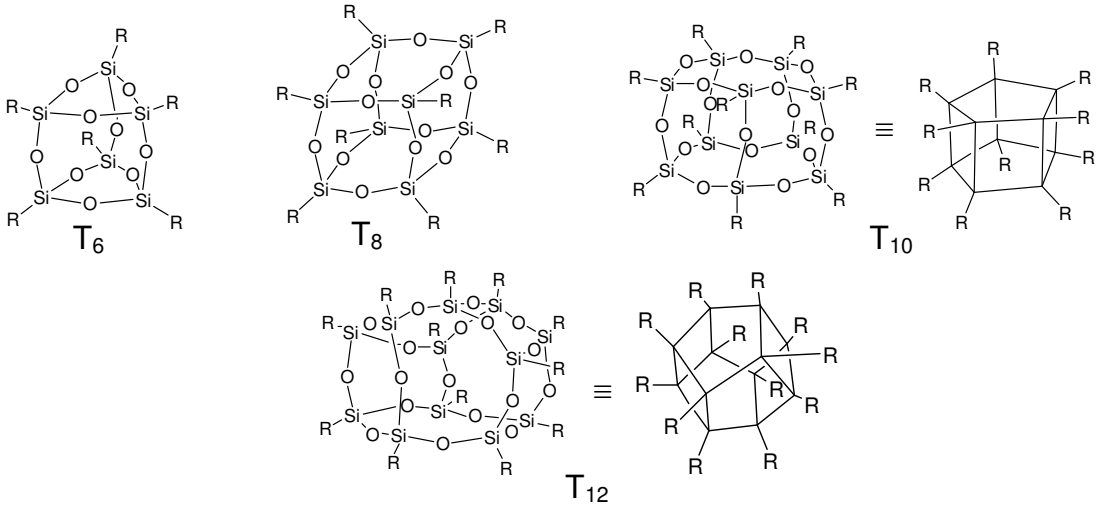

Figure 1.3. Completely condensed polyhedral silsesquioxane cage structures.[10]

1.3.2 Formation of Silsesquioxane Cages and Networks

The hydrolytic condensation reactions of $RSiX_3$ to produce silsesquioxanes are a complex, time-consuming, multistep process, even though it can be represented by a seemingly simple scheme:

$$n\ RSiX_3 + 1.5n\ H_2O \rightarrow (RSiO_{1.5})_n + 3n\ HX$$

These reactions are influenced by a whole host of reaction conditions such as concentration of $RSiX_3$, solvent, characters of R and X groups, catalyst, water addition, and

solubility of the condensation products.[1,50] During this reaction, numerous intermediates are formed and they are in equilibrium with one another. Some of these intermediates have been isolated and identified as linear oligosiloxanes with two to four silicon atoms, cyclic oligosiloxanes, as well as condensed polycyclosiloxanes.[51-55]

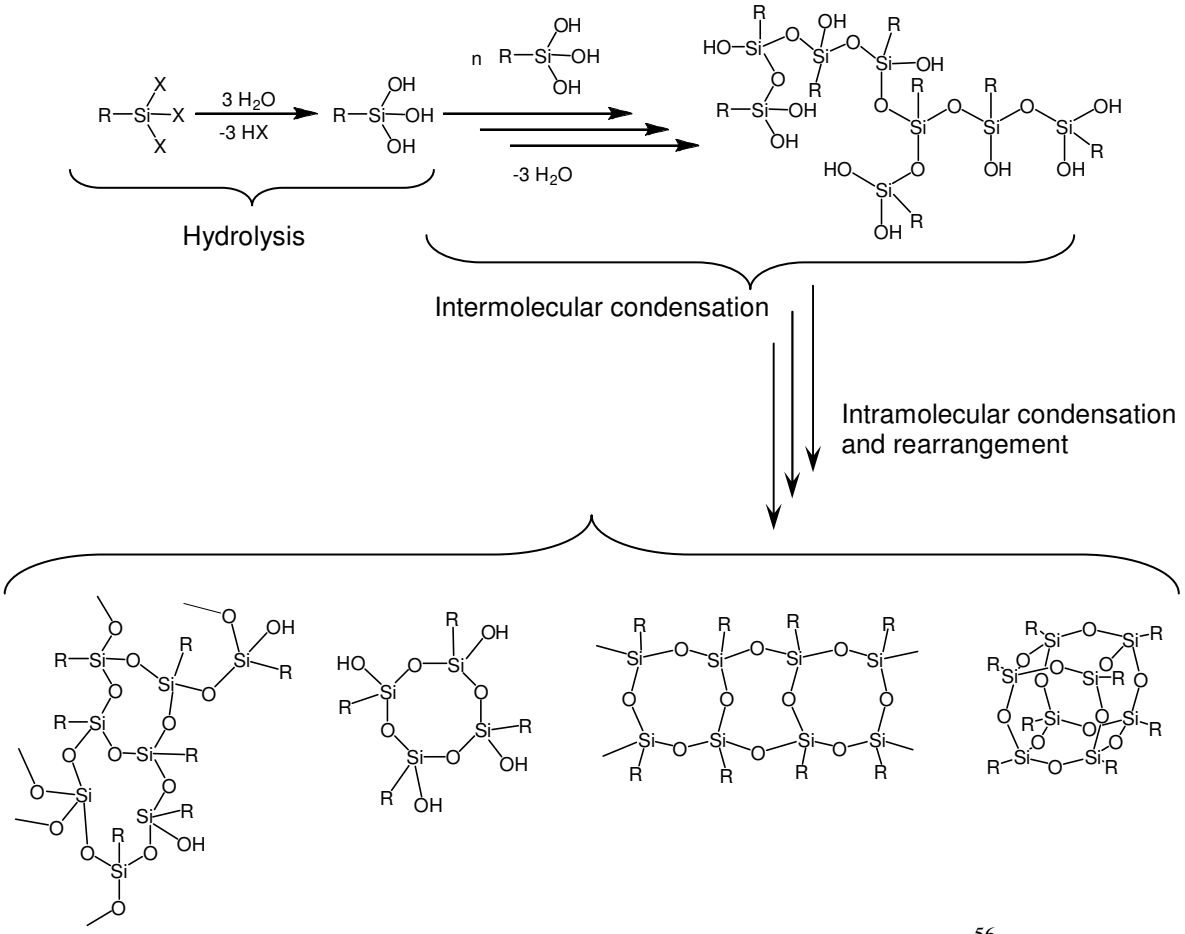

Scheme 1.1. Hydrolysis and condensation of silsesquioxanes.[56]

It should be noted that due to the complicated nature of the condensation process and the strong interdependence of the reaction conditions, there are no universal procedures that can be applied to the syntheses of silsesquioxanes. However, by carefully controlling the reaction conditions, the equilibria of the intermediates can be tipped to favor the formation of specific structures. Recently, there have been numerous procedures developed for the synthesis of specific silsesquioxanes, causing an increase in the number of published papers and patents on silsesquioxanes.[10,49]

Even if there are no universal procedures for the syntheses of silsesquioxanes, there are some general trends observed with respect to how a certain reaction condition may

affect the structures of the silsesquioxane product. As mentioned above, high concentrations of $RSiX_3$ monomer favor the formation of silsesquioxane polymers, while intramolecular cyclization dominates in dilute reaction solutions to yield polyhedral silsesquioxanes. Polar solvents, especially alcohols, solvate the siloxane intermediates and favor polymer formation, whereas inert, organic non-polar solvents decrease the degree of intermolecular association and favor intramolecular condensation. More reactive R and X groups, such as R = hydrogen, methyl and X = Cl, OH, undergo faster hydrolysis and favor the formation of silsesquioxane polymers. Low reaction pH supports cyclization of the reaction intermediates, but high pH supports their polymerization. Water is needed to achieve hydrolysis and cyclization, but too much water in the reaction causes polymer formation. The solubility of a specific silsesquioxane species formed during the condensation reaction, which in part is dictated by the type of R group on the monomer, has a large influence over the yield of that species. The less soluble silsesquioxane species precipitate out of the reaction mixture, pushing the equilibrium of the reaction intermediates towards forming more of that species. This process continues until a point is reached in which the amounts of the intermediates in the reaction solution are back in equilibrium with one another.[1,50]

1.3.3 Silsesquioxanes as Nanobuilding Blocks

The best candidate for nanobuilding blocks should have the following properties: nanometer dimensions, high symmetry, and multiple functionalities. Having nanometer dimension would aid in the assembly of new materials at the finest length-scales possible. The high symmetry of the building blocks will increase the probability in minimizing defects in assembled 2-D and 3-D structures, since misaligned but highly symmetrical components would be able to realign easily (with less energy required) with adjacent assembled components. Nanobuilding blocks with multiple functionalities are essential in building new materials, as they are the key to forming multiple bonds with adjacent components in 1-, 2-, and 3-dimensions, anchoring them permanently in the new materials. These functionalities should also be easily modified, so that they can be customized at will to tailor to whatever functional groups are needed for different purposes. Therefore, considering the criteria for successful nanobuilding blocks, molecules with cubic symme-

try could be exceptional candidates to develop routes to well-defined molecular nano-building blocks.

At the molecular level, there are numerous highly symmetrical 2-D molecules described in literature. There are also sets of molecules that offer highly symmetrical 3-D functionality, such as tetrahedranes, adamantanes, cubanes, and dodecahedral boranes. However, only a small set of molecules offer high 3-D symmetry, ease of synthesis and/or modifications, and octafunctionality such that there is a functional group in each octant in the three-dimensional coordinate system. To date, only the cubane family of compounds and cubic silsesquioxanes offer the requisite 3-D symmetry. However, cubanes are synthesized from complex, multistep synthetic protocols where systematic and controlled substitution of functional groups onto the cubane frame has proven to be difficult.[57-59]

Octameric silsesquioxanes are unique molecules consisting of rigid silica cores (body diagonal = 0.53 nm) with eight organic functional groups anchored to the vertices of the silica core. Together, the silica core and the organic moieties create sphere-like organic-inorganic molecule 1-2 nm in diameter with volumes less than 2 nm^3 (Figure **1.4a**). Each functional group is located in a separate octant in three-dimensional space, orthogonal (or in opposition) to each other (see Figure **1.4b**).

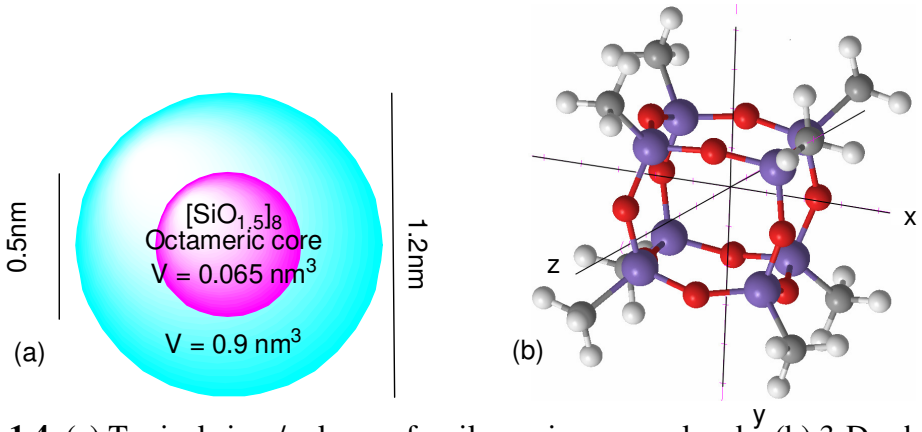

Figure 1.4. (a) Typical sizes/volume of a silsesquioxane molecule. (b) 3-D schematic drawing of octamethylsilsesquioxane showing the functional groups in different octants in three-dimensional space.

Silsesquioxanes can be prepared in large quantities using simple and straightforward syntheses.[5,9-13] The organic groups on the corners of the molecules can be further functionalized or modified using simple chemistries.[1-13] The position of the organic functional

groups and the large variety of these groups, together with the size of octameric silsesquioxanes, provide unique opportunities to build nanocomposites in 1-, 2-, or 3-dimensions, one nanometer at a time. The silica core adds rigidity and heat capacity of silica to the resulting compounds, improving the mechanical and thermal properties of these compounds.

1.3.4 Octaphenylsilsesquioxane (OPS): Synthesis and Derivatives

OPS was first synthesized by Olsson in 1958 as a product of hydrolysis of phenyltrichlorosilane ($PhSiCl_3$) in refluxing methanol with aqueous HCl as catalyst, with a 9% yield.[60] Since then, various efforts have been made to optimize the synthesis of OPS by modifying the reaction conditions.[53,61-64]

Our group has optimized the synthesis of OPS developed by Brown[53] to achieve greater than 90% yield from commercially available $PhSiCl_3$,[65] which is reacted with

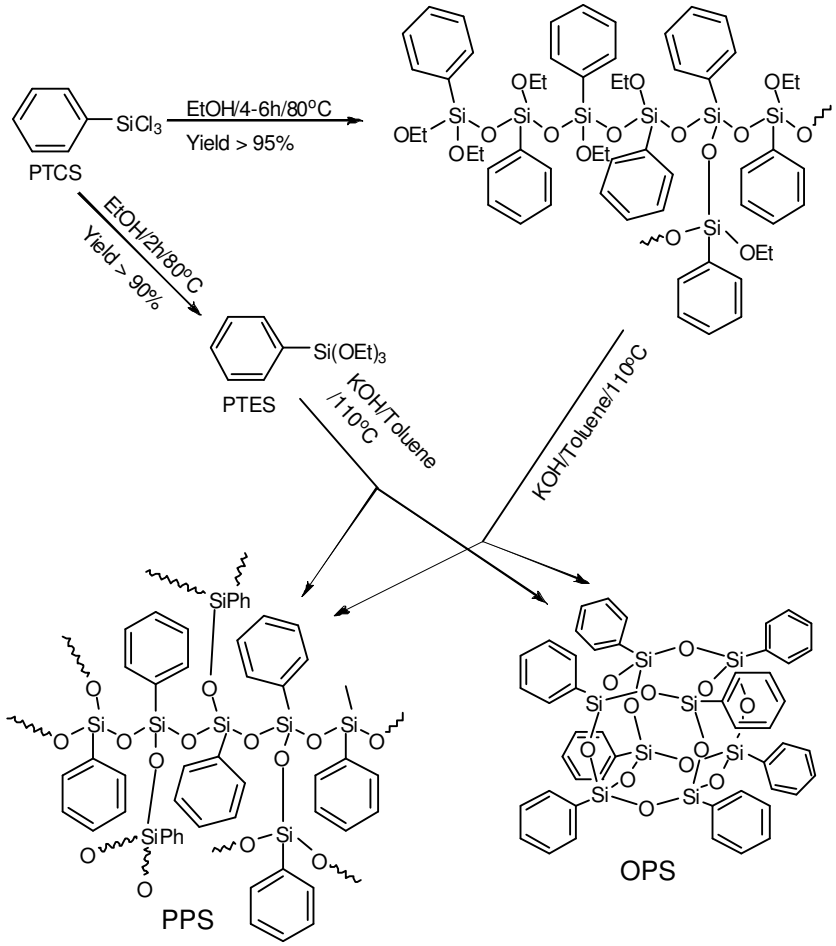

Scheme 1.2. General pathways for the synthesis of OPS.[65]

ethanol to form either phenyltriethoxysilane, $PhSi(OEt)_3$, or its hydrolyzed oligomers depending on the reaction conditions (2 h vs. 4-6 h reflux time). Condensation of either types of $PhSi(OEt)_3$ with catalytic amounts of KOH and minimal amounts of water in toluene produces OPS and a byproduct, polymeric phenyl silsesquioxanes [$(PhSiO_{1.5})_n$, PPS] with a molecular weight of approximately 3000 Da.

OPS is obtained as white microcrystalline powder with very low solubility in common organic solvents. It has high thermal stability in air (up to 500°C) and gives a high yield of ceramic residue (70%) when heated in nitrogen.[66] Even though OPS has excellent thermal stability, nanometer dimension, high 3-D symmetry, and relatively simple preparation, it has seen limited use in nanocomposite application due to its high insolubility and the fact that it decomposes before melting. The utility of OPS is improved by increasing its solubility and reactivity by introducing functional groups on the phenyl rings. Various papers have reported the functionalization of OPS via electrophilic aromatic substitution reactions, some of which are summarized in the following sections.

1.3.4.1 Octa(nitrophenyl)silsesquioxane (ONPS) and Octa(aminophenyl)silsesquioxane (OAPS)

The nitration of OPS was first reported by Olsson and Gröwall in 1961,[61] resulting from the dissolution of OPS in cold, fuming nitric acid, giving one nitro group per phenyl ring.[67] The authors' efforts to reduce the nitro groups to amino groups were reported to be unsuccessful and the paper was unnoticed for decades. Our group revisited this reaction and found that the nitration occurs on the *ortho*-, *meta*-, and *para*-position relative to the silicon atom with an approximate ratio of 10:65:25 *o*:*m*:*p*.[67] Furthermore, the nitro groups can be easily reduced to amino groups using formic acid/triethylamine as the reducing agent and Pd/C as the catalyst in THF solution.

The strongly electron-withdrawing nitro groups prevent electrophilic attack by a second nitro group under ambient temperature. However, it is possible to di-nitrate each phenyl ring in OPS using a mixture of nitric and sulfuric acids at 50°C.[68] This material decomposes explosively around 400°C. Octa(dinitrophenyl)silsesquioxane can be reduced to form its amino derivatives, octa(diaminophenyl)silsesquioxane, using a similar

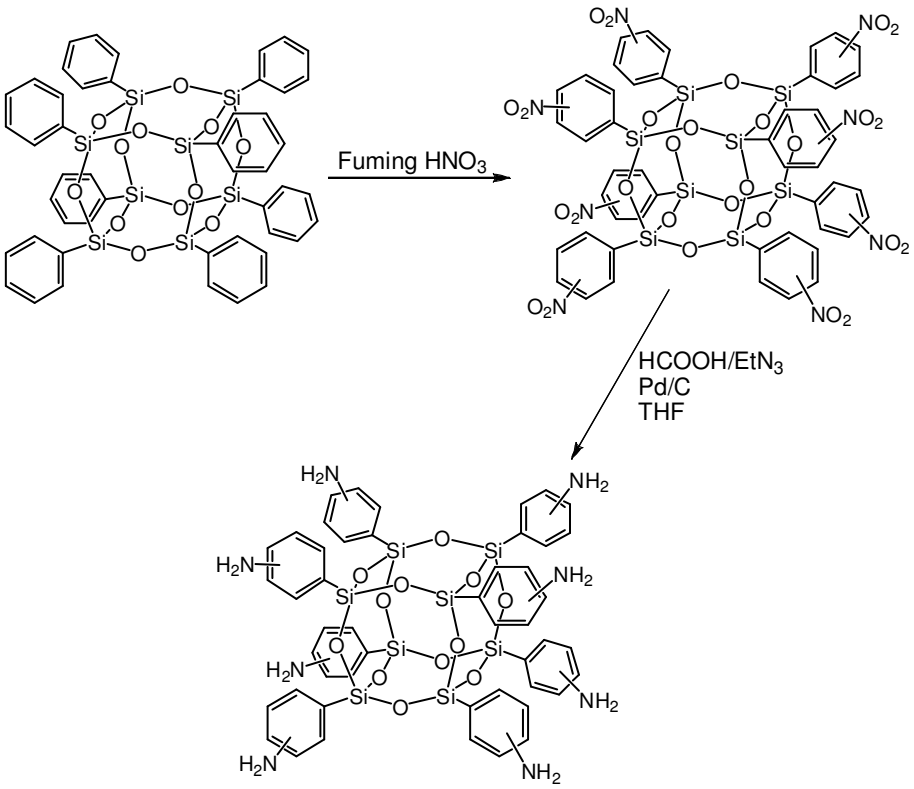

Scheme 1.3. Synthesis of ONPS and OAPS.

procedure for OAPS, but this synthesis is difficult because this material is strongly basic, which can easily destroy the silsesquioxane cage structure.

The amino-functionalized silsesquioxanes can be used to form a variety of derivatives for numerous potential applications. A multitude of work has been done using OAPS as a component in nanocomposites.[69-73] Of particular interest for the work described here (Chapter **6**) is the use of OAPS in epoxy resins. Choi et al. investigated the mechanical properties of OAPS-based epoxy nanocomposites[69] and found that the highest rubbery modulus is obtained when the NH_2:epoxy molar ratio is 1:1 to form linear tethers (see Figure **1.5a**), which suggests that the highest crosslink density is achieved at this composition. Bifurcated tethers, with NH_2:epoxy molar ratio of 0.5:1 (Figure **1.5b**), cannot be formed efficiently due to steric hindrance around the secondary amine hydrogen, which limits reaction with epoxide groups, producing nanocomposites with high numbers of defects.

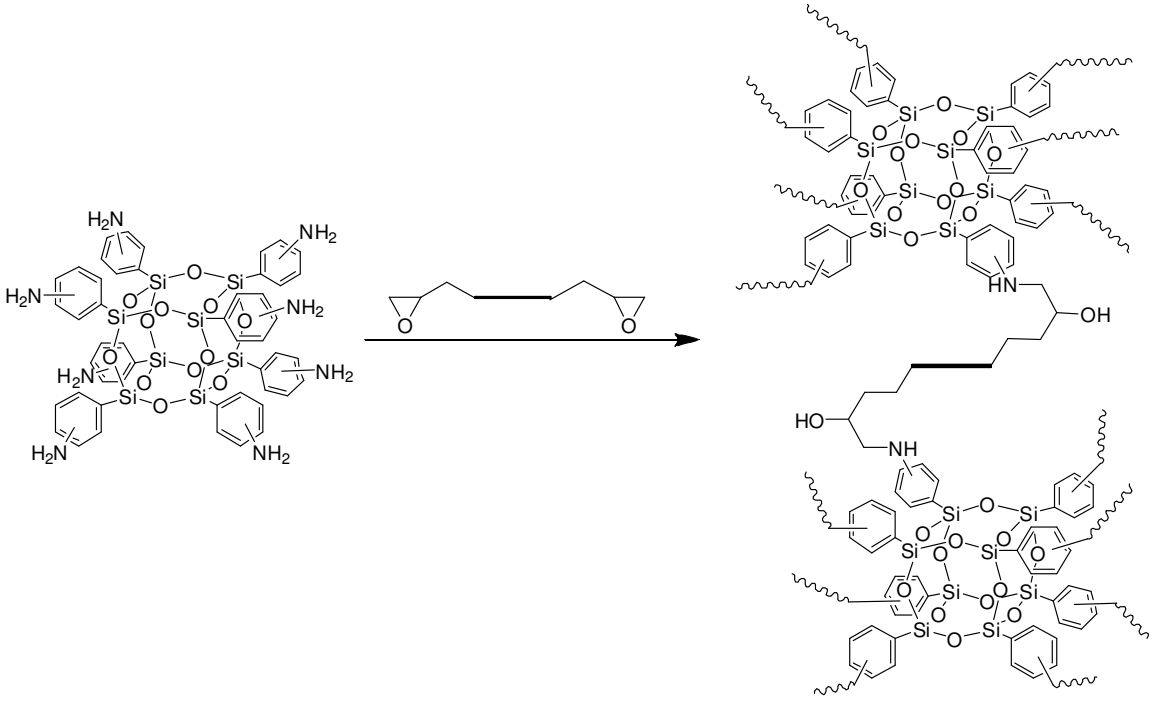

Scheme 1.4. OAPS/epoxy nanocomposite.

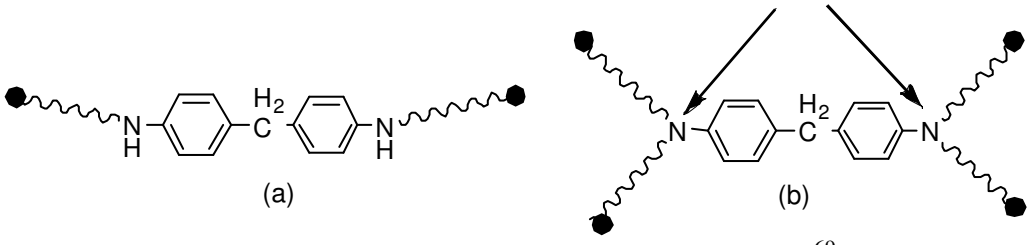

Figure 1.5. Linear (a) and bifurcated (b) tethers.[69]

1.3.4.2 Brominated OPS (Br_xOPS)

Preliminary studies done in our group to brominate OPS use bromine (Br_2) as the brominating agent and iron [Fe(0)] as the catalyst in dichloromethane solutions.[74] Singly brominated OPS is obtained when the ratio of Br_2:OPS is less than 8:1, with the most predominant product being $Br_{5.3}$OPS. Oxidative cleavage of the brominated phenyl groups from the silsesquioxane core using KF/H_2O_2 allows investigation of the substitution pattern of the resulting bromophenols by ^{1}H-NMR, which determine that the substitution pattern of $Br_{5.3}$OPS was 10:25:65 *o*:*m*:*p*.

Higher ratios of Br_2:OPS produce dibrominated OPS up to $Br_{15.7}$OPS with almost 80% having a 2,5- substitution pattern (*ortho* and *meta*-to the silicon atom). This indicates extensive rearrangement of the *para*-positioned bromo groups, the predominant

species in monobrominated OPS, to *ortho*- or *meta*-positioned bromo groups so that the more stable 2,5-dibrominated phenyl rings can be formed.

$Br_{5.3}$OPS have been shown to undergo further modifications by various cross-coupling reactions including Heck, Suzuki, Sonogashira, and Buchwald-Hartwig amination reactions.[74,75]

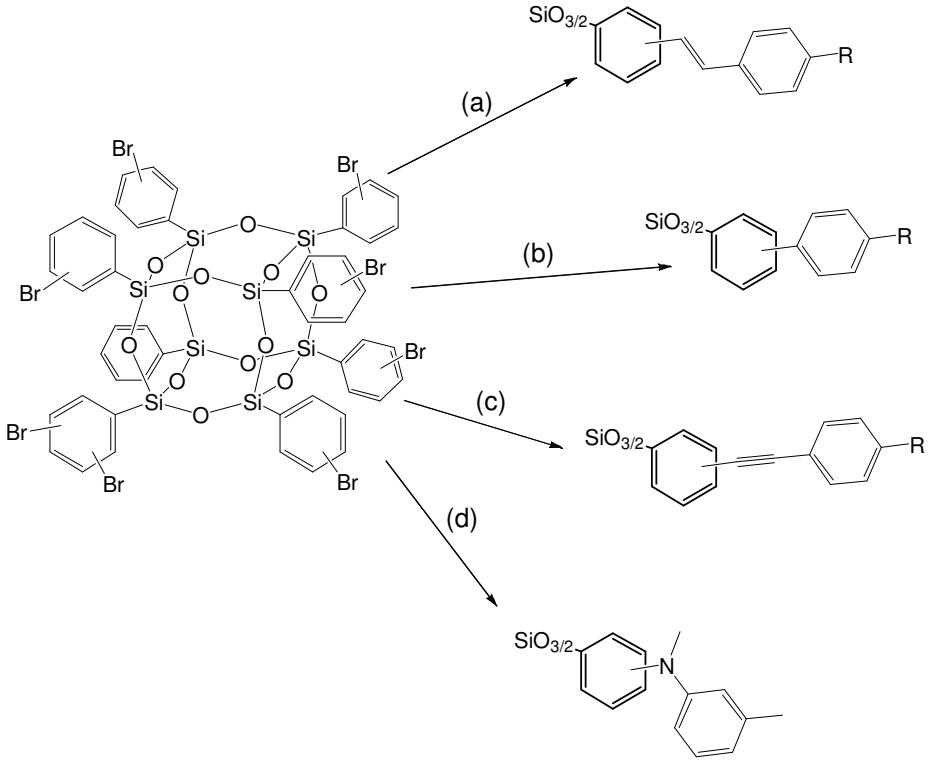

Scheme 1.5. Functionalization of $Br_{5.3}$OPS via (a) Heck, (b) Suzuki, (c) Sonogashira, and (d) Buchwald-Hartwig amination reactions.[74,75]

More recently, studies done in our group have expanded our knowledge of bromination reactions on OPS. Br_xOPS (x = 8, 16, 24) were synthesized by careful manipulation of reaction conditions such as catalyst, total concentration, temperature, and the sequence of reagent addition.[76,77] Crystalline samples are collected from multiple recrystallization from the crude products with yields up to 25% and purities greater than 95%.

Bromination of OPS in dilute dichloromethane solution without added catalyst affords octa-brominated OPS with a narrow distribution in substitution number. The substitution pattern for this material is found to be 85:15 *o*:*p*. This is highly unusual since uncatalyzed bromination of phenyl rings only occurs with activated aromatic systems such as phenols and anisoles.[78] Furthermore, the substitution reaction should occur

mostly on the *para* position rather than the *ortho* position simply because of steric hindrance around the *ortho* position.

It is postulated that the silsesquioxane cage faces promotes bromination of OPS by forming a complex with Br_2 (see Figure **1.6**), polarizing the Br_2 molecule, such that $Br^{\delta+}$ forms close to the *ortho* position next to the silicon atom, leading to electrophilic attack by the phenyl ring to give *ortho*-bromophenyl moiety.

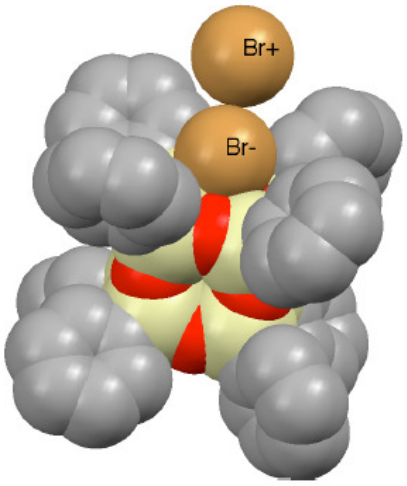

Figure 1.6. Proposed complexation of Br_2 with OPS cage face.[77]

The uncatalyzed bromination of OPS introduces up to an average of fourteen bromo groups per OPS molecule. The use of $FeBr_3$ as a homogenous catalyst can increase the number of bromo groups incorporated onto an OPS molecule beyond fourteen. The slow addition of Br_2 into a suspension of OPS and $FeBr_3$ in cold dichloromethane produces microcrystalline 2,5-Br_{16}OPS, which precipitates out of the reaction solution.[76,77] The substitution pattern of this material is > 95% 2,5-dibromophenyl, as determined by ^{1}H-NMR data of the oxidative cleavage products.

The addition of $FeBr_3$ catalyst after an initial uncatalyzed bromination reaction of OPS has subsided, produces soluble Br_{16}OPS with 2:1 ratio of 2,5-dibromophenyl and 3,4-dibromophenyl substitution patterns.[76,77] If more Br_2 is added to this reaction mixture, the degree of bromination can be increased up to twenty-four. However, significant Si-C bond cleavage is observed as a side reaction, and the crude product has to be purified by multiple recrystallizations to obtain crystalline Br_{24}OPS. *o*-Br_8OPS, 2,5-Br_{16}OPS, and Br_{24}OPS are used as starting materials in Chapter **4** to synthesize polyfunctional luminescent silsesquioxane molecules.

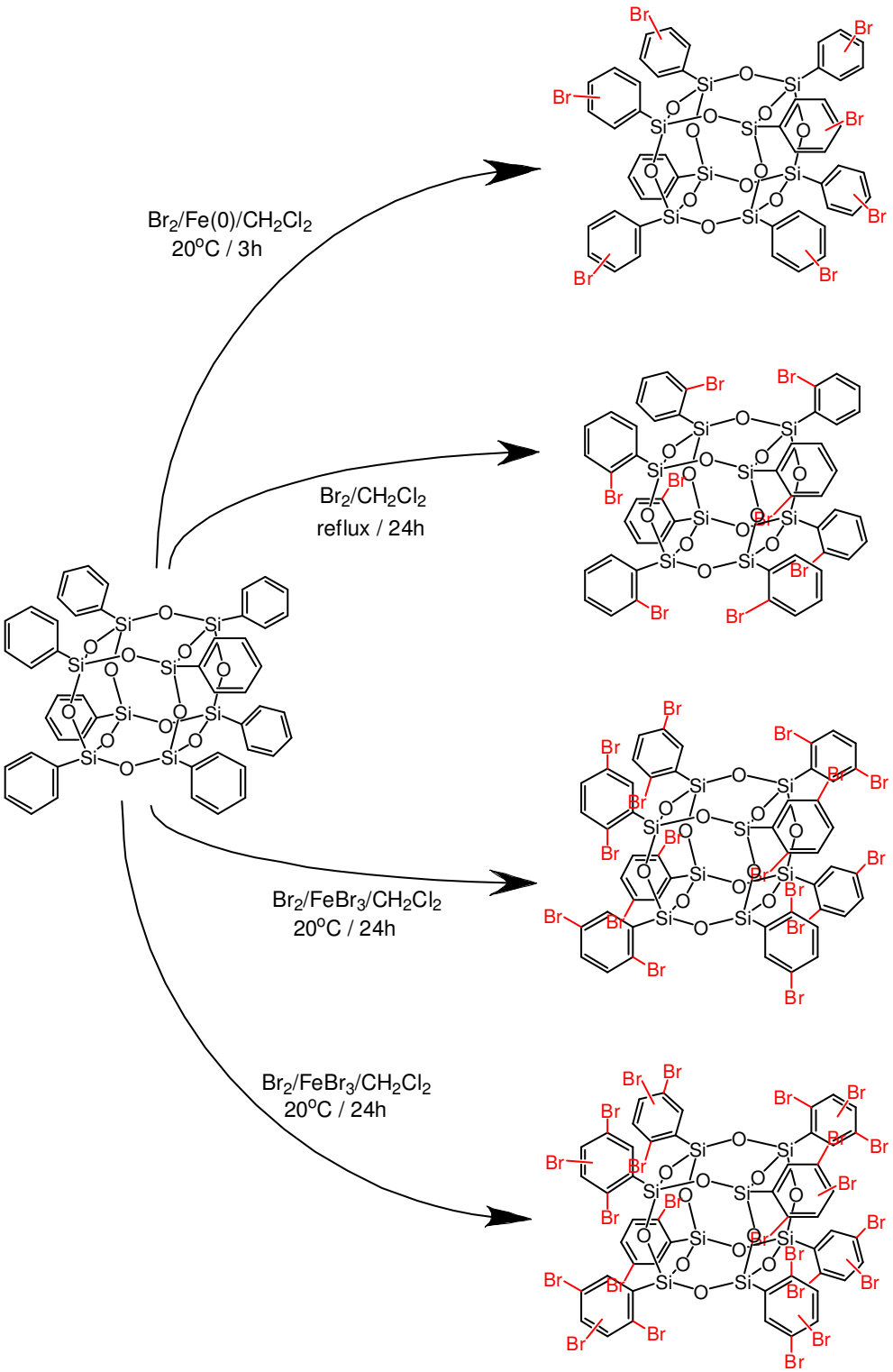

Scheme 1.6. Bromination of OPS.

1.3.4.3 Octa(*p*-iodophenyl)silsesquioxane (*p*-I_8OPS)

The iodination of OPS is achieved by reacting OPS with iodine monochloride (ICl) in dichloromethane at -40°C and then slow warm-up to room temperature. The crude product of this reaction is 90% I_8OPS, which is purified by recrystallization from ethyl acetate to give crystalline materials that are 99% octa-substituted and 93% *para*-substituted in up to 40% yield.[77,79] Unlike brominated OPS products, *p*-I_8OPS preserves the cubic symmetry of the parent OPS compound and this material has been used as a starting point to build highly-ordered porous nanostructures.[77,79,80] *p*-I_8OPS is highly soluble in common organic solvents and has been shown to undergo various cross-coupling reactions such as Heck, Suzuki, Sonogashira, amination, and phosphonation reactions.[79]

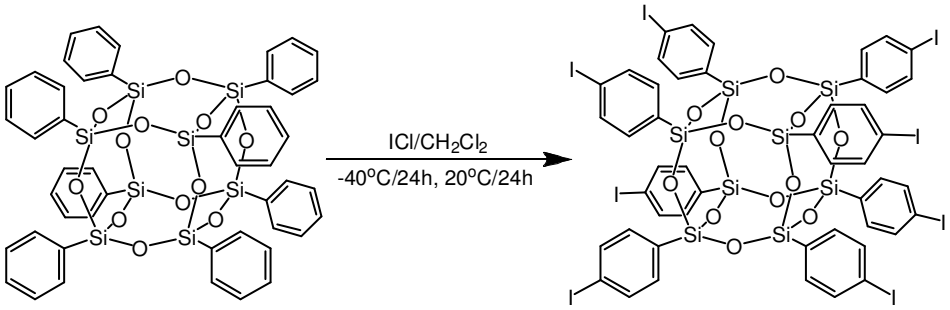

Scheme 1.7. Iodination of OPS.

1.3.5 Octavinylsilsesquioxane (OVS): Synthesis and Functionalization

OVS was first synthesized in 1978 by Andrianov et al. from the hydrolysis of vinyltrichlorosilane ($ViSiCl_3$) in low yields (< 10%).[54] Multiple groups have since tried to improve this synthesis with little success[81-83] until Harrison and Hall published their work in 1997,[84] obtaining 20-30% yield using aqueous ethanol as the medium for the hydrolysis of $ViSiCl_3$. More recently, the use of Amberlite cation exchange resin as a catalyst for the hydrolysis and condensation of $ViSiCl_3$ in methanol afforded the synthesis of OVS with yields up to 40%.[64] This catalyst can be regenerated and reused repeatedly, making the synthesis more economically viable. An even better yield of up to 80% was reported when tetramethylammonium hydroxide (Me_4NOH) was used as phase transfer catalyst for the hydrolysis and condensation of vinyltriethoxysilane [$ViSi(OEt)_3$] in methanol.[85]

OVS can be functionalized with a variety of chemical reactions applicable to regular alkene group, such as thioether addition, phosphination, hydrosilylation, and epoxidation.

Radical addition of thiols such as thiophenol and cyclohexylthiol across the vinyl groups of OVS with AIBN as radical initiator or under UV irradiation have been reported.[86-88]

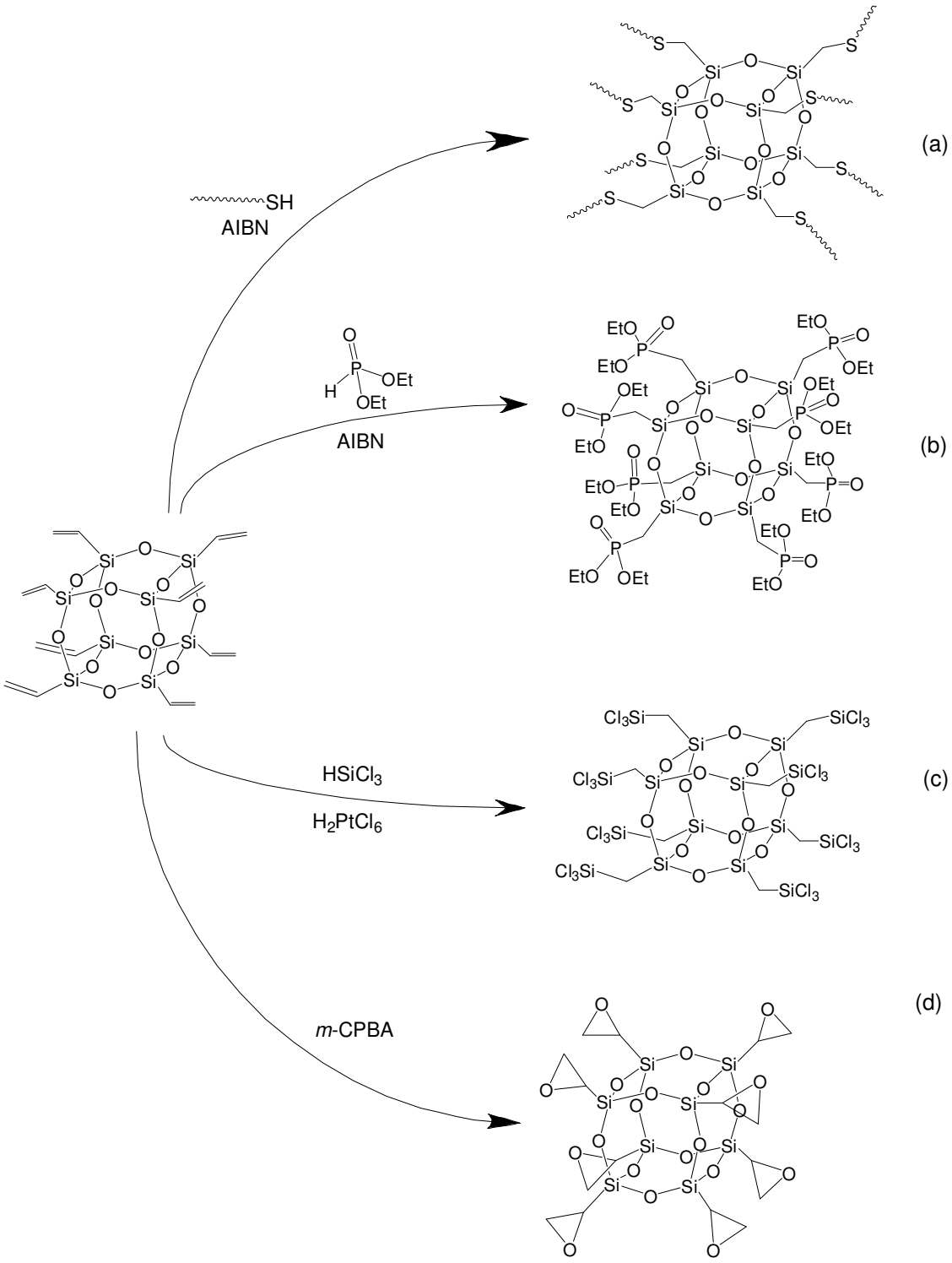

Scheme 1.8. Reactions across the vinyl groups in OVS: (a) thioether, (b) phosphonation, (c) hydrosilylation, (d) epoxidation.

The radical addition of phosphines and phosphonates, such as diethylphosphine or diethylphosphonate, onto the vinyl groups of OVS provides phosphine-functionalized silsesquioxane molecules, which can then be used as ligands for transition metals such as rhodium.[89]

Platinum-catalyzed hydrosilylation reactions of OVS with di- and tri-chlorosilanes have extended the number of functional groups per molecules to 16 and 24, forming the starting point for silsesquioxane-based dendrimers.[89-91] Syntheses of highly-porous silsesquioxane-based polymer network have been investigated by hydrosilylation of OVS and $Q_8(SiMe_2Vi)_8$ ($Si_8O_{12}(OSiMe_2Vi)_8$) with T_8H_8 ($Si_8O_{12}H_8$) and $Q_8(SiMe_2H)_8$ ($Si_8O_{12}(OSiMe_2H)_8$) to form four types of network.[26]

Oxidation of the vinyl groups on OVS using *m*-chloroperoxybenzoic acid (*m*-CPBA) gives epoxy-functionalized silsesquioxanes. However, only the product from partial oxidation (3 equivalent *m*-CPBA used, 2 vinyl groups oxidized) was isolated. Efforts to isolate the fully oxidized product produced intractable gels, instead. These epoxy-functionalized silsesquioxanes polymerize readily using Lewis acid initiators or diamines to give organic/inorganic nanocomposites.[92]

Heck coupling reactions of OVS with various large, mono-haloaromatic compounds have been reported. Interestingly, di-substitution of the vinyl groups of OVS was obtained easily when the aromatic compounds were added in excess. It was suggested that the already substituted vinyl groups may be activated towards the second substitution inspite of steric constraints around the silsesquioxane cores.[93-95]

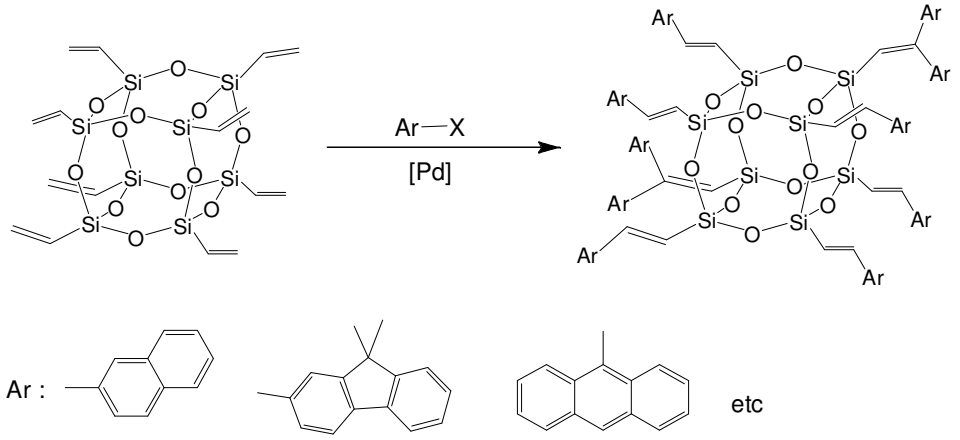

Scheme 1.9. Heck coupling reaction of OVS.

The Feher group has shown that OVS undergoes cross-metathesis reactions with various simple alkenes, such as pentene, 4-octene, and styrene, using both Grubbs and Schrock catalysts.[96] Similar work done by the Marciniec group demonstrated that silylative coupling catalyst can be used in coupling reactions in which the Grubbs catalyst is not active, most notably with functionalized alkenes such vinylsilanes, vinyl ethers, and vinylpyrrolidinone.[97] Chapter **3** describes cross-metathesis reactions of OVS with R-styrenes to form the starting platform for the syntheses of other novel silsesquioxane molecules with unique properties.

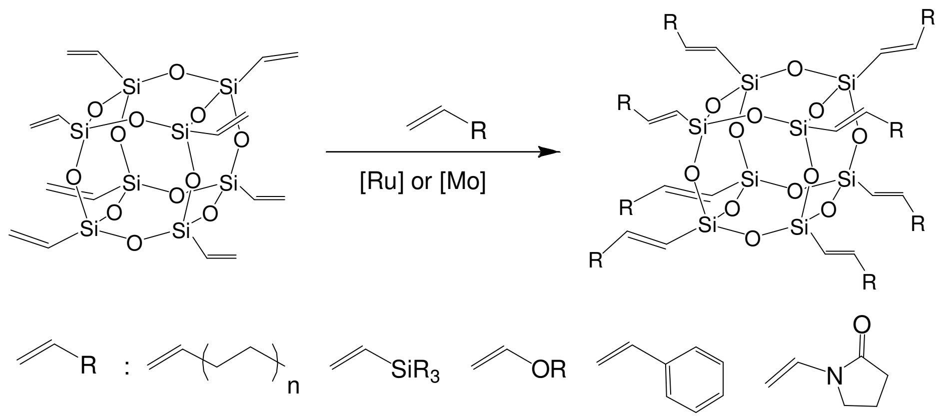

Scheme 1.10. Cross-metathesis of OVS.

1.3.6 Electrophilicity of Silsesquioxane Core

Conventionally, silsesquioxanes have been regarded as insulators due to their similarities with silica. The structure of the incompletely condensed trisilanol cubic silsesqui-

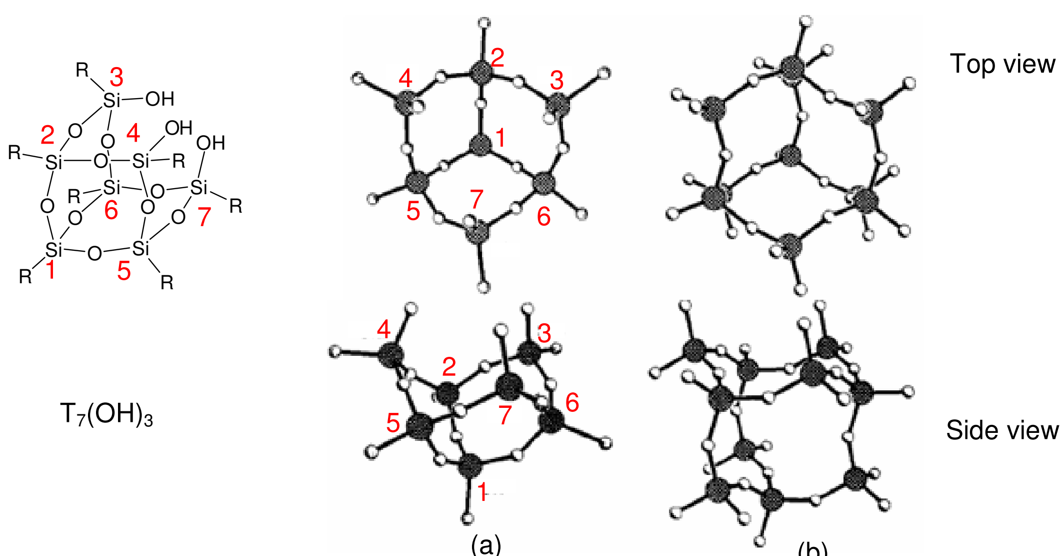

Figure 1.7. ORTEP plot of (a) $R_7T_7(OH)_3$ and (b) idealized β-cristobalite.[36] For clarity, only C atoms attached to Si are shown.

oxane [$R_7T_7(OH)_3$] bears a close resemblance to coordination sites on the surface of the β-cristobalite form of silica[36] (Figure **1.7**) and as a consequence, silsesquioxanes are used as models for silica surfaces.[36-38] Indeed, the silsesquioxane inorganic core has been touted as the smallest single crystal of silica.[8,13,36]

Computational modeling studies of the simplest cubic silsesquioxane, H_8T_8,[2,98-102] show that the highest occupied molecular orbital (HOMO) of this molecule consists of atomic orbitals of the lone pair electrons on the oxygen atoms and the lowest unoccupied molecular orbital (LUMO) is a combination of atomic orbitals of the silicon, oxygen, and hydrogen atoms. Furthermore, the LUMO is spherical and located in the center of the silsesquioxane core. These studies also predicted that the energy gap between its HOMO and LUMO to be approximately 6-7 eV,[99,101,102] which indicates that it is an insulator.

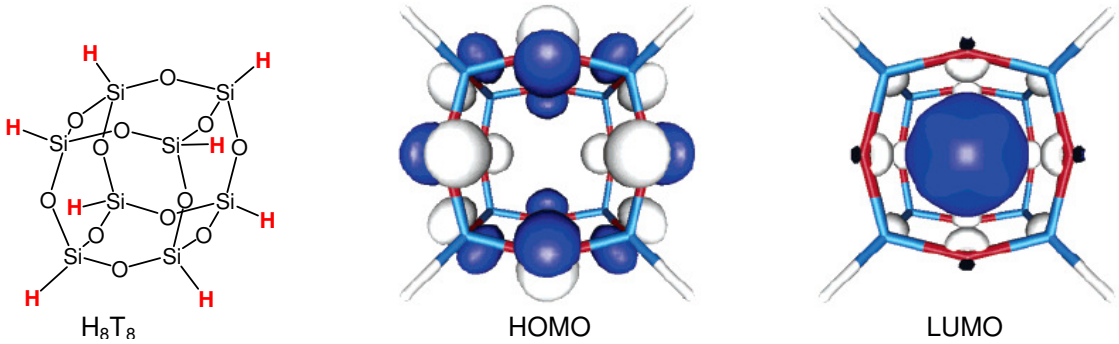

Figure 1.8. HOMO and LUMO of H_8T_8.[100]

Considering the low electronegativity of silicon atoms (1.90 vs. 2.55 for carbon atom on the Pauling scale), one would assume that any organic groups on the corners of the silsesquioxane core would experience electron donation from the silicon atoms. On the contrary, there has been considerable evidence that the silsesquioxane core is actually electrophilic. Feher and Budzichowski discovered that benzylic chloride groups attached to a silsesquioxane core are not susceptible towards hydrolysis and other substitution reactions.[103] From the ^{13}C-NMR chemical shifts data, they determined that the electron-withdrawing characteristics of the silsesquioxane core is comparable to that of a trifluoromethyl group (-CF_3).

Other evidence supporting the idea of electrophilic silsesquioxane cores is the encapsulation of fluoride (F^-) ions inside the cubic silsesquioxane cores.[104-106] These compounds can only be isolated if the organic group tethers are at least mildly electron-

withdrawing, such as phenyl, vinyl, and perfluorinated alkyl groups.[106] X-ray diffraction data for these compounds show that the presence of the F^- ion causes only minimal disturbance to the cage structure. For OPS and fluoride-encapsulating-OPS, the distance between silicon atoms on opposite corners (i.e. body diagonal) is only slightly shorter in the fluoride-encapsulating cores than in the empty structure (5.31 Å vs. 5.38 Å, respectively).[104,105]

X-ray diffraction data along with ^{19}F- and ^{29}Si-NMR data suggest that there is only a weak, electrostatic interaction between the fluoride ion and the eight equivalent silicon atoms surrounding it.[104,105] In fluoride-encapsulating-OPS, the distance between the silicon atoms and fluoride ion is 2.65 Å, which is much longer than a full Si-F covalent bond (1.71 Å).[104] The ^{19}F-NMR spectrum of this molecule shows a sharp peak at δ = -26.4 ppm, which is one of the highest shift for a fluoride salt, and indicates that the fluoride ions is essentially "naked".[104] The ^{29}Si-NMR spectrum shows a signal at δ = -80.6 ppm, which is shifted upfield by only 0.9 ppm from the signal for OPS.

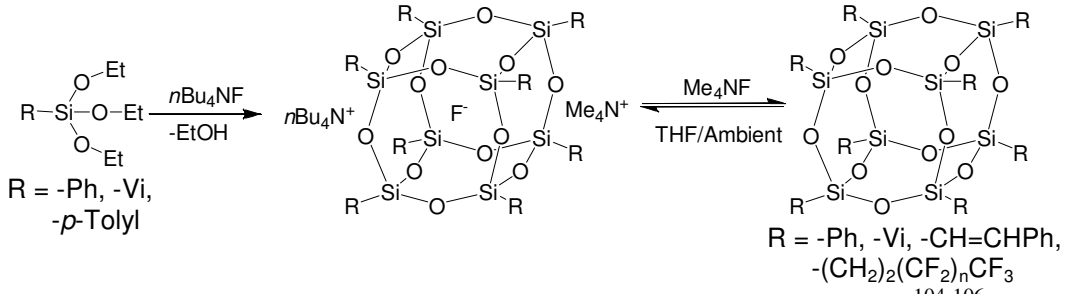

Scheme 1.11. Encapsulation of F^- ions inside silsesquioxane cage.[104-106]

Theoretical modeling studies of H_8T_8 molecules complexed with various ionic impurities reveal that the formation of F^-/H_8T_8 endohedral complexes (with the ion inside the silsesquioxane core) was favored by 60-80 kcal/mol,[100] while most positively-charged alkali metal ions prefer to form exohedral complexes (with the ion outside the silsesquioxane core).[100] This highlights the electrophilicity of the silsesquioxane core. Furthermore, atomic hydrogen can also be trapped inside the silsesquioxane cores via γ-irradiation, but modeling studies indicate that the separated $H\cdot/H_8T_8$ system is more energetically favorable, indicating that hydrogen atom trapping is a kinetic process.[107-108]

The *ortho*-bromination of OPS without any catalyst as reported by our group provides additional evidence for the electrophilicity of the silsesquioxane core.[76,77] As mentioned

earlier in this chapter (see Section **1.3.4.2** and Figure **1.6**), the complexation between OPS and Br_2 leads to spontaneous polarization of Br_2, with $Br^{\delta-}$ at the silsesquioxane cage face and $Br^{\delta+}$ close to the *ortho* position on the phenyl ring next to the silicon atom. This facilitates electrophilic attack on $Br^{\delta+}$ by the phenyl ring leading to substitution on the *ortho* position.

1.3.6.1 Electron Delocalization Involving Silsesquioxane Core

As mentioned above, the calculated values for the HOMO-LUMO bandgaps for cubic silsesquioxanes with simple tethers, such as H and alkyl groups, are 6-7 eV. However, photoluminescence studies of these compounds found that the measured HOMO-LUMO bandgaps are approximately 4-5 eV. As an example, for H_8T_8, the calculated bandgap is about 6.0 eV, but the measured value is 4.4 eV.[109,110] Azinovic et al.[110] attributed this discrepancy in the energy gap to the negative Coulomb integral, estimated to be approximately 2 eV for these molecules.[111]

Attaching conjugated aromatic groups on the corners of the silsesquioxane molecules would lower their HOMO-LUMO bandgaps further because now the electronic transitions would be localized on these organic groups. Consequently, the photophysical behavior of these materials would be expected to be similar to their free analogs (unbound to a silsesquioxane core). Indeed, numerous studies have been published on the use of silsesquioxane core as an anchor for organic chromophores for photonic applications such as OLEDs,[11] and these compounds show photophysical behavior similar to the unbound chromophores, sometimes with higher quantum yields because the silsesquioxane cores prevent π-π stacking that leads to quenching of the luminescence.[112,113]

However, a series of papers recently published by several research groups have shown that the silsesquioxane cores can act as more than just an observing anchor for organic chromophores. This set of investigations focuses on smaller conjugated organic groups, such as stilbene and biphenyl, attached to the silsesquioxane core. The absorption spectra of these molecules are similar to the small unbound molecules, but the photoluminescence spectra are red-shifted compared to the small molecules by a significant amount such that they resemble spectra from more conjugated molecules.

André et al. investigates the photophysical behavior of silsesquioxane-tethered *para*-substituted vinylbiphenyl moieties.[114] The absorption and photoluminescence spectra of these molecules in CH_2Cl_2 are only slightly red-shifted from their small molecule analogs: ~10 nm for absorption and ~15 nm for emission. Theoretical studies of these molecules suggest that the slight red-shifts in the photophysical spectra are caused by partial electron delocalization from the organic tethers to the silsesquioxane core and that there exists a possibility for intramolecular charge-transfers. However, no such interactions were observed experimentally, most probably due to the bulky *para*-substituents that prevent the formation of charge-transfer states, and other non-radiative relaxation processes are considered to be more likely to occur.

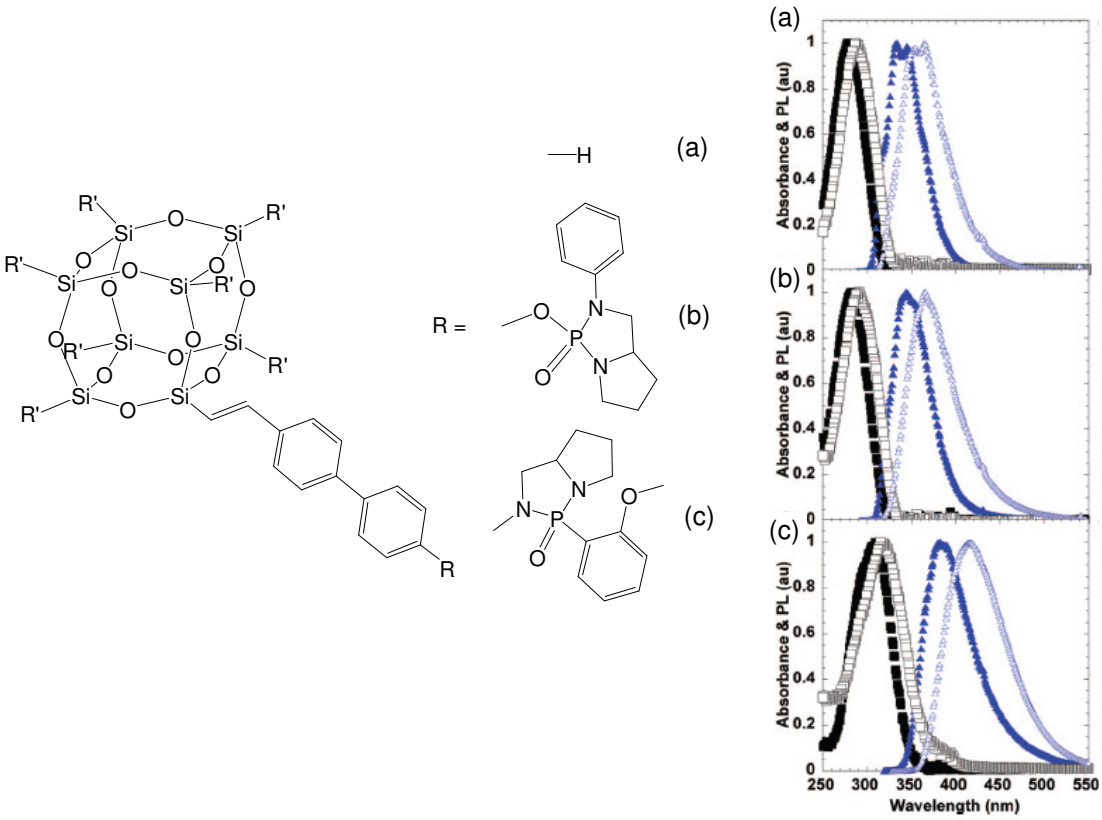

Figure 1.9. Absorption and photoluminescence spectra of *para*-substituted vinylbiphenyl silsesquioxane.[114]

A paper published by the same group[115] examines the change in fluorescence behavior of silsesquioxane molecules with 4'-vinylbiphenyl-3,5-dicarbaldehyde tethers when reduced to the dialcohol derivative (see Scheme **1.12** and Figure **1.10**). They discovered that the absorption spectra of both dialdehyde and dialcohol compounds are slightly red-

shifted (~7 nm) compared to their small molecule analogs (free, unbound to silsesquioxane core). Photoluminescence spectra of the dialdehyde compounds, both free and tethered to the silsesquioxane core (Figure **1.10a**), show that the presence of the aldehyde groups quenched the luminescence of the vinylbiphenyl moiety. However, photoluminescence spectra of the dialcohol compounds (Figure **1.10b**) show that the macromolecule's emission spectrum is red-shifted by 60 nm compared to the small molecule, which is unexpected if the silsesquioxane core is only assumed to be an observer in the electronic transition process.

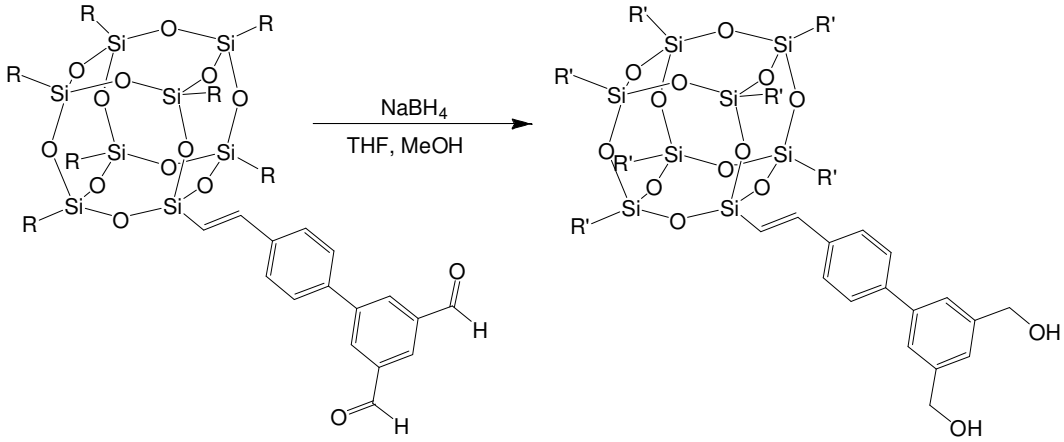

Scheme 1.12. Reduction of octa(4'-vinylbiphenyl-3,5-dicarbaldehyde)silsesquioxane to its dialcohol derivative.[115]

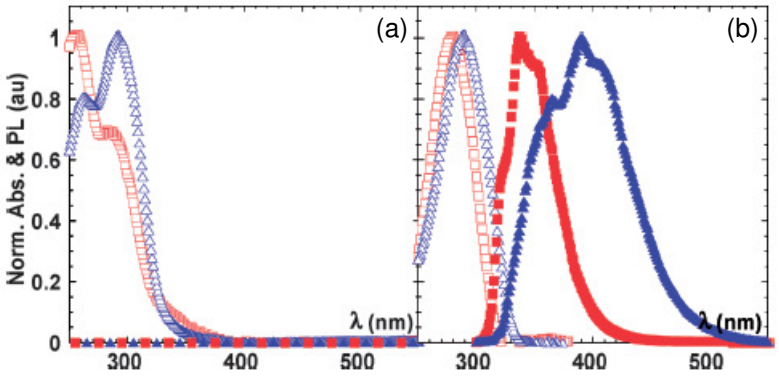

Figure 1.10. Normalized absorbance (empty symbols) and photoluminescence (full symbols) spectra of the dialdehyde (a) and dialcohol (b) compounds – small molecule analog (■) and silsesquioxane-tethered (▲). Solvent: THF-methanol.[115]

Furthermore, if the silsesquioxane core is just simply electron-withdrawing, comparable to a $-CF_3$ group as argued by Feher and Budzichowski, then both the absorption and photoluminescent spectra of the dialcohol compound should be blue-shifted compared to

the spectra of the small molecule analog instead of red-shifted, and especially the photoluminescent spectrum should not be red-shifted by 60 nm. The photoluminescent spectrum of the dialcohol compound suggests that the molecule has longer conjugation than just the individual organic substituent on each corner. Indeed, the authors attributed this large red-shift to electron-delocalization to the silsesquioxane core based on their theoretical studies on the *para*-subsituted vinylbiphenyl silsesquioxane compounds discussed above.

Zhen et al. published a paper describing the use of frontier orbital theory to characterize a set of cubic silsesquioxane molecules functionalized with one electron-donating (4-carbazolephenyl) and/or one electron-withdrawing (4-cyanophenyl) groups.[116] Their calculations found that when both electron-donating and electron-withdrawing groups are attached to the silsesquioxane core (see Figure **1.11**), the HOMO-LUMO bandgap is reduced to 3.70 eV, corresponding to energy of near violet light. The authors assert that the silsesquioxane core cannot be considered as simply non-conjugated moiety, that there is electron delocalization between the organic tethers and the silsesquioxane core and the silsesquioxane core acts as electron acceptor.

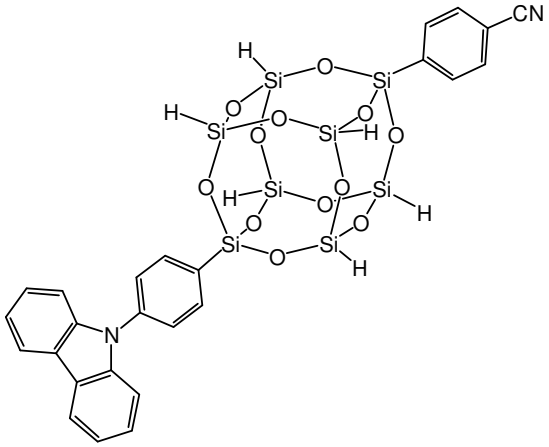

Figure 1.11. Silsesquioxane molecule with electron-donating 4-carbazolephenyl group and electron-withdrawing 4-cyanophenyl group.[116]

Our group has also published a paper on the photophysical behavior of cubic silsesquioxane molecules with functionalized stilbene tethers.[117] Compared to molecular *trans*-stilbene, the absorption spectrum of octastilbenesilsesquioxane ($Stil_8OS$) shows only slight red-shifts (~5 nm), but the photoluminescence spectrum is red-shifted by ~60 nm,

suggesting electron delocalization between the organic tethers and the silsesquioxane core as observed by Vautravers et al. discussed above.[115]

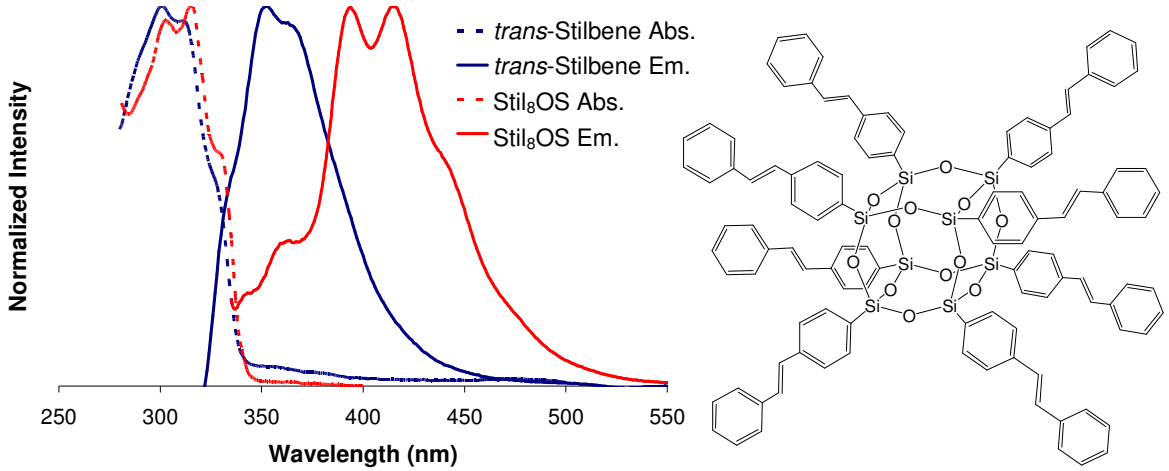

Figure 1.12. UV-Vis absorption and photoluminescence spectra of $Stil_8OS$.[117]

Collaboration with the Ugo group in Universita di Milano gave our group access to dimethylaminostilbene-functionalized siloxane and cyclosiloxane molecules that are equivalent to corner units and halves of the cubic silsesquioxane molecules, respectively.[117] Comparisons of photophysical behavior of these molecules along with the octameric silsesquioxane analog allow us to assess the extent of conjugation between the organic tethers and different degrees of silsesquioxane units.

The absorption and photoluminescence spectra of the "corner" and "half" molecules (Figure **1.13**) in CH_2Cl_2 and THF are essentially identical, while those of the "cubic" molecules are slightly red-shifted (~5 nm for absorption and ~10 nm for emission). The low photoluminescence quantum yields and structureless emission spectra of these molecules point to charge-transfer processes, and solvatochromism studies show 15-25 nm red-shifts in the absorption and emission spectra in 20% THF/80% CH_3CN.

Photoluminescence quantum yields for the three molecules are 6% for the "corner" molecule, 8% for the "half", and 3% for the "cube". Two-photon absorption (TPA, see Section **1.7**) studies of these three molecules found that the TPA cross-sections of the "corner" molecule is 12 GM/moiety, the "half" is 8 GM/moiety, and the "cube" is 26 GM/moiety. If the charge-transfer characteristics of these molecules are identical, then their TPA cross-section/moiety will also be identical. Considering that the "cube" mole-

cule has the lowest photoluminescence quantum yield and the highest TPA cross-section/moiety, it stands to reason that this molecule has the highest charge-transfer characteristics among the three molecules investigated. The influence of the silsesquioxane core as a whole on the photophysical behavior of the molecule is more than just a sum of the influence of 8 $SiO_{3/2}$ fragments.

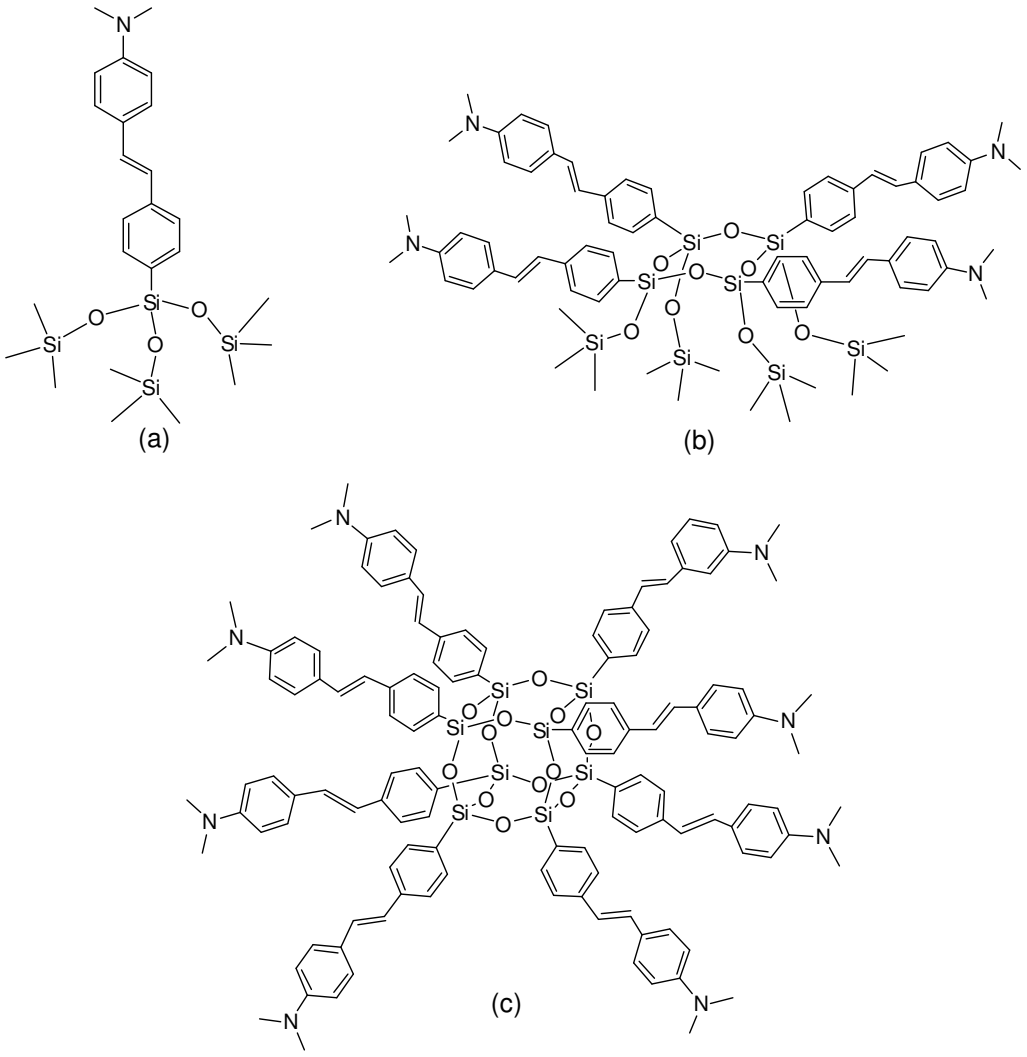

Figure 1.13. Dimethylaminostilbene-functionalized (a) "corner", (b) "half", and (c) "cubic" silsesquioxane molecules.[117]

Modeling studies on stilbene-functionalized silsesquioxanes show that the HOMO of $Stil_8OS$ is the π-state of the stilbene tethers and the LUMO is localized on the interactions between the silicon atoms and the π*-state of the stilbene tethers. The HOMO-LUMO gap of $Stil_8OS$ is 2.6 eV, and the gap between the HOMO and the molecular orbital inside

the silsesquioxane core ("core MO") is 4.2 eV. However, as discussed earlier in this section, the measured HOMO-LUMO bandgap of H_8T_8 ("silsesquioxane core") is 1.6 eV lower than the calculated value (4.4 eV measured vs. 6.0 eV calculated).[107,108] If the calculated energy gap between the HOMO and the core MO for $StilI_8OS$ is also too high by 1.6 eV, then this energy gap is now closer to 2.6 eV, approximately the same as the organic tether-based bandgap, and the core MO has the same energy as the excited state of the stilbene tethers. This offers another argument for electron delocalization involving the silsesquioxane core to the extent that there is a possibility of 3-D conjugation through the core.

Table 1.1. DFT HOMO-LUMO calculations for select silsesquioxane molecules.[117] All values in eV.

	H_8T_8	OPS	$StilSi(OSiMe_3)_3$*	$StilI_1(SiO_{3/2})_8$**	$StilI_8OS$
HOMO	-7.519	-5.529	-5.165	-5.466	-4.519
Core/LUMO	-0.541	-0.035	-0.213	-0.406	-0.293
Organic/LUMO		-0.865	-2.461	-2.767	-1.906
Core gap	6.978	5.564	4.95	5.056	4.227
Organic gap		4.664	2.70	2.695	2.613

* Stilbene-functionalized "corner" molecule. ** Silsesquioxane molecule with 7 H atoms and 1 stilbene tether.

Another paper published by our group discusses the photophysical properties of silsesquioxane-based beads-on-a chain (BoC) oligomers with divinylbenzene linkers between deca- and dodecameric silsesquioxane molecules (Figure **1.14**).[118] A model compound was also synthesized with $–Si(OEt)_3$ end-caps (Figure **1.15**) to simulate the $–Si(O-)_3$ corners of the BoC oligomers. Figure **1.16** shows similar absorption maxima for the BoC oligomers and the model compound at ~260 nm; however, the emission maximum for the BoC oligomers is red-shifted by ~60 nm from the emission maximum of the model compounds (386 nm for BoC vs 326 nm for model compounds). These results imply that the conjugation length of the BoC is increased by connecting the silsesquioxane cages with conjugated linkers and that electron delocalization in the silsesquioxane cages occurs in the excited state. Furthermore, these results corroborate that red-shifts in the emission spectra of silsesquioxane molecules with simple conjugated organic tethers are not caused by the individual $–Si(OR)_3$ moiety, but by the silsesquioxane cage as a whole.

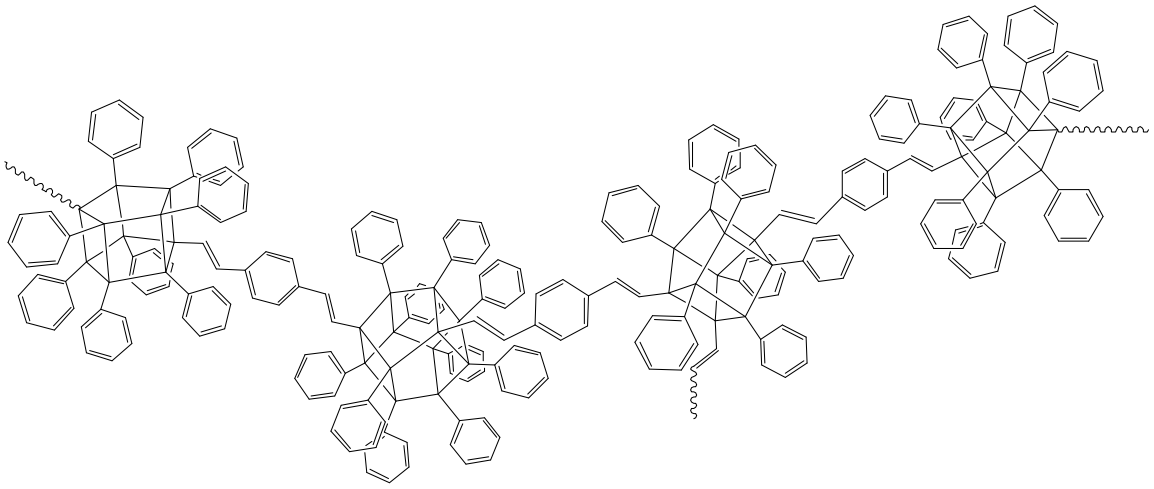

Figure **1.14**. General structure of silsesquioxane-based BoC oligomers.[118]

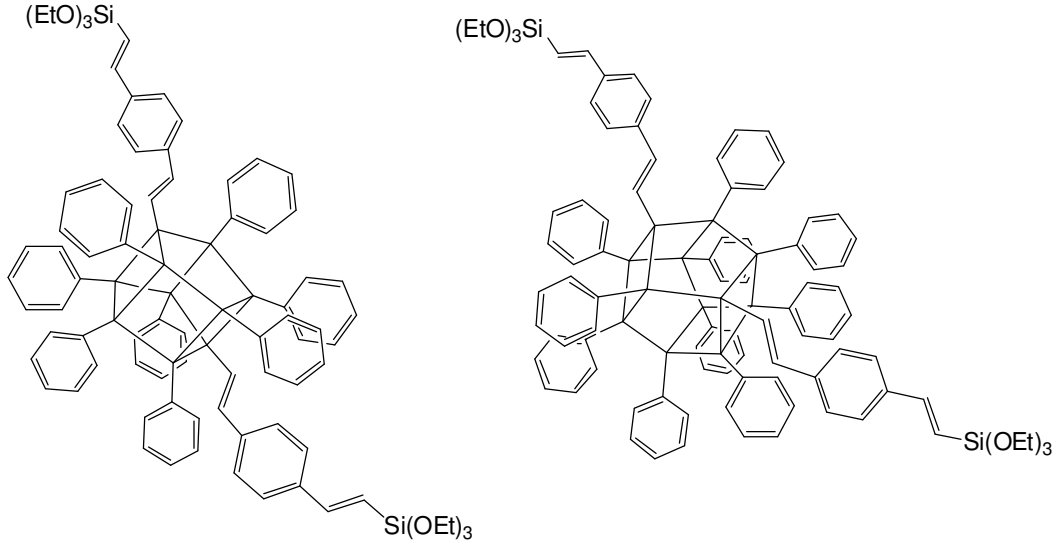

Figure **1.15**. Model compounds of silsesquioxane-based BoC oligomers with –$Si(OEt)_3$ endcaps. [118]

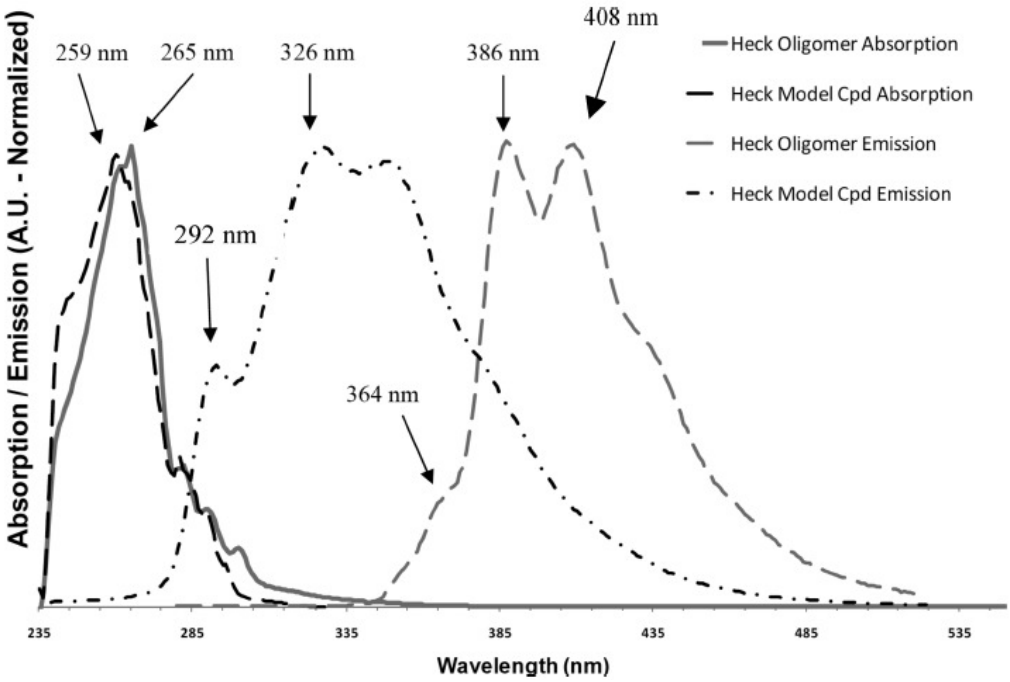

Figure **1.16**. Absorption and emission spectra of silsesquioxane BoC oligomers and model compounds (λ_{ex} = 265 nm).[118]

1.4 Olefin Metathesis Reactions

Olefin metathesis is a transition metal-catalyzed reaction which involves the mutual exchange of alkylidene groups between two substituted alkenes, comprising cleavage and formation of double bonds. Scheme **1.13** shows a simplified reaction scheme for an olefin metathesis reaction. These reactions are in principle equilibrium reactions under thermodynamic control; however, there are various means to kinetically control them. For example, reactions involving two terminal alkenes produce ethylene gas, the volatility of which displaces the reactions towards the product formation.

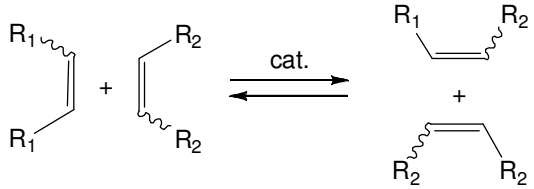

Scheme 1.13. General schematic of olefin metathesis.

Metathesis reactions have been used in the petroleum industry as early as the 1950's.[119] One of the classic examples of this application is the Phillips triolefin process in which propene is converted into ethylene and 2-butene (Scheme **1.14**).[120] Catalysts

used during the early days of metathesis reactions were poorly defined and were mainly heterogeneous systems. These "classical" catalytic systems utilized transition metals such as W, Mo, Re, and Ru, and were either oxides such as WO_3/SiO_2 or Ziegler-Natta derived systems such as WCl_6 (or $MoCl_5$) + AlX_nR_{3-n} (or SnR_4).[121-123] These catalysts were generally easily deactivated (or sometimes decomposed) by functional groups on the substrates, particularly those close or adjacent to the double bonds.[120]

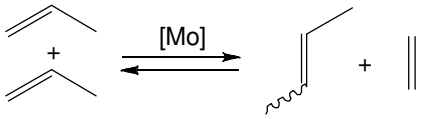

Scheme 1.14. Phillips triolefin process.

The generally accepted mechanism for metathesis reactions were developed by Chauvin in 1970, with the postulate that the reaction proceeds via a metallcyclobutane intermediate.[124] The catalytic cycle (see Figure **1.17**) starts with [2+2]cycloaddition between a C=C bond and a metallacarbene complex to form the metallacyclobutane intermediate, followed cycloreversion in the direction perpendicular to the initial olefin insertion the to form the new olefin. All individual steps in the catalytic cycle are reversible and therefore an equilibrium mixture of olefins is obtained.

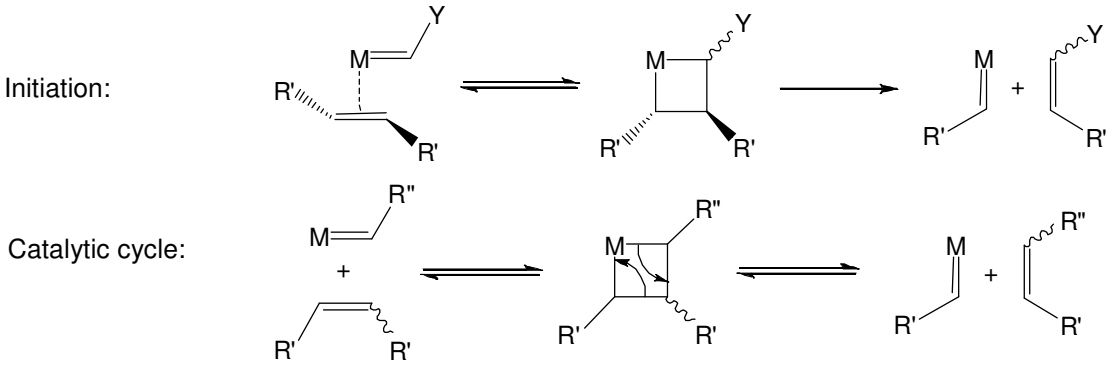

Figure 1.17. Mechanism of olefin metathesis reactions.

The introduction of stable alkylidene-transition metal complexes has been significant in the application of olefin metathesis in organic syntheses.[121,123,125] These complexes should be correctly referred to as initiators, since they must first be converted into the actual catalytically active metallacarbene complex by alkylidene exchange with a C=C bond. Schrock's molybdenum-based catalysts[126,127] and Grubbs' ruthenium-based cata-

lysts[128-132] constitute the most commonly used homogeneous catalysts in metathesis reactions.

Schrock catalysts (e.g. Figure **1.18a**) are quite sensitive towards oxygen and moisture and require rigorously dried reaction conditions. However, these catalysts have much higher reactivity, which also allows the conversion of sterically demanding double bonds.[133] Furthermore, the molybdenum complexes are hardly affected by the electronic properties of the olefinic substrates and reacts with both electron-rich (e.g. enol ethers)[134-137] and electron-poor olefins (e.g. acrylonitrile).[138]

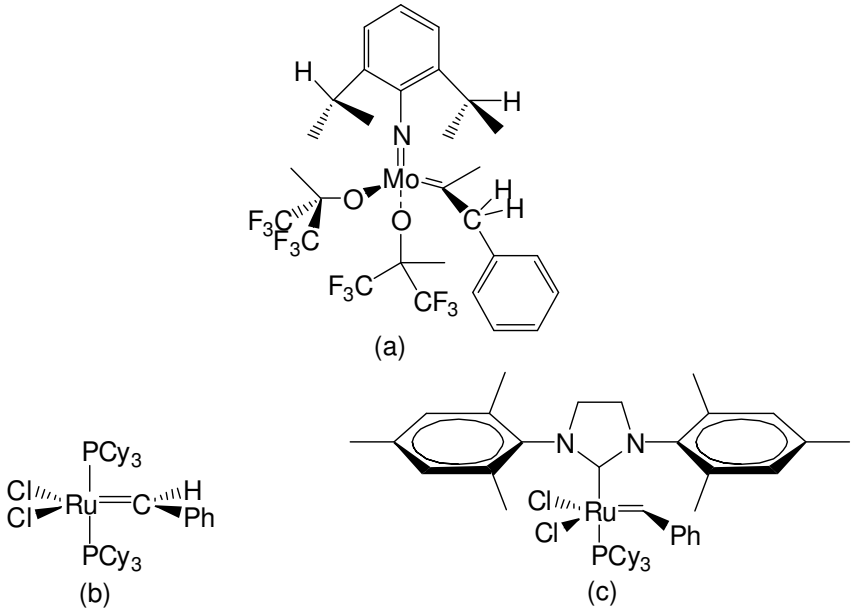

Figure 1.15. Metal-alkylidene catalysts for metathesis reactions. a. Schrock catalyst. b. Grubbs 1st generation. c. Grubbs 2nd generation.

Grubbs' ruthenium-based catalysts (Figure **1.18b** and **c**) are more practical to use because of their reasonable stability against oxygen, water, and minor impurities in the solvent. They also show higher tolerance towards a large number of polar functional groups that limit the usefulness of Schrock's molybdenum-based catalysts.[139] Grubbs 1st generation catalyst show lower reactivity compared to Schrock catalyst, but the reactivity of the 2nd generation catalyst is comparable to Schrock catalyst, especially with strained olefins. The ruthenium-based catalysts are not tolerant towards electron-rich or electron-poor olefins such as amines and nitriles, respectively.

As mentioned above, the Feher[96] and Marciniec[97] groups have demonstrated that OVS undergoes cross-metathesis reactions with simple alkenes. In Chapter **3**, we de-

scribe cross-metathesis reactions of OVS with functionalized styrenes catalyzed by Grubbs 1st generation catalyst to produce RStyrenylOS as the starting platform for the syntheses of other novel silsesquioxane molecules.

1.5 The Heck Reaction

The Pd(0)-catalyzed vinylation of aryl halides was first discovered in the early 1970's independently by Mizoroki[140] and Heck[141] and then developed by Heck into a general method in organic chemistry. The Heck reaction, also called the Mizoroki-Heck reaction, is now broadly defined as the Pd(0)-mediated coupling of an aryl or alkenyl halide or triflate with an alkene to form a new C-C bond by replacing a hydrogen atom in the alkene with a carbon substituent (see Scheme **1.15**). The Heck reaction has been studied extensively by numerous academic and industrial research groups, and as a result, it is now one of the most versatile catalytic methods for C-C bond formations.[142-144] Recent research has focused on the asymmetric variant of the Heck reaction as a method to construct stereocenters and also on the use of Heck reaction as a key step in complex organic syntheses.[145,146]

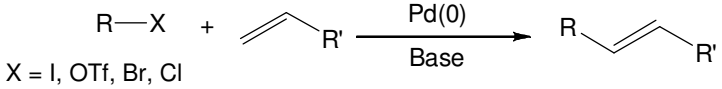

Scheme 1.15. General schematic of Heck reactions.

The generally accepted mechanism for the Heck reaction is shown in Figure **1.19**. Although key features of this mechanism have remained unchanged, recent developments in the syntheses of more efficient ligands and asymmetric catalyses have come up with new proposals on the exact nature of the catalytically active species and the influence of associated ligands.

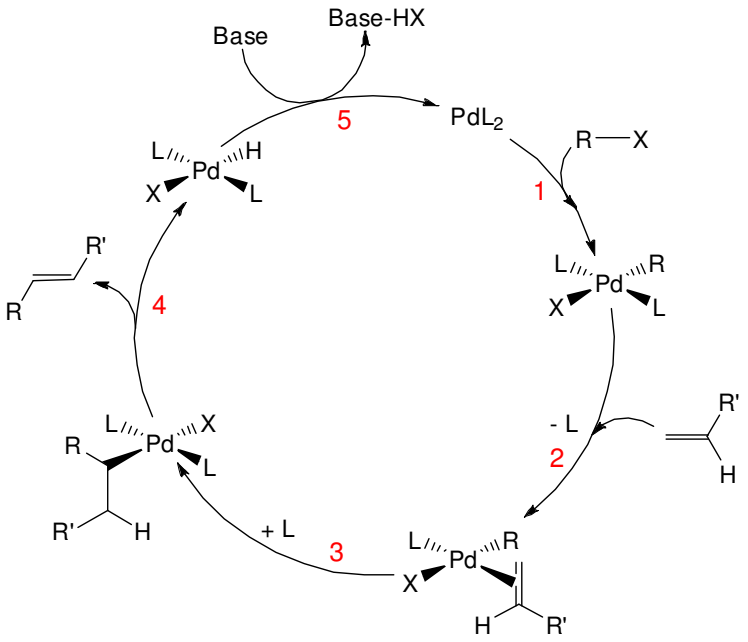

Figure 1.19. General mechanism for Heck reactions.

The active catalytic species is the coordinately unsaturated, 14-electron species $Pd(0)L_2$, regardless of the nature of the palladium precursor. The first step is the oxidative addition of the organic halide or triflate to the Pd(0) complex (step 1) to form a σ-aryl- or σ-alkenylpalladium(II) complex. Coordination of an alkene (step 2) and subsequent insertion into the Pd-C bond by *syn* addition (step 3) provides the σ-alkylpalladium intermediate. This intermediate readily undergoes β-hydride elimination to generate the alkene Heck product and the catalytically inactive $HPdXL_2$ (step 4). A base is required to reduce the $HPdXL_2$ to regenerate the active Pd(0) complex to complete the catalytic cycle (step 5).

Previous work done in our group[74,77,79,117] demonstrated the use of Heck coupling to synthesize a variety of compounds from Br_xOPS and *p*-I_8OPS with various olefins such as R-styrenes and methacrylates. Our group has also extended this work to the coupling of T_{10} and T_{12} molecules with mixed aryl bromide/phenyl and vinyl/phenyl functionalities to form beads-on-a-chain oligomers.[118] The use of $Pd_2(dba)_3$ and $Pd(P\text{-}tBu_3)_2$ as the pre-catalyst system and dicyclohexylmethylamine (NCy_2Me) as base at room temperature[147] allows for complete conversion without the need for strong acids or bases which can destroy the silsesquioxane core.

In this dissertation, the syntheses of conjugated silsesquioxane molecules via Heck coupling have been expanded to include several other bromo-functionalized silsesquioxane molecules. In Chapter **3**, the cross-metathesis product of OVS with 4-bromostyrene, BrStyrenylOS, is used as starting material for the synthesis of a series of luminescent molecules, R'VinylStilbeneOS. In Chapter **4**, crystalline polybrominated OPS (*o*-Br_8OPS, 2,5-Br_{16}OPS, and Br_{24}OPS) are coupled with functionalized styrenes to produce 8-, 16-, and 24-functionalized OPS molecules with interesting photophysical properties.

1.6 Two-photon Absorption (TPA)

The phenomenon of simultaneous absorption of two photons by an atom or a molecule leading to an electronic transition to an excited state was first proposed by Maria Göppert-Mayer in 1931.[148] In 1961, soon after the invention of the first laser device, Kaiser and Garrett published the first paper on the two photon-induced fluorescence of europium-doped Ca_2F crystal.[149] The availability of sub-picosecond pulsed lasers (particularly the Ti:sapphire laser) in the 1990's has led to an explosion in the investigation of two-photon spectroscopy.[150] TPA increases with the square of the light intensity since it involves the simultaneous interaction of two photons; therefore, the investigation of TPA requires intense laser beams, particularly focused pulsed lasers, which generate a very high instantaneous photon density. TPA is an alternate way to access an excited state with photons of half the energy (or twice the wavelength) of the corresponding one-photon transition.

The theoretical description of TPA involves the concept of an intermediate state between the ground and excited states.[151,152] The electronic transition of a molecule from the ground to the excited states induced by simultaneous absorption of two photons can be visualized as a two-step event. In the first step, the molecule absorbs the energy of one photon and is excited from its ground state to the intermediate state, which only exists while the molecule experiences the field of the first photon (~ 5 fs).[153] In the second step, the molecule absorbs the energy of another photon and completes the transition from the intermediate state to the excited state. Since the lifetime of the intermediate state is infinitely short compared to the final excited state, the two-step process of TPA essentially a simultaneous process.

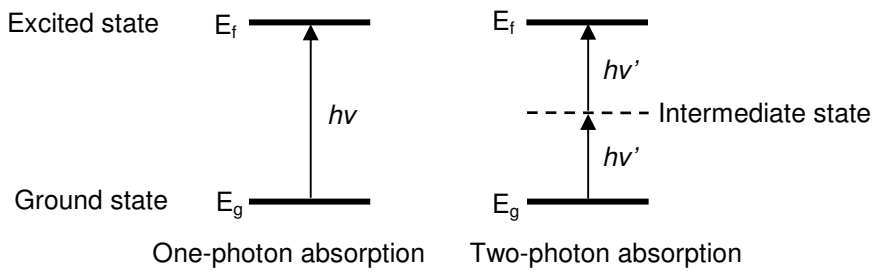

Figure 1.20. Schematic diagrams of one- and two photon-induced electron transition processes.

The sensitivity of a molecule towards TPA is quantified by its TPA cross-section, δ, which is usually reported in Göppert-Mayer (GM) units (1 GM ≡ 10^{-50} cm^4 s $photon^{-1}$) in honor of its discoverer. The TPA cross-section is an intrinsic property as it is controlled by the molecular structure. There is a strong relationship between intramolecular charge transfer processes and two-photon absorptivity, as the absorption of photons induces polarization of the molecule. Therefore, molecules with permanent ground-state dipole moments or transitional dipole moments connected with either the ground or excited state are of great interest in two-photon spectroscopy.

Design strategies for organic molecules for use as highly active TPA chromophores are driven by concerns of intramolecular charge-transfer processes. There are three essential components that are a definite requirement: a strong π-electron donor (D), a polarizable π-bridge (π), and a strong π-electron acceptor (A). Furthermore, there are three molecular structure motifs for TPA chromophores.[153,154] Type I chromophores are symmetrical and consists of two terminal donor or acceptor groups linked by a π-bridge, which in turn can have acceptor or donor characteristics, respectively (D-π-D and A-π-A). Type II chromophores are asymmetrical and composed of electron-rich π-bridge with a donor group on one side and an acceptor group on the other (D-π-A). Type III chromophores consists of multibranched (or multiarmed) organic molecules with two or more Type II chromophores joined together with extended conjugation. The flow of intramolecular charge transfer in Type III chromophores can be from the terminals to the center of the molecule or vice versa.

The donor and acceptor groups in TPA chromophores can function as terminal groups or as part of the π-bridge. The most widely used terminal donor groups are dialkyl and

diaryl amino groups, due to their ease of availability as well as their oxidative stability and electron-donating capability. Commonly used electron-withdrawing groups include nitro,[155-159] trifluoromethyl,[158,159] cyano,[158-160] sulfonyl,[161-163] aldehyde,[164,165] phosphonates,[155] and many electron-deficient heterocycles such as pyridyl,[164,165] quinoline,[166] and triazole.[167]

An efficient π-conjugated bridge is required to aid the electron flow in an intramolecular charge-transfer process. Phenylene-vinylene, 2,7-fluorenyl, and phenylene-ethynyl are the most commonly used organic π-bridges.[153] Attaching electron-withdrawing groups to the center of π-bridge in D-π-D-type chromophores leads to an increase in the TPA cross-section.[152] Systems with electron-rich centers tend to be less stable than electron-deficient ones in normal aerobic environments and therefore have not been widely investigated.[152] Increasing the conjugation length of the π-bridge results in extended charge separation and higher TPA cross-section.[160,168] Electron delocalization is optimized when a π-system assumes a planar geometry, with maximum π-orbital overlap, and therefore TPA cross-section values are dependent on the conformation of the π-bridge.[152,153]

The advantages of two-photon spectroscopy over one-photon spectroscopy are based on two characteristics of two-photon processes: (1) the coherent light used in two-photon spectroscopy has much longer wavelength, which causes less photochemical damage in biological samples, and (2) the absorption increases with the square of the light intensity at the focal area and falls off rapidly away from the focus, which provides much sharper resolution and prevents unwanted emission or photochemical conversion outside the focal area. Some examples of applications using two-photon spectroscopy include biological probes,[169-171] drug delivery,[172,173] frequency-upconversion imaging and microscopy,[174,175] frequency-upconversion lasing,[1756] optical microfabrication,[177] optical data storage,[178-180] and optical power limiting.[181-182]

References Cited:

1. Voronkov, M.G.; Lavrent'yev, V.I. "Polyhedral Oligosilsesquioxanes and Their Homo Derivative." *Top. Curr. Chem*. **1982**, *102*, 199-236.

2. Calzaferri, G. "Octasilsesquioxanes." In *Tailor-Made Silicon-Oxygen Compounds, from Molecules to Materials*; Corriu, R. and Jutzi, P., Eds.; Friedr. Vieweg & Sohn mbH: Braunschweig/Wiesbaden, Germany, 1996; pp. 149-169.

3. Lichtenhan, J. "Silsesquioxane-based Polymers." In *Polymeric Materials Encyc.*; Salmone, J.C., Ed.; CRC Press: N.Y., 1996; Vol. 10; pp. 7768-7777.

4. Provatas, A.; Matisons, J.G. "Synthesis and Applications of Silsesquioxanes." *Trends Polym. Sci.* **1997**, *5*, 327-333.

5. Li, G.; Wang, L.; Ni, H.; Pittman Jr., C.U. "Polyhedral Oligomeric Silsesquioxane (POSS) Polymers and Copolymers: A Review." *J. Inorg. Organomet. Chem*. **2001**, *11*, 123-151.

6. Duchateau, R. "Incompletely Condensed Silsesquioxanes: Versatile Tools in Developing Silica-Supported Olefin Polymerization Catalyst." *Chem. Rev.* **2002**, *102*, 3525-3542.

7. Abe, Y.; Gunji, T. "Oligo- and Polysiloxanes." *Prog. Polym. Sci*. **2004**, *29*, 149-182.

8. Phillips, S.H.; Haddad, T.S.; Tomczak, S.J. "Developments in Nanoscience: Polyhedral Oligomeric Silsesquioxane (POSS)-Polymers." *Curr. Opin. Solid State Mater. Sci.* **2004**, *8*, 21-29.

9. Laine, R.M. "Nano-Building Blocks Based on the $[OSiO_{1.5}]_8$ Silsesquioxanes." *J. Mater. Chem*. **2005**, *15*, 3725-3744.

10. Lickiss, P.D.; Rataboul, F. "Fully Condensed Polyhedral Oligosilsesquioxanes (POSS): From Synthesis to Application." *Adv. Organomet. Chem*. **2008**, *57*, 1-116.

11. Chan, K.L.; Sonar, P.; Sellinger, A. "Cubic Silsesquioxanes for Use in Solution Processable Organic Light Emitting Diodes (OLED)." *J. Mater. Chem*. **2009**, *19*, 9103-9120.

12. Cordes, D.B.; Lickiss, P.D.; Rataboul, F. "Recent Developments in the Chemistry of Cubic Polyhedral Oligosilsesquioxanes." *Chem. Rev*. **2010**, *10*, 2081-2173.

13. Laine, R.M.; Roll, M.F. "Polyhedral Phenylsilsesquioxanes." *Macromol*. **2011**, *44*, 1073-1109.

14. McCallister, W. *Materials Science and Engineering: An Introduction*, 8th ed.; Wiley: New York, 2010, pp. 630.

15. Mathews, F.L.; Rawlings, R.D. *Composite Materials: Engineering and Science*, CRC Press LLC: Boca Raton, FL, 1999, pp. 12-14.

16. Judeinstein, P.; Sanchez, C. "Hybrid Organic-Inorganic Materials: A Land of Multidisciplinarity." *J. Mater. Chem*. **1996**, *6*, 511-525.

17. Morin, J.-F.; Shirai, Y.; Tour, J. M. "En Route to a Motorized Nanocar." *Org. Lett.* **2006**, *8* 1713-1716.

18. Sasaki, T.; Osgood, A.J.; Alemany, L.B.; Kelly, K.F.; Tour, J.M. "Synthesis of a Nanocar with an Angled Chassis. Toward Circling Movement." *Org. Lett*. **2008,** *10*, 229-232.

19. Zhang, Z.L.; Horsch, M.A.; Lamm, M.H.; Glotzer, S.C. "Tethered Nano Building Blocks: Toward a Conceptual Framework for Nanoparticle Self-Assembly." *Nano Lett.* **2003**, *3*, 1341-1346.

20. Lanznaster, M.; Heeg, M.J.; Yee, G.T.; McGarvey, B.R.; Verani, C.N. "Design of Modular Scaffolds Based on Unusual Geometries for Magnetic Modulation of Spin-Diverse Complexes with Selective Redox Response." *Inorg. Chem.* **2007**, *46*, 72-78.

21. Large-Toumi, B.; Salvia, M.; Vincent, L. "Fiber/Matrix Interface Effect on Monotonic and Fatigue Behavior of Unidirectional Carbon/Epoxy Composites." In *Fiber, Matrix, and Interface Properties*; Spragg, C., Drzal, T., Eds.; ASTM STP 1290; ASTM: Philadelphia, PA, 1996; pp. 182-200.

22. Mäder, E.; Jacobasch, H.; Grundki, K.; Gietzelt, T. "Influence of an Optimized Interphas on the Properties of Polypropylene/Glass Fibre Composites." *Composites Part A* **1996**, *27A*, 907-912.

23. Novak, B.M. "Hybrid Nanocomposite Materials – Between Inorganic Glasses and Organic Polymers." *Adv. Mater.* **1993**, *5*, 422-433.

24. Loy, D.A.; Shea, K.J. "Bridged Polysilsesquioxanes. Highly Porous Organic-Inorganic Materials." *Chem. Rev.* **1995**, *95*, 1431-1442.

25. Ajayan, P.M. "Nanotubes from Carbon." *Chem. Rev.* **1999**, *99*, 1787-1799.

26. Zhang, C.; Babonneau, F.; Bonhomme, C.; Laine, R.M.; Soles, C.L.; Hristov, H.A.; Yee, A.F. "Highly Porous Polyhedral Silsesquioxane Polymers. Synthesis and Characterization." *J. Am. Chem. Soc.* **1998**, *120*, 8380-8391.

27. Sellinger, A.; Laine, R.M. "Silsesquioxanes as Synthetic Platforms. 3. Photocurable, Liquid Epoxides as Inorganic/Organic Hybrid Precursors." *Chem. Mater.* **1996**, *8*, 1592-1593.

28. Choi, J.; Kim, S.G.; Laine, R.M. "Organic/Inorganic Hybrid Epoxy Nanocomposites from Aminophenylsilsesquioxanes." *Macromol.* **2004**, *37*, 99-109.

29. Choi, J.; Yee, A.F.; Laine, R.M. "Organic/Inorganic Hybrid Composites form Cubic Silsesquioxanes. Epoxy Resins of Octa(dimethylsiloxyethylcyclohexyl-epoxide) silsesquioxane." *Macromol.* **2003**, *36*, 5666-5682.

30. Takamura, N.; Viculis, L.; Zhang, C.; Laine, R.M. "Completely Discontinuous Organic/Inorganic Hybrid Nanocomposites by Self-Curing of Nanobuilding Blocks Constructed from Reactions of $[HMe_2SiOSiO_{1.5}]_8$ with Vinylcyclohexene." *Polym. Int.* **2007**, *56*, 1378-1391.

31. Asuncion, M.Z.; Laine, R.M. "Silsesquioxane Barrier Materials." *Macromol.* **2007**, *40*, 555-562.

32. Feher, F.J.; Blanski, R.L. "Olefin Polymerization by Vanadium-Containing Silsesquioxanes: Synthesis of a Dialkyl-oxo-vanadium (V) Complex that Initiates Ethylene Polymerization." *J. Am. Chem. Soc.* **1992**, *114*, 5886-5887.

33. Feher, F.J.; Budzichowski, T.A. "Silasesquioxanes as Ligands in Inorganic and Organometallic Chemistry." *Polyhedron* **1995**, *14*, 3239-3253.

34. Ropartz, L.; Morris, R.E.; Schwarz, G.P.; Foster, D.F.; Cole-Hamilton, D.J. "Dendrimer-Bound Tertiary Phosphines for Alkene Hydroformylation." *Inorg. Chem. Commun.* **2000**, *3*, 714-717.

35. Riollet, V.; Quadrelli, E.A.; Copéret, C.; Basset, J.-M.; Andersen, R.A.; Köhler, K.; Böttcher, R.-M.; Herdtweck, E. "Grafting of [Mn(CH_2*t*Bu)$_2$(tmeda)] on Silica and Comparison with Its Reaction with a Silsesquioxane." *Chem.-Eur. J.* **2005**, *11*, 7358-7365.

36. Feher, F.J.; Newman, D.A.; Walzer, J.F. "Silsesquioxanes as Models for Silica Surfaces." *J. Am. Chem. Soc*. **1989**, *111*, 1741-1748.

37. Feher, F.J.; Budzichowski, T.A.; Blanski, R.L.; Weller, K.J.; Ziller, J.W. "Facile Syntheses of New Incompletely Condensed Polyhedral Oligosilsesquioxanes: [(*c*-$C_5H_9)_7Si_7O_9(OH)_3$], [(*c*-$C_7H_{13})_7Si_7O_9(OH)_3$], and [(*c*-$C_7H_{13})_6Si_6O_7(OH)_4$]." *Organomet*. **1991**, *10*, 2526-2528.

38. Contreras-Torres, F.F.; Basiuk, V.A. "Imidazo[1,2-*a*]pyrazine-3,6-diones Derived from α-Amino Acids: A Theoretical Mechanistic Study of Their Formation via Pyrolysis and Silica-Catalyzed Process." *J. Phys. Chem. A* **2006**, *110*, 7431-7440.

39. Maschmeyer, T.; Klunduk, M.C.; Martin, C.M.; Shephard, D.S.; Thomas, J.M.; Johnson, B.F.G. "Modeling the Active Sites of Heterogeneous Titanium-Centred Epoxidation Catalysts with Soluble Silsesquioxane Analogues." *Chem. Comm.* **1997**, 1847-1848.

40. Duchateau, R.; Abbenhuis, H.C.L.; van Santen, R.A.; Meetsma, A.; Thiele, S.K.-H.; van Tol, M.F.H. "Half-Sandwich Titanium Complexes Stabilized by a Novel Silsesquioxane Ligand: Soluble Model Systems for Silica-Grafted Olefin Polymerization Catalysts." *Organomet*. **1998**, *17*, 5222-5224.

41. Solans-Monfort, X.; Filhol, J.-S.; Copéret, C.; Eisenstein, O. "Structure, Spectroscopic and Electronic Properties of a Well Defined Silica Supported Olefin Metathesis Catalyst, [(≡SiO)Re(≡CR)(=CHR)(CH_2R)], through DFT Periodic Calculations: Silica is Just a Large Siloxy Ligand." *New J. Chem*. **2006**, *30*, 842-850.

42. Leu, C. M.; Reddy, M.; Wei, K.-H.; Shu, C.-F. "Synthesis and Dielectric Properties of Polyimide-Chain-End Tethered Polyhedral Oligomeric Silsesquioxane Nanocomposites." *Chem. Mater.* **2003**, *15,* 2261-2265.

43. Leu, C.-M.; Chang, Y.-T.; Wei, K.-H. "Synthesis and Dielectric Properties of Polyimide-Tethered Polyhedral Oligomeric Silsesquioxane (POSS) Nanocomposites via POSS-Diamine." *Macromol.* **2003**, *36*, 9122-9127.

44. Liu, Y.-L.; Lee, H.-C. "Preparation and Properties of Polyhedral Oligosilsesquioxane Tethered Aromatic Polyamide Nanocomposites through Michael Addition between Maleimide-Containing Polyamides and an Amino-Functionalized Polyhedral Oligosilsesquioxane." *J. Polym. Sci., Part A: Polym. Chem*., **2006**, *44*, 4632-4643.

45. Chojnowski, J.; Fortuniak, W.; Rościszewski, P.; Werel, W.; Lukasiak, J.; Kamysz, W.; Halasa, R. "Polysilsesquioxanes and Oligosilsesquioxanes Substituted by Alkylammonium Salts as Antibacterial Biocides." *J. Inorg. Organomet. Polym. Mater*. **2006**, *16*, 219-230.

46. Majumdar, P.; Lee, E.; Gubbins, N.; Stafslien, S.J.; Daniels, J.; Thorson, C.J.; Chisolm, B.J. "Synthesis and Antimicrobial Activity of Quaternary Ammonium-Functionalized POSS (Q-POSS) and Polysiloxane Coatings Containing Q-POSS." *Polymer* **2009**, *50*, 1124-1133.

47. Gromilov, S.A.; Basova, T.V.; Emel'yanov, D.Y.; Kuzmin, A.V.; Prokhorova, S.A. "Layer Arrangement in the Structure of Octakis-(trimethylsiloxy)octasilsesquioxane and Dodecakis-(trimethylsiloxy)octasilsesquioxane." *J. Struct. Chem. (Engl. Trans.)* **2004**, *45*, 471-475.

48. Gromilov, S.A.; Emel'yanov, D.Y.; Kuzmin, A.V.; Prokhorova, S.A. "Structural Organization of Layers in Octakis-(trimethylsiloxy)octasilsesquioxane." *J. Struct. Chem. (Engl. Trans.)* **2003**, *44*, 704-706

49. Baney, R.H.; Itoh, M.; Sakakibara, A.; Suzuki, T. "Silsesquioxanes*." Chem. Rev.* **1995**, *95*, 1409-1430.

50. Harrison, P.G. "Silicate Cages: Precursors to New Materials." *J. Organomet. Chem.* **1997**, *542*, 141-183.

51. Sprung, M.M.; Guenther, F.O. "The Partial Hydrolysis of Ethytriethoxysilane." *J. Am. Chem. Soc.* **1955**, *77*, 3996-4002.

52. Sprung, M.M.; Guenther, F.O. "The Partial Hydrolysis of Methyltri-*n*-propoxysilane, Methyltriisopropoxysilane, and Methyltri-*n*-butoxysilane." *J. Am. Chem. Soc*. **1955**, *77*, 6045-6047.

53. Brown Jr., J.F. "The Polycondensation of Phenylsilanetriol." *J. Am. Chem. Soc*. **1965**, *87*, 4317-4324.

54. Andrianov, K.A.; Petrovnina, N.M.; Vasil'eva, T.V.; Skhlover, V.E.; D'yanchenko, B.I. "Products of the Hydrolytic Polycondensation of Methyl- and Vinyltrichlorosilane." *Zh. Obshch. Khim*. **1978**, *48*, 2692-2695.

55. Wallace, W.E.; Guttman, C.M.; Antonucci, J. M. "Polymeric Silsesquioxanes: Degree-of-Intramolecular-Condensation Measured by Mass Spectrometry." *Polymer*, **2000**, *41*, 2219-2226.

56. Pakjamsai, C.; Kawakami, Y. "Tendency of Loop Formation of Oligosilsesquioxanes Obtained from (4-Substituted Phenyl)trimethoxysilane Catalyzed by Benzyltrimethylammonium Hydroxide in Benzene." *Polymer Journal* **2004**, *36*, 455-464.

57. Eaton, P.E. "Cubane: Starting Materials for the Chemistry of the 1990s and the New Century." *Angew. Chem. Int. Ed.* **1992**, *31*, 1421-1436.

58. Detken, A.; Zimmermann, H.; Haeberlen, U.; Poupko, R.; Luz, Z. "Molecular Reorientation and Self-Diffusion in Solid Cubane by Deuterium and Proton NMR." *J. Phys. Chem*. **1996**, *100*, 9598-9604.

59. Yildirim, T.; Gehring, P.M.; Neumann, D.A.; Eaton, P.E.; Emrick, T. "Solid Cubane: A Brief Review." *Carbon* **1998**, *36*, 809-815.

60. Olsson, K. "Improved Preparation of Octakis(alkylsilsesquioxanes)." *Ark. Kemi* **1958**, *13*, 367-378.

61. Olsson, K.; Gröwall, C. "Octa(arylsilsesquioxanes), $(ArSi)_8O_{12}$ I. Phenyl, 4-Toyl, and 1-Naphthyl Compounds." *Ark. Kemi* **1961**, *17*, 529-540.

62. Brown Jr., J.F.; Vogt, L.H.; Prescott, P.I. "Preparation and Characterization of the Lower Equilibrated Phenylsilsesquioxanes." *J. Am. Chem. Soc*. **1964**, *86*, 1120-1125.

63. Bassindale, A.R.; Liu, Z.; MacKinnon, I.A.; Taylor, P.G.; Yang, Y.; Light, M.E.; Horton, P.N.; Hursthouse, M.B. "A Higher Yielding Route for T_8 Silsesquioxane Cages and X-Ray Crystal Structures of Some Novel Spherosilicates." *Dalton Trans*. **2003**, 2945-2949.

64. Dare, E.O.; Liu, L.-K.; Peng, J. "Modified Procedure for Improved Synthesis of Some Octameric Silsesquioxanes *via* Hydrolytic Polycondensation in the Presence of Amberlite Ion-Exchange Resins." *Dalton Trans*. **2006**, 3668-3671.

65. Kim, S.-G.; Sulaiman, S.; Fargier, D.; Laine, R.M. "Octaphenyloctasilsesquioxane and Polyphenylsilsesquioxane for Nanocomposite." In *Materials Syntheses. A Practical Guide*; Schubert, U., Hüsing, N., Laine, R., Eds.; Springer-Verlag: Wien, 2008; pp. 179-191.

66. Fina, A.; Tabuani, D.; Carniato, F.; Frache, A.; Boccaleri, E.; Camino, G. "Polyhedral Oligomeric Silsesquioxanes (POSS) Thermal Degradation." *Thermochim. Acta* **2006**, *440*, 36-42.

67. Tamaki, R.; Tanaka, Y.; Asuncion, M.Z.; Choi, J.; Laine, R.M. "Octa(aminophenyl)silsesquioxane as a Nanoconstruction Site." *J. Am. Chem. Soc.* **2001**, *123*, 12416-12417.

68. Takahashi, K.; Sulaiman, S.; Katzenstein, J.M.; Snoblen, S.; Laine, R.M. "New Aminophenylsilsesquioxanes – Synthesis, Properties, and Epoxy Nanocomposites." *Aust. J. Chem*. **2006**, *59*, 564-570.

69. Choi, J.; Kim, S.G.; Laine, R.M. "Organic/Inorganic Hybrid Epoxy Nanocomposites from Aminophenylsilsesquioxanes." *Macromol*. **2004**, *37*, 99-109.

70. Choi, J.; Tamaki, R.; Kim, S.G.; Laine, R.M. "Organic/Inorganic Imide Nanocomposites from Aminophenylsilsesquioxanes." *Chem. Mater*. **2003**, *15*, 3365-3375.

71. Nagendiran, S.; Alagar, M.; Hamerton, I. "Octasilsesquioxane-Reinforced DGEBA and TGDDM Epoxy Nanocomposites: Characterization of Thermal, Dielectric, and Morphological Properties." *Acta Materialia* **2010**, *58*, 3345-3356.

72. Zhang, J.; Xu, R.-W.; Yu, D.-S. "A Novel and Facile Method for the Synthesis of Octa(aminophenyl)silsesquioxane and Its Nanocomposites with Bismaleimide-Diamine Resin." *J. Appl. Poly. Sci*. **2007**, *103*, 1004-1010.

73. Asuncion, M.Z.; Laine, R.M. "Silsesquioxane Barrier Materials." *Macromol*. **2007**, *40*, 555-562.

74. Brick, C.M.; Tamaki, R.; Kim, S.G.; Asuncion, M.Z.; Roll, M; Nemoto, T.; Ouchi, Y.; Chujo, Y.; Laine, R.M. "Spherical, Polyfunctional Molecules Using Poly(bromophenylsilsesquioxane)s as Nanoconstruction Sites." *Macromol*. **2005**, *38*, 4655-4660.

75. Asuncion, M.Z.; Roll, M.F.; Laine, R.M. "Octaalkynylsilsesquioxanes, Nano Sea Urchin Molecular Building Blocks for 3-D-Nanostructures." *Macromol.* **2008**, *41,* 8047–8052.

76. Roll, M.F.; Mathur, P.; Takahashi,K.; Kampf, J.W.; Laine, R.M. "$[PhSiO_{1.5}]_8$ Promotes Self-Bromination to Produce $[o\text{-}BrPhSiO_{1.5}]_8$. Further Bromination Gives Crystalline $[2,5\text{-}Br_2PhSiO_{1.5}]_8$ with a Density of 2.38 g/cc and Calculated Refractive Index of 1.7 (RI of Sapphire is 1.76) or the Tetraisocosa Bromo Compound $[Br_3PhSiO_{1.5}]_8$." *J. Mater. Chem.* **2011**, *21*, 11167-11176.

77. Roll, M.F. "Symmetric Functionalization of Polyhedral Phenylsilsesquioxanes as a Route to Nano-Building Blocks." Ph.D. Dissertation, University of Michigan, Ann Arbor, MI, 2010.

78. Ege, S. *Organic Chemistry: Structure and Reactivity*, 4th ed.; Houghton Mifflin: Boston, 1999, pp. 769-770, 776-778.

79. Roll, M.F.; Asuncion, M.Z.; Kampf, J.; Laine, R.M. "*para*-Octaiodophenylsilsesquioxane, $[p\text{-}IC_6H_4SiO_{1.5}]_8$, a Nearly Perfect Nano-Building Block." *ACS Nano* **2008**, *2*, 320-326.

80. Kim, Y.; Koh, K.; Roll, M.F.; Laine, R.M.; Matzger, A.J. "Porous Networks Assembled from Octaphenylsilsesquioxane Building Blocks" *Macromol.* **2010**, *43*, 6995-7000.

81. Voronkov, M.G.; Martynova, T.N.; Mirskov, R.G.; Belyi, V.I. "Octavinylsilsesquioxane." *Zh. Obshch. Khim.* **1979**, *49*, 1522-1525.

82. Kovrigin, V.M.; Lavrent'ev, V.I. "Chromatographic-Mass-Spectroscopic Study of the Mechanism of Fomation of Pervinyloctasilsesquioxane in Polycondensation of Vinyltrichlorosilane in Butanol." *Zh. Obshch. Khim*. **1989**, *59*, 377-83.

83. Bonhomme, C.; Tolédano, P.; Maquet, J.; Livage, J.; Bonhomme-Coury, L. "Studies of Octameric Vinylsilsesquioxane by Carbon-13 and Silicon-29 Cross Polarization Magic Angle Spinning and Inversion Recovery Cross Polarization Nuclear Magnetic Resonance Spectroscopy." *J. Chem. Soc. Dalton Trans.* **1997**, 1617-1626

84. Harrison, P.G.; Hall, C. "Preparation and Characterization of Octasilsesquioxane Cage Monomers." *Main Group Met. Chem*. **1997**, *20*, 515-529.

85. Gao, J.-G.; Wang, S.-C.; Zhang, X.-J.; Run, M.-T. "Synthesis of Cage Octa(vinyl)silsesquioxane." *Youjigui Cailiao* **2005**, *19*, 5-7.

86. Koenig, H.J.; Marsmann, H.C.; Letzel, M.C. "Thioether Functionalized Octasilsesquioxanes." In *Organosilicon Chemistry V: From Molecules to Materials*; Auner, N. Weis, J., Eds.; Wiley-VCH: Weinheim, 2003; pp. 425-428.

87. Gao, Y.; Eguchi, A.; Kakehi, K.; Lee, Y.C. "Efficient Preparation of Glycoclusters from Silsesquioxanes." *Org. Lett*. **2004**, *6*, 3457-3460.

88. Lücke, S.; Stoppek-Langner, K.; Kuchinke, J.; Krebs, B. "Octakis-(dimethylphosphanoethyl)-octasilsesquioxane – Synthesis, Characterization, and Reactivity." *J. Organomet. Chem*. **1999**, *584*, 11-15.

89. Ropartz, L.; Morris, R.E.; Schwarz, G.P.; Foster, D.F.; Cole-Hamilton, D.J. "Dendrimer-Bound Tertiary Phosphines for Alkene Hydroformylation." *Inorg. Chem. Commun*. **2000**, *3*, 714-717.

90. Jaffrés, P.-A.; Morris, R.E. "Synthesis of Highly Functionalized Dendrimers Based on Polyhedralsilsesquioxane Cores." *J. Chem. Soc. Dalton Trans*. **1998**, 2767-2770.

91. Ropartz, L.; Foster, D.F.; Morris, R.E.; Slawin, A.M.Z.; Cole-Hamilton, D.J. "Hydrocarbonylation Reactions using Alkylphosphine-Containing Dendrimers Based on a Polyhedral Oligosilsesquioxane Core." *J. Chem. Soc. Dalton Trans*. **2002**, 1997-2008.

92. Zhang, C.; Laine, R.M. "Silsesquioxaes as Synthetic Platforms. II. Epoxy-Functionalized Inorganic-Organic Hybrid Species." *J. Organomet. Chem*. **1996**, *521*, 199-201.

93. Sellinger, A.; Tamaki, R.; Laine, R.M.; Ueno, K.; Tanabe, H.; Williams, E.; Jabbour, G.E. "Heck Coupling of Haloaromatics with Octavinylsilsesquioxane: Solution Processable Nanocomposites for Applications in Electroluminescent Devices." *Chem. Commun*. **2005**, 3700-3702.

94. Lo, M.Y.; Ueno, K.; Tanabe, H.; Sellinger, A. "Silsesquioxane-Based Nanocomposite Dendrimers with Photoluminescent and Charge Transport Properties." *Chem. Rec.* **2006**, *6*, 157-168.

95. Lo, M.Y.; Zhen, C.; Lauters, M.; Jabbour, G.E.; Sellinger, A. "Organic-Inorganic Hybrids Based on Pyrene-Functionalized Octavinylsilsesquioxane Cores for Application in OLEDs." *J. Am. Chem. Soc.* **2007**, *129*, 5808-5809.

96. Feher, F.J.; Soulivong, D.; Eklund, A.G.; Wyndham, K.D. "Cross-Metathesis of Alkenes with Vinyl-Substituted Silsesquioxanes and Spherosilicates: A New Method for Synthesizing Highly-Functional Si/O Frameworks." *Chem. Commun.* **1997**, 1185-1186.

97. Itami, Y.; Marciniec, B.; Kubicki, M. "Functionalization of Octavinylsilsesquioxane by Ruthenium-Catalyzed Silylative Coupling versus Cross-Metathesis." *Chem.-Eur. J.* **2004**, *10*, 1239-1248.

98. Calzaferri, G.; Hoffman, R. "The Symmetrical Octasilsesquioxanes $X_8Si_8O_{12}$: Electronic Structure and Reactivity." *J. Chem. Soc. Dalton Trans*. **1991**, 917-928.

99. Xiang, K.H.; Pandey, R.; Pernisz, U.C.; Freeman, C. "Theoretical Study of Structural and Electronic Properties of H-Solsesquioxanes." *J. Phys. Chem. B* **1998**, *102*, 8704-8711.

100. Park, S.S.; Xiao, C.; Hagelberg, F.; Hossain, D.; Pittman Jr, C.U.; Saebo, S. "Endohedral and Exohedral Complexes of Polyhedral Double Four-Membered Ring (D4R) Units with Atomic and Ionic Impurities." *J. Phys. Chem. A* **2004**, *108*, 11260-11272.

101. Lin, T.; He, C.; Xiao, Y. "Theoretical Studies of Monosubstituted and Higher Phenyl-Substituted Octahydrosilsesquoxane." *J. Phys. Chem. B* **2003**, *107*, 13788-13792.

102. Schneider, K.S.; Zhang, Z.; Banaszak-Holl, M.; Orr, B.G.; Pernisz, U.C. "Determination of Spherosiloxane Cluster Bonding to Si(100)-2 x 1 by Scanning Tunneling Microscopy." *Phys. Rev. Lett.* **2000**, *85*, 602-605.

103. Feher, F.J.; Budzichowski, T.A. "Syntheses of Highly-Functionalized Polyhedral Oligosilsesquioxanes." *J. Organomet. Chem*. **1989**, *379*, 33-40.

104. Bassindale, A.R.; Pourny, M.; Taylor, P.G.; Hursthouse, M.B.; Light, M.E. "Fluoride-Ion Encapsulation within a Silsesquioxane Cage." *Angew. Chem. Int. Ed.* **2003**, *42*, 3488-3490.

105. Bassindale, A.R.; Parker, D.J.; Pourny, M.; Taylor, P.G.; Horton, P.N.; Hursthouse, M.B. "Fluoride Ion Entrapment in Octasilsesquioxane Cages as Models for Ion Entrapment in Zeolites. Further Examples, X-Ray Crystal Structure Studies, and Investigations into How and Why They May Be Formed." *Organomet*. **2004**, *23*, 4400-4405.

106. Anderson, S.E.; Bodzin, D.J.; Haddad, T.S.; Boatz, J.A.; Mabry, J.M.; Mitchell, C.; Bowers, M.T. "Structural Investigation of Encapsulated Fluoride in Polyhedral Oligomeric Silsesquioxane Cages Using Ion Mobility Mass Spectrometry and Molecular Mechanics." *Chem. Mater*. **2008**, *20*, 4299-4309.

107. Päch, M.; Stösser, R. "Scavenger Assisted Trapping of Atomic Hydrogen in Si_8O_{12}-Cages." *J. Phys. Chem. A* **1997**, *101*, 8360-8365.

108. Mattori, M.; Mogi, K.; Sakai, Y.; Isobe, T. "Studies on the Trapping and Detrapping Transition Steas of Atomic Hydrogen in Octasilsesquioxane Using the Density Functional Theory B3LYP Method." *J. Phys. Chem. A* **2000**, *104*, 10868-10872.

109. Ossadnik, C.; Vepřek, S.; Marsmann, H.C.; Rikowski, E. "Photoluminescent Properties of Substituted Silsesquioxanes of the Composition $R_n(SiO_{1.5})_n$." *Monat. fur Chemie* **1999**, *130*, 55-68.

110. Azinović, D.; Cai, J.; Eggs, C.; König, H.; Marsmann, H.C.; Vepřek, S. "Photoluminescence from Silsesquioxanes $R_8(SiO_{1.5})_8$." *J. Luminescence* **2002**, *97*, 40-50.

111. Slater, J.C. *Quantum Theory of Molecules and Solids, Vol. 1: Electronic Structure of Molecules*; McGraw-Hill: New York, 1963, p. 263.

112. Xiao, S.; Nguyen, M.; Gong, X.; Cao, Y.; Wu, H.B.; Moses, D.; Heeger, A.J. "Stabilization of Semiconducting Polymers with Silsesquioxane." *Adv. Funct. Mater.* **2003**, *13*, 25-29.

113. Lee, J.; Cho, H.J.; Cho, N.S.; Hwang, D.H.; Shim, H.K. "Synthesis of Polyhedral Oligomeric Silsesquioxane-Functionalized Polyfluorenes: Hybrid Organic-Inorganic π-Conjugated Polymers." *Synth. Met*. **2006**, *156*, 590-596.

114. André, P.; Cheng, G.; Ruseckas, A.; van Mourik, T.; Früchtl, H.; Crayston, J.A.; Morris, R.E.; Cole-Hamilton, D.; Samuel, I.D.W. "Hybrid Dendritic Molecule with Confined Chromophore Architecture to Tune Fluorescence Efficiency." *J. Phys. Chem. B* **2008**, *112*, 16382-16392.

115. Vautravers, N.R.; André, P.; Cole-Hamilton, D. "Fluorescence Activation of a Polyhedral Oligomeric Silsesquioxane in the Presence of Reducing Agents." *J. Mater. Chem.* **2009**, *19*, 4545-4550.

116. Zhen, C.-G.; Becker, U.; Kieffer, J. "Tuning Electronic Properties of Functionalized Polyhedral Oligomeric Silsesquioxanes: A DFT and TDDFT Study." *J. Phys. Chem. A* **2009**, *113*, 9707-9714.

117. Laine, R.M.; Sulaiman, S.; Brick, C.; Roll, M.; Tamaki, R.; Asuncion, M.Z.; Neurock, M.; Filhol, J.-S.; Lee, C.-Y.; Zhang, J.; Goodson III, T.; Ronchi, M.; Pizzotti, M.; Rand, S.C.; Li, Y. "Synthesis and Photophysical Properties of Stilbeneoctasilsesquioxanes. Emission Behavior Coupled with Theoretical Modeling Studies Suggest a 3-D Excited State Involving the Silica Core." *J. Am. Chem. Soc.* **2010**, *132*, 3708-3722.

118. Asuncion, M.Z.; Laine, R.M. "Fluoride Rearrangement Reactions of Polyphenyl- and Polyvinylsilsesquioxanes as a Facile Route to Mixed Functional Phenyl, Vinyl T_{10} and T_{12} Silsesquioxanes." *J. Am. Chem. Soc.* **2010**, *132*, 3723-3726.

119. Warwel, S. "Industrial Chemicals via Olefin Metathesis of Natural Fatty Acid Esters." *Nachr. Chem. Tech. Lab*. **1992**, *40*, 314-316.

120. Banks, R.L.; Bailey, G.C. "Olefin Disproportionation." *Ind. Eng. Chem., Prod. Res. Dev.* **1964**, *3*, 170-173.

121. Schuster, M., Blechert, S. "Olefin Metathesis in Organic Chemistry." *Angew. Chem. Int. Ed. Engl.* **1997**, *36*, 2036-2056.

122. Trnka, T.M.; Grubbs, R.H. "The Development of $L_2X_2Ru{=}CHR$ Olefin Metathesis Catalyst: An Organometallic Success Story." *Acc. Chem. Res*. **2001**, *34*, 18-29.

123. Astruc, D. "The Metathesis Reactions: From a Historical Perspective to Recent Developments." *New J. Chem*. **2005**, *29*, 42-56.

124. Herrison, J.L.; Chauvin, Y. "Catalysis of Olefin Transformations by Tungsten Complexes. II. Telomerization of Cyclic Olefins in the Presence of Acyclic Olefins." *Makromol. Chem*. **1970**, *141*, 161-167.

125. Fürstner, A. "Olefin Metathesis and Beyond." *Angew. Chem. Int. Ed*. **2000**, *39*, 3012-3043.

126. Schrock, R.R.; Murzdek, J.S.; Bazan, G.C.; Robbins, J.; DiMare, M.; O'Regan, M. "Synthesis of Molybdenum Imido Alkylidene Complexes and Some Reactions Involving Acyclic Olefins." *J. Am. Chem. Soc*. **1990**, *112*, 3875.

127. Schrock, R.R. "Olefin Metathesis by Molybdenum Imido Alkylidene Catalysts." *Tetrahedron* **1999**, *55*, 8141-8153.

128. Nguyen, S.T.; Grubbs, R.H.; Ziller, J.W. "Syntheses and Activities of New Single-Component, Ruthenium-Based Olefin Metathesis Catalyst." *J. Am. Chem. Soc.* **1993**, *115*, 9856-9857.

129. Schwab, P.; Grubbs, R.H.; Ziller, J.W. "Synthesis and Applications of $RuCl_2(=CHR')(PR_3)_2$: The Influence of the Alkylidene Moiety on Metathesis Activity." *J. Am. Chem. Soc.* **1996**, *118*, 100-110.

130. Schwab, P.; France, M.B.; Ziller, J.W.; Grubbs, R.H. "A Series of Well-Defined Metathesis Catalysts – Synthesis of $[RuCl_2(=CHR')(PR_3)_2]$ and Its Reactions." *Angew. Chem. Int. Ed. Engl*. **1995**, *34*, 2039-2041.

131. Scholl, M.; Trnka, T.M.; Morgan, J. P.; Grubbs, R.H. "Increased Ring Closing Metathesis Activity of Ruthenium-Based Olefin Metathesis Catalysts Coordinated with Imidazolin-2-ylidene Ligands." *Tetrahedron Lett*. **1999**, *40*, 2247-2250.

132. Scholl, M.; Ding, S.; Lee, C.W.; Grubbs, R.H. "Synthesis and Activity of a New Generation of Ruthenium-Based Olefin Metathesis Catalysts Coordinated with 1,3-Dimesityl-4,5-dihydroimidazol-2ylidene Ligands." *Org. Lett*. **1999**, *1*, 953-956.

133. Kirkland, T.A.; Grubbs, R.H. "Effects of Olefin Substitution on the Ring-Closing Metathesis of Dienes." *J. Org. Chem*. **1997**, *62*, 7310-7318.

134. Fujimura, O.; Fu, G.C.; Grubbs, R.H. "The Synthesis of Cyclic Enol Ethers via Molybdenum Alkylidene-Catalyzed Ring-Closing Metathesis." *J. Org. Chem*. **1994**, *59*, 4029-4031.

135. Clark, J.S.; Kettle, J.G. "Synthesis of Brevetoxin Sub-Units by Sequential Ring-Closing Metathesis and Hydroboration." *Tetrahedron Lett.* **1997**, *38*, 123-126.

136. Clark, J.S.; Kettle, J.G. "Enantioselective Synthesis of Medium-Ring Sub-Units of Brevetoxin A by Ring-Closing Metathesis." *Tetrahedron Lett.* **1997**, *38*, 127-130.

137. Calimente, D.; Postema, M.H.D. "Preparation of *C*-1 Glycals via Olefin Metathesis. A Convergent and Flexible Approach to *C*-Glycoside Synthesis." *J. Org. Chem*. **1999**, *64*, 1770-1771.

138. Crowe, W.E.; Goldberg D.R.; "Acrylonitrile Cross-Metathesis: Coaxing Olefin Metathesis Reactivity from a Reluctant Substrate." *J Am Chem Soc*. **1995**, *117*, 5162-5163.

139. Grubbs, R.H. "The Development of Functional Group Tolerant ROMP Catalyst." *J. Macromol. Sci.-Pure Appl. Chem*. **1994**, *A31*, 1829-1833.

140. Mizoroki, T.; Mori, K.; Ozaki, A. "Arylation of Olefin with Aryl Iodide Catalyzed by Palladium." *Bull. Chem. Soc. Jpn*. **1971**, *44*, 581.

141. Heck, R.F.; Nolley, J.P. "Palladium-Catalyzed Vinylic Hydrogen Substitution Reactions with Aryl, Benzyl, and Styryl Halides." *J. Org. Chem*. **1972**, *14*, 2320-2322

142. de Meijere, A.; Meyer, F.E. "Fine Feathers Make Fine Birds: The Heck Reaction in Modern Garb." *Angew. Chem. Int. Ed. Engl*. **1994**, *11*, 2379-2411.

143. Beletskaya, I.P.; Cheprakov, A.V. "The Heck Reaction as a Sharpening Stone of Palladium Catalysis." *Chem. Rev*. **2000**, *100*, 3009-3066.

144. Crisp, G.T. "Variations on a Theme – Recent Developments on the Mechanism of the Heck Reaction and Their Implications for Synthesis." *Chem. Soc. Rev*. **1998**, *27*, 427-436.

145. Loiseleur, O.; Hayashi, M.; Keenan, M.; Schmees, N.; Pfaltz, A. "Enantioselective Heck Reactions using Chiral P,N-Ligands." *J. Organomet. Chem*. **1999**, *576*, 16-22.

146. Dounay, A.B.; Overman, L.E. "The Asymetric Intramolecular Heck reaction in Natural Product Total Synthesis." *Chem. Rev*. **2003**, *103*, 2945-2963.

147. Littke, A.F.; Fu, G.C. "A Versatile Catalyst for Heck Reactions of Aryl Chlorides and Aryl Bromides under Mild Conditions." *J. Am. Chem. Soc*. **2001,** *123,* 6989-7000.

148. Göppert-Mayer, M. "Elementary Processes with Two Quantum Jumps." *Ann. Phys*. **1931**, *401*, 273-294.

149. Kaiser, W.; Garrett, C.G.B. "Two-Photon Excitation in CaF_2:Eu^{2+}." *Phys. Rev. Lett*. **1961**, *7*, 229-231.

150. Marder, S.R. "Organic Nonlinear Optical Materials: Where We Have Been and Where We Are Going." *Chem. Commun*., **2006**, 131-134.

151. Pawlicki, M.; Collins, H.A.; Denning, R.G.; Anderson, H.L. "Two-Photon Absorption and the Design of Two-Photon Dyes." *Angew. Chem. Int. Ed.* **2009**, *48*, 3244-3266.

152. He, G.S.; Tan, L.-S.; Zheng, Q.; Prasad, P.N. "Multiphoton Absorbing Materials: Molecular Design, Characterizations, and Applications." *Chem. Rev*. **2008**, *108*, 1245-1330.

153. Birge, R.R.; Pierce, B.M. "Semiclassical Time-Dependent Theory of Two-Photon Spectroscopy. The Effect of Dephasing in the Virtual Level on the Two-Photon Excitation Spectrum of Isotachysterol." *Int. J. Quantum Chem*. **1986**, *29*, 639-656.

154. Reinhardt, B.A.; Brot, L.L.; Clarson, S.J.; Dillard, A.G.; Bhatt, J.C.; Kannan, R.; Yuan, L.; He, G.S.; Prasad, P.N. "Highly Active Two-Photon Dyes: Design, Synthesis, and Characterization toward Application." *Chem. Mater*. **1998**, *10*, 1863-1874.

155. Belfield, K.D.; Hagan, D.J.; Van Stryland, E.W.; Schafer, K.J.; Negres, R.A. "New Two-Photon Absorbing Fluorene Derivatives: Synthesis and Nonlinear Optical Characterization." *Org. Lett*. **1999**, *1*, 1575-1578.

156. Stellacci, F.; Bauer, C.A.; Meyer-Friedrichsen, T.; Wenseleers, W.; Marder, S.R.; Perry, J.W. "Ultrabright Supramolecular Beacons Based on the Self-Assembly of Two-Photon Chromophores on Metal Nanoparticles." *J. Am. Chem. Soc*. **2003**, *125*, 328-329.

157. Aujard, I.; Benbrahim, C.; Gouget, M.; Ruel, O.; Baudin, J.-B.; Neveu, P.; Jullien, L. "*o*-Nitrobenzyl Photolabile Protecting Groups with Red-Shifted Absorption: Syntheses and Uncaging Cross-Sections for One- and Two-Photon Excitation." *Chem.-Eur. J*. **2006**, *12*, 6865-6879.

158. Zeng, Z.; Guan, Z.; Xu, Q.-H.; Wu, J. "Octupolar Polycyclic Aromatic Hydrocarbons as New Two-Photon Absorption Chromophores: Synthesis and Application for Optical Power Limiting." *Chem. Eur. J*. **2011**, *17*, 3837-3841.

159. Santos-Pérez, J.; Crespo-Hernández, C.E.; Reichardt, C.; Cabrera, C.R.; Feliciano-Ramos, I.; Arroyo-Ramirez, L.; Meador, M.A. "Synthesis, Optical Characterization, and Electrochemical Properties of Isomeric Tetraphenylbenzodifurans Containing Electron Acceptor Groups." *J. Phys. Chem. A* **2011** ASAP Article.

160. Albota, M.; Beljonne, D.; Bredas, J.L.; Ehrlich, J.E.; Fu, J.Y.; Heikal, A.A.; Hess, S.E.; Kogej, T.; Levin, M.D.; Marder, S.R.; McCord-Maughon, D.; Perry, J.W.; Rockel, H.; Rumi, M.; Subramaniam, G.; Webb, W.W.; Wu, X.L.; Xu, C. "Design of Organic Molecules with Large Two-Photon Absorption Cross Sections." *Science* **1998**, *281*, 1653.

161. Strehmel, B.; Sarker, A.M.; Detert, H. "The Influence of σ and π Acceptors on Two-Photon Absorption and Solvatochromism of Dipolar and Quadrupolar Unsaturated Organic Compounds." *ChemPhysChem* **2003**, *4*, 249-259

162. Le Droumaguet, C.; Mongin, O.; Werts, M.H.V.; Blanchard-Desce, M. "Towards 'Smart' Multiphoton Fluorophores: Strongly Solvatochromic Probes for Two-Photon Sensing of Micropolarity." *Chem. Commun*. **2005**, 2802-2804.

163. Lee, H.J.; Sohn, J.; Hwang, J.; Park, S.Y.; Choi, H.; Cha, M. "Triphenylamine-Cored Bifunctional Organic Molecules for Two-Photon Absorption and Photorefraction." *Chem. Mater*. **2004**, *16*, 456-465.

164. Huang, Z.-L.; Lei, H.; Li, N.; Qiu, Z.-R.; Wang, H.-Z.; Guo, J.D.; Luo, Y.; Zhong, Z.-P.; Liu, X.-F.; Zhou, Z.-H. "Novel Heterocycle-Based Organic Molecules with Two-Photon Induced Blue Fluorescent Emission." *J. Mater. Chem*. **2003**, *13*, 708-711.

165. Shao, P.; Huang, B.; Chen, L.; Liu, Z.; Qin, J.; Gong, H.; Ding, S.; Wang, Q. "Synthesis and Two-Photon Absorption Properties of Novel Heterocycle-Based Organic Molecules." *J. Mater. Chem*. **2005**, *15*, 4502-4506.

166. Kim, O.-K.; Lee, K.-S.; Woo, H.Y.; Kim, K.-S.; He, G.S.; Swiatkiewicz, J.; Prasad, P.N. "New Class of Two-Photon-Absorbing Chromophores Based on Dithienothiophene." *Chem. Mater*. **2000**, *12*, 284-286.

167. Parent, M.; Mongin, O.; Kamada, K.; Katan, C.; Blanchard-Desce, M. "New Chromophores from Click Chemistry for Two-Photon Absorption and Tuneable Photoluminescence." *Chem. Commun.* **2005**, 2029-2031.

168. Marder, S.R.; Torruellas, W.E; Blanchard-Desce, M.; Ricci, V.; Stegeman, G.I.; Gilmour, S.; Bredas, J.L.; Li, J.; Bublitz, G.U.; Boxer, S.G. "Large Molecular Third-Order Optical Nonlinearities in Polarized Carotenoids." *Science* **1997**, *276*, 1233-1236.

169. Bozio, R.; Cecchetto, G.; Fabbrini, G.; Ferrante, C.; Maggini, M.; Menna, E.; Pedron, D.; Ricco, R.; Signorini, R.; Zerbetto, M. "One- and Two-Photon Absorption and Emission Properties of a Zn(II) Chemosensor." *J. Phys. Chem. A* **2006**, *110*, 6459-6464.

170. Bhaskar, A.; Ramakrishna, G.; Twieg, R.J.; Goodson III, T. "Zinc Sensing via Enhancement of Two-Photon Excited Fluorescence." *J. Phys. Chem. C* **2007**, *111*, 14607-14611.

171. Liu, Z.-Q.; Shi, M.; Li, F.-Y.; Fang, Q.; Chen, Z.-H.; Yi, T.; Huang, C.-H. "Highly Selective Two-Photon Chemosensors for Fluoride Derived from Organic Boranes." *Org. Lett*. **2005**, *7*, 5481-5484.

172. Wecksler, S.; Mikhailovsky, A.; Ford, P.C. "Photochemical Production of Nitric Oxide via Two-Photon Excitation with NIR Light." *J. Am. Chem. Soc*. **2004**, *126*, 13566-13567.

173. Goodwin, A.P.; Mynar, J.L.; Ma, Y.; Fleming, G.R.; Frechet, J.M.J. "Synthetic Micelle Sensitive to IR Light via a Two-Photon Process." *J. Am. Chem. Soc*. **2005**, *127*, 9952-9953.

174. Zipfel, W.R.; Williams, R.M.; Webb, W.W. "Nonlinear Magic: Multiphoton Microscopy in the Biosciences." *Nat. Biotechnol*. **2003**, *21*, 1369-1377.

175. Helmchen, F.; Denk, W. "Deep Tissue Two-Photon Microscopy." *Nat. Methods* **2005**, *2*, 932-940.

176. Lin, T.-C.; Chung, S.-J.; Kim, K.S.; Wang, X.; He, G.S.; Swiatkiewicz, J.; Pudavar, H.E.; Prasad, P.N. "Organics and Polymers with High Two-Photon Activities and Their Applications." *Adv. Polym. Sci*. **2003**, *161*, 157-193.

177. LaFratta, C.N.; Fourkas, J.T.; Baldacchini, T.; Farrer, R.A. "Multiphoton Fabrication." *Angew. Chem. Int. Ed*. **2007**, *46*, 6238-6258.

178. Parthenopoulos, D.A.; Rentzepis, P.M. "Three-Dimensional Optical Storage Memory." *Science* **1989**, *245*, 843-845.

179. Kawata, S.; Kawata, Y. "Three-Dimensional Optical Data Storage Using Photochromic Materials." *Chem. Rev*. **2000**, *100*, 1777-1788.

180. Walker, E.; Rentzepis, P.M. "Two-Photon Technology: A New Dimension." *Nat. Photonics* **2008**, *2*, 406-408.

181. Spangler, C.W. "Recent Development in the Design of Organic Materials for Optical Power Limiting." *J. Mater. Chem*. **1999**, *9*, 2013-2020.

182. Ehrlich, J.E.; Wu, X.L.; Lee, I.-Y.S.; Hu, Z.-Y.; Rockel, H.; Marder, S.R.; Perry, J.W. "Two-Photon Absorption and Broadband Optical Limiting with Bis-Donor Stilbenes." *Opt. Lett.* **1997**, *22*, 1843-1845.

Chapter 2
Experimental Techniques and Syntheses

2.1 Materials

Dichloromethane (CH_2Cl_2) and acetonitrile (CH_3CN) were purchased from Fisher and distilled from CaH_2 under N_2 prior to use. Tetrahydrofuran (THF), 1,4-dioxane, hexane, and toluene were purchased from Fisher and distilled from Na/benzophenone prior to use. Grubbs 1st generation catalyst [$RuCl_2(=CHPh)(PCy_3)_2$] and $Pd_2(dba)_3$ were purchased from Sigma-Aldrich and used as received. $Pd(P\text{-}t Bu_3)_2$ was purchased from Strem Chemicals and used as received.

Octavinylsilsesquioxane (OVS) and polyvinylsilsesquioxane (PVSQ) were produced according to procedures developed by Harrison and Hall.[1] Crystalline octa(*o*-bromophenyl)silsesquioxane (*o*-Br_8OPS), octa(2,5-dibromophenyl)silsesquioxane (Br_{16}OPS), and octa(tribromophenylsilsesquioxane) (Br_{24}OPS) were synthesized by bromination of octaphenylsilsesquioxane (OPS) using previously reported methods.[2] Octa(aminophenyl)silsesquioxane (OAPS) was synthesized from reduction of octa(nitrophenyl)silsesquioxane (ONPS).[3] Octa(dimethylsiloxyglycidyl)silsesquioxane (OG) and octa(dimethylsiloxyethylcyclohexylepoxide)silsesquioxane (OC) were synthesized from hydrosilylation reaction of octa(dimethylsiloxy)silsesquioxane with allyl glycidyl ether and vinyl cyclohexene epoxide, respectively.[4,5]

3,5-Dibromobenzoyl chloride was synthesized from 3,5-dibromobenzoic acid and thionyl chloride.[6] *p*-Vinylstilbene was produced according to literature methods.[7] 4-NBocStyrene was synthesized from reaction of 4-vinylaniline with di-*tert*-butyl-dicarbonate.[8] The diglycidyl ether of bisphenol A (DGEBA, MW = 340) was obtained from Dow Chemical Co. (Midland, MI) and tetraglycidyl-*m*-xylene (TGMX) was received as a gift from Dr. Rafil Basheer of Delphi Research Lab (Shelby Township, MI). All other chemicals were purchased from Fisher or Sigma-Aldrich and used as received.

2.2 Analytical Techniques

Matrix-Assisted Laser Desorption/Time-of-Flight Spectrometry (MALDI-ToF)

All MALDI-ToF analyses was done on a Micromass TofSpec-2E equipped with a 337 nm nitrogen laser in positive-ion reflectron mode using poly(ethylene glycol) as calibration standard, dithranol as matrix, and $AgNO_3$ as ion source. Samples were prepared by mixing solutions of 5 parts matrix (10 mg/mL in THF), 5 parts sample (1 mg/mL in THF), and 1 part $AgNO_3$ (2.5 mg/mL in water) and blotting the mixture on target plate.

Gel Permeation Chromatography (GPC)

All GPC analyses were done on a Waters 440 system equipped with Waters Styragel columns (7.8 x 300, HT 0.5, 2, 3, 4) with RI detection using Waters refractometer and THF as solvent. The system was calibrated using polystyrene standards and toluene as reference.

Thermogravimetric analyses (TGA)

All TGA were run on a 2960 simultaneous TGA-DTA instrument (TA Instruments, Inc., New Castle, DE) or a SDT Q600 Simultaneous Differential DTA-TGA Instrument (TA Instruments, Inc., New Castle, DE). Samples (15-25 mg) were loaded in alumina pans and ramped at 10^oC/min to 1000^oC under dry air with a flow rate of 60 mL/min.

Nuclear Magnetic Resonance (NMR)

All ^{1}H-NMR and ^{13}C-NMR were performed in $CDCl_3$, CD_3OD, or DMSO-d_6 and recorded on a Varian INOVA 400 MHz spectrometer. All ^{29}Si-NMR were performed in $CDCl_3$ or DMSO-d_6 and recorded on a Bruker Avance DRX-500 spectrometer. ^{1}H-NMR spectra were collected at 400 MHz using a 6000 Hz spectral width, a relaxation delay of 0.5 s, 30k data points, a pulse width of 38^o, and TMS (0.00 ppm) as the internal reference. ^{13}C-NMR spectra were collected at 100 MHz using a 25000 Hz spectral width, a relaxation delay of 1.5 s, 75k data points, a pulse width of 40°, and TMS (0.00 ppm) as the internal reference. ^{29}Si-NMR spectra were collected at 100 MHz using a 14000 Hz spectral width, a relaxation delay of 20 s, 65k data points, a pulse width of 7^o, and TMS (0.00 ppm) as the internal reference.

FTIR Spectra.

Diffuse reflectance Fourier transform (DRIFT) spectra were recorded on a Mattson Galaxy Series FT-IR 3000 spectrometer (Mattson Instruments, Inc., Madison, WI) or a Nicolet 6700 FT-IR spectrometer (ThermoScientific, Waltham, MA). Optical grade, random cuttings of KBr (International Crystal Laboratories, Garfield, NJ) were ground, with 1.0 wt% of the sample to be analyzed. For DRIFT analysis, samples were packed firmly and leveled off at the upper edge to provide a smooth surface. The FTIR sample chamber was flushed continuously with N_2 prior (10 min) to data acquisition in the range 4000-400 cm^{-1}.

Differential Scanning Calorimetry (DSC)

All DSC experiments were performed on materials using a DSC 2910 (TA Instruments, Inc., New Castle, DE) under N_2 flow rate of 60 mL/min. Sample (5-10 mg) was placed in a pan without capping and ramped to the desired temperature at a rate of 10^oC/min. The heat flow difference between the reference blank and the sample pan was recorded.

UV-Vis Spectrometry

UV-Vis spectra were taken on a Shimadzu UV-1601 UV-Vis transmission spectrometer. Samples were dissolved in solvents of choice and diluted to a concentration (10^{-6}-10^{-7} M) where the absorption maximum was less than 10% for a 1 cm path length.

Photoluminescence Spectrometry

Photoluminescent spectra were taken on a Fluoromax-2 fluorimeter using 260 nm excitation for R-styrenylOS and 320 nm excitation for R-vinylstilbeneOS. Samples of RStyrenylOS from UV-Vis spectroscopy were used without dilution, while all other samples from UV-VIS spectroscopy were diluted (10^{-7} to 10^{-8} M) to avoid excimer formation and fluorimeter detector saturation.

Photoluminescence Quantum Yields (Φ_{PL}).

Φ_{PL} was determined by a modification of the relative method described by Demas and Crosby[9] using anthracene[10] and 9,10-diphenylanthracene[11] as references. The absorption at 320 nm was determined for each material at three different concentrations (maximum absorption of 20%). These samples were then diluted by equal amounts in order to avoid fluorimeter saturation and excimer formation, and the total area of the emission spectrum calculated. For each solution, absorption and emission measurements were repeated a minimum of two times and averaged. The slope of a plot of emission versus absorption was determined for each material, and relative quantum efficiency calculated according to the equation:

$$\Phi_{PL}(x) = \left(\frac{A_s}{A_x}\right)\left(\frac{F_x}{F_s}\right)\left(\frac{n_x}{n_s}\right)^2 \Phi_{PL}(s)$$

where Φ_{PL} is the quantum yield, A is the absorption at the excitation wavelength, F is the total integrated emission, and n is the refractive index of the solution, which can be approximated to be the refractive index of the solvent, considering the low concentration of the solution. Subscripts x and s refer to the sample to be measured and the reference, respectively.

Two Photon Spectroscopy

a. Steady State Measurements

All compounds were dissolved in tetrahydrofuran (THF) or dichloromethane (CH_2Cl_2) (Sigma-Aldrich, spectrophotometric grade) for carrying out the optical measurements. The absorption spectra of the molecules were measured using an Agilent (Model No. 8341) spectrophotometer. The fluorescence spectra were acquired using a Spex-fluorolog spectrofluorimeter. The quantum yields of the molecules were measured using a known procedure[12] with bis-MSB [*p*-bis(*o*-methyl-styryl) benzene] as the standard. The absorbance was limited to equal to or less than 0.03. The solutions were purged with argon for 3 minutes prior to measuring their emission spectra.

b. Two-Photon Excited Fluorescence Measurements

In order to measure the two photon absorption cross sections, we followed the two photon excited fluorescence (TPEF) method.[13] Bis-MSB dissolved in cyclohexane (620 nm to 710 nm) and C-307 in methanol (710 nm to 800 nm) were used as references for measuring TPA cross-sections at different wavelength regions. The laser used for the measurements was an amplified femtosecond laser (Spitfire, Spectraphysics) pumped optical parametric amplifier (OPA-800C, Spectraphysics) which gives tunable wavelengths from 300 nm to 2000 nm. The input power from the laser was varied by using a neutral density filter. An iris was placed prior to the neutral density filter in order to ensure a circular beam. The beam was directed on to the sample cell (quartz cuvette, 0.5cm path length) and the resultant fluorescence was collected in a direction perpendicular to the incident beam. A 1" focal length plano-convex lens was used to direct the collected fluorescence into a monochromator. The output from the monochromator was coupled to a PMT. The photons were converted into counts by a photon counting unit. A logarithmic plot between collected fluorescence photons and input intensity gave a slope of two, ensuring a quadratic dependence. The intercept enabled us to calculate the two photon absorption cross sections at different wavelengths.

Coefficient of Thermal Expansion (CTE) Measurements

The thermal expansion behavior of cured samples was studied using a Perkin-Elmer TMA7 (Boston, MA). Cured samples were polished to ≈ 1.5 x 5.5 x 5.5 mm with 400C-grade sandpaper. The thermal properties were measured under helium from 30^{o}C to 230^{o}C with a ramp rate of 10^{o}C/min.

2.3 Syntheses

2.3.1 Elaboration of Octavinylsilsesquioxane

General Metathesis Reactions of OVS

To a dry 10 mL Schlenk flask under N_2 was added 0.40 g (5.1 mmol –CH=CH_2) of OVS and 21.0 mg (0.0265 mmol, 0.5 mol %) of 1st generation Grubbs catalyst. Dry CH_2Cl_2 (6 mL) was added via a syringe followed by R-styrene (7.56 mmol). The mixture was stirred at room temperature for 72 h and then quenched by precipitation into 200 mL

of methanol. The resulting powder was filtered and further purified according to published procedure.[14]

HStyrenylOS: Styrene = 0.87 mL; Yield = 82%; Conversion = 100%; MALDI-ToF (Ag^+): m/z = 1349.2 (100%), Calculated = 1349.7 Da; GPC: M_n = 1025, M_w = 1034, PDI = 1.01; TGA (air, 1000°C): Found = 38.6%, Calculated = 38.7%, $T_{d5\%}$ = 395°C; DSC (10°C/min, N_2): T_m = 270°C; ^{1}H-NMR ($CDCl_3$): 6.32 ppm (d, 8H, =C*H*-Si); 7.28-7.42 ppm (m, 8H, =C*H*-Ph, 24H, Ph); 7.50 ppm (d, 16H, Ph); ^{13}C-NMR ($CDCl_3$): 117.3 ppm (Si*C*H=CHPh), 126.7 ppm (*o*-Ph), 128.6 ppm (*m*-Ph), 128.9 ppm (*p*-Ph), 137.3 ppm (*ipso*-Ph), 149.2 ppm (SiCH=*C*HPh); ^{29}Si-NMR ($CDCl_3$): 78.23 ppm.

MeStyrenylOS: 4-Methylstyrene = 1.00 mL; Yield = 75%; Conversion = 94%; MALDI-ToF (Ag^+): m/z = 1236 (14%), 1344 (24%), 1462 (62%), Calculated = 1461.9 Da; GPC: M_n = 1257, M_w = 1278, PDI = 1.02; TGA (air, 1000°C): Found = 33.5%, Calculated = 35.5%, $T_{d5\%}$ = 283°C; DSC (10°C/min, N_2): T_m = 315°C; ^{1}H-NMR ($CDCl_3$): 2.35 (s, 24H, -C*H*$_3$); 6.24 (d, 8H, =C*H*-Si); 7.14, (d, 16H, Ph); 7.28 (d, 8H, =C*H*-Ph); 7.33 (d, 16H, Ph).

MeOStyrenylOS: 4-Vinylanisole = 1.00 mL; Yield = 83%; Conversion = 100%; MALDI-ToF (Ag^+): m/z = 1589.1 (100%), Calculated = 1589.9 Da; GPC: M_n = 1262, M_w = 1283, PDI = 1.02; TGA (air, 1000°C): Found = 33.6%, Calculated = 32.4%, $T_{d5\%}$ = 323°C; DSC (10°C/min, N_2): T_m = 345°C; ^{1}H-NMR ($CDCl_3$): 3.83 (s, 24H, -OC*H*$_3$); 6.14 (d, 8H, =C*H*-Si); 6.87, (d, 16H, Ph); 7.30 (d, 8H, =C*H*-Ph); 7.43 (d, 16H, Ph); ^{13}C-NMR ($CDCl_3$): 55.3 (-O*C*H$_3$), 113.9 (*m*-Ph), 114.8 (Si*C*H=CHPh), 128.3 (*o*-Ph), 130.4 (*ipso*-Ph), 148.4 (SiCH=*C*HPh), 160.1 (*C*-OCH$_3$).

ClStyrenylOS: 4-Chlorostyrene = 0.91 mL; Yield = 76%; Conversion = 100%; MALDI-ToF (Ag^+): m/z = 1626.8 (100%), Calculated = 1625.2 Da; GPC: M_n = 1387, M_w = 1403, PDI = 1.01; TGA (air, 1000°C): Found = 31.5%, Calculated = 31.7%, $T_{d5\%}$ = 362°C; DSC (10°C/min, N_2): T_m = 310°C; ^{1}H-NMR ($CDCl_3$): 6.21 (d, 8H, =C*H*-Si); 7.25 (d, 8H, =C*H*-Ph); 7.28 (d, 16H, Ph); 7.35 (d, 16H, Ph).

BrStyrenylOS: 4-Bromostyrene = 0.99 mL; Yield = 82%; Conversion = 100%; MALDI-ToF (Ag^+): m/z = 1981.3 (100%), Calculated = 1980.8 Da; GPC: M_n = 1321, M_w = 1350, PDI = 1.02; TGA (air, 1000°C): Found = 25.7%, Calculated = 25.6%, $T_{d5\%}$ = 318°C; DSC (10°C/min, N_2): T_m = 330°C; ^{1}H-NMR ($CDCl_3$): 6.27 (d, 8H, =C*H*-Si); 7.26 (d, 8H, =C*H*-Ph); 7.33 (d, 16H, Ph); 7.49 (d, 16H, Ph); ^{29}Si-NMR ($CDCl_3$): 78.45 ppm.

NO_2StyrenylOS: 3-Nitrostyrene = 1.05 mL; Yield = 81%; Conversion = 100%; MALDI-ToF (Ag^+): m/z = 1710.1 (100%), Calculated = 1709.7 Da; GPC: M_n = 1561, M_w = 1607, PDI = 1.03; TGA (air, 1000°C): Found = 29.8%, Calculated = 30.0%, $T_{d5\%}$ = 331°C; ^{1}H-NMR ($CDCl_3$): 6.50 (d, 8H, =C*H*-Si); 7.43 (d, 8H, =C*H*-Ph); 7.58 (m, 8H, Ph); 7.82 (m, 8H, Ph); 8.20 (m, 8H, Ph); 8.37 (m, 8H, Ph); ^{29}Si-NMR ($CDCl_3$): 78.45 ppm.

General Heck Reaction of BrStyrenylOS.

To a dry 50 mL Schlenk flask under N_2 was added 0.50 g (2.14 mmol –Br) BrStyrenylOS, 19 mg (0.04 mmol) Pd[P(*t*-Bu_3)]$_2$, and 18 mg (0.02 mmol) $Pd_2(dba)_3$. 1,4-dioxane (10 ml) was then added by syringe, followed by NCy_2Me (2.11 mmol, 0.45 ml) and R-styrene (6.41 mmol). The mixture was stirred at room temperature for 72 h and then quenched by filtering through 1 cm Celite, which was washed with 5 ml THF. The solution was then precipitated into 200 ml methanol, filtered, and the solid re-dissolved in 10 ml THF. This solution was then filtered again through a 1 cm Celite column to remove any remaining Pd particles, and re-precipitated into 200 ml methanol. The product was further purified by column chromatography (silica, 1:10 THF:hexane).

HVinylStilbeneOS: Styrene = 0.74 mL; Yield = 79%; Conversion = 100%; MALDI-ToF (Ag^+): m/z = 2162.7 (100%), Calculated = 2166.7 Da; GPC: M_n = 1511, M_w = 1596, PDI = 1.06; TGA (air, 1000°C): Found = 23.4%, Calculated = 23.8%, $T_{d5\%}$ = 400°C; ^{1}H-NMR ($CDCl_3$): 6.31 (d, 8H, =C*H*-Si); 7.09 (dd, 16H, Ph-C*H*=C*H*-Ph); 7.24-7.39 (m, 8H, Si-CH=C*H*-Ph, 24H, Ph); 7.48 (m, 48H, Ph); ^{13}C-NMR ($CDCl_3$, ppm): 117.1, 126.5, 126.7, 127.3, 127.7, 128.1, 128.7, 129.2, 136.6, 137.1, 138.0, 148.7; ^{29}Si-NMR ($CDCl_3$): 78.15 ppm.

MeVinylStilbeneOS: 4-Methylstyrene = 0.85 mL; Yield = 74%; Conversion = 100%; MALDI-ToF (Ag^+): m/z = 2279.9 (100%), Calculated = 2279.0 Da; GPC: M_n = 17751, M_w = 1876, PDI = 1.06; TGA (air, 1000°C): Found = 22.1%, Calculated = 21.1%, $T_{d5\%}$ = 390°C; ^{1}H-NMR ($CDCl_3$): 2.33 (s, 24H, -C*H*$_3$); 6.34 (d, 8H, =C*H*-Si); 7.09 (dd, 16H, Ph-C*H*=C*H*-Ph); 7.17, (d, 16H, Ph); 7.41 (m, 8H, Si-CH=C*H*-Ph, 16H, Ph); 7.49 (m, 32H, Ph).

MeOVinylStilbeneOS: 4-Vinylanisole = 0.85 mL; Yield = 79%; Conversion = 100%; MALDI-ToF (Ag^+): m/z = 2404.6 (100%), Calculated = 2406.9 Da; GPC: M_n = 1880, M_w = 2096, PDI = 1.12; TGA (air, 1000°C): Found = 20.9%, Calculated = 22.%, $T_{d5\%}$ = 315°C; ^{1}H-NMR ($CDCl_3$): 3.83 (s, 24H, -OC*H*$_3$); 6.33 (d, 8H, =C*H*-Si); 6.90, (d, 16H, Ph); 7.03 (dd, 16H, Ph-C*H*=C*H*-Ph); 7.39 (d, 8H, Si-CH=C*H*-Ph); 7.47 (m, 48H, Ph); ^{13}C-NMR ($CDCl_3$, ppm): 55.3, 114.1, 116.8, 126.0, 126.4, 127.3, 127.8, 128.7, 130.0, 136.2, 138.3, 148.7, 159.4; ^{29}Si-NMR ($CDCl_3$): 78.12 ppm.

NH_2VinylStilbeneOS: 4-Vinylaniline = 0.75 mL; Yield = 73%; Conversion = 100%; MALDI-ToF (Ag^+): m/z = 2287.6 (100%), Calculated = 2286.9 Da; GPC: M_n = 1374, M_w = 1549, PDI = 1.13; TGA (air, 1000°C): Found = 22.1%, Calculated = 20.1%, $T_{d5\%}$ = 345°C; ^{1}H-NMR ($CDCl_3$): 3.72 (s, 16H, -N*H*$_2$); 6.32 (d, 8H, =C*H*-Si); 6.67 (d, 16H, Ph); 6.98 (dd, 16H, Ph-C*H*=C*H*-Ph); 7.34 (m, 8H, Si-CH=C*H*-Ph, 16H, Ph); 7.46 (m, 32H, Ph); ^{29}Si-NMR ($CDCl_3$): 78.06ppm.

Reaction of NH_2VinylStilbeneOS with difunctional benzoylchlorides.

To a dry 10 mL Schlenk flask under N_2 was added 0.1 g (0.37 mmol –NH_2) NH_2VinylStilbeneOS dissolved in 1 mL of THF. A solution of 0.74 mmol of the corresponding benzoylchloride in 1 mL of THF was then added to the flask via syringe, followed by 0.05 mL (0.36 mmol) triethylamine. The mixture was stirred at room temperature for 24 h and then quenched by filtering through 1 cm Celite. The filtrate was then precipitated into 50 mL of hexane and the product collected by suction filtration.

$(NO_2)_2$BenzamideOS: 3,5-Dinitrobenzoyl chloride = 0.17 g; Yield = 90%; Conversion = 100%; GPC: M_n = 2003, M_w = 2089, PDI = 1.04; TGA (air, 1000°C): Found = 10.5%, Calculated = 12.9%, $T_{d5\%}$ = 170°C; ^{1}H-NMR ($CDCl_3$): 6.55 (d, 8H, SiC*H*=CHPh), 7.27 (d, 16H, PhC*H*=C*H*Ph), 7.42 (d, 8H, SiCH=C*H*Ph),7.65 (s, 16H, Ph), 7.82 (d, 16H, Ph), 8.85 (dd, 32H, Ph), 8.99 (s, 8H, Ph), 9.16 (s, 16H, Ph), 10.9 (s, 8H, -N(*H*)C(=O); ^{13}C-NMR ($CDCl_3$, ppm): 117.0, 119.9, 121.1, 127.1, 127.4, 128.0, 128.4, 128.9, 133.5, 136.1, 137.8, 148.2, 148.5, 164.9.

Br_2BenzamideOS: 3,5-Dibromobenzoyl chloride = 1.10 g; Yield = 92%; Conversion = 100%; GPC: M_n = 2178, M_w = 2533, PDI = 1.16; TGA (air, 1000°C): Found = 10.5%, Calculated = 11.2%, $T_{d5\%}$ = 335°C; ^{1}H-NMR ($CDCl_3$): 6.50 (d, 8H, SiC*H*=CHPh), 7.22 (d, 16H, PhC*H*=C*H*Ph), 7.37 (d, 8H, SiCH=C*H*Ph),7.57 (m, 24H, Ph), 7.73 (d, 16H, Ph), 8.06 (m, 24H, Ph), 10.4 (s, 8H, -N(*H*)C(=O); ^{13}C-NMR ($CDCl_3$, ppm): 116.9, 120.9, 123.0, 127.1, 127.2, 127.4, 128.0, 129.2, 130.1, 133.2, 136.0, 138.7, 149.3, 162.8; ^{29}Si-NMR ($CDCl_3$): 77.40ppm.

2.3.2 Synthesis, Characterization, and Photophysical Properties of Polyfunctional Phenylsilsesquioxanes

General Heck Reaction of *o*-Br_8OPS.

To a dry 10-mL Schlenk flask under N_2 was added 0.50 g (0.3 mmol, 2.4 mmol-Br) of *o*-Br_8OPS, 22 mg (0.046 mmol)of Pd[P(*t*-Bu_3)]$_2$, and 21 mg (0.023 mmol) of $Pd_2(dba)_3$. 1,4-dioxane (3 ml) was then added by syringe, followed by NCy_2Me (3.7 mmol, 0.8 ml) and R-styrene (8.70 mmol). The mixture was stirred at 70°C for 24 h and then quenched by filtering through 1 cm Celite, which was washed with 5 ml THF. The solution was then precipitated into 200 ml methanol, filtered, and the solid re-dissolved in 10 ml THF. This solution was then filtered again through a 1 cm Celite column to remove any remaining Pd particles, and re-precipitated into 200 ml methanol. The product is collected via suction filtration and dried in vacuo.

o-$MeStyr_8$OPS: 4-methylstyrene = 1.14 mL; Yield = 91%; Conversion = 100%; MALDI-ToF: m/z = 1953.9 (*o*-$MeStyr_7$OPS/Ag^+, 5%), 1961.9 (*o*-$MeStyr_7$OPS/H^+, 4%), 2070.9

(*o*-MeStyr$_8$OPS/Ag$^+$, 91%), Calculated = 2070.7 (*o*-MeStyr$_8$OPS/Ag$^+$); GPC: M_n = 1212, M_w = 1225, PDI = 1.01; TGA (air, 1000^{o}C): Found = 24.6%, Calculated = 24.5%, $T_{d5\%}$ = 370^{o}C.

o-NBocStyr$_8$OPS: 4-NBocstyrene = 1.20 g; Yield = 87%; Conversion = 100%; MALDI-ToF (as *o*-NH$_2$Styr$_8$OPS): m/z = 1969.2 (*o*-NH$_2$Styr$_8$OS/H$^+$, 83%), 2074.4 (*o*-NH$_2$Styr$_8$OS/Ag$^+$, 7%), 2087.3 (*o*-NH$_2$Styr$_9$OS/H$^+$, 10%), Calculated = 1971.7 Da (*o*-NH$_2$Styr$_8$OS/H$^+$); GPC: M_n = 2382, M_w = 2431, PDI = 1.02; TGA (air, 1000^{o}C): Found = 15.4%, Calculated = 17.3%, $T_{d5\%}$ = 180^{o}C.

o-AceStyr$_8$OPS: 4-acetoxystyrene = 1.33 mL; Yield = 89%; Conversion = 100%; MALDI-ToF : m/z = 2221.3 (*o*-AceStyr$_6$HOStyrOPS/Ag$^+$, 5%), 2262.2 (*o*-AceStyr$_7$OPS/Ag$^+$, 19%), 2336.2 (*o*-AceStyr$_6$HOStyr$_2$OPS/Ag$^+$, 7%), 2380.2 (*o*-AceStyr$_7$HOStyrOPS/Ag$^+$, 26%), 2422.2 (*o*-AceStyr$_8$OPS/Ag$^+$, 44%), Calculated = 2422.7 Da (*o*-AceStyr$_8$OPS/Ag$^+$); GPC: M_n = 1535, M_w = 1570, PDI = 1.02; TGA (air, 1000^{o}C): Found = 20.3%, Calculated = 20.8%, $T_{d5\%}$ = 400^{o}C.

General Heck Reaction of Br$_{16}$OPS.

To a dry 10-mL Schlenk flask under N_2 was added 0.50 g (0.22 mmol, 3.5 mmol-Br) of Br$_{16}$OPS, 22 mg (0.046 mmol)of Pd[P(*t*-Bu$_3$)]$_2$, and 21 mg (0.023 mmol) of Pd$_2$(dba)$_3$. 1,4-dioxane (5 ml) was then added by syringe, followed by NCy$_2$Me (5.6 mmol, 1.2 ml) and R-styrene (10.5 mmol). The mixture was stirred at 70^{o}C for 24 h and then quenched by filtering through 1 cm Celite, which was washed with 5 ml THF. The solution was then precipitated into 200 ml methanol, filtered, and the solid re-dissolved in 10 ml THF. This solution was then filtered again through a 1 cm Celite column to remove any remaining Pd particles, and re-precipitated into 200 ml methanol. The product is collected via suction filtration and dried in vacuo.

MeStyr$_{16}$OPS: 4-methylstyrene = 1.38 mL; Yield = 92%; Conversion = 100%; MALDI-ToF: m/z = 2775.0 (MeStyr$_{15}$OPS/H$^+$, 1.2%), 2882.0 (MeStyr$_{15}$OPS/Ag$^+$, 11.6%), 2890.0 (MeStyr$_{16}$OPS/H$^+$, 19.8%), 2999.5 (MeStyr$_{16}$OPS/Ag$^+$, 67.1%), 3115.8

($MeStyr_{17}OPS/Ag^+$, 0.3%) Calculated = 2999.9 ($MeStyr_{16}OPS/Ag^+$); GPC: M_n = 2032, M_w = 2057, PDI = 1.01; TGA (air, 1000°C): Found = 17.2%, Calculated = 16.6%, $T_{d5\%}$ = 420°C.

$NBocStyr_{16}OPS$: 4-NBocstyrene = 1.50 g; Yield = 86%; Conversion = 100%; MALDI-ToF (as $NH_2Styr_{16}OPS$): m/z = 2906.8 ($NH_2Styr_{16}OPS/H^+$, 9%), 3013.9 ($NH_2Styr_{16}OPS/Ag^+$, 91%), Calculated = 3015.7 ($NH_2Styr_{16}OPS/Ag^+$); GPC: M_n = 3749, M_w = 3809, PDI = 1.02; TGA (air, 1000°C): Found = 11.5%, Calculated = 10.2%, $T_{d5\%}$ = 190°C.

$AceStyr_{16}OPS$: 4-acetoxystyrene = 1.61 mL; Yield = 89%; Conversion = 100%; MALDI-ToF: m/z = 3498.4 ($AceStyr_{14}HOStyrOPS/Ag^+$, 3%), 3541.5 ($AceStyr_{15}OPS/Ag^+$, 5%), 3619.5 ($AceStyr_{14}HOStyr_2OPS/Ag^+$, 13%), 3660.6 ($AceStyr_{15}HOStyrOPS/Ag^+$, 19%), 3702.7 ($AceStyr_{16}OPS/Ag^+$, 41%), 3777.9 ($AceStyr_{15}HOStyrOPS/Ag^+$, 2%), 3821.6 ($AceStyr_{16}HOStyrOPS/Ag^+$, 4%), 3862.5 ($AceStyr_{17}OPS/Ag^+$, 5%), 3942.8 ($AceStyr_{16}HOStyr_2OPS/Ag^+$, 2%), 3979.8 ($AceStyr_{17}HOStyr_1OPS/Ag^+$, 2%), 4024.4 ($AceStyr_{18}OPS/Ag^+$, 4%), Calculated = 3704.1 ($AceStyr_{16}OPS/Ag^+$); GPC: M_n = 2542, M_w = 2614, PDI = 1.03; TGA (air, 1000°C): Found = 13%, Calculated = 13.4%, $T_{d5\%}$ = 360°C.

General Heck Reaction of $Br_{24}OPS$.

To a dry 10-mL Schlenk flask under N_2 was added 0.50 g (0.17 mmol, 3.9 mmol-Br) of $Br_{24}OPS$, 22 mg (0.046 mmol)of $Pd[P(t\text{-}Bu_3)]_2$, and 21 mg (0.023 mmol) of $Pd_2(dba)_3$. 1,4-dioxane (3 ml) was then added by syringe, followed by NCy_2Me (6.2 mmol, 1.32 ml) and R-styrene (12 mmol). The mixture was stirred at 70°C for 24 h and then quenched by filtering through 1 cm Celite, which was washed with 5 ml THF. The solution was then precipitated into 200 ml methanol, filtered, and the solid re-dissolved in 10 ml THF. This solution was then filtered again through a 1 cm Celite column to remove any remaining Pd particles, and re-precipitated into 200 ml methanol. The product is collected via suction filtration and dried in vacuo.

$MeStyr_{24}OPS$: 4-methylstyrene = 1.88 mL; Yield = 84%; Conversion = 99%; MALDI-ToF: m/z = 3697 ($MeStyr_{22}OPS/Ag^+$, 20%), 3776 ($MeStyr_{22}BrOPS/Ag^+$, 5%), 3812 ($MeStyr_{23}OPS/Ag^+$, 45%), 3891 ($MeStyr_{23}BrOPS/Ag^+$, 6%), 3928 ($MeStyr_{24}OPS/Ag^+$, 23%) Calculated = 3813.1 ($MeStyr_{23}OPS/Ag^+$); GPC: M_n = 2522, M_w = 2565, PDI = 1.01; TGA (air, 1000°C): Found = 13.5%, Calculated = 13 %, $T_{d5\%}$ = 385°C.

$NBocStyr_{24}OPS$: 4-NBocstyrene = 2.48 g; Yield = 80%; Conversion = 99%; GPC: M_n = 4290, M_w = 4390, PDI = 1.02; TGA (air, 1000°C): Found = 7%, Calculated = 8%, $T_{d5\%}$ = 185°C.

$AceStyr_{24}OPS$: 4-acetoxystyrene = 1.83 g; Yield = 79%; Conversion = 99%; GPC: M_n = 3593, M_w = 3893, PDI = 1.08; TGA (air, 1000°C): Found = 5.7%, Calculated = 10.2%, $T_{d5\%}$ = 345°C.

Removal of Residual Pd catalyst.

To a dry 50-mL Schlenk flask under N_2 was added 1.0 g of $RStilbene_xOS$ dissolved in 10 mL of toluene and 0.1 g of *N*-acetyl-*L*-cysteine dissolved in 1 mL of THF. The solution was stirred overnight at room temperature and then filtered through a short silica gel column to remove the insoluble Pd-cysteine complex. The filtrate was then concentrated by rotary evaporation and precipitated into 200 mL of methanol or hexane. The product was filtered and dried in vacuo overnight.

Deprotection of $NBocStilbene_xOS$.

To a dry vial under N_2 was added 10 mg of $NBocStilbene_xOS$ dissolved in 1 mL of THF and 1 mL of 37% HCl solution. The reaction was stirred overnight at room temperature. The reaction was then neutralized with saturated $NaHCO_3$ solution and extracted with CH_2Cl_2 (3 x 10 mL). The combined organic layer was washed with DI H_2O (3 x 10 mL), dried over Na_2SO_4, and the solvent evaporated in vacuo to give light brown solid as product.

2.3.3 Fluoride Ion-Catalyzed Rearrangement of PVSQ and PMSQ

Synthesis of Polymethylsilsesquioxane (PMSQ).

To a dry 100-mL 1-necked round-bottomed flask was added 20 mL (0.14 mol) of methyltrimethoxysilane and 40 mL of ethanol, followed by 10 mL (0.12 mol) or 37% HCl solution. The reaction solution was stirred at room temperature under N_2 gas for 72 h, during which a white solid was formed. The product was then collected via suction filtration, washed with ether (3 x 10 mL), and then dried in vacuo. Yield = 90%; FT-IR (KBr): $\nu_{C\text{-}H}$ (2971, 1408 cm^{-1}), $\nu_{Si\text{-}C}$ (1271 cm^{-1}), $\nu_{Si\text{-}O\text{-}Si}$ (1121, 1035 cm^{-1}).

PMSQ dissolution.

To a dry 50-mL 1-necked round-bottomed flask was added 1.0 g (14.4 mmol $MeSiO_{1.5}$) PMSQ and 20 mL THF, followed by 0.4 mL (0.4 mmol) 1.0 M nBu$_4$NF solution in THF. The mixture was stirred at room temperature under N_2 for 48 h. Undissolved material was then filtered off from the solution and $CaCl_2$ (0.3 g) was added to the filtrate to quench the F- catalyst. The mixture was stirred for 3-4 h and then the solid was removed by filtration. The product was collected by removing the solvent in vacuo or by precipitation into cold methanol. Yield = 25%; MALDI-ToF (Ag^+): m/z = 739 [$Me_9Si_9O_{12}(OH)_3$], 781 ($Me_{10}T_{10}$); GPC: M_n = 575, M_w = 578, PDI = 1.00; FT-IR (KBr) : $\nu_{C\text{-}H}$ (2970, 1413 cm^{-1}), $\nu_{Si\text{-}C}$ (1270 cm^{-1}), $\nu_{Si\text{-}O\text{-}Si}$ (1123 cm^{-1}).

Synthesis of Vinyl$_{10}$T$_{10}$ and Vinyl$_{12}$T$_{12}$ cages from Polyvinylsilsesquioxane (PVSQ)

To a 100-mL 1-necked round-bottomed flask was added 5g (63.0 mmol $ViSiO_{1.5}$) PVSQ and 50 mL THF, followed by 0.5 mL (0.5 mmol) 1.0 M nBu$_4$NF solution in THF. The reaction solution was stirred at room temperature under N_2 for 24 h. $CaCl_2$ (1.5 g) was then added to quench the F- catalyst. The mixture was stirred for 3-4 h and then the solid was removed by filtration. The filtrate was concentrated by rotary evaporation and then precipitated into 100 mL of cold methanol. The product was collected by suction filtration and dried in vacuo. Yield = 92%; MALDI-ToF (Ag^+): m/z = 898.7 ($Vi_{10}T_{10}$), 1056.7 ($Vi_{12}T_{12}$); GPC: M_n = 1062, M_w = 1196, PDI = 1.13.

General Synthesis of T_8, T_{10} and T_{12} cages from Polyvinylsilsesquioxane (PVSQ) and Polymethylsilsesquioxane (PMSQ).

To a 100-mL 1-necked round-bottomed flask was added PVS, solvent, and 1.0 M nBu$_4$NF solution in THF. The reaction solution was stirred at room temperature under N_2 until all PVSQ was dissolved. PMSQ was then added to the reaction solution and the mixture was stirred for 48 h at room temperature or refluxed for 6 h. Undissolved material was then filtered off from the solution and $CaCl_2$ (0.3 g) was added to the filtrate to quench the F- catalyst. The mixture was stirred for 3-4 h and then the solid was removed by filtration. The product was collected by removing the solvent in vacuo or by precipitation into cold methanol. All yields are based on mass of material recovered from the soluble fraction.

PMSQ concentration effect:

Experiment 1. PVSQ = 1 g (12.6 mmol), PMSQ = 0.87 g (12.6 mmol), nBu$_4$NF = 0.4 ml, (0.4 mmol), THF = 20 ml, room temperature/48 h. Yield = 80%; MALDI-ToF (Ag^+): m/z = 691 ($Me_4Vi_4T_8$), 703 ($Me_3Vi_5T_8$), 715 ($Me_2Vi_6T_8$), 852 ($Me_4Vi_6T_{10}$), 864 ($Me_3Vi_7T_{10}$), 876 ($Me_2Vi_8T_{10}$), 998 ($Me_5Vi_7T_{12}$), 1010 ($Me_4Vi_8T_{12}$), 1022 ($Me_3Vi_9T_{12}$), 1024 ($Me_2Vi_{10}T_{12}$) ; GPC: M_n = 779, M_w = 789, PDI = 1.01; FT-IR (KBr): $\nu_{C\text{-}H(Me)}$ (2959, 1408 cm^{-1}), $\nu_{C\text{-}H(Vi)}$ (3061, 1487 cm^{-1}), $\nu_{C=C}$ (1602 cm^{-1}), $\nu_{Si\text{-}C}$ (1273 cm^{-1}), $\nu_{Si\text{-}O\text{-}Si}$ (1120 cm^{-1}).

Experiment 2. PVSQ = 1 g (12.6 mmol), PMSQ = 0. 4.36 g (63mmol), nBu$_4$NF = 0.4 ml, (0.4 mmol), THF = 30 ml, room temperature/48 h. Yield = 87%; MALDI-ToF (Ag^+): m/z = 679 ($Me_5Vi_3T_8$), 691 ($Me_4Vi_4T_8$), 703 ($Me_3Vi_5T_8$), 715 ($Me_2Vi_6T_8$), 827 ($Me_6Vi_4T_{10}$), 837 ($Me_5Vi_5T_{10}$), 848 ($Me_4Vi_6T_{10}$), 972 ($Me_7Vi_5T_{12}$), 984 ($Me_6Vi_6T_{12}$), 997 ($Me_5Vi_7T_{12}$) ; GPC: M_n = 760, M_w = 770, PDI = 1.01; FT-IR (KBr): $\nu_{C\text{-}H(Me)}$ (2969, 1408 cm^{-1}), $\nu_{C\text{-}H(Vi)}$ (3061 cm^{-1}), $\nu_{C=C}$ (1602 cm^{-1}), $\nu_{Si\text{-}C}$ (1272 cm^{-1}), $\nu_{Si\text{-}O\text{-}Si}$ (1118 cm^{-1}).

Solvent effect:

Experiment 3. PVSQ = 1 g (12.6 mmol), PMSQ = 4.36 g (63 mmol), nBu$_4$NF = 0.4 ml (0.4 mmol), toluene = 30 ml, room temperature/48 h. Yield = 30%. MALDI-ToF (Ag^+):

m/z = 741 (Vi_8T_8), 899 ($Vi_{10}T_{10}$), 1057 ($Vi_{12}T_{12}$), 1690 ($Vi_{20}T_{20}$); GPC: M_n = 762, M_w = 773, PDI = 1.01. FT-IR (KBr): $\nu_{C\text{-}H(Me)}$ (2958, 1409 cm^{-1}), $\nu_{C\text{-}H(Vi)}$ (3061, 3023 cm^{-1}), $\nu_{C=C}$ (1602 cm^{-1}), $\nu_{Si\text{-}C}$ (1274 cm^{-1}), $\nu_{Si\text{-}O\text{-}Si}$ (1126, 1047 cm^{-1}).

Experiment 4. PVSQ = 1 g (12.6 mmol), PMSQ = 1.74 g (25 mmol), *n*Bu_4NF = 0.4 ml (0.4 mmol), THF = 20 ml, and ethanol = 20 ml, room temperature/48 h. Yield = 50%; GPC: M_n = 835, M_w = 847, PDI = 1.02; MALDI-ToF (Ag^+): m/z = 739 (Vi_8T_8), 899 ($Vi_{10}T_{10}$), 1057 ($Vi_{12}T_{12}$), 1690 ($Vi_{20}T_{20}$).

Experiment 5. PVSQ = 1 g (12.6 mmol), PMSQ = 1.74 g (25 mmol), *n*Bu_4NF = 0.4 ml (0.4 mmol), THF = 25 ml and ethanol = 6.25 ml, room temperature/48 h. Yield = 52%; MALDI-ToF (Ag^+): m/z = 828 ($Me_6Vi_4T_{10}$), 850 ($Me_4Vi_6T_{10}$), 862 ($Me_3Vi_7T_{10}$), 874 ($Me_2Vi_8T_{10}$), 996 ($Me_5Vi_7T_{12}$), 1009 ($Me_4Vi_8T_{12}$), 1020 ($Me_3Vi_9T_{12}$); FT-IR (KBr): $\nu_{C\text{-}H(Me)}$ (2972, 1409 cm^{-1}), $\nu_{C\text{-}H(Vi)}$ (3061 cm^{-1}), $\nu_{C=C}$ (1602 cm^{-1}), $\nu_{Si\text{-}C}$ (1272 cm^{-1}), $\nu_{Si\text{-}O\text{-}Si}$ (1133, 1036 cm^{-1}).

Experiment 6. PVSQ =1 g (12.6 mmol), PMSQ = 1.74 g (25 mmol), *n*Bu_4NF = 0.4 ml (0.4 mmol), THF = 6.25 ml and ethanol = 25 ml. Yield = 33 %; MALDI-ToF (Ag^+): m/z = 793 ($Me_9Vi_1T_{10}$), 899 ($Vi_{10}T_{10}$), 973 ($Me_7Vi_5T_{12}$), 1057 ($Vi_{12}T_{12}$).

Temperature effect.

Experiment 7. PVSQ = 1 g (12.6 mmol), PMSQ = 1.74 g (25 mmol), *n*Bu_4NF = 0.4 ml (0.4 mmol), and THF = 20 ml, reflux/6 h. Yield = 75%; MALDI-ToF (Ag^+): m/z = 729 ($Me_1Vi_7T_8$), 739 (Vi_8T_8), 793 ($Me_9Vi_1T_{10}$), 861 ($Me_3Vi_7T_{10}$), 899 ($Vi_{10}T_{10}$), 997 ($Me_5Vi_7T_{12}$), 1009 ($Me_4Vi_8T_{12}$), 1021 ($Me_3Vi_9T_{12}$), 1057 ($Vi_{12}T_{12}$); GPC: M_n = 721, M_w = 739, PDI = 1.03; FT-IR (KBr): $\nu_{C\text{-}H(Me)}$ (2959, 1409 cm^{-1}), $\nu_{C\text{-}H(Vi)}$ (3061, 3023 cm^{-1}), $\nu_{C=C}$ (1602 cm^{-1}), $\nu_{Si\text{-}C}$ (1273 cm^{-1}), $\nu_{Si\text{-}O\text{-}Si}$ (1122, 1044 cm^{-1}).

2.3.4 Silsesquioxane-based Epoxy Resins

Preparation of OAPS/TGMX Resins (N = 0.5)

OAPS (0.45 g, 3.13 mmol of $-NH_2$), tetraglycidyl-*m*-xylene (TGMX, 0.49 g, 6.25 mmol of epoxy) and THF (10 mL) were added to a vial equipped with a magnetic stir bar and stirred until a homogeneous solution is formed. The solvent was then removed by vacuum, and the mixture poured into a circular PTFE mold, which was then placed in the oven at 50°C overnight under N_2 atmosphere to remove residual solvent. The system is then heated at 20°C/hr to 200°C and cured for 20 hr. The cured resin was then cooled to room temperature and used to make samples for CTE measurements.

Preparation of OAPS/TGMX Resins (N = 1.0)

OAPS (0.80 g, 5.56 mmol of $-NH_2$), tetraglycidyl-*m*-xylene (TGMX, 0.56 g, 5.56 mmol of epoxy) and THF (10 mL) were added to a vial equipped with a magnetic stir bar and stirred until a homogeneous solution is formed. The solvent was then removed by vacuum, and the mixture poured into a circular PTFE mold, which was then placed in the oven at 50°C overnight under N_2 atmosphere to remove residual solvent. The system is then heated at 20°C/hr to 200°C and cured for 20 hr. The cured resin was then cooled to room temperature and used to make samples for CTE measurements.

Preparation of OAPS/TGMX Resins (N = 1.0) with 10 wt% Al_2O_3

OAPS (0.80 g, 5.56 mmol of $-NH_2$), tetraglycidyl-*m*-xylene (TGMX, 0.56 g, 5.56 mmol of epoxy), and THF (10 mL) were added to a vial equipped with a magnetic stir bar and stirred until a homogeneous solution is formed. Al_2O_3 (1.4g) was added to the solution and the mixture was ultrasonicated to dispersed the nanopowder. The solvent was then removed by vacuum, and the mixture poured into a circular PTFE mold, which was then placed in the oven at 50°C overnight under N_2 atmosphere to remove residual solvent. The system is then heated at 20°C/hr to 200°C and cured for 20 hr. The cured resin was then cooled to room temperature and used to make samples for CTE measurements.

Preparation of OAPS/ECHX Resins (N = 0.5)

OAPS (0.45 g, 3.13 mmol of $-NH_2$), 3,4-epoxycyclohexylmethyl-3,4-epoxycyclohexanecarboxylate (ECHX, 0.79 g, 6.25 mmol of epoxy), and THF (10 mL) were added to a vial equipped with a magnetic stir bar and stirred until a homogeneous solution is formed. The solvent was then removed by vacuum, and the mixture poured into a circular PTFE mold, which was then placed in the oven at 50°C overnight under N_2 atmosphere to remove residual solvent. The system is then heated at 20°C/hr to 200°C and cured for 20 hr. The cured resin was then cooled to room temperature and used to make samples for CTE measurements.

Preparation of OAPS/ECHX Resins (N = 1.0)

OAPS (0.80 g, 5.56 mmol of $-NH_2$), 3,4-epoxycyclohexylmethyl-3,4-epoxycyclohexanecarboxylate (ECHX, 0.79 g, 5.56 mmol of epoxy), and THF (10 mL) were added to a vial equipped with a magnetic stir bar and stirred until a homogeneous solution is formed. The solvent was then removed by vacuum, and the mixture poured into a circular PTFE mold, which was then placed in the oven at 50°C overnight under N_2 atmosphere to remove residual solvent. The system is then heated at 20°C/hr to 200°C and cured for 20 hr. The cured resin was then cooled to room temperature and used to make samples for CTE measurements.

Preparation of OAPS/DGEBA Resins (N = 0.5)

OAPS (0.45 g, 3.13 mmol of $-NH_2$), DGEBA (1.16 g, 6.25 mmol of epoxy), and THF (10 mL) were added to a vial equipped with a magnetic stir bar and stirred until a homogeneous solution is formed. The solvent was then removed by vacuum, and the mixture poured into a circular PTFE mold, which was then placed in the oven at 50°C overnight under N_2 atmosphere to remove residual solvent. The system is then heated at 20°C/hr to 200°C and cured for 20 hr. The cured resin was then cooled to room temperature and used to make samples for CTE measurements.

Preparation of OAPS/DGEBA Resins (N = 1.0)

OAPS (0.80 g, 5.56 mmol of $-NH_2$), DGEBA (1.03 g, 5.56 mmol of epoxy), and THF (10 mL) were added to a vial equipped with a magnetic stir bar and stirred until a homogeneous solution is formed. The solvent was then removed by vacuum, and the mixture poured into a circular PTFE mold, which was then placed in the oven at 50°C overnight under N_2 atmosphere to remove residual solvent. The system is then heated at 20°C/hr to 200°C and cured for 20 hr. The cured resin was then cooled to room temperature and used to make samples for CTE measurements.

Preparation of OAPS/OG Resins (N = 0.5)

OAPS (0.45 g, 3.13 mmol of $-NH_2$), OG (1.61 g, 6.25 mmol of epoxy), and THF (10 mL) were added to a vial equipped with a magnetic stir bar and stirred until a homogeneous solution is formed. The solvent was then removed by vacuum, and the mixture poured into a circular PTFE mold, which was then placed in the oven at 50°C overnight under N_2 atmosphere to remove residual solvent. The system is then heated at 20°C/hr to 200°C and cured for 20 hr. The cured resin was then cooled to room temperature and used to make samples for CTE measurements.

Preparation of OAPS/OG Resins (N = 1.0)

OAPS (0.80 g, 5.56 mmol of $-NH_2$), OG (1.43 g, 5.56 mmol of epoxy), and THF (10 mL) were added to a vial equipped with a magnetic stir bar and stirred until a homogeneous solution is formed. The solvent was then removed by vacuum, and the mixture poured into a circular PTFE mold, which was then placed in the oven at 50°C overnight under N_2 atmosphere to remove residual solvent. The system is then heated at 20°C/hr to 200°C and cured for 20 hr. The cured resin was then cooled to room temperature and used to make samples for CTE measurements.

Preparation of OAPS/OC Resins (N = 0.5)

OAPS (0.45 g, 3.13 mmol of $-NH_2$), OC (1.69 g, 6.25 mmol of epoxy), and THF (10 mL) were added to a vial equipped with a magnetic stir bar and stirred until a homogeneous solution is formed. The solvent was then removed by vacuum, and the mixture

poured into a circular PTFE mold, which was then placed in the oven at 50°C overnight under N_2 atmosphere to remove residual solvent. The system is then heated at 20°C/hr to 200°C and cured for 20 hr. The cured resin was then cooled to room temperature and used to make samples for CTE measurements.

Preparation of OAPS/OC Resins (N = 1.0)

OAPS (0.80 g, 5.56 mmol of $-NH_2$), OC (1.51 g, 5.56 mmol of epoxy), and THF (10 mL) were added to a vial equipped with a magnetic stir bar and stirred until a homogeneous solution is formed. The solvent was then removed by vacuum, and the mixture poured into a circular PTFE mold, which was then placed in the oven at 50°C overnight under N_2 atmosphere to remove residual solvent. The system is then heated at 20°C/hr to 200°C and cured for 20 hr. The cured resin was then cooled to room temperature and used to make samples for CTE measurements.

References Cited:

i. Harrison, P.G.; Hall, C. "Preparation and Characterization of Octasilsesquioxane Cage Monomers." *Main Group Met. Chem*. **1997**, *20*, 515-529.

2. Roll, M.F.; Mathur, P.; Takahashi,K.; Kampf, J.W.; Laine, R.M. "$[PhSiO_{1.5}]_8$ Promotes Self-Bromination to Produce $[o\text{-}BrPhSiO_{1.5}]_8$. Further Bromination Gives Crystalline $[2,5\text{-}Br_2PhSiO_{1.5}]_8$ with a Density of 2.38 g/cc and Calculated Refractive Index of 1.7 (RI of Sapphire is 1.76) or the Tetraisocosa Bromo Compound $[Br_3PhSiO_{1.5}]_8$, submitted to *J. Mater. Chem.*.

3. Tamaki, R.; Tanaka, Y.; Asuncion, M.Z.; Choi, J.; Laine, R.M. "Octa(aminophenyl)-silsesquioxane as a Nanoconstruction Site." *J. Am. Chem. Soc.* **2001**, *123*, 12416-12417.

4. Sellinger, A.; Laine, R.M. "Silsesquioxanes as Synthetic Platforms. 3. Photocurable, Liquid Epoxides as Inorganic/Organic Hybrid Precursors." *Chem. Mater*. **1996**, *8*, 1592-1593.

5. Choi, J.; Yee, A.F.; Laine, R.M. "Organic/Inorganic Hybrid Composites from Cubic Silsesquioxanes. Epoxy Resins of Octa(dimethylsiloxycyclohexylepoxide) Silsesquioxane." *Macromol*. **2003**, *36*, 5666-5682.

6. Laatsch, H.; Pudleiner, H. "Marine Bacteria. I. Synthesis of Pentabromopseudilin, a Cytotoxic Phenylpyrrole from Alteromonas Luteoviolaceus." *Leibigs Ann. Chem*. **1989**, 863-881.

7. Bezou, P.; Hilberer, A.; Hadziioannou, G. “Efficient Synthesis of *p*-Vinyl-*trans*-Stilbene.” *Synthesis* **1996**, *4*, 449-451.

8. Kessler, A.; Coleman, C.M.; Charoenying, P.; O’Shea, D.F. “Indole Synthesis by Controlled Carbolithiation of *o*-Aminostyrenes.” *J. Org. Chem*. **2004**, *69*, 7836-7846.

9. Crosby, G.A.; Demas, J.N. “The Measurement of Photoluminescence Quantum Yields. A Review.” *J. Phys. Chem*. **1971**, *75*, 991-1024.

10. *Standards for Fluorescence Spectrometry,* J.N. Miller Ed.; Chapman and Hall: London, 1981.

11. Hamai, S.; Hirayama, F. "Actinometric Determination of Absolute Fluorescence Quantum Yields." *J. Phys. Chem*. **1983**, *87*, 83-89.

12. Maciejewski, A.; Steer, R.P. ”Spectral and Photophysical Properties of 9,10-Diphenylanthracene in Perfluoro-n-hexane: The Influence of Solute-Solvent Interactions.” *J. Photochem.* **1986**, *35*, 59-69.

13. Xu, C.; Webb, W.W. “Measurement of Two-Photon Excitation Cross Sections of Molecular Fluorophores with Data from 690 to 1050 nm.” *J. Opt. Soc. Am. B* **1996**, *13*, 481-491.

14. Ahn, Y.M.; Yang, K.L.; Georg, G.I. “A Convenient Method for the Efficient Removal of Ruthenium Byproducts Generated during Olefin Metathesis Reactions.” *Org. Lett*. **2001**, *3*, 1411-1413.

Chapter 3

Elaboration of Octavinylsilsesquioxane via Cross-Metathesis and Heck Reactions to Form Luminescent Star Molecules

Published in Chemistry of Materials vol. 20, pp. 5563-5573, 2008.

With contributions from Ms. Jin Zhang and Professor Ted Goodson III (Macromolecular Science and Engineering Center and Chemistry Department, University of Michigan).

Abstract

Octavinylsilsesquioxane (OVS, $[VinylSiO_{1.5}]_8$) with perfect 3-D or cubic symmetry is elaborated through metathesis with substituted styrenes to produce a series of RStyrenylOS compounds. *p*-BrStyrenylOS is then further reacted with other sets of *p*-substituted styrenes via Heck coupling to produce a set of R'VinylStilbeneOS compounds. NH_2VinylStilbeneOS is then reacted with 3,5-dibromo- or dinitro-benzoyl chloride to produce hexadecafunctional 3-D stars. These synthetic methods provide perfect single core and then core-shell 3-D stars, including branch points in the third generation, such that these molecules can be used for the synthesis of new dendrimers or hyperbranched molecules. Furthermore, the second set of materials is fully conjugated. Investigation of the UV-Vis, emission and two-photon absorption properties of R'VinylStilbeneOS, especially where R' = NH_2, reveals exceptional red shifts (120 nm), CT behavior, and excellent two photon absorption properties that may suggest that the silsesquioxane cage serves the role of electron acceptor in the system.

3.1 Introduction

There is widespread interest in developing building blocks for constructing materials with architectures tailored at nanometer length scales.[1-5] The ability to assemble materials at such length scales should provide high reproducibility of global properties and the opportunity to precisely predict and fine-tune those properties.[6-10] There is the potential to identify new properties in nano-scale building blocks not available in the bulk, which can then be used to create entirely new materials by ordering these nano-components over large length scales or simply using them as is.[10,11]

In principle, nanometer-sized molecules with high symmetry, functionality and a means to modify that functionality at will to aid in assembling 1-, 2- or 3-D structures nanometer by nanometer would seem to offer the best potential for complete control of properties over all length scales. To this end, molecules with cubic symmetry could be exceptional candidates to develop routes to well-defined, molecular nanobuilding blocks.

To date, only the cubane family of compounds and cubic silsesquioxanes (Q_8 ($RO\text{-}SiO_{1.5})_8$ and T_8 $(RSiO_{1.5})_8$) offer the requisite symmetry.[8,9,12-42] Of these, only the silsesquioxanes are easily prepared in large quantities and readily octafunctionalized. A further advantage is the single crystal silica cage, which provides the heat capacity of silica making these systems unusually robust.[36] The 3-D symmetry also provides materials that are very soluble and therefore easily purified by standard methods.

In this paper, motivated by work by Marciniec et al,[43] Feher et al,[44] and Sellinger et al[45] on octavinylsilsesquioxane (OVS, $[vinylSiO_{1.5}]_8$), our efforts target the development of nano-building blocks for nanoconstruction, but also access to 3-D stars with cubic symmetry built on OVS cores. We report here, as illustrated in Scheme **3.1**, functionalization of OVS with functionalized styrenes via cross-metathesis reactions, forming the first generation star materials, octa(RStyrenyl)silsesquioxane (RStyrenylOS). A variety of R groups are used to demonstrate the versatility of this reaction.

Octa(*p*-bromostyrenyl)silsesquioxane (BrStyrenylOS) is further functionalized via Heck reactions with functionalized styrenes to give octa(R'vinylstilbene)silsesquioxane (R'VinylStilbeneOS, second generation) stars (Scheme **3.3**). A further goal of the work initiated here is to methodically explore the luminescence properties of these materials based on the initial findings of Sellinger et al,[45] who are the only researchers to examine

the luminescence properties of silsesquioxanes where the cage is conjugated to the organic lumiphore. Finally, octa(*p*-aminovinylstilbene)silsesquioxane (NH_2Vinyl-StilbeneOS) is reacted with difunctional benzoylchlorides (Scheme **3.3**) to give octa(R"$_2$benzamide-vinylstilbene)silsesquioxane (R"$_2$BenzamideOS), third generation molecules with increased functional group density and potential for further functionalization and branching.

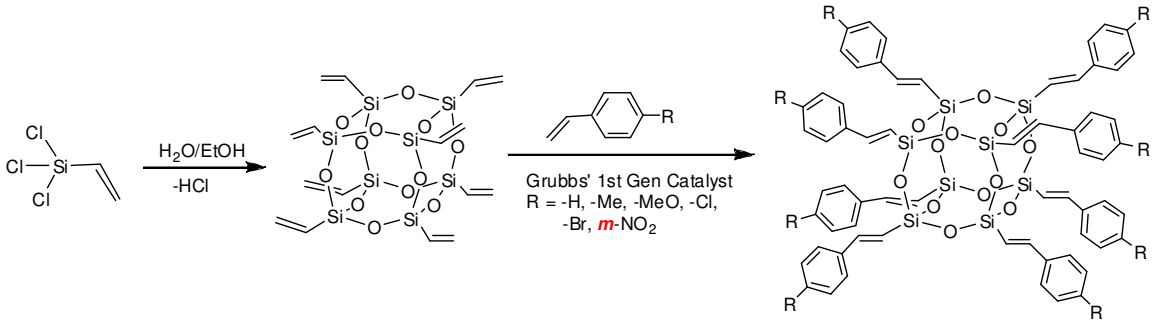

Scheme 3.1. Synthesis of OVS (30-40 % yield) and RStyrenylOS.

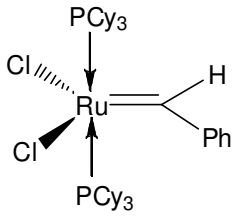

Figure 3.1. Grubbs catalyst, 1st generation.[46]

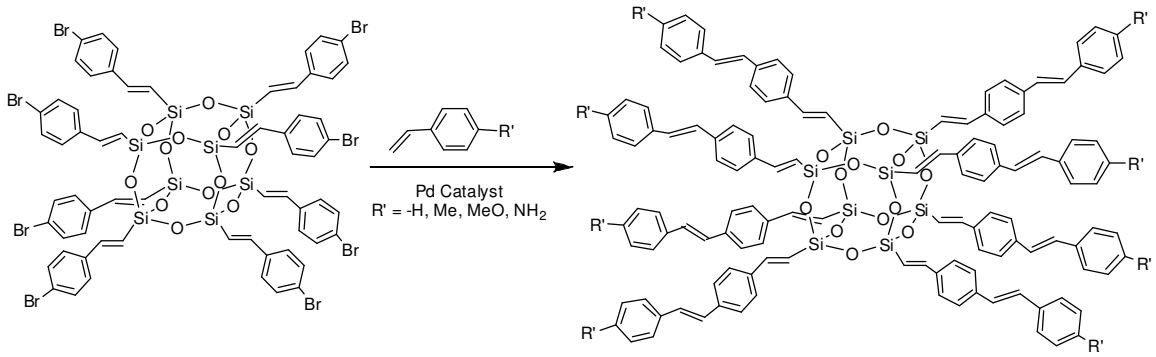

Scheme 3.2. Synthesis of R'VinylStilbeneOS from BrStyrenylOS.

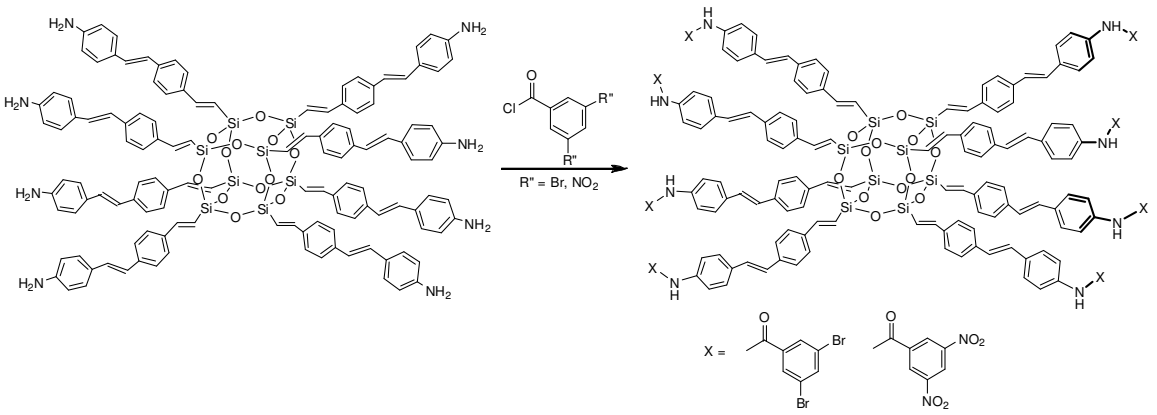

Scheme 3.3. Synthesis of R"$_2$BenzamideOS from NH_2VinylStilbeneOS.

3.2 Experimental Procedures

The synthetic methods and characterization techniques are described in Chapter 2, along with more detailed experimental data.

3.3 Results and Discussion

The objectives of the work undertaken here were: (1) to explore the utility of combining methathesis and Heck chemistry to produce perfect, conjugated core-shell stars from OVS; (2) to realize functionality in the first and second shells for further elaboration; (3) develop general synthetic routes to branch points providing access to octa- and hexadecafunctional 3-D cores as starting points for the synthesis of more complex stars, dendrimers, or hyperbranched molecules and nanostructured materials there from and (4) to investigate the photoluminescence properties of these novel system for comparison with more highly conjugated appended aromatics as described by Sellinger et al.[45]

In the following sections, we discuss the synthesis and characterization of these materials and their photoluminescence properties in order of their complexity starting with the RStyrenylOS systems followed R'VinylStilbenes and ending with hexadecafunctionalized R"$_2$BenzamideOS stars.

3.3.1 Synthetic Methods

Cross-metathesis reactions were carried out using commercially available functionalized styrenes and 1st generation Grubbs catalyst.[46] The reaction mixture was stirred for 72

h to ensure complete conversion of the vinyl groups. Since metathesis is an equilibrium reaction, the reaction can be driven to > 99% conversion of OVS to RStyrenylOS by blowing a gentle stream of N_2 above the reaction mixture to remove ethylene formed.

Heck coupling reactions of BrStyrenylOS were run using R-styrenes having functional groups with different electron-donor groups using a 2:1 molar mixture of Pd[P(*t*-Bu_3)]$_2$ and $Pd_2(dba)_3$ as the catalyst system.[56]

NH_2VinylStilbeneOS was acylated with 3,5-difunctional (NO_2- or Br-) benzoyl chloride using standard procedure to provide the first examples of a branch point at the ends of the star arms. The nitro derivative can be reduced to the amino derivative, which then introduces 16 functional groups as a first generation 3-D dendrimer as will be reported later. The bromo derivatives should permit further functionalization via various coupling reactions. They also can serve as 3-D cores for dendrimer materials.

3.3.2 Solubilities

RStyrenylOS and R'VinylStilbeneOS are soluble in various organic solvents such as THF, toluene, dioxane, CH_2Cl_2, and $CHCl_3$. R"$_2$BenzamideOS are soluble in polar solvents such as THF and DMSO.

3.3.3 Molecular Characterization of RStyrenylOS, R'VinylStilbeneOS, and R"$_2$BenzamideOS

MALDI-ToF data for first and second generation stars are given in Tables **3.1** (RStyrenylOS) and **3.2** (R'VinylStilbeneOS). Figure **3.2** provides representative spectra for RStyrenylOS. With the exception of MeStyrenylOS, all RStyrenylOS are perfectly octasubstituted. For R'VinylStilbeneOS, no double Heck reactions on BrStyrenylOS akin to those targeted by Sellinger et al[45] are observed, due to the large excess of R-styrene used. We were not able to obtain MALDI-ToF data for R"$_2$BenzamideOS, but ^{1}H- and ^{13}C-NMR spectra of these compounds confirm their complete conversion from their parent material (NH_2VinylStilbeneOS).

GPC analyses are presented in Tables **3.1**-**3.3**. These materials exhibit narrow molecular weight distributions, indicating that they retain their silsesquioxane cage structures. The values of M_n and M_w as measured by GPC are smaller than the molecular

weight measured by MALDI-TOF, but expected from GPC characterization of rigid, spherical molecules using flexible, linear standards, based on previous results.[36]

Table 3.1. MALDI-ToF and GPC data for RStyrenylOS.

R group	m/z (Ag^+ adduct)		GPC			
	MALDI-ToF	Calc.	M_n	M_w	FW	PDI
H	1349.2	1349.7	1025	1034	1241.8	1.01
p-Me (octamer)	1461.6	1461.9	1257	1278	1354.0	1.02
p-MeO	1589.1	1589.9	1262	1283	1482.0	1.02
p-Cl	1626.8	1625.2	1387	1403	1517.4	1.01
p-Br	1981.3	1980.8	1321	1350	1872.0	1.02
m-NO_2	1710.1	1709.7	1561	1607	1601.8	1.03

Table 3.2. MALDI-ToF and GPC data for R'VinylStilbeneOS.

R' group	m/z (Ag^+ adduct)		GPC			
	MALDI-ToF	Calc.	M_n	M_w	FW	PDI
H	2162.7	2166.7	1511	1597	2058.9	1.06
p-Me	2279.9	2279.0	1775	1876	2171.1	1.06
p-MeO	2404.6	2406.9	1880	2096	2299.1	1.12
p-NH_2	2287.6	2286.9	1374	1549	2179.0	1.13

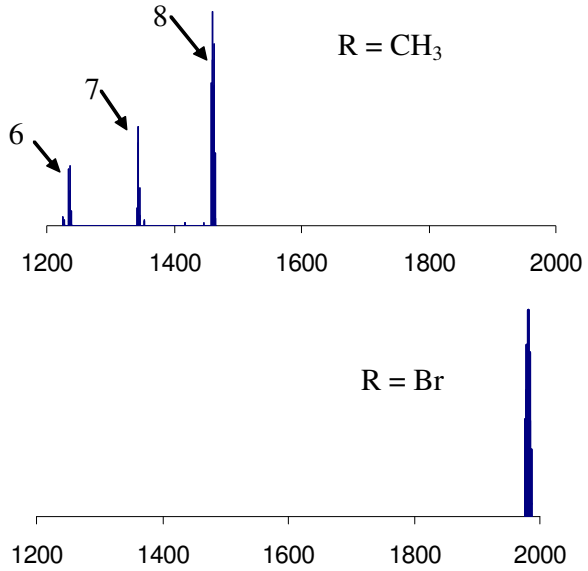

Figure 3.2. MALDI-TOF spectra for RStyrenylOS. Octasubstitution was observed for all RStyrenylOS except a. MeStyrenylOS, b. BrStyrenylOS shown for comparison.

TGA were run in air at heating rates of 10°C/min. Figures **3.3**-**3.5** show the TGA traces for RStyrenylOS, R'VinylStilbeneOS and R"$_2$BenzamideOS, respectively. All of

RStyrenylOS are stable in air to > 300°C, with the exception of MeStyrenylOS, due to the presence of the *p*-methyl group which should readily oxidize given its benzylic structure. HStyrenylOS has the highest thermal stability, as expected from its completely aromatic structure.

Table 3.3. TGA and melting point data for RStyrenylOS.

R group	Ceramic yield (%)		$T_{d5\%}$ (^oC)	T_m (^oC,N_2)
	Actual	Calc.		
H	38.6	38.7	395	270
p-Me (octamer)	33.5	35.5	283	315
p-MeO	33.6	32.4	323	345
p-Cl	31.5	31.7	362	310
p-Br	25.7	25.6	318	330
m-NO_2	29.8	30.0	331	n.a.

Table 3.4. TGA data for R'VinylStilbeneOS.

R' group	Ceramic yield (%)		$T_{d5\%}$ (^oC)
	Actual	Calc.	
H	23.4	23.8	400
p-Me	22.1	21.1	390
p-MeO	20.9	22.6	315
p-NH_2	22.1	20.1	345

Table 3.5. Characterization data for R"$_2$BenzamideOS.

R" group	GPC				Ceramic yield (%)		$T_{d5\%}$ (^oC)
	M_n	M_w	FW	PDI	Actual	Calc.	
NO_2	2003	2089	3087.8	1.04	10.5	12.9	170
Br	2178	2533	3155.6	1.16	10.5	11.2	335

The same trend in thermal decomposition is also observed with the second generation materials. With the exception of the amino derivative, the rest of R'VinylStilbeneOS are air stable to > 300^{o}C. The amino derivative exhibits a mass gain at ~250^{o}C, which might arise from oxidation of the amino groups. $(NO_2)_2$BenzamideOS exhibits a lower onset of mass loss, 170°C, likely because of loss of the nitro groups. Table **3.5** summarizes the decomposition temperatures and ceramic yields for R"$_2$BenzamideOS. As can be seen from the calculated and actual ceramic yields, the compositions of the compounds are in keeping with the MALDI-ToF and GPC data.

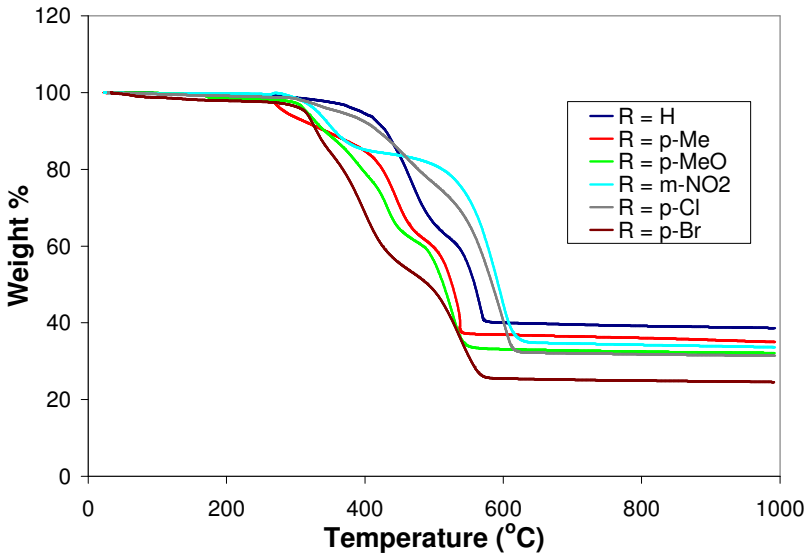

Figure 3.3. TGA data in air (10°C/min) for RStyrenylOS.

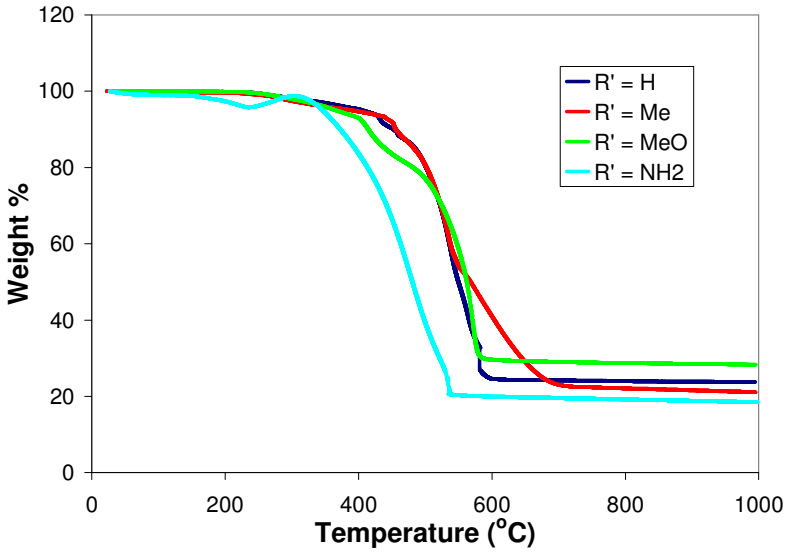

Figure 3.4. TGA data in air (10°C/min) for R'VinylStilbeneOS.

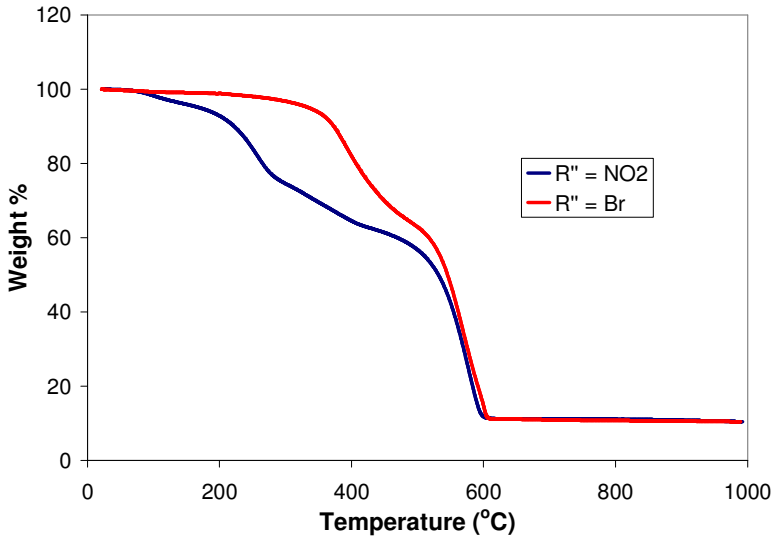

Figure 3.5. TGA data in air (10°C/min) for R"$_2$BenzamideOS

^{29}Si-NMR data for selected compound can be found in Appendix **1** (Table **A1.3**, **A1.6**, and **A1.9**). All of the decoupled spectra show a single resonance at ~ -78 ppm, which indicates that (a) all of the silicon atoms in each silsesquioxane cage are magnetically equivalent and (b) the magnetic environment around the silicon atoms does not change from the first generation compounds to the second and third generation compounds. This is expected since the different functional groups on the styrenyl moieties of the first generation compounds are too far away from the silicon atoms to influence their magnetic environment. The different functional groups on the second and third generation compounds are even farther away from the silicon atoms, and as such do not have an influence on the silicon atoms' magnetic environment.

3.3.4 Thermal Behavior of HStyrenylOS

It occurred to us that having a silica cage with pendant styrene groups might permit the polymerization of these groups to form a very novel, highly crosslinked polystyrene with perfectly dispersed, monosized nano-silica particles within the polystyrene matrix in considerable contrast to every other type of filled polystyrene.[48,49]

The first step in these studies was to run DSCs as illustrated in Figure **3.6** for HStyrenylOS. The first heating cycle traces for HStyrenylOS show endotherms near 210°C and 260°C but no exotherms on cooling. These endotherms disappear in a second cycle

(red trace). Hot stage optical microscopy shows that these materials melt over a range of 240-280°C.

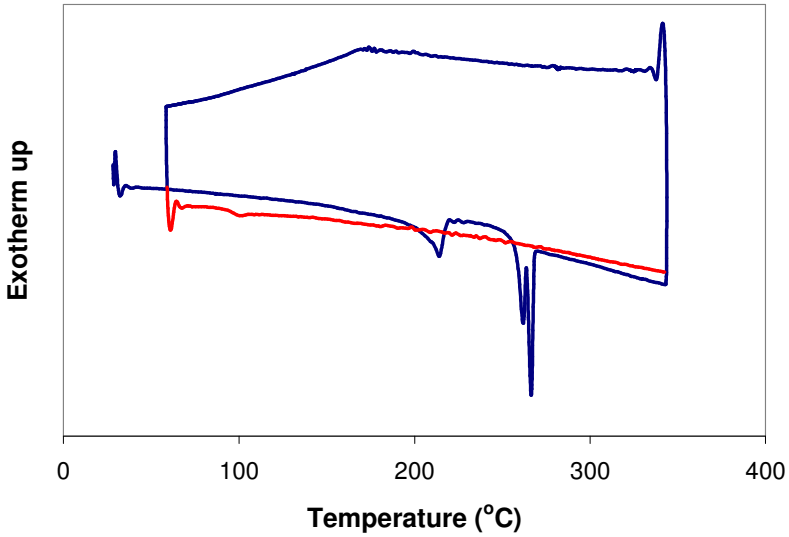

Figure 3.6. DSC thermogram of HStyrenylOS. Red trace indicates second heating cycle.

X-ray diffraction patterns (Figure **3.7**) of HStyrenylOS before and after heating to 300°C show that the molten material does not crystallize on cooling leading to the essentially amorphous XRD. This also explains the absence of any exotherms in the cooling cycle and the endotherms in the second heating cycle in the DSC. FTIR spectra (Figure **3.8**) of the material before and after heating to 300°C do not show any distinct differ-

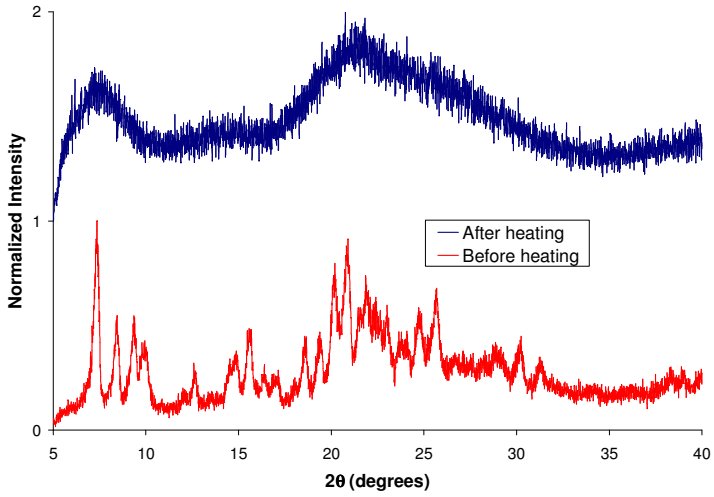

Figure 3.7. X-ray diffraction pattern of HStyrenylOS before and after heating to 300°C.

ences. This leads us to conclude that crystalline HStyrenylOS melts but does not polymerize, and upon cooling forms an amorphous phase.

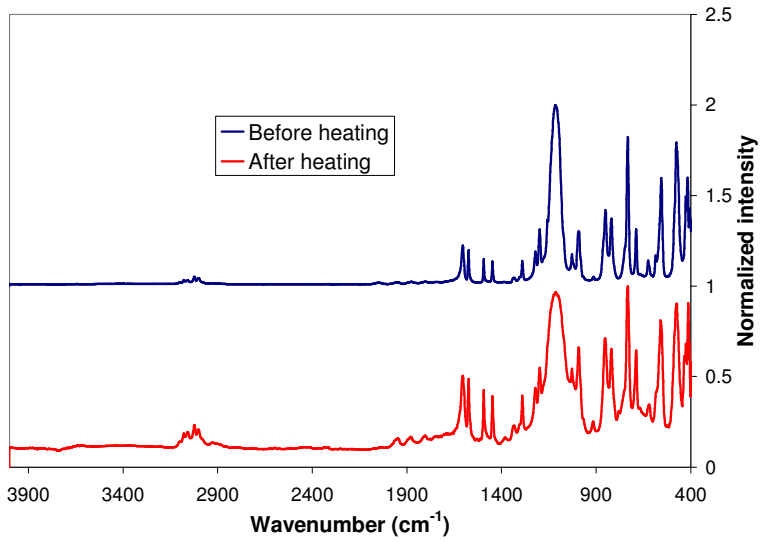

Figure 3.8. FTIR spectra of HStyrenylOS before and after heating to 300°C.

As seen in Figure **3.9**, the $T_{d5\%}$ value for polystyrene is ~ 290°C whereas that for polymerized HStyrenylOS is 400°C. This > 100°C increase in oxidative stability could arise for a number of reasons. First, the very uniform dispersion of silica nanoparticles within HStyrenylOS provides significant added heat capacity thereby limiting oxidative degra-

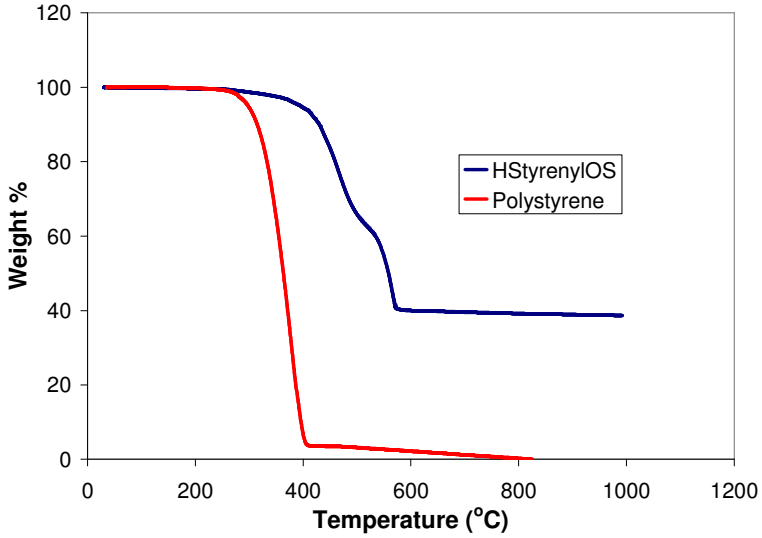

Figure 3.9. Decomposition of HStyrenylOS and polystyrene (TGA in air, 10°C/min).

dation. Second, as the organic material is oxidized away from the surface, the remaining residue becomes enriched in silica and provides a barrier to further oxidation. Similar observations have been made for silsesquioxane-enriched materials exposed to atomic oxygen.[15]

3.3.5 Photophysical Properties

UV-Vis absorption and photoluminescence (PL) of RStyrenylOS and R'VinylStilbeneOS in THF are shown in Figures **3.10** and **3.11**. Both the absorption and emission spectra show red-shifts from the corresponding small molecule analogues (styrene and *p*-vinylstilbene) untethered to the silsesquioxane cage. RStyrenylOS show smaller red-shifts than R'VinylStilbeneOS (10-40 nm shifts vs 30-80 nm shifts). This is expected because the conjugation lengths for the R'VinylStilbeneOS compounds are twice those of the RStyrenylOS compounds. Within both series of compounds, the red-shifts from the small molecules become larger as the functional groups at the silsesquioxane's vertex become more electron-donating. The photoluminescence from NH_2VinylStilbeneOS is quenched on reaction with 3,5-difunctional benzoyl chlorides.

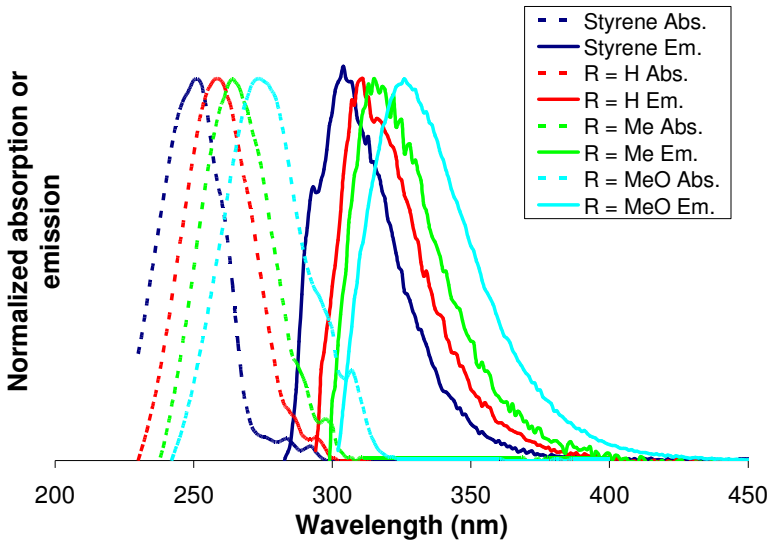

Figure 3.10. UV absorption and PL emission of RStyrenylOS in THF.

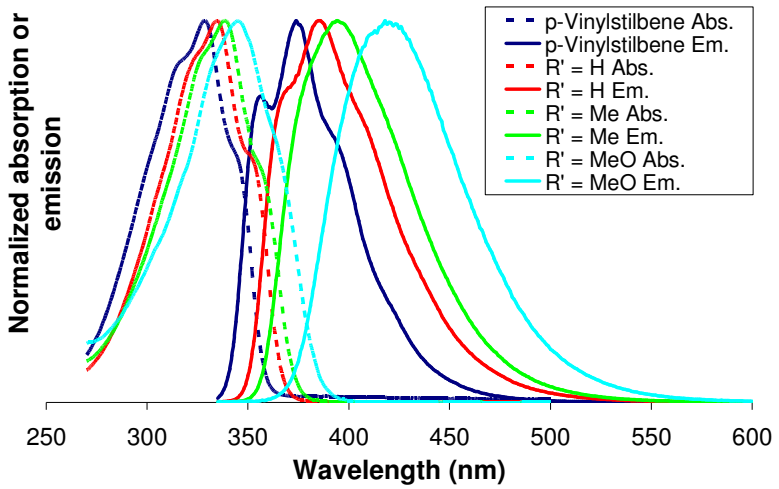

Figure 3.11. UV-Vis and PL spectra of R'VinylStilbeneOS in THF.

The absorption and emission spectra of HStyrenylOS and HVinylStilbeneOS (shown in Figure **3.12)** allow us to compare the photophysical properties of the first and second generation materials. The two sets of materials demonstrate similar Stokes shifts of ~50 nm. Both absorption and emission spectra for R'VinylStilbeneOS are red-shifted ~70 nm from those for RStyrenylOS. The spectra show normal 0-0 transitions typical for conjugated aromatic compounds suggesting that the silica cage has little influence other than the slight red shifts compared with the organic compounds alone.

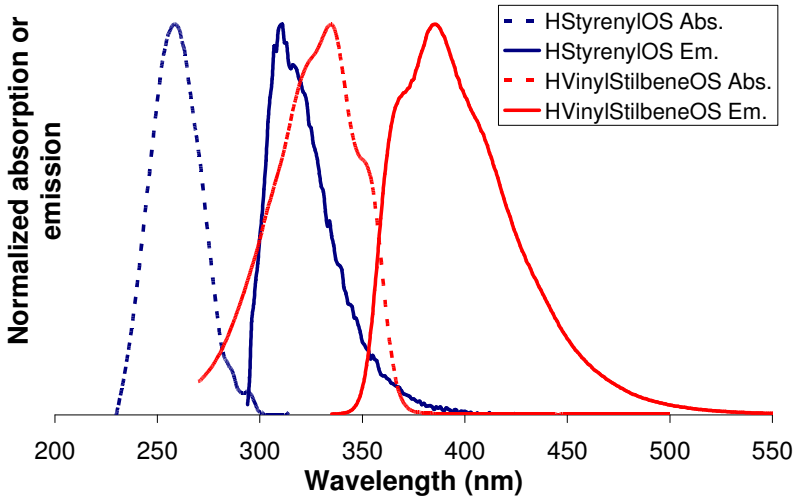

Figure 3.12. UV-Vis and PL spectra of HStyrenylOS and HVinylStilbeneOS.

The PL quantum yields (Φ_{PL}'s) for RStyrenylOS are very low, as observed from the need to characterize their PL behavior using samples from UV-Vis absorption measurements without dilution. Φ_{PL}'s for R'VinylStilbeneOS were measured at 320 nm at high dilution to avoid the formation of aggregates in solution. Φ_{PL}'s were calculated using anthracene and 9,10-diphenylanthracene as standards.[51-53] Their values are shown in Table **3.6**. The observed Φ_{PL} for HVinylStilbeneOS is 36%, which is comparable to that measured for the corresponding small molecule, *p*-vinylstilbene. The measured Φ_{PL} for NH_2VinylStilbeneOS is six times lower as a result of charge transfer (CT) effects in the solution, which partially funnel the energy away from luminescence but greatly improve the two-photon cross-section (see Table **3.6** and Figure **3.13**) which led to the two photon studies as follows.

3.3.6 Two Photon Cross-Section Studies

Molecular components assembled in a well-defined three dimensional geometry can potentially lead to novel electronic, optical and nonlinear optical properties. Among nonlinear optical properties, two-photon absorption (TPA, a third order optical nonlinearity) has received tremendous research attention in recent years because of their applications in different areas of science.[54] Several molecular architectures such as branched,[55-58] dendritic,[59,60] macrocyclic topologies[61,62] have shown enhanced TPA cross-sections over their linear counterparts. It has also been shown that when the chromophores are decorated on silver nanoparticles, there is a strong electronic coupling between the chromophores and thereby enhancing the nonlinear optical properties.[63] However when the chromophores are adsorbed on a nanoparticle it is difficult to judge the orientation and geometry of chromophore on the nanoparticle. If the chromophores are covalently attached to a known three dimensional geometry, it is easy to understand the influence of the molecular orientation as well as charge transfer character on the two-photon absorption properties. To this effect, we have investigated the two-photon absorption properties of the donor-acceptor derivatives of selected R'VinylStilbeneOS shown in Scheme **3.2** using methods described in the experimental section.

3.3.6.1 Steady-State Measurements

As noted above the absorption and emission spectra of the investigated systems dissolved in THF are shown in Figure **3.11**. The corresponding optical properties are summarized in Table **3.6**. It can be noted from the figure that the absorption spectrum of the more polar derivative (NH_2VinylStilbeneOS) shows structureless and red-shifted absorption when compared to the less polar ones (HVinylStilbeneOS and MeOVinylStilbeneOS) suggesting the involvement of a charge transfer transition.

It can also be observed from Figure **3.11** and Table **3.6** that the Stoke's shift increases with increases in the strength of donor (from HVinylStilbeneOS to NH_2VinylStilbeneOS) suggesting an increased charge transfer character. The reduction of the quantum yield from HVinylStilbeneOS to NH_2VinylStilbeneOS is also in accordance with the increased charge transfer character of the chromophores. It will be interesting to observe how the arrangement of chromophores and the charge transfer character influence the two-photon absorption properties as will be explored at a later date.

3.3.6.2 Two-Photon Absorption Measurements

TPA cross-sections as a function of wavelength are plotted in Figure **3.13** for all the investigated chromophores. It is clear from the TPA cross-sections that the cross-section

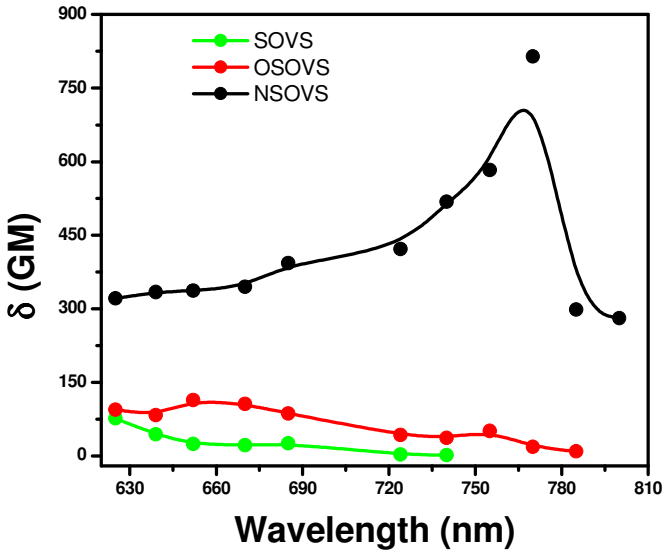

Figure 3.13. Two photon cross-section of R'VinylStilbeneOS where R' = -H (SOVS), -MeO (OSOVS), -NH_2 (NSOVS).

increases with the increases in donor-strength on the chromophore. It can also be noted that the cross-section per molecule has also increased (Table **3.6**) and it is increased by 35 times when the donor is changed from HVinylStilbeneOS to NH_2VinylStilbeneOS. This 35 fold increase of TPA cross-section can be explained by increased change in dipole-moment term (major factor responsible in sum-over states formalism).[62-64]

Table 3.6. Spectral data of RStyrenylOS and R'VinylStilbeneOS.

Compound	UV λ_{max} (nm)	PL λ_{max} (nm)	Φ_{PL} (%)	Stokes shift $\Delta\nu$ (cm^{-1})	δ (GM) @780 nm	δ/group (GM)
HStyrenylOS	260	311	n.a.			
MeStyrenylOS	265	315	n.a.			
MeOStyrenylOS	275	326	n.a.			
Styrene	251	304	n.a.			
HVinylStilbeneOS	335	385	36	3966	25	3.1
MeVinylStilbeneOS	338	394	22			
MeOVinylStilbeneOS	345	418	16	4947	110	13.8
NH_2VinylStilbeneOS	358	482	6	6458	810	101
p-Vinylstilbene	329	374	24			

3.3.7 Solvent-Dependence of Emission Spectra

The identification of the CT behavior in NH_2VinylStilbeneOS motivated efforts to explore the effects of solvent polarity on its emission behavior. Figure **3.14** provides UV-Vis and emission data for MeVinylStilbeneOS in several solvents while Figure **3.15** records the same type of data for NH_2VinylStilbeneOS. What is immediately apparent is

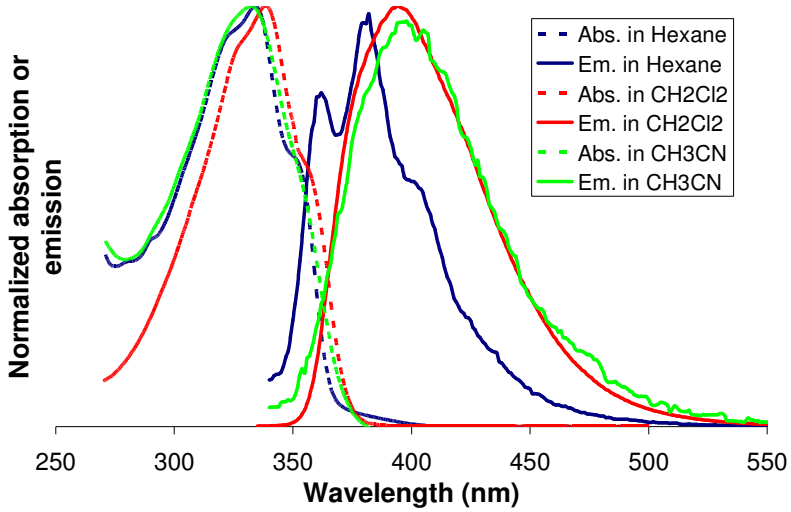

Figure 3.14. UV-Vis and emission data for MeVinylStilbeneOS in three solvents.

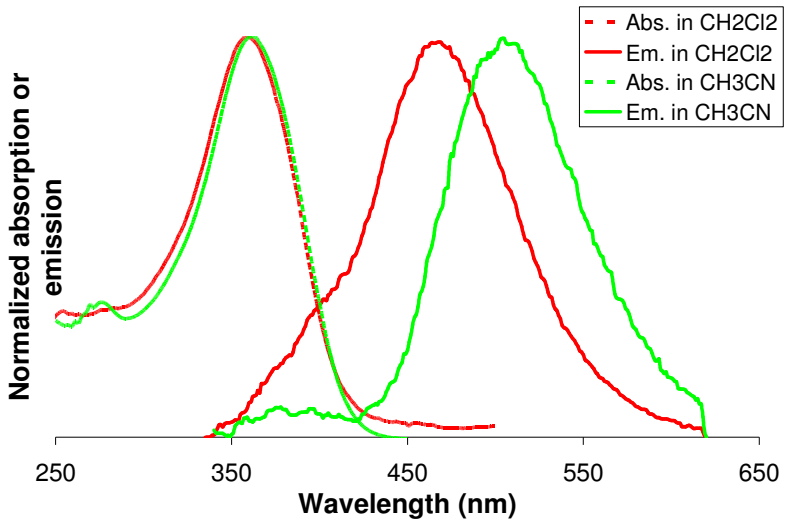

Figure 3.15. UV-Vis and emission data for NH_2VinylStilbeneOS in two good solvents.

that while the red shifts seen for MeVinylStilbeneOS are modest with changes in solvent polarity, those of NH_2VinylStilbeneOS are quite large by comparison. The extent of the shift is more impressive when considered against the shifts of all of these molecules as a function of solvent polarity. A search of the literature provides a better perspective of the degree of shift observed. Table **3.7** lists sets of representative organic molecule UV-Vis and emission properties as a function of solvent and type of substitution.

The simplest member of this system, stilbene, absorbs at 307 nm (in CH_3CN) and emits at 350 nm. The addition of a *p*-vinyl group shifts these values to 325 and 369 nm in the same solvent. Attaching a *p*-vinylstilbene group to the silsesquioxane cage (HVinyl-StilbeneOS), leads to a red shift (331 and 388 nm) of less than 10 nm in the same solvent. The addition of a *p*-CH_3 group causes a nominal red shift in the UV-Vis absorption from the parent HVinylStilbeneOS and a 20 nm shift in emission, to 398 nm, with essentially no change in luminescence quantum efficiencies. However, the addition of a *p*-CH_3O group shifts the UV-Vis about 10 nm from the parent HVinylStilbeneOS but results in a 40 nm red shift in the emission maximum to 430 nm. Most surprising of all is that addition of a *p*-NH_2 group red shifts the UV-Vis by 30 nm from the parent HVinylStilbeneOS but shifts the emission by 120 nm in the same solvent.

Table 3.7. Spectral data of RStyrenylOS and R'VinylStilbeneOS as a function of solvent and two photon cross-sections of selected compounds

Compound	UV λ_{max} (nm)	PL λ_{max} (nm)	Solvent	Φ_{PL} %	Ref
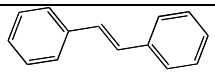	307	350	CH_3CN		64
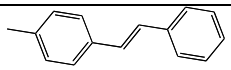	311	354	CH_3CN		64
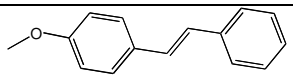	318	375	CH_3CN		64
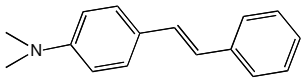	347 349 352 348 351	379 407 418 433 440	Hexane, Et_2O BuCl EtOH CH_3CN		65 65 65 65 65
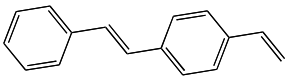	324 329 325	370 374 369	Hexane CH_2Cl_2 CH_3CN	24	66 66 66
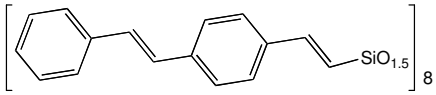	329 335 331	375 385 388	Hexane CH_2Cl_2 CH_3CN	36	66 66 66
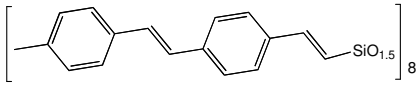	335 338 334	384 394 398	Hexane CH_2Cl_2 CH_3CN	22	66 66 66
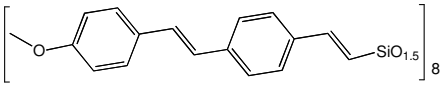	339 345 343	378 418 **431**	Hexane CH_2Cl_2 CH_3CN	12	66 66 66
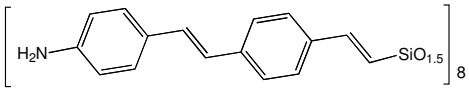	358 361	482 **507**	CH_2Cl_2 CH_3CN	6	66 66

There have now been several modeling studies of octasilsesquioxane cages, $[RSiO_{1.5}]_8$ (R = H, F, HO, NH_2 alkyl, etc), done by multiple groups, which suggest HOMO-LUMO band gaps that range between 5 and 7 eV, typical of insulators.[67-72] The majority of these studies find that the HOMO involves 2p lone pair states of A_{2g} symmetry on the oxygen atoms, Figure **3.16a**. Likewise they also find that the LUMO has $4A_1$ symmetry and involves contributions from all silicon, oxygen atoms and the organic substituents, is spherical, and resides in the cage center, Figure **3.16b**.[67-72] This "core" state is highly electrophilic and may influence emission behavior.

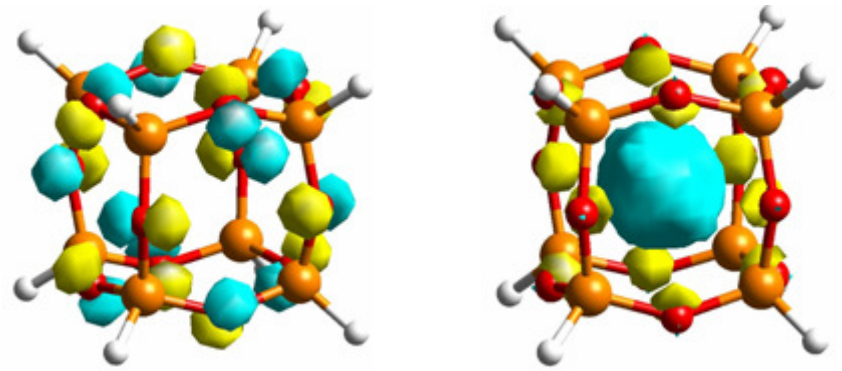

Figure 3.16. HOMO and LUMO of $[XSiO_{1.5}]_{8.}$[72]

In a previously published paper,[72] we have shown that, for stilbene-functionalized silsesquioxane, the energy difference between the lowest unoccupied core state of the silsesquioxane cage (core LUMO) and the HOMO (π-state on stilbene) is 4.23 eV, and that between the π and π* states of the stilbene tethers is 2.61 eV. Marsmann et al[68] have shown that the calculated band gap of $[RSiO_{1.5}]_8$ cage are approximately 1.6eV higher than experimental values. This suggests that the actual band gap between the core LUMO and the HOMO of $[StilbeneSiO_{1.5}]_8$ is closer to 2.6 eV, similar to that for the stilbene tethers, which means that the cage-centered or "core" orbital may be of the same energy as the excited state of the stilbene, leading to possible 3-D conjugation through the cage.

Bassindale et al[73,74] recently synthesized silsesquioxane cage with encapsulated F^- and suggest that their stability may be enhanced by interaction with a low lying LUMO within the cage, suggesting that the idea is not novel to us and further supporting our proposed explanation. In contrast, Pach et al[75] recently studied and modeled the behavior of H^+ and D^+ in $[HSiO_{1.5}]_8$ and $[MeSiO_{1.5}]_8$ cages. They find that "…H is more stable outside the cage.", indirectly agreeing with Bassindale and with previous theoretical findings that the interior is electrophilic.

Consequently, one interpretation of the data obtained for NH_2VinylStilbeneOS would be that the highly electrophilic core LUMO acts as a strong acceptor for the CT electron from the amine group. This means that the silsesquioxane cage is actually able to interact electronically with the conjugated vinyl stilbene and can no longer be considered as a classical insulating silica cage. Second, if the LUMO is indeed 3-D, then all eight vinyl-

stilbene groups may interact simultaneously setting the stage for some form of 3-D electronic interactions. Efforts to develop 3-D luminescent molecules have been discussed in the literature recently.[76-79]

3.4 Conclusions

The current work suggests that cubic silsesquioxanes offer unique opportunities to build new types of 3-D molecular structures around a nanometer size octafunctional core with cubic symmetry. The chemistries explored here were meant only to be representative of the many diverse simple and complex molecular structures that can be created using these simple cages as a basic starting point. It is also clear that these compounds offer unique properties in their own rights as witnessed by the novel luminescence properties that may suggest 3-D conjugation in the excited state and in the formulation of nanocomposites with important new properties as evidenced by the polymerized styrenyl cage materials.

References Cited:

1. Seidel, S.R.; Stang, P.J. "High-Symmetry Coordination Cages via Self-Assembly." *Acc. Chem. Res.* **2002**, *35*, 972-983.
2. Addicott, C.; Das, N.; Stang, P.J. "Self-Recognition in the Coordination Driven Self-Assembly of 2-D Polygons." *Inorg. Chem.* **2004**, *43*, 5335-5338.
3. Stewart, M.D.; Willson, C.G. "Imprint Materials for Nanoscale Devices." *MRS Bulletin* **2005**, *30*, 947-951.
4. Levins, C.G.; Schafmeister, C.F. "The Synthesis of Functional Nanoscale Molecular Rods of Defined Length." *J. Am. Chem. Soc.* **2003**, *125*, 4702-4703.
5. Yaghi, O.M.; Li, H.; Davis, C.; Richardson, D.; Groy, T.L. "Synthetic Strategies, Structure Patterns, and Emerging Properties in the Chemistry of Modular Porous Solids." *Acc. Chem. Res.* **1998**, *31*, 474-484.
6. Lanznaster, M.; Heeg, M.J.; Yee, G.T.; McGarvey, B.R.; Verani, C.N. "Design of Molecular Scaffolds Based on Unusual Geometries for Magnetic Modulation of Spin-Diverse Complexes with Selective Redox Response." *Inorg. Chem.* **2007**, *46*, 72-78.
7. Laine, R.M.; Choi, J.; Lee, I. "Organic-Inorganic Nanocomposites with Completely Defined Interfacial Interactions." *Adv. Mater.* **2001**, *13*, 800-803.
8. Eaton, P.E. "Cubanes: Starting Materials for the Chemistry of the 1990s and the New Century." *Angew. Chem. Int. Ed. Eng.* **1992**, *31*, 1421-1436.

9. Roll, M.F.; Asuncion, M.Z.; Kampf, J.; Laine, R.M. "*para*-Octaiodophenylsilsesquioxane, $[p\text{-}IC_6H_4SiO_{1.5}]_8$, a Nearly Perfect Nano-Building Block." *ACS Nano* **2008**, *2*, 320-326.

10. Morin, J.-F.; Shirai, Y.; Tour, J.M. "En Route to a Motorized Nanocar." *Org. Lett.* **2006**, *8*, 1713-1716.

11. Sasaki, T.; Osgood, A.J.; Alemany, L.B.; Kelly, K.F.; Tour, J.M. "Synthesis of a Nanocar with an Angled Chassis. Toward Circling Movement." *Org. Lett.* **2008**, *10*, 229-232.

12. Detken, A.; Zimmerman, H.; Haeberlen, U.; Poupko, R.; Luz, Z. "Molecular Reorientation and Self-Diffusion in Solid Cubane by Deuterium and Proton NMR." *J. Phys. Chem.* **1996**, *100*, 9598-9604.

13. Yildrim, T.; Gehring, P.M.; Neumann, D.A.; Eaton, P.E.; Emrick, T. "Solid Cubane: A Brief Review." *Carbon* **1998**, *36*, 809-815.

14. For reviews see: (a) Voronkov, M.G.; Lavrent'yev, V.I. "Polyhedral Oligosilsesquioxanes and Their Homo Derivatives." *Top. Curr. Chem.* **1982**, *102*, 199-236. (b) Baney, R.H.; Itoh, M.; Sakakibara, A.; Suzuki, T. "Silsesquioxane." *Chem. Rev.* **1995**, *95*, 1409-1430. (c) Provatas, A.; Matisons, J.G. "Silsesquioxanes: Synthesis and APplications." *Trends Polym. Sci.* **1997**, *5*, 327-333. (d) Loy, D.A.; Shea, K.J. "Bridged Polysilsesquioxanes. Highly Porous Hybrid Organic-Inorganic Materials." *Chem. Rev.* **1995**, *95*, 1431-1442. (e) Lichtenhan, J. "Silsesquioxane-based Polymers." In *Polymeric Materials Encyc.*; Salmone, J.C., Ed.; CRC Press: N.Y., 1996; Vol. 10; pp. 7768-7777. (f) Laine, R.M. "Nanobuilding Blocks Based on the $[OSiO_{1.5}]_x$ (x = 6,8,10) Octasilsesquioxanes." *J. Mater. Chem.*, **2005**, 3725-3744. (g) Calzaferri, G. "Octasilsesquioxanes." In *Tailor-Made Silicon-Oxygen Compounds, from Molecules to Materials*; Corriu, R. and Jutzi, P., Eds.; Friedr. Vieweg & Sohn mbH: Braunschweig/Wiesbaden, Germany, 1996; pp. 149-169.

15. (a) Lichtenhan, J.D.; Vu, H.Q.; Carter, J.A.; Gilman, J.W.; Feher, F.J. "Silsesquioxane-Siloxane Copolymers from Polyhedral Silsesquioxanes." *Macromol.* **1993**, *26*, 2141-2142. (b) Gilman, J.W.; Schlitzer, D.S.; Lichtenhan, J.D. "Low Earth Orbit Resistant Siloxane Copolymers." *J. Appl. Poly. Sci.* **1996**, *60*, 591-596. (c) Gonzalez, R.I.; Phillips, S.H.; Hoflund, G.B. "In Situ Oxygen-Atom Erosion Study of Polyhedral Oligomeric Silsesquioxane-Siloxane Copolymer." *J. Spacecraft and Rockets* **2000**, *37*, 463-467.

16. (a) Weidner, R.; Zeller, N.; Deubzer, B.; Frey, V. "Organooligosilsesquioxanes." U.S. Patent 5,047,492, Sept. 1991. (b) Dathe, S.; Popowski, E.; Sonnek, G.; Feiher, T.; Jancke, H.; Schelm, U. "Organophilic Double-Ring Silicilic-Acid Derivatives with Cage Structures, Process for Their Preparation and Their Use." Euro. Patent 0,348, 705, A1 1989. (c) Freyer, C.; Wolferseder, J.; Peetz, U. "Organosilicon Compounds Having a Cage-like Structure." Euro. Patent, 0, 624,691 A1 1993.

17. (a) Zhang, Y.; Lee, S.H.; Liang, K.; Toghiani, H.; Pittman, C.U. "Phenolic Resin-Trisilanolphenyl Polyhedral Oligomeric Silsesquioxane (POSS) Hybrid Nanocomposites: Structure and Properties." *Polymer* **2006**, *47*, 2984-2996. (b) Patel, R.R.; Mohanraj, R.; Pittman, C.U. "Properties of Polystyrene and Polymethyl Methacrylate

Copolymers of Polyhedral Oligomeric Silsesquioxanes: A Molecular Dynamics Study." *J. Polym. Sci. B-Polym. Phys*. **2006**, *44*, 234-248. (c) Liang, K.; Li, G.Z.; Toghiani, H.; Koo, J.H.; Pittman, C.U. "Cyanate Ester/Polyhedral Oligomeric Silsesquioxane (POSS) Nanocomposites: Synthesis and Characterization." *Chem. Mater*. **2006**, *18*, 301-312.

18. Stewart, M.D.; Wetzel, J.T.; Schmid, G.M.; Palmieri, F.; Thompson, E.; Kim, E.K.; Wang, D.; Sotodoeh, K.; Jen, K.; Johnson, S.C.; Hao, J.; Dickey, M.D.; Nishimura, Y.; Laine, R.M.; Resnick, D.J.; Willson, C.G. "Direct Imprinting of Dielectric Materials for Dual Damascene Processing." *Proc. SPIE-Int. Soc. Opt. Eng*. **2005**, *5751*, 210-218.

19. (a) Hasegawa, I.; Sakka, S.; Sugahara, Y.; Kuroda, K.; Kato, C. "Silicate Anions Formed in Tetramethylammonium Silicate Methanolic Solutions as Studied by ^{29}Si Nuclear Magnetic Resonance." *J. Chem. Soc., Chem. Comm.* **1989**, 208-210. (b) Hasegawa, I.; Motojima, S. "Dimethylvinylsilylation of $Si_8O_{20}^{8-}$ Silicate Anion in Methanol Solutions of Tetramethylammonium Silicate." *J. Organomet. Chem*. **1992**, *441*, 373-380. (c) Hasegawa, I.; Sakka, S. "Rapid Solidification of (2-Hydroxyethyl)trimethyl-ammonium Silicate." *Chem. Lett.* **1988**, *17*, 1319-1322.

20. Agaskar, P. A. "New Synthetic Route to the Hydridospherosiloxanes O_h-$H_8Si_8O_{12}$ and D_{5h}-$H_{10}Si_{10}O_{15}$." *Inorg. Chem*. **1991**, *30*, 2707-2708.

21. (a) Hoebbel, D.; Endres, K.; Reinert, T.; Pitsch, I. "Inorganic-Organic Polymers Derived from Functional Silicic Acid Derivatives by Additive Reaction." *J. Noncryst. Sol.* **1994**, *176*, 179-188. (b) Hoebbel, D.; Pitsch, I.; Heidmann, D. "Inorganic Organic Polymers with Defined Silicic Acid Units." In *Eurogel '91*; Vilminot, S., Nass, R., and Schmidt, H., Eds.; Elsevier Sci. Publ.: Amsterdam, 1992; pp. 467-473.

22. (a) Hong, B.; Thoms, T.P.S.; Murfee, H.J.; Lebrun, M.J. "Highly Branched Dendritic Macromolecules with Core Polyhedral Silsesquioxane Functionalities." *Inorg. Chem*. **1997**, *36*, 6146-6147. (b) Feher, F.J.; Wyndham, K.D. "Amine and Ester-Substituted Silsesquioxanes: Synthesis, Characterization and Use as a Core for Starburst Dendrimers." *Chem. Comm.* **1998**, 323-324. (c) Dvornic, P.R.; Hartmann-Thompson, C.; Keinath, S.E.; Hill, E.J. "Organic-Inorganic Polyamidoamine (PAMAM) Dendrimer-Polyhedral Oligosilsesquioxane (POSS) Nanohybrids." *Macromol*. **2004**, *37*, 7818-7831.

23. (a) Waddon, A.J.; Coughlin, E.B. "Crystal Structure of Polyhedral Oligomeric Silsesquioxane (POSS) Nano-materials: A Study by X-ray Diffraction and Electron Microscopy." *Chem. Mater*. **2003**, *15*, 4555-4561. (b) Cardoen, G.; Coughlin, E.B. "Hemi-Telechelic Polystyrene-POSS Copolymers as Model Systems for the Study of Well-Defined Inorganic/Organic Hybrid Materials." *Macromol*. **2004**, *37*, 5123-5126.

24. (a) Fu, B.X.; Hsiao, B.S.; White, H.; Rafailovich, M.; Mather, P.; Joen, H.G.; Phillips, S.; Lichtenhan, J.; Schwab, J. "Nanoscale Reinforcement of Polyhedral Oligomeric Silsesquioxane (POSS) in Polyurethane Elastomer." *Poly. Inter*. **2000**, *49*, 437-440. (b) Fu, B.X.; Zhang, W.; Hsiao, B.S.; Rafailovich, M.; Sokolov, J.; Johansson, G.; Sauer, B.B.; Phillips, S.; Blanski, R. "Synthesis and Characterization of Segmented

Polyurethanes Containing Polyhedral Oligomeric Silsesquioxanes Nanostructured Molecules." *High Perform. Polym*. **2000**, *12*, 565-571.

25. (a) Imae, I.; Kawakami, Y. "Unique Photoluminescence Property of a Novel Perfectly Carbazole-Substituted POSS." *J. Mater. Chem*. **2005**, *15*, 4581-4583. (b) Lin, H.-C.; Kuo, S.-W.; Huang, C.-F.; Chang, F.-C. "Thermal and Surface Properties of Phenolic Nancomposites Containing Octaphenyl Polyhedral Oligomeric Silsesquioxane." *Macromol. Rapid Comm*. **2006**, *27*, 537-541.

26. (a) Baker, E.S.; Gidden, J.; Anderson, S.E.; Haddad, T.S.; Bowers, M.T. "Isomeric Structural Characterization of Polyhedral Oligomeric Silsesquioxanes (POSS) with Styryl and Epoxy Phenyl Capping Agents." *Nano Lett*. **2004**, *4*, 779-785. (b) Fu, B.X., Lee, A.; Haddad, T.S. "Styrene-Butadiene-Styrene Triblock Copolymers Modified with Polyhedral Oligomeric Silsesquioxanes." *Macromol*. **2004**, *37*, 5211-5218. (c) Kopesky, E.T.; Haddad, T.S.; Cohen, R.E.; McKinley, G.H. "Thermomechanical Properties of Poly(methyl methacrylate)s Containing Tethered and Untethered Polyhedral Oligomeric Silsesquioxanes." *Macromol*. **2004**, *37*, 8992-9004. (d) Tuteja, A.; Choi, W.; Ma, M.; Mabry, J.M.; Mazella, S.A.; Rutledge, G.C.; McKinley, G.H.; Cohen, R.E. "Designing Superoleophobic Surfaces." *Science* **2007**, *318*, 1618-1622.

27. (a) Kim, G.-M.; Qin, H.; Fang, X.; Sun, F.C.; Mather, P.T. "Hybrid Epoxy-Based Thermosets Based on Polyhedral Oligosilsesquioxane: Cure Behavior and Toughening Mechanisms." *J. Poly. Sci. B-Polym. Phys*. **2003**, *41*, 3299-3313. (b) Kim, B.S.; Mather, P.T. "Amphiphilic Telechelics Incorporating Polyhedral Oligosilsesquioxane: 1. Synthesis and Characterization." *Macromol*. **2002**, *35*, 8378-8384.

28. Sellinger, A.; Laine, R.M. "Silsesquioxanes as Synthetic Platforms. Thermally Curable and Photocurable Inorganic/Organic Hybrids." *Macromol*. **1996**, *29*, 2327-2330.

29. Choi, J.; Harcup, J.; Yee, A.F.; Zhu, Q.; Laine, R.M. "Organic/Inorganic Hybrid Composites from Cubic Silsesquioxanes." *J. Am. Chem. Soc*. **2001**, *123*, 11420-11430.

30. Choi, J.; Yee, A.F.; Laine, R.M. "Organic/Inorganic Hybrid Composites from Cubic Silsesquioxanes. Epoxy Resins of Octa(dimethylsiloxyethylcyclohexylepoxide) Silsesquioxane." *Macromol*. **2003**, *15*, 5666-5682.

31. Tamaki, R.; Tanaka, Y.; Asuncion, M.Z.; Choi, J.; Laine, R.M. "Octa(aminophenyl) silsesquioxane as a Nanoconstruction Site." *J. Am. Chem. Soc*. **2001**, *123*, 12416-12417.

32. (a) Tamaki, R.; Choi, J.; Laine, R.M. "A Polyimide Nanocomposite from Octa-(aminophenyl)silsesquioxane." *Chem. Mater*. **2003**, *15*, 793-797. (b) Choi, J.; Tamaki, R.; Kim, S.G.; Laine, R.M. "Organic/Inorganic Imide Nanocomposites from Aminophenylsilsesquioxanes." *Chem. Mater*. **2003**, *15*, 3365-3375.

33. Neumann, D.; Fisher, M.; Tran, L.; Matisons, J.G. "Synthesis and Characterization of an Isocyanate Functionalized Polyhedral Oligosilsesquioxane and the Subsequent Formation of an Organic-Inorganic Hybrid Polyurethane." *J. Am. Chem. Soc.* **2002**, *124*, 13998-13999.

34. Maitra, P.; Wunder, S.L. "Oligomeric Poly(ethylene oxide)-Functionalized Silsesquioxanes: Interfacial Effects on T_g, T_m, and ΔH_m." *Chem. Mater.* **2002**, *14*, 4494-4497.

35. Mehl, G.H.; Goodby, J.W. "Liquid-Crystalline, Substituted Octakis-(dimethylsiloxy)octasilsesquioxanes: Oligomeric Supermolecular Materials with Defined Topology." *Angew. Chem. Intl. Ed. Engl.* **1996**, *35*, 2641-2643.

36. Brick, C.M.; Ouchi, Y.; Chujo, Y.; Laine, R.M. "Robust Polyaromatic Octasilsesquioxanes from Polybromophenylsilsesquioxanes, Br_xOPS, via Suzuki Coupling." *Macromol.* **2005**, *38*, 4661-4665.

37. Zhang, Z.L.; Horsch, M.A.; Lamm, M.H.; Glotzer, S.C. "Tethered Nano Building Blocks: Toward a Conceptual Framework for Nanoparticle Self-Assembly." *Nano Lett.* **2003**, *3*, 1341-1346.

38. Takahashi, K.; Sulaiman, S.; Katzenstein, J.M.; Snoblen, S.; Laine, R.M. "New Aminophenylsilsesquioxanes – Synthesis, Properties, and Epoxy Nanocomposites." *Aust. J. Chem.* **2006**, *59*, 564-570.

39. Sulaiman, S.; Brick, C.M.; De Sana, C.M.; Katzenstein, J.M.; Laine, R.M.; Basheer, R.A. "Tailoring the Global Properties of Nanocomposites. Epoxy Resins with Very Low Coefficients of Thermal Expansion." *Macromol.* **2006**, *39*, 5167-5169.

40. Asuncion, M.Z.; Laine, R.M. "Silsesquioxane Barrier Materials." *Macromol.* **2007**, *40*, 555-562.

41. Brick, C.M.; Chan, E.R.; Glotzer, S.C.; Martin, D.C.; Laine, R.M. "Self-Lubricating Nano-Ball-Bearings." *Adv. Mater.* **2007**, *19*, 82-86.

42. (a) Takamura, N.; Viculis, L.; Laine, R.M. "Completely Discontinuous Organic/Inorganic Hybrid Nanocomposites by Self-Curing of Nanobuilding Blocks Constructed from Reactions of $[HMe_2SiOSiO_{1.5}]_8$ with Vinylcyclohexene." *Polym. Int.* **2007**, *56*, 1378-1391. (b) Laine, R.M.; Roll, M.; Asuncion, M.; Sulaiman, S.; Popova, V.; Bartz, D.; Krug, D.J.; Mutin, P.H. "Perfect and Nearly Perfect Silsesquioxane (SQs) Nanoconstruction Sites and Janus SQs." *J. Sol-Gel Sci. Tech.* **2008**, *46*, 335-347.

43. (a) Marciniec, B.; Pietraszuk, C. "Synthesis of Unsaturated Organosilicon Compounds via Alkene Metathesis and Metathesis Polymerization." *Current Org. Chem.* **2003**, *7*, 691-735. (b) Kujawa-Welten, M.; Pietraszuk, C.; Marciniec, B. "Cross-Metathesis of Vinylsilanes wtih Allyl Alkyl Ethers Catalyzed by Ruthenium-Carbene Complexes." *Organomet.* **2002**, *21*, 840-845. (c) Itami, Y.; Marciniec, B.; Kubicki, M. "Functionalization of Octavinylsilsesquioxane by Ruthenium-Catalyzed Silylative Coupling versus Cross-Metathesis." *Chem. Eur. J.* **2004**, *10*, 1239-1248.

44. Feher, F.J.; Soulivong, D.; Eklund, A.G.; Wyndham, K.D. "Cross-Metathesis of Alkenes with Vinyl-Substituted Silsesquioxanes and Spherosilicates: A New Method for Synthesizing Highly-Functionalized Si/O Frameworks." *Chem. Comm.* **1997**, 1185.

45. (a) Sellinger, A.; Tamaki, R.; Laine, R.M.; Ueno, K.; Tanabe, H.; Williams, E.; Jabbour, G.E. "Heck Coupling of Haloaromatics with Octavinylsilsesquioxane: Solution Processable Nanocomposites for Application in Electroluminescent Devices." *Chem.*

Comm., **2005**, 3700-3702. (b) Lo, M.Y.; Zhen, C.; Lauters, M.; Jabbour, G.E.; Sellinger, A. "Organic-Inorganic Hybrids Based on Pyrene Functionalized Octavinylsilsesquioxane Cores for Application in OLEDS." *J. Am. Chem. Soc*. **2007**, *129*, 5808-5809.

46. Grubbs, R.H. *Handbook of Metathesis*, Wiley-VCH: Germany, 2003.
47. Littke, A.F.; Fu, G.C. "A Versatile Catalyst for Heck Reactions of Aryl Chlorides and Aryl Bromides under Mild Conditions." *J. Am. Chem. Soc.* **2001**, *123*, 6989-7000.
48. Lee, J.; Hong, C.K.; Choe, S.; Shim, S.E. "Synthesis of Polystyrene/Silica Composite Particles by Soap-Free Emulsion Polymerization Using Positively Charged Colloidal Silica." *J. Colloid Interface Sci.* **2007**, *310*, 112-120.
49. Bachmann, S.; Wang, H.; Albert, K.; Partch, R. "Graft Polymerization of Styrene Initiated by Covalently Bonded Peroxide Groups on Silica." *J. Colloid Interface Sci.* **2007**, *309*, 169-175.
50. Feher, F.J.; Budzichowski, T.A. "Syntheses of Highly-Functionalized Polyhedral Oligosilsesquioxanes." *J. Organomet. Chem.* **1989**, *379*, 33-40.
51. Crosby, G.A.; Demas, J.N. "The Measurement of Photoluminescence Quantum Yields. A Review." *J. Phys. Chem*. **1971**, *75*, 991-1024.
52. *Standards for Fluorescence Spectrometry,* J.N. Miller Ed.; Chapman and Hall, London, 1981.
53. Hamai, S.; Hirayama, F. "Actinometric Determination of Absolute Fluorescence Quantum Yields." *J. Phys. Chem*. **1983**, *87*, 83-89.
54. Albota, M.; Beljonne, D.; Bredas, J.-L.; Ehrlich, J.E.; Fu, J.-Y.; Heikal, A.A.; Hess, S.E.; Kogej, T.; Levin, M.D.; Marder, S.R.; McCord-Maughon, D.; Perry, J.W.; Rockel, H.; Rumi, M.; Subramaniam, G.; Webb, W.W.; Wu, X.-L.; Xu, C. "Design of Organic Molecules with Large Two-Photon Absorption Cross Sections." *Science* **1998**, *281*, 1653-1656.
55. (a) Chung, S.-J.; Kim, K.-S.; Lin, T.-C.; He, G.S.; Swiatkiewicz, J.; Prasad, P.N. "Cooperative Enhancement of Two-Photon Absorption in Multi-branched Structures." *J. Phys. Chem. B* **1999**, *103*, 10741-10745. (b) Wang, Y.; He, G.S.; Prasad, P.N.; Goodson III, T. "Ultrafast Dynamics in Multibranched Structures with Enhanced Two-Photon Absorption." *J. Am. Chem. Soc.* **2005**, *127*, 10128-10129.
56. Bhaskar, A.; Ramakrishna, G.; Lu, Z.; Twieg, R.J.; Hales, J.M.; Hagan, D.J.; Van Stryland, E.; Goodson III, T. "Investigation of Two-Photon Absorption Properties in Branched Alkene and Alkyne Chromophores." *J. Am. Chem. Soc*. **2006**, *128*, 11840-11849.
57. Ramakrishna, G.; Bhaskar, A.; Goodson III, T. "Ultrafast Excited State Relaxation Dynamics of Branched Donor-π-Acceptor Chromophore: Evidence of a Charge-Delocalized State." *J. Phys. Chem. B* **2006**, *110*, 20872-20878.
58. Ramakrishna, G.; Goodson III, T. "Excited-State Deactivation of Branched Two-Photon Absorbing Chromophores: A Femtosecond Transient Absorption Investigation." *J. Phys. Chem. A* **2007**, *111*, 993-1000.

59. Ramakrishna, G.; Bhaskar, A.; Bauerle, P.; Goodson III, T. "Oligothiophene Dendrimers as New Building Blocks for Optical Applications." *J. Phys. Chem. A* **2008**, *112*, 2018-2026.

60. Varnavski, O.P.; Xan, X.; Mongin, O.; Blanchard-Desce, M.; Goodson III, T. "Strongly Interacting Organic Conjugated Dendrimers with Enhanced Two-Photon Absorption." *J. Phys. Chem. C,* **2007** *111*, 149-162.

61. Bhaskar, A.; Ramakrishna, G.; Hagedorn, K.; Varnavski, O.; Osteritz, E.M.; Bauerle, P.; Goodson, T. III. "Enhancement of Two-Photon Absorption Cross-Section in Macrocyclic Thiophenes with Cavities in the Nanometer Regime." *J. Phys. Chem. B* **2007**, *111*, 946-954.

62. Williams-Harry, M.; Bhaskar, A.; Ramakrishna, G.; Goodson III, T.; Imamura, M.; Matawari, A.; Nakao, K.; Enozawa, H.; Nishinaga, T.; Iyoda, M. "Giant Thienylene-Acetylene-Ethylene Macrocycles with Large Two-Photon Absorption Cross Section and Semishape-Persistence." *J. Am. Chem. Soc.* **2008**, *130*, 3252-3253.

63. Varnavski, O.P.; Ranasinghe, M.I.; Yan, X.; Bauer, C.A.: Chuang, S.-J.; Perry, J.W.; Marder, S.R.; Goodson III, T. "Ultrafast Energy Migration in Chromophore Shell-Metal Nanoparticle Assemblies." *J. Am. Chem. Soc.* **2006**, *128*, 10988-10989.

64. Samori, S.; Hara, M.; Tojo, S.; Fujitsuka, M.; Majima, T. "Important Factors for the Formation of Radical Cation of Stilbene and Substituted Stilbenes during Resonant Two-Photon Ionization with a 266- or 355-nm Laser." *J. Photochemistry Photobiology A: Chemistry* **2006**, *179*, 115-124.

65. Letard, J.-F.; Lapouyade, R.; Rettig, W. "Structure-Photophysics Correlation in a Series of 4-(Dialkylamino)stilbenes: Intramolecular Charge Transfer in the Excited State as Related to the Twist around the Single Bonds." *J. Am. Chem. Soc*. **1993**, *115*, 2441-2447.

66. Measured in this work.

67. (a) Calzaferri, G.; Hoffman, R. "The Symmetrical Octasilsesquioxanes $X_8Si_8O_{12}$: Electronic Structure and Reactivity." *J. Chem. Soc. Dalton Trans*., **1991**, 917-928. (b) Schneider, K.S.; Zhang, Z.; Banaszak-Holl, M.M.; Orr, B.G.; Pernisz, U.C. "Determination of Spherosiloxane Cluster Bonding to Si(100)-2 x 1 by Scanning Tunneling Microscopy." *Phys. Rev. Lett.* **2000**, *85*, 602-605.

68. Ossadnik, C.; Veprek, S.; Marsmann, H.C.; Rikowski, E. "Photoluminescent Properties of Substituted Silsesquioxane of the Composition $R_n(SiO_{1.5})_n$." *Monat. fur Chem*. **1999**, *130*, 55-68.

69. Azinovic, D.; Cai, J.; Eggs, C.; Konig, H.; Marsmann, H.C.; Veprek, S. "Photoluminescence from Silsesquioxanes $R_8(SiO_{1.5})_8$." *J. Luminescence* **2002**, *97*, 40-50.

70. (a) Xiang, K.-H.; Pandey, R.; Pernisz, U.C.; Freeman, C. "Theoretical Study of Structural and Electronic Properties of H-Silsesquioxanes." *J. Phys. Chem. B*, **1998**, *102*, 8704-8711. (b) Cheng, W.-D.; Xiang, K.-H.; Pandey, R.; Pernisz, U.C. "Calculations of Linear and Non-Linear Optical Properties of H-Silsesquioxanes." *J. Phys. Chem. B* **2000**, *104*, 6737-6742.

71. Lin, T.; He, C.; Xiao, Y. "Theoretical Studies of Monosubstituted and Higher Phenyl-Substituted Octahydrosilsesquioxanes." *J. Phys. Chem. B* **2003**, *107*, 13788-13792.

72. Laine, R.M.; Sulaiman, S.; Brick, C.; Roll, M.; Tamaki, R.; Asuncion, M.Z.; Neurock, M.; Filhol, J.-S.; Lee, C.-Y.; Zhang, J.; Goodson III, T.; Ronchi, M.; Pizzotti, M.; Rand, S.C.; Li, Y. "Synthesis and Photophysical Properties of Stilbeneoctasilsesquioxanes. Emission Behavior Coupled with Theoretical Modeling Studies Suggest a 3-D Excited State Involving the Silica Core." *J. Am. Chem. Soc*. **2010**, *132*, 3708-3722.

73. Bassindale, A.R.; Pourny, M.; Taylor, P.G.; Hursthouse, M.B.; Light, M.E. "Fluoride-Ion Encapsulation within a Silsesquioxane Cage." *Angew. Chem. Int. Ed.* **2003**, *42*, 3488-3490.

74. Bassindale, A.R.; Parker, D.J.; Pourny, M.; Taylor, P.G.; Horton, P.N.; Hursthouse, M.B. "Fluoride Ion Entrapment in Octasilsesquioxane Cages as Models for Ion Entrapment in Zeolites. Further Examples, X-ray Crystal Structure Studies, and Investigations into How and Why They May Be Formed." *Organomet*. **2004**, *23*, 4400-4405.

75. Pach, M.; Stosser, R. "Scavenger Assisted Trapping of Atomic Hydrogen in Si_8O_{12}-Cages." *J. Phys. Chem. A* **1997**, *101*, 8360-8365.

76. Ganesan, P.; Yang, X.; Loos, J.; Savenije, T.J.; Abellon, R.D.; Zuilhof, H.; Sudholter, E.J.R. "Tetrahedral n-Type Materials: Efficient Quenching of the Excitation of p-type Polymers in Amorphous Films." *J. Am. Chem. Soc*. **2005**, *127*, 14530-14531.

77. Oldham Jr., W.J.; Lachicotte, R.J.; Bazan, G.C. "Synthesis, Spectroscopy, and Morphology of Tetrastilbenoidmethanes." *J. Am. Chem. Soc*. **1998**, *120*, 2987-2988.

78. Robello, D.R.; Andre, A.; McCovick, T.A.; Kraus, A.; Mourey, T.H. "Synthesis and Characterization of Star Polymers Made from Simple, Multifunctional Initiators." *Macromol.* **2002**, *35*, 9334-9344.

79. Wang, S.; Oldham Jr., W.J.; Hudack Jr., R.A.; Bazan, G.C. "Synthesis, Morphology, and Optical Properties of Tetrahedral Oligo(phenylenevinylene) Materials." *J. Am. Chem. Soc*. **2000**, *122*, 5695-5709.

Chapter 4

Synthesis, Characterization, and Photophysical Properties of Polyfunctional Phenylsilsesquioxanes: [*o*-$RPhSiO_{1.5}$]$_8$, [2,5-$R_2PhSiO_{1.5}$]$_8$, and [$R_3PhSiO_{1.5}$]$_8$

Published in Journal of Materials Chemistry vol. 21, pp. 11177-11187, 2011.

With contributions from Ms. Jin Zhang and Professor Ted Goodson III (Macromolecular Science and Engineering Center and Chemistry Department, University of Michigan).

Abstract

The availability of pure *o*-Br_8OPS, 2,5-Br_{16}OPS, and Br_{24}OPS provides a rare opportunity to synthesize sets of corresponding stilbene derivatives: *o*-$RStyr_8$OPS, $RStyr_{16}$OPS, and $RStyr_{24}$OPS where R = 4-methyl (Me), Boc-protected 4-amino (NBoc), or 4-acetoxy (Ace). These derivatives show unique UV-Vis absorption and photoluminescent behavior that point to interesting interactions between the organic tethers with the silsesquioxane cage. *o*-$RStyr_8$OPS show blue-shifts in the absorption spectra compared to *p*-$MeStyr_8$OPS, suggesting that the stilbene groups sit over and interact with the face of the electrophilic silsesquioxane cage as is the case with the parent molecule, *o*-Br_8OPS. The emission spectra of *o*-$RStyr_8$OPS are similar to *p*-$MeStyr_8$OPS indicating similar excited state involving the core LUMO. $RStyr_{16}$OPS exhibit absorption and emission spectra as well as Φ_{PL} similar to 1,4-distyrylbenzene, pointing to disruption in conjugation with the silsesquioxane cage because of steric interactions. $RStyr_{24}$OPS offer absorption maxima that are blue-shifted and emission maxima that are red-shifted relative to $RStyr_{16}$OPS. We speculate that $RStyr_{24}$OPS are so sterically hindered that interactions with the cage face must occur. $NBocStyr_{24}$OPS and $AceStyr_{24}$OPS show moderate Φ_{PL} and high two

photon cross-section values, leading us to conclude that there are two excited states of nearly equivalent energy in these molecules with similar decay rates: normal radiative π-π* transition and charge transfer involving the silsesquioxane cage. These same functional groups can be anticipated to offer much greater two photon absorption if different methods can be found for protecting the free amine from oxidation or replacing the acetoxy group (e.g. perhaps using alkyl or aryl groups).

4.1 Introduction

In the past few years, we and others have sought to use the 3-D nature of functionalized silsesquioxanes[1-4] to develop novel hybrid organic/inorganic components for electronic and photonic devices.[3,5-13] The rationale for this effort comes from the fact that the T_8 and Q_8 derivatives, see Figure **4.1**, place functional groups in each octant in Cartesian space providing good-to-excellent solubility allowing facile purification. Furthermore, the central cage provides the heat capacity of silica often improving thermal stabilities up to 100°C higher compared to all-organic compounds with structures similar to silsesquioxanes or its organic tethers[14-16] or model compounds such as organic triethoxysilanes. In addition, these compounds are easily made in 0.1-1 kilogram quantities in short periods of time.[17,18]

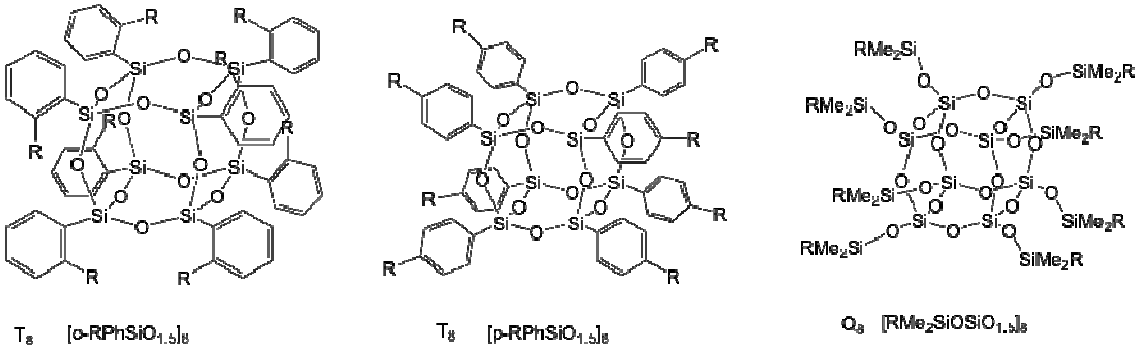

Figure 4.1. 3-D symmetrical T_8 and Q_8 compounds.

Perhaps most importantly, recent work indicates that the cage is not an innocuous insulating component but rather appears to offer 3-D conjugation in the excited state promising novel semiconductor properties.[11-13] In the latter case we have shown that the pure

methyl-stilbene silsesquioxanes, [*o*-MeStyrPhSiO$_{1.5}$]$_8$ (*o*-MeStyr$_8$OPS) and [*p*-MeStyrPhSiO$_{1.5}$]$_8$ (*p*-MeStyr$_8$OPS), show red-shifts in their emission behavior of up to 80 nm relative to molecular *trans*-stilbene as seen in Figure **4.2**.[12]

Furthermore, we also find that the two photon absorption (TPA) cross-sections per moiety of methoxy- and amino-vinylstilbene silsesquioxanes, [*p*-MeOStilCH=CHSiO$_{1.5}$]$_8$ and [*p*-NH$_2$StilCH=CHSiO$_{1.5}$]$_8$, are quite high relative to model compounds (see Table **4.1**). In these instances, the observed behaviors can be directly correlated with the formation of charge transfer (CT) excited states wherein the peripheral MeO- and NH$_2$ groups donate electron density to the cage in the excited state as supported by solvatochromism studies.[11,12]

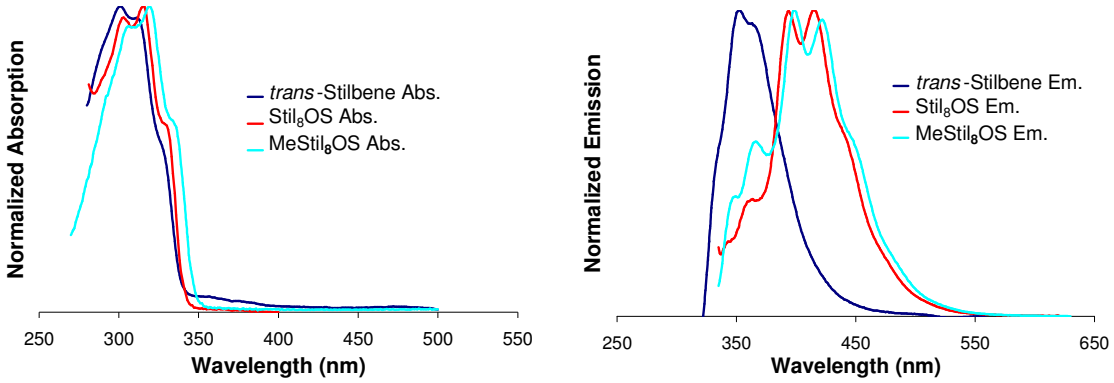

Figure 4.2. UV-Vis absorption (top) and PL emission (bottom) of *trans*-stilbene and *p*-Me(H)Stil$_8$OS in THF.[12]

Table 4.1. TPA properties of silsesquioxane derivatives.[11,12]

Sample	δ (GM)	δ /moiety (GM)	λ_{max} (nm)
[*p*-MeStilSiO$_{1.5}$]$_8$	11	1.2	735
[*p*-Me$_2$NStilSiO$_{1.5}$]$_8$	211	26	755
[StilCH=CHSiO$_{1.5}$]$_8$	25	3	705
[*p*-MeOStilCH=CHSiO$_{1.5}$]$_8$	110	14	705
[*p*-NH$_2$StilCH=CHSiO$_{1.5}$]$_8$	810	101	720

These results coupled with our recent discovery of methods of making very pure [*o*-BrPhSiO$_{1.5}$]$_8$, [2,5-Br$_2$PhSiO$_{1.5}$]$_8$, [Br$_3$PhSiO$_{1.5}$]$_8$, provided the impetus to explore the functionalization of these compounds.[19] In principle, these brominated [PhSiO$_{1.5}$]$_8$ or OPS (octaphenylsilsesquioxane) derivatives offer the potential to introduce 8, 16 or ≈ 24 functional groups in the same volume. Furthermore, these functional groups are expected to offer extended conjugation via the central phenyl ring and through the center of the

cage. Also of potential interest is the fact that the molecules synthesized here have some of the highest densities of functional groups per unit volume possible. Assuming spherical shapes, these polyfunctional silsesquioxanes have diameters of approximately 1.5 nm.[20] In contrast, for example, PAMAM dendrimers[21] with comparable number of functional groups (see Table **4.2**) at much greater diameters and only as surface functional groups.

Table 4.2. Physical characteristics of PAMAM dendrimers.[21]

Generation	No. of surface groups	Molecular weight[a]	Diameter (nm)[b]
0	4	517	1.5
1	8	1430	2.2
2	16	3256	2.9
3	32	6909	3.6

[a] Molecular weight is based on defect-free, ideal-structure, amine-terminated dendrimers. [b] Molecular dimensions determined by size-exclusion chromatography.

We have chosen functional groups per unit volume of individual molecules and compared them to dendrimers as opposed to total densities of molecules per cc. In our crystal structures,[20] we do not see interdigitation; thus, these values are realistic at all length scales.

The extended conjugation in each functional group coupled with the potential for 3-D conjugation, considerable charge transfer behavior and the fact that in earlier studies we saw exceptional two-photon absorption cross-sections suggest possible applications in optical limiting and enhanced solar energy harvesting. As we report below, the results of these studies provide unexpected properties that may be useful for these applications.

4.2 Experimental Procedures

The synthetic methods and characterization techniques are described in Chapter 2, along with more detailed experimental data.

4.3 Results and Discussion

In previous studies, we used Heck coupling as a means to introduce a variety of functional groups to brominated- (Scheme **4.1**) and iodinated- (Scheme **4.2**) OPS.[18,22] In these studies, we had not as yet learned to control bromination selectivity and opted for com-

pounds with less than eight bromines to minimize the potential for double substitution at a single phenyl group. Even so, double bromination was still observed at 3-5 % of the total bromine incorporated. This was the motivation for moving to the iodination studies where double iodination was not observed. With our recent discovery of routes to pure *o*-Br_8OPS, Br_{16}OPS, and Br_{24}OPS,[19] we can now extend our studies to making sets of octa-, hexadeca- and tetraicosa-styrenyl substituted OPS compounds. The motivation, as noted above, is to extend our knowledge concerning the cage-moiety interactions as it affects photophysical properties. Scheme **4.3** shows the general reaction schemes explored.

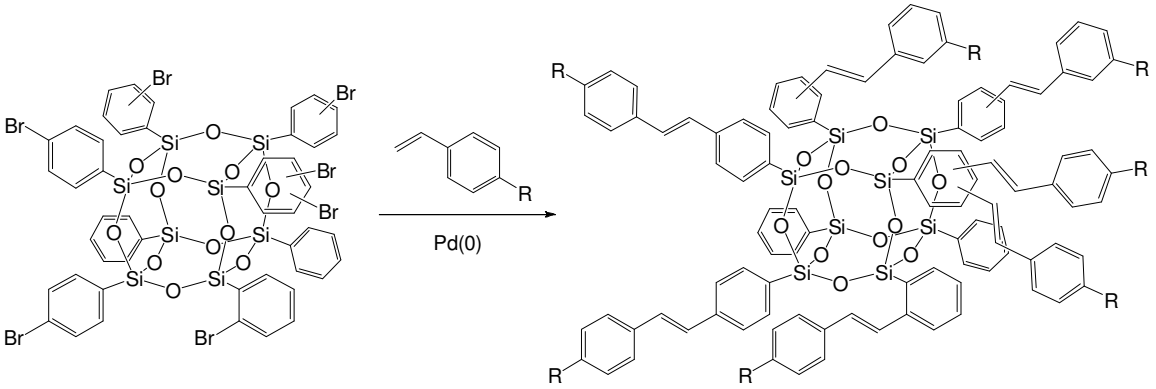

Scheme 4.1. Heck coupling reaction of $Br_{5.3}$OPS with RStyrenes.[12,22]

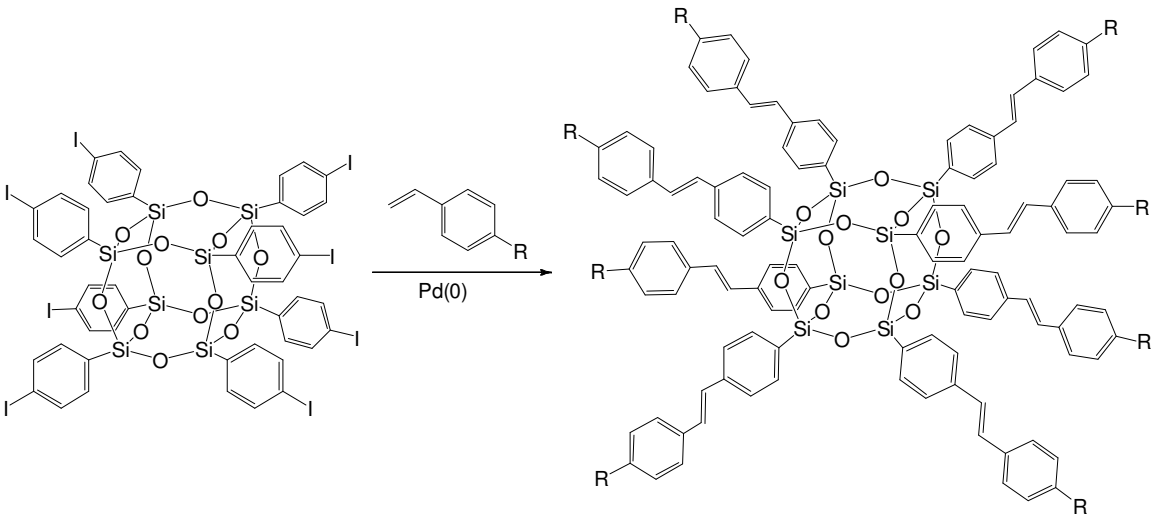

Scheme 4.2. Heck coupling reaction of *p*-I_8OPS with RStyrenes.[12,18]

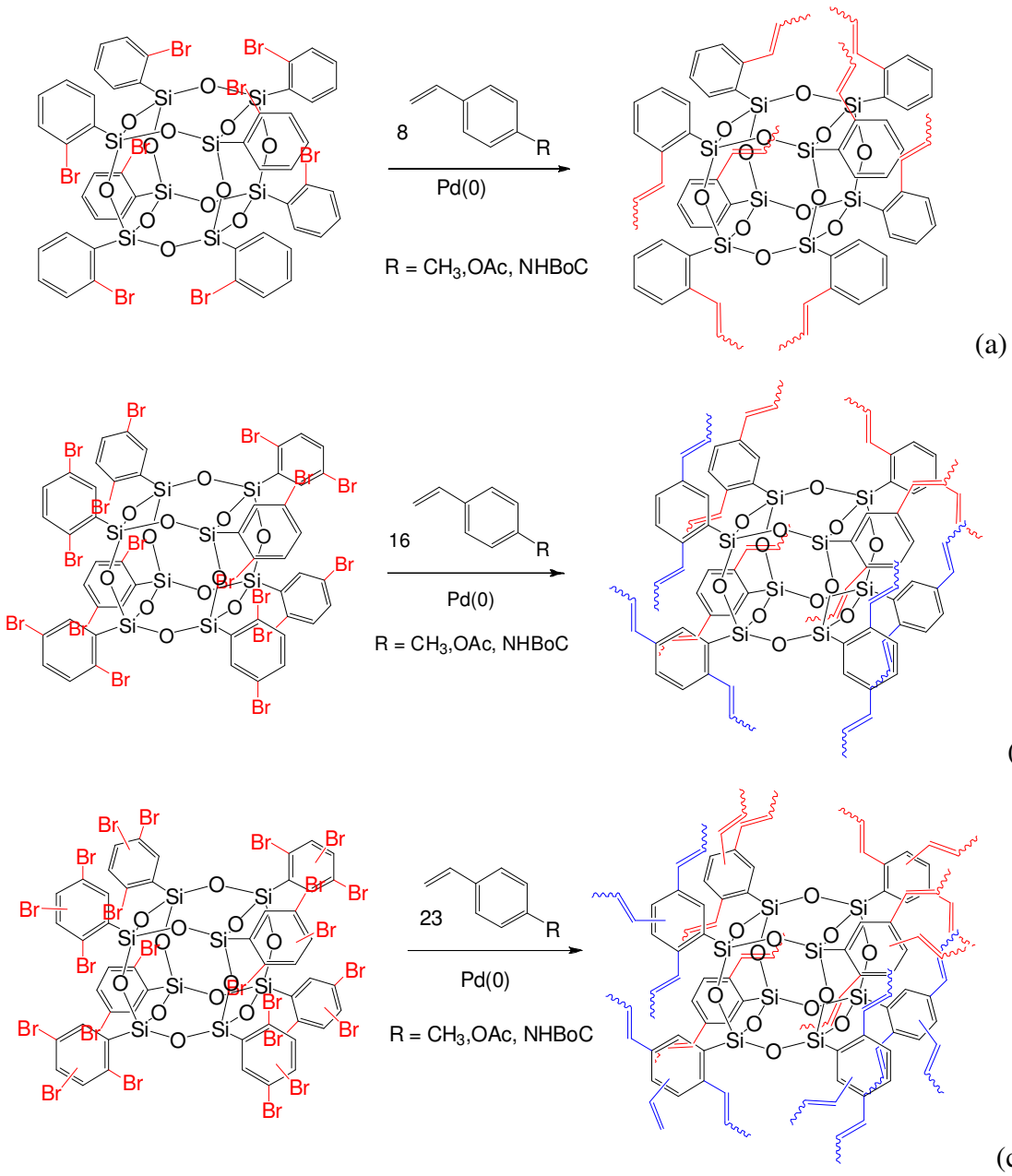

Scheme 4.3. Heck coupling studies on *o*-Br_8OPS, 2,5-Br_{16}OPS and Br_{24}OPS. Preparation of selected functionalized stilbenes for comparison of photophysical properties.[19]

We begin with a discussion of our synthetic methods as a prelude to discussing characterization and thereafter photophysical properties for a set of three different StyreneOPS systems: the *para*-methyl, -acetoxy and -NBoc-protected amine.

4.3.1 Synthetic Methods

Heck coupling at the *ortho* position is relatively slow because of steric interactions, (Scheme **4.3a** and Figure **4.3**). As a consequence, most reactions were run at 70°C/24 h, in contrast to our earlier studies where the reactions were run at room temperature (48 h).[11,12] Tables **4.6**-**4.8** list general characterization data for the compounds prepared. In general, purities were quite high as witnessed by the ceramic yields, which are close to those calculated, Table **4.7**. Table **4.8** provides data for NBocStyr$_x$OPS separately as the analyses need some explanation.

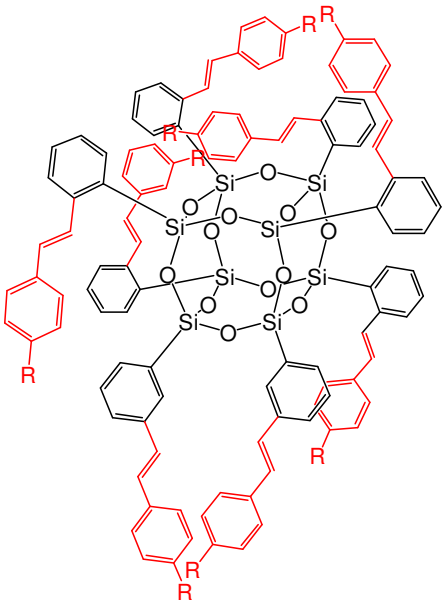

Figure 4.3. *o*-RStyr$_x$OPS with exaggerated bond lengths and angles for clarity.

Heck coupling reactions between crystalline Br$_x$OPS (x =8, 16, 24) and the target *p*-RStyrene were run under much more rigorous conditions compared to our previous work using BrStyrenylOS.[11,22] The close proximity of the *ortho*-Br groups to the silsesquioxane cage presents a challenge in obtaining complete conversion to the Heck coupling product. This was achieved using higher concentrations of *p*-RStyrene and elevated temperatures.

As noted above, we chose three different R groups in this work. The simplest methyl derivatives are used for comparison with the small molecule analog and as a baseline for the other derivatives. NH2VinylStilbeneOS previously synthesized from *p*-BrStyrenylOS shows CT behavior in solution, and we would like to investigate how this phenomenon is affected by increases in the number of chromophores in the NH$_2$Stry$_x$OPS systems. How-

ever, due to the basic nature of $–NH_2$ groups and the instability of silsesquioxane cages in base, –NBoc protection was used to prevent unwanted degradation during synthesis. Deprotection was possible for the octa-*ortho*-compound but the higher functionality congeners were found to oxidize rapidly during deprotection and thus photophysical properties were measured for the NBoc derivatives. The acetoxy- group was chosen as it can be hydrolyzed to give hydroxyl- groups, which can be used as a starting point for further functionalization to make supramolecular or 3-D nanoarchitectures.

It is well-known that silsesquioxane cages have high affinity for the transition metals commonly used as catalyst in coupling reactions, such as palladium and ruthenium.[23] The Heck coupling products of Br_xOPS still contain residual palladium catalyst, even after several precipitation steps, as evidenced by the grayish tint of the products. Further removal of residual palladium was achieved by treating the crude products with the well-known palladium complexing additive *N*-acetyl-*L*-cysteine.[24] The palladium-cysteine complex is soluble in polar solvents such as THF and methanol, but highly insoluble in non-polar solvents such as toluene. Therefore, the palladium-cysteine complex can be removed either during filtration of the original reaction mixture, as it precipitated out of toluene, or during the precipitation as it goes into solution in methanol.

The Heck coupling reactions of Br_xOPS produced some unwanted byproducts, which according to the GPC analyses are most likely dimeric in nature (i.e. two silsesquioxane molecules bridged by an organic tether). These byproducts were not observed in our earlier work with BrStyrenylOS.[11] We believe that dimer formation arises because of the harsher reaction conditions used in this set of experiments, especially the high concentration of reagents in the reaction mixture. The byproducts were removed either by column chromatography or selective precipitation to give pure products per GPC analyses.

4.3.2 Solubilities.

All of the synthesized compounds are soluble in moderately polar organic solvents such as THF, 1,4-dioxane, CH_2Cl_2, and $CHCl_3$. MeStyr$_x$OPS and AceStyr$_x$OPS are insoluble in highly polar solvents such as methanol, and in nonpolar solvents such as hexane. NBocStyr$_x$OPS are soluble in MeOH, and were therefore purified by precipitation into hexane.

4.3.3 Molecular Characterization of $RStyr_xOPS$

MALDI-ToF spectra of $RStyr_xOPS$ are shown in Figures **A2.1**-**A2.7**. It should be noted that although the compounds synthesized in this work are labeled as having 8, 16, or 24 groups per molecule, those numbers reflect an average of the actual number of functional groups present per molecule. The starting materials used in this work (*o*-Br_8OPS, $Br_{16}OPS$, and $Br_{24}OPS$) were purified by multiple recrystallization; however, MALDI-ToF spectra of these materials still show small amounts of other brominated species (e.g. Br_7OPS, $Br_{15}OPS$, $Br_{22}OPS$, etc) present in the system.[19,20]

Tables **4.3**-**4.5** detail the different molecular species present in $RStyr_xOPS$ and their percentages based on MALDI-ToF data. Even though each set of compounds (*o*-$RStyr_8OPS$, $RStyr_{16}OPS$, and $RStyr_{24}OPS$) was synthesized using starting material from the same batch, their MALDI-ToF data show different compositions of molecular species. For example, MALDI-ToF data for *o*-$MeStyr_8OPS$ and *o*-$AceStyr_8OS$ show different percentages for the 7-mer and the 8-mer, and *o*-NH_2Styr_8OS show the presence of the

Table 4.3. Molecular species present in $MeStyr_xOPS$.

o-$MeStyr_8OPS$		$MeStyr_{16}OPS$		$MeStyr_{24}OPS$	
Species present	%	Species present	%	Species present	%
o-$MeStyr_7OPS$	5	$MeStyr_{14}OPS$	2.4	$MeStyr_{22}OPS$	18.5
o-$MeStyr_8OPS$	95	$MeStyr_{15}OPS$	30.5	$MeStyr_{22}BrPh_1OPS$	5.1
		$MeStyr_{16}OPS$	62.2	$MeStyr_{23}OPS$	47.0
		$MeStyr_{17}OPS$	4.9	$MeStyr_{23}BrOPS$	5.8
Average: 7.95		Average: 15.7		$MeStyrenyl_{24}OPS$	23.6

Table 4.4. Molecular species present in NH_2Styr_xOPS.

o-NH_2Styr_8OPS		$NH_2Styr_{16}OPS$	
Species present	%	Species present	%
o-NH_2Styr_8OPS	89.6	$NH_2Styr_{16}OPS$	100
o-NH_2Styr_9OPS	10.4		
Average: 8.1		Average: 16.0	

Table 4.5. Molecular species present in $AceStyr_xOPS$.

o-$AceStyr_8OPS$		$AceStyr_{16}OPS$	
Species present	%	Species present	%
o-$AceStyr_7OPS$	23.6	$AceStyr_{15}OPS$	10.6
o-$AceStyr_8OPS$	76.4	$AceStyr_{16}OPS$	74.4
		$AceStyr_{17}OPS$	15.1
Average: 8.1		Average: 16.05	

9-mer, which is not present in the other two compounds. We attribute these results to differences in ionization potentials of the compounds rather than substitutional variations.

Complete conversion of the –Br groups is observed in the MALDI-ToF spectra for almost all the compounds, with the exception of $MeStyr_{24}OPS$, which shows small amounts of unreacted –Br groups. This is not completely unexpected, considering the steric hindrance associated with having three –Br groups on a phenyl ring attached to the silsesquioxane cage, especially for *o*-Br groups.

The MALDI-ToF data of $NBocStyr_xOPS$ show a series of low intensity peaks close to the mass of the deprotected species. We were able to collect MALDI-ToF data for two of the deprotected compounds: *o*-NH_2Styr_8OS and $NH_2Styr_{16}OPS$. No MALDI-ToF data were obtained for $NH_2Styr_{24}OPS$ and $AceStyr_{24}OPS$, most probably due to their complex structures, which makes them unstable under the UV laser of MALDI-ToF such that they fragment. GPC and ceramic yield data for these two compounds (Tables **4.6** to **4.8**) suggest that nearly all of the –Br groups were converted to the organic derivatives.

Table 4.6. MALDI-ToF and GPC data for $RStyr_xOPS$.

R group	x	m/z (Ag^+ adduct)		GPC			
		MALDI[a]	Calc.	M_n	M_w	FW	PDI
Me	8	2068.6	2070.7	1212	1225	1962.8	1.01
	16	2890.4[b]	2983.8	2032	2057	2875.9	1.01
	24	3812	3821.3	2522	2565	3705.2	1.01
NBoc	8	1969.2[b,c]	1971.7[b,c]	2382	2431	2771.6	1.02
	16	3013.9[c]	3015.7[c]	3749	3809	4509.7	1.02
	24	N.A	3845.1[c]	4290	4390	6030.6	1.02
Ace	8	2422.2	2422.7	1535	1570	2314.9	1.02
	16	3702.7	3704.1	2542	2614	3596.2	1.03
	24	N.A	4877.6	3593	3893	4717.4	1.08

[a]Highest intensity peak detected. [b]As H^+ adduct. [c]As deprotected species (NH_2Styr_xOPS).

GPC analyses of $RStyr_xOPS$ (Table **4.6**) show that these materials exhibit narrow molecular weight distributions, indicating that they retain their silica cage structures following reaction. As expected, the methyl derivatives show the lowest molecular weights due to their simple structures. Within each set of functional groups, the molecular weight increases as the number of functional groups per molecule increases. The values of M_n and M_w, as measured by GPC, are smaller than those measured by MALDI-TOF, but ex-

pected from GPC characterization of rigid, spherical molecules using flexible, linear standards, based on previous results.[11-13]

TGA data for Me- and AceStyr$_x$OPS, Figure **4.4,** show mass-loss onset temperatures greater than 350^{o}C. Table **7** details the actual and theoretical ceramic yields for Me- and AceStyr$_x$OPS. We have also included theoretical ceramic yields calculated using average FW from MALDI-ToF data. With the exception of AceStyr$_{24}$OPS, the actual and theoretical values of Me- and AceStyr$_x$OPS are in close agreement with each other, confirming that the compositions of the compounds are in accord with the MALDI-ToF data.

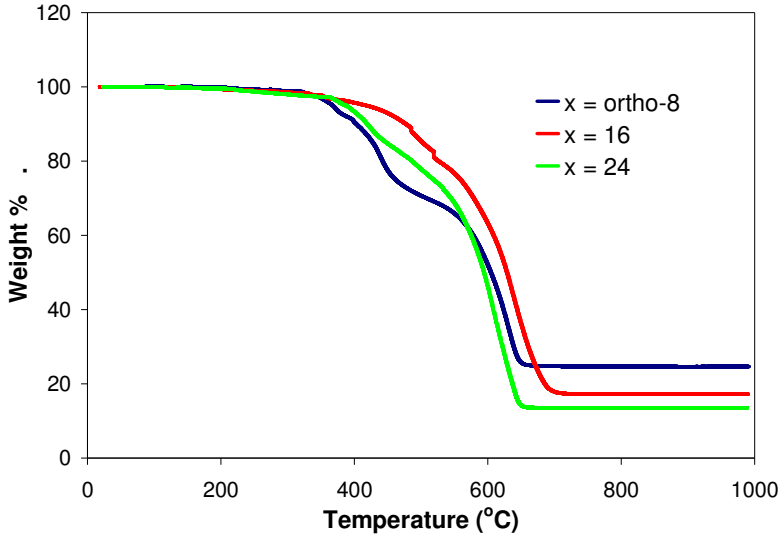

(a)

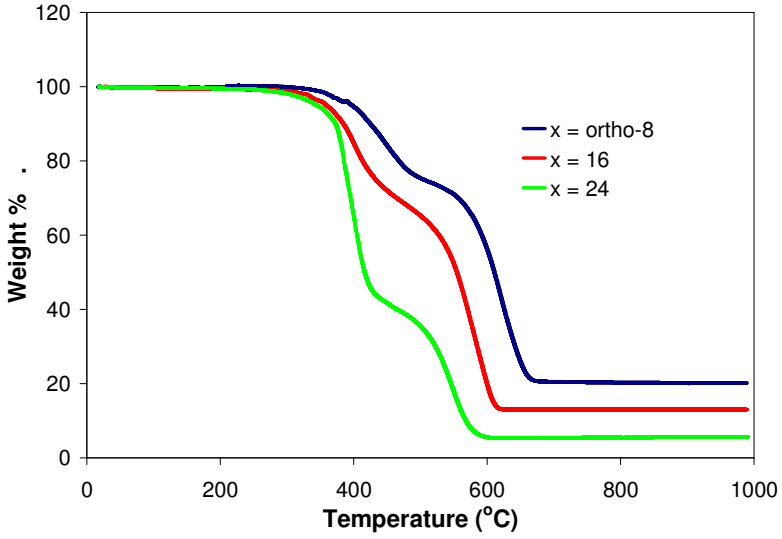

(b)

Figure 4.4. TGA data in air (10^{o}C/min) for (a) MeStyr$_x$OPS and (b) AceStyr$_x$OPS.

Table 4.7. TGA data for MeStyr$_x$OS and AceStyr$_x$OS.

R group	x	Ceramic yield (%)			$T_{d5\%}$ (°C)
		Actual	Calc.	Calc. with ave FW[a]	
Me	8	24.6	24.5	24.6	367
	16	17.2	16.6	16.8	417
	24	13.5	13	12.9	386
Ace	8	20.3	20.8	21.1	397
	16	13	13.4	13.3	359
	24	5.7	10.2	N.A.	344

[a]Average FW calculated from MALDI-ToF data (Tables **4.2** and **4.4**).

TGA data for NBocStyr$_x$OPS (Figure **4.5**) have two distinct mass loss steps: The first step at ~200 °C arises from the loss of the –Boc protecting group, while the second step at ~400°C points to the oxidative decomposition of the phenyl groups generatingsilica as the final ceramic product. Table **4.8** summarizes the thermal decomposition data of NBocStyr$_x$OPS. The mass loss from the –NBoc groups can be used to estimate the average number of these functional groups per silsesquioxane molecule.

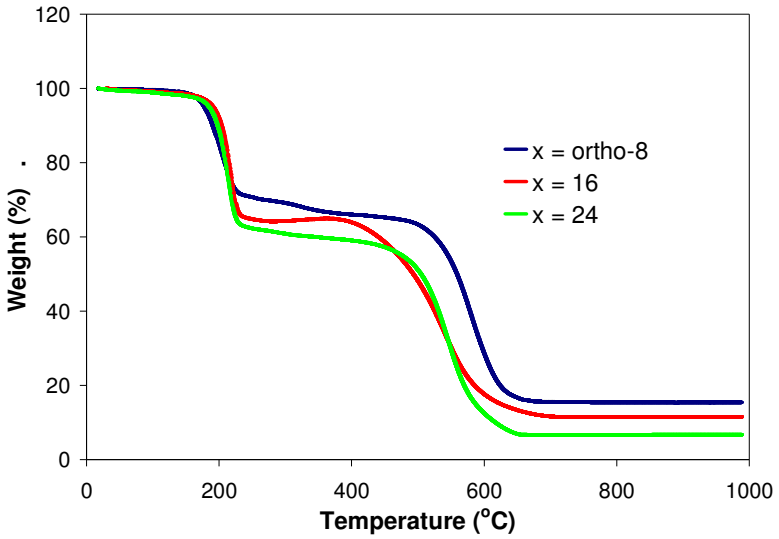

Figure 4.5. TGA data in air (10°C/min) for NBocStyr$_x$OPS.

Since the actual and theoretical mass loss from the –NBoc groups are comparable, we can assume that all of the –Br groups are converted to the –NBocStyrene groups, in agreement with the MALDI-ToF data.

Table 4.8. TGA data for NBocStyr$_x$OPS.

x	Ceramic yield (%)			$T_{d5\%}$ (^oC)	Boc group mass %	
	Actual	Calc.	Calc. with ave FW[a]		Actual	Calc.
8	15.4	17.3	17.2	177 / ~400	29	29.2
16	11.5	10.2	10.2	190 / ~440	35	35.9
24	7	8	N.A.	184 / ~450	38	38.6

[a]Average FW calculated from MALDI-ToF data (Table **4.2**).

4.3.4 Photophysical Properties

The UV-Vis absorption and photoluminescence spectra for RStyr$_x$OPS are shown in Figures **4.6-4.8.** The photophysical data are summarized in Table **4.9**. Within each series of compounds with the same R group, we observed the same trends as discussed below. While consistent in their trends, there are still some important surprises.

First, the absorption and emission spectra for RStyr$_{16}$OPS are red-shifted from those for *o*-RStyr$_8$OPS as expected because of the longer conjugation length. However, the absorption spectra for RStyr$_{24}$OPS are blue-shifted from those for RStyr$_{16}$OPS, whereas the emission spectra are red-shifted. Furthermore, for RStyr$_8$OPS Φ_{PL} are typical of those seen previously at ca. 0.04 whereas for the RStyr$_{16}$OPS Φ_{PL} are an order of magnitude higher at 0.40-0.60. Unexpectedly the Φ_{PL} for RStyr$_{24}$OPS are 0.10-0.30 lower than RStyr$_{16}$OPS. This is surprising because it might be anticipated that RStyr$_{24}$OPS would exhibit more extensive conjugation resulting in red-shifts in both the absorption and emission spectra relative to those of RStyr$_{16}$OPS. This should lead to more stabilization in the excited state leading to higher Φ_{PL} values.

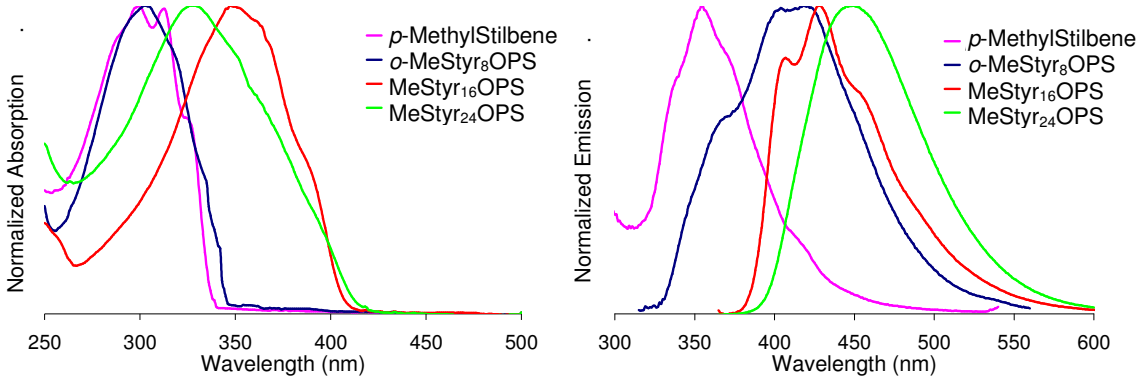

Figure 4.6. (a) Absorption and (b) emission spectra for MeStyr$_x$OPS.

Table 4.9. Photophysical data for $RStyr_xOPS$ (THF, CH_2Cl_2 peak positions are identical).

Compound	x	Absorption λ_{max} (nm)	Emission λ_{max} (nm)	Φ_{PL} %	Stoke's shift $\Delta\nu(cm^{-1})$	δ (GM)	δ / group (GM)
p-MeStilbene[25]		298, 311	355	9			
1,4-Distyrylbenzene[26]		353	385, <u>408</u>	62			
1,2,4-Tristyrenylbenzene[27]		<u>320</u>, 355[b]					
1,3,5-Tristyrenylbenzene[28]		297	412 (toluene) 384 (*n*-hexane)				
p-$MeStyr_8OPS$[a]		320	400, 422	4			
$MeStyr_xOPS$	*o*-8	303	<u>405</u>	4	8312[c]		
	16	349	407,<u>431</u>,457	57	5451[c]		
	24	329	<u>444</u>	39	7873[c]		
$NBocStyr_xOPS$	*o*-8	317	386, <u>422</u>, 445[b]	5	7849[c]	1	~0
	16	364	429, <u>453</u>	43	5398[c]	50	~3
	24	346	440,[b]<u>461</u>	8	7210[c]	270	~12
$AceStyr_xOPS$	*o*-8	300	402, <u>422</u>	4	9637[c]	~0	~0
	16	347	407, <u>429</u>, 451	45	5508[c]	~1	~0
	24	317	<u>435</u>, 453[b]	19	8557[c]	221	~10

[a] *p*-$MeStyr_8OPS$ synthesized from *p*-I_8OPS.[12]
[b] Shoulder.
[c] There are several emission bands; the emission maximum (underlined) is used to calculate the Stoke's shift.

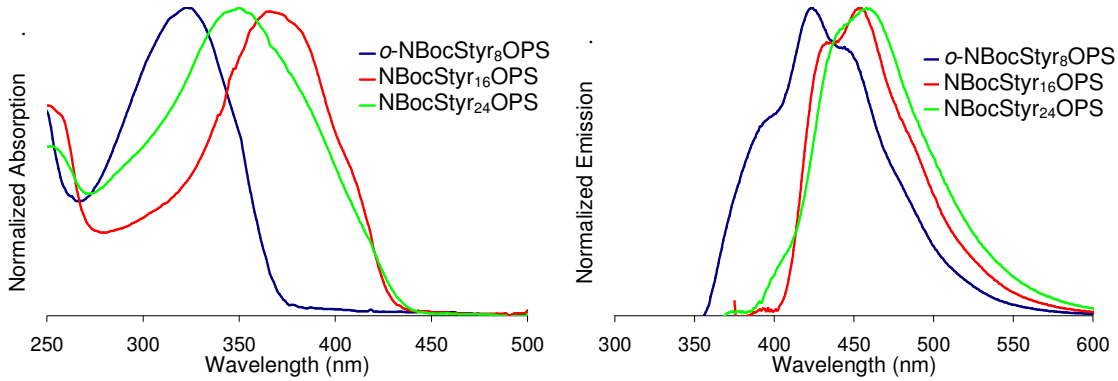

Figure 4.7. Absorption and emission spectra for NBocStyr$_x$OPS.

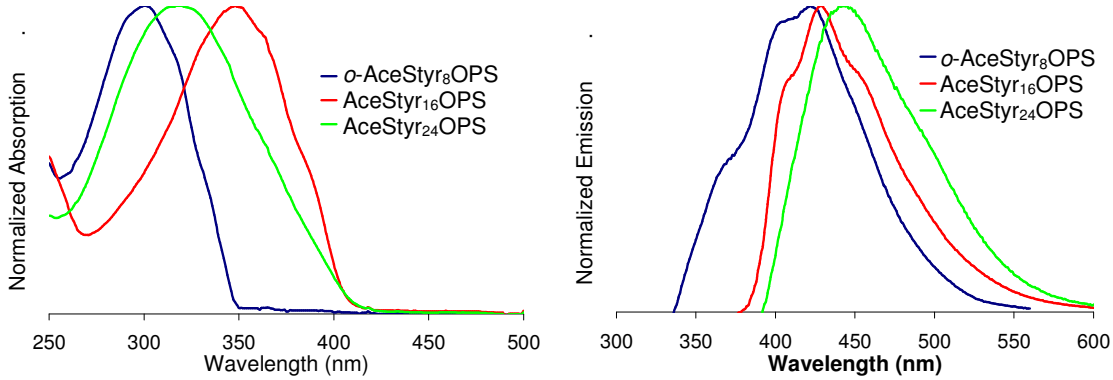

Figure 4.8. Absorption and emission spectra for AceStyr$_x$OS.

In order to explain these results we must first compare the observed behavior with their organic analogs.[25-28] The comparative data are also provided in Table **4.9**. Thus, the absorption spectrum of *o*-MeStyr$_8$OPS has the same λ_{max} as *p*-methylstilbene (Table **4.9**). This is ≈ 20 nm blue-shifted from the absorption λ_{max} of *p*-MeStyr$_8$OPS synthesized from *p*-I$_8$OPS.[11] In contrast, the emission λ_{max} for *p*-methylstilbene is 355 nm compared to 400 nm and 420 nm for *p*-MeStyr$_8$OPS and 405 nm for *o*-MeStyr$_8$OPS.

A comparison of 1,4-distryenylbenzene with MeStyr$_{16}$OPS shows similar absorption λ_{max} of 353 nm and 349 nm suggesting similar ground states. The emitting λ_{max} are 408 nm vs 431 nm, which may be accounted for in part by the methyl substituent. In addition, the Φ_{PL} values are quite similar at 62 % and 57 % (ethanol vs THF).

Finally, comparing 1,2,4-tristyrenylbenzene, 1,3,5-tristyrenylbenzene and MeStyr$_{24}$OPS, we see that the all *meta* 1,3,5-tristyrenylbenzene has an absorption λ_{max} at ≈ 300 nm whereas the 1,2,4-isomer has an absorption λ_{max} at ≈ 320 nm. The emission λ_{max} for the 1,2,4-isomer is not reported but that for the 1,3,5-isomer is 412 nm in toluene.

The data suggest that the absorption and emission max for $MeStyr_{24}OPS$ are quite red-shifted from the 1,3,5-tristyrenylbenzene analog but may be similar to or red-shifted from the 1,2,4-isomer as well. Thus, the blue shift for $MeStyr_{24}OPS$ seems explainable in terms of the organic analogs. However, the Φ_{PL} values remain difficult to explain.

Multiple theoretical calculations suggest that the cage is highly electrophilic,[29] which is supported by the fact that it auto-catalyzes bromination as discussed in a previous paper.[19] Further support for this comes from our recent studies offering considerable evidence for charge transfer transitions in the excited state leading, for example, to quite high two photon absorption cross sections as discussed below.[11,12] As also noted in the accompanying paper, the cage interacts with aromatic ring substituents as if it were a electron withdrawing substituent equivalent to a CF_3 or NO_2 group.[30]

Consequently, one might expect to see such an electron withdrawing effect on the stilbene substituents prepared here ($RStyr_8OPS$) whether they are *ortho*- or *para*-substituents. The implication is that the cages should cause considerable blue shifts in both the absorption and emission maxima. This is contrary to what is seen. Therefore this argument cannot be used to explain the blue shift in the absorption data for the *ortho*-stilbene (*o*-$MeStyr_8OPS$). The only other possible explanation that seems valid is that the styrenyl group in the *ortho* position is forced to spend some of its time above the cage face. The crystal structure of the starting [*o*-$BrPhSiO_{1.5}$] indicates that the bromo group sits over the face of the very electrophilic cage.[19,20] Indeed, this interaction might actually be stabilized if the cage is considered to be highly electrophilic. In fact, Bowers et al calculate that the highly electrophilic behavior extends beyond the cage,[29] supporting the suggestion that the cage face polarizes Br_2 promoting *ortho*-substitution and the possibility that the styrenyl group prefers to sit above the electrophilic cage face.[19,20] This latter interaction could explain the blue shift relative to the *para* analog (*p*-$MeStyr_8OPS$).

However, the emission spectrum of *o*-$MeStyr_8OPS$ is clearly red-shifted from that of *p*-methylstilbene and similar to that of *p*-$MeStyr_8OPS$. The quantum yield of *o*-$MeStyr_8OPS$ is also similar to *p*-$MeStyr_8OPS$. In our previous work, we attributed the red-shifts in the absorption and emission spectra of *p*-$MeStyr_8OPS$ compared to molecular stilbene to 3-D conjugation as involving the LUMO of the silsesquioxane cage.[12] It appears that the excited states of both *o*- and *p*-$MeStyr_8OPS$ are quite similar allowing for

the argument that both excited states access the same LUMO inside the silsesquioxane cage.

The absorption and emission spectra of NBocStyr$_x$OPS are only slightly red-shifted from those of MeStyr$_x$OPS and AceStyr$_x$OPS. This is expected given that the amino groups are masked by the Boc protecting groups, which are electron withdrawing. We would expect much larger red-shifts from free amino groups due to their strong donor characteristics, as seen previously.[11,12] Normally, *para*-alkoxysubstituents exhibit good-to-excellent electron donating properties; however, the AceStyr$_x$OS absorption and emission spectra are similar to MeStyr$_x$OS suggesting roughly equivalent electron-donating abilities. Thus the electron-withdrawing characteristics of the acyl group seems to balance the normal electron donating properties of a *para* oxygen substituent, but the TPA data suggest this is not quite a correct assessment (see below).

The absorption and emission spectra of RStyr$_{16}$OPS are both red-shifted from those of *o*-RStyr$_8$OPS as expected considering the longer conjugation lengths. The absorption maxima and quantum yields for RStyr$_{16}$OPS are comparable to those for the small molecule analog, 1,4-distyrylbenzene, while the emission spectra are red-shifted from 1,4-distyrylbenzene (20-45 nm depending on the R-group). The emission spectra of RStyr$_{16}$OPS exhibit structured bands typical for conjugated aromatic compounds. These compounds also have low two-photon cross-sections (GM values, see below). All of these observations, as briefly noted above, suggest that the HOMO and LUMO of RStyr$_{16}$OS are similar to those of 1,4-distyrylbenzene without any contributions from the silsesquioxane cage.[27] The simplest explanation for this behavior is that the presence of the second styrenyl group on each corner of the cage causes overcrowding around the cage, forcing the distyrenylphenyl groups away from the cage face. It also may interrupt the 3-D interaction with the cage in the excited state. Thus we observe photophysical behavior expected for an electronically isolated organic fragment. This contrasts with the RStyr$_{24}$OPS compounds.

The blue-shifts in the RStyr$_{24}$OPS absorption spectra compared to those of RStyr$_{16}$OPS likely arise from the *meta*-styrenyl groups present on each central phenyl ring (see Figure **4.9**). As discussed in a previous paper on the polybromination of OPS,[19,20] Br substitution starts at the *ortho*-position (position 1 in Figure **4.9**). The second

Br- adds (almost exclusively) *para*- to the first Br- (position 5 in Figure **4.9**). We believe that at this point, the steric hindrance will prevent addition of a third Br to the other *ortho*-position (position 6, Figure **4.9**). Therefore, addition of a third Br would be expected to occur at either of the two other positions on the phenyl rings (positions 3 and 4 in Figure **4.9**), as supported by the X-ray single crystal data from a previous paper,[19,20] which show partial occupancy at both positions. This means that there will always be two styrenyl groups *meta* to each other in $RStyr_{24}OPS$.

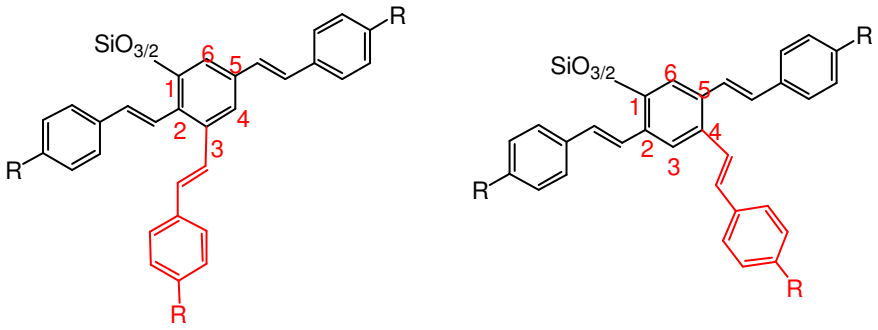

Figure 4.9. Two possible configurations of $RStilbene_{24}OS$ corner.

Previous work on 1,2,4-tristyrylbenzene[27] suggests that its absorption spectrum can be considered as a summation of the 1,3-distyrylbenzene and 1,4-distyrylbenzene spectra, with a maximum (320 nm) in between the maxima of the two distyrylbenzenes (300 nm and 355 nm) and a shoulder corresponding to the absorption maximum of 1,4-distyrylbenzene (355 nm). The authors attribute this phenomenon to interactions between the two conjugated distyrylbenzene "fragments" of the molecule. However, no rationalization as to what these interactions might be is available in the literature.

Related work suggests that *meta*-substituted phenylenevinylene units in *meta*-distyrylbenzene and oligo(phenylenevinylene) can be considered "conjugative insulators" that disrupt the interaction between phenylenevinylene units.[31] The 1,3,5-tristyrylbenzene absorption λ_{max}, where all phenylenevinylene units are *meta*-, is 297 nm (toluene or *n*-hexane) and the emission λ_{max} at 412 nm in toluene.[28]

In comparison, we begin by considering the widths of the absorption bands for $RStyr_{24}OPS$. For each series of R-groups, the absorption spectrum of $RStyr_{24}OPS$ has an onset similar to that for *o*-$RStyr_8OPS$ that tails into the absorption spectrum for $RStyr_{16}OPS$. Each has a λ_{max} in between the maxima of *o*-$RStyr_8OPS$ and $RStyr_{16}OPS$.

This implies that the absorption spectra for each RStyr$_{24}$OPS actually consist of contributions from all "fragments" of the tristyrenylphenyl groups. Basically we observe a sum of the interaction between the *ortho*-stilbenes with the face of the silsesquioxane cage (Figure **4.10a**) with the longer conjugation of the distyrylbenzene units (Figure **4.10b**) coupled with the disruption in overall conjugation caused by the *meta*-positioned styrenyl (a.k.a. phenylenevinylene) units (Figure **4.10c**). The presence of the third styrenyl group on each corner of the cage causes even more crowding around the cage and some of the organic groups are forced to approach the face of the cage, thus giving rise to an interaction (blue shift) between the cage face and the organic groups observed in the absorption spectra.

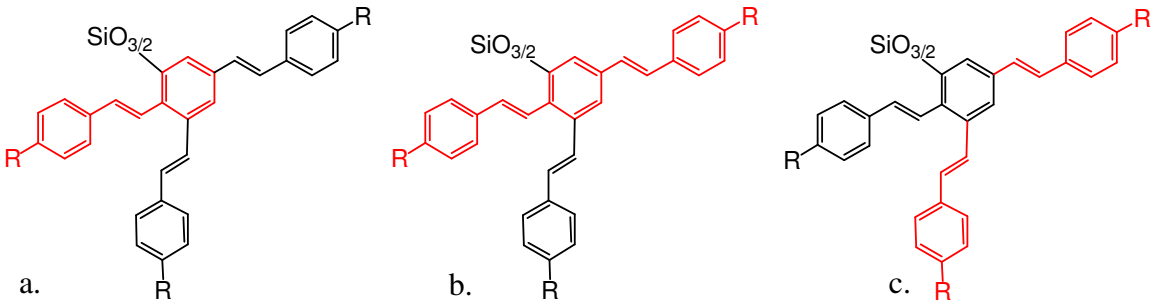

Figure 4.10. Interactions of "fragments" of tristyrenylphenyl groups on each corner of RStyr$_{24}$OS.

The emission spectra for RStyr$_{24}$OPS are red-shifted from their respective RStyr$_{16}$OPS and show no band structure. Their quantum yields are slightly lower, but the two-photon cross-section values are much higher for the NBoc and Acetoxy groups, see below. The data suggest that there are actually two pathways for the transition from the excited to the ground state: charge transfer (CT) and normal radiative emission from a π^* state.

The CT effects explain the lack of structure in their emission spectra and the high TPA values (see below). Normally CT funnels energy away from luminescence and gives rise to low quantum yields. However, in the case of RStyr$_{24}$OPS, the Φ_{PL} values are not as low as expected if CT is the only mechanism for excited-to-ground state transition. The normal π^* radiative emission provides another option, and explains the Φ_{PL} values of RSyr$_{24}$OS. For both mechanisms to be active, both processes must have roughly equivalent decay rates and energies otherwise one would dominate over the other. Indeed, this

suggests that one might promote the CT transition by using a more polar solvent to stabilize the CT transition state and perhaps improve the TPA values at the expense of the Φ_{PL} values. Such studies are planned in the future.

One final comment about these results should be made. Because of the very high density of functional groups, it is possible that some form of 3-D through space interactionsare also involved in their absorption and emission behavior. At this point, we have no proof but believe the possibility should be mentioned as higher densities of functional groups affect absorption and emission behavior in cyclic polystyrenes albeit mostly causing blue shifts.[32]

As mentioned above, efforts to deprotect NBocStyr$_x$OPS to give NH$_2$Styr$_x$OPS for MALDI-ToF samples led to rapid oxidation of the amino groups because of the aqueous acidic reaction conditions. Attempts to deprotect the NBoc groups using trifluoroacetic acid were also not successful. Our previous work with hexadecaaminophenylsilsesquioxane, $[(NH_2)_2PhSiO_{1.5}]_8$, shows it to be very basic and very susceptible to air oxidation at room temperature.[33] Thus, we were concerned that similar efforts to generate samples for photophysical studies would risk including contributions from oxidized materials. Therefore, we decided that it was best to assess the photophysical properties of the NBocStyr$_x$OPS and AceStyr$_x$OPS as discussed below.

4.3.5 Two-photon Excited Fluorescence Measurements

The interaction of the functional groups at the corners of the cage can be very strong and it has been shown previously that this interaction can lead to new optical properties.[12] The possibility of enhancement of the cage macromolecule's two-photon absorption cross-section may result in possible applications in not only optical limiting and sensor protection but the enhanced transition moment of these systems may also lead to enhanced solar energy harvesting devices. In this section we discuss the linear and nonlinear optical properties of this new class of silsesquioxanes and probe their two-photon absorption properties both in magnitude and spectral width.

Table **4.9** provides much of the data taken in the current studies. The steady state absorption and emission spectra shown in Figures **4.6-4.8** are displayed comprehensively in Figure **A2.8**. As noted above, our efforts were directed towards understanding the photo-

physical effects of increasing functional group density in the same volume. Our previous studies provide a baseline for the studies conducted here.[11,12] In addition to the steady state studies summarized in the Table **4.9** data, we also carried out TPA measurements to investigate the charge transfer character.

Two-photon excited-state fluorescence (TPEF) measurements with a femtosecond laser were used to measure TPA cross-sections as a function of wavelength. It is clear from Figure **4.11** that the NBocStyr$_x$OPS compounds offer superior TPA cross-sections when compared with the AceStyr$_x$OPS compounds for RStyr$_{16}$OPS and RStyr$_{24}$OPS. This can be explained by the greater strength of the donor group and by changes in the dipole-moment.[34,35] It was also noted that TPA cross sections increase with an increase in the number of chromophores attached to the phenyl group. As seen in Table **4.9**, the cross-sections "per chromophore" in RStyr$_{24}$OPS are also enhanced by the additional chromophores in comparison with RStyr$_{16}$OPS and *o*-RStyr$_8$OPS systems.

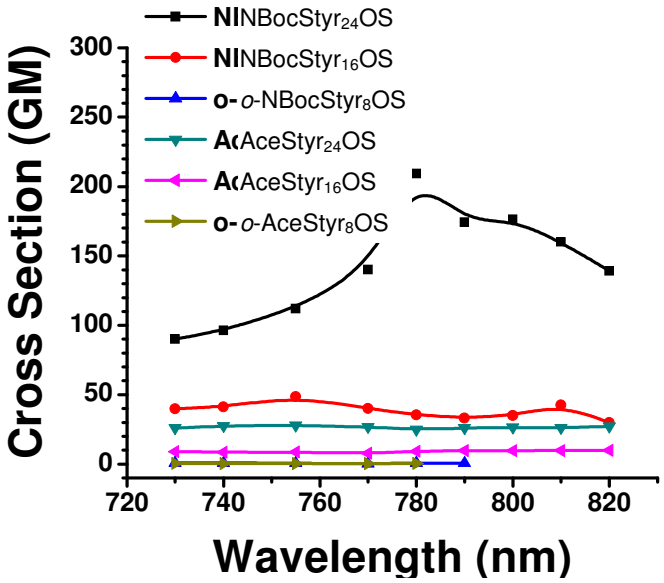

Figure 4.11. TPA cross section measurements of the investigated chromophores.

For NBocStyr$_{24}$OPS and NBocStyr$_{16}$OPS, the cross-section increases by a factor of 4.4, while the cross-section increase per chromophore is by a factor of 3. This seems to correlate well with the increase of the cross-section per chromophore, which seems to correlate well with the steady-state measurements of Table **4.9**. In the case of RStyr$_{16}$OPS, although the absorption measurements showed a red shift, the fluorescence emissions and

quantum yields suggest that the system possesses less charge transfer character. The literature suggests that molecular systems with symmetric charge transfer from the ends of a conjugation to the middle gives enhanced TPAs,[36] such as found here for $RStyr_{16}OPS$ and $RStyr_{24}OPS$. Similar trends are observed in $AceStyr_xOPS$ systems as well. Note that *o*-$NBocStyr_8OPS$ and *o*-$AceStyr_8OPS$ with cross-sections below 1 GM, do not appear to be promising two photon materials, but it may be that on deprotection they will offer TPAs equivalent to the *para* systems we have studied before.[11] Finally, time-resolved measurements are underway in order to understand the actual mechanism of the charge transfer character of these systems.[37]

4.4 Conclusions

A series of stilbene-silsesquioxanes ($RStyr_xOPS$, x = 8, 16, 24; R = 4-methylstyrenyl, 4-acetoxystyrenyl, Boc-protected 4-aminostyrenyl) have been synthesized from the corresponding bromophenyl-silsesquioxanes, $[o\text{-}BrPhSiO_{1.5}]_8$, $[2,5\text{-}Br_2PhSiO_{1.5}]_8$, and $[Br_3PhSiO_{1.5}]_8$. These molecules have some of the highest densities of functional groups/unit volume of any molecules even when compared to silsesquioxane dendrimers.[4-13,38-40] The blue shift in the absorption spectra and red shift in the emission spectra of *o*-$RStyr_8OPS$ compared to the small molecule analog suggests interactions between the electrophilic face of the silsesquioxane cage with the *ortho*-positioned organic group. In contrast, $RStyr_{16}OPS$ exhibit absorption and emission spectra as well as quantum efficiencies typical of simple organic compounds, most likely because of steric interaction forcing the organic groups away from the cage and disrupts the 3-D conjugation involving LUMO inside the silsesquioxane cage. $RStyr_{24}OPS$ exhibits photophysical behavior that shows characteristics of both regular π-π^* transition and charge transfer, suggesting that there are two excited states of nearly equivalent energy with similar decay rates, involving the LUMO inside the silsesquioxane cage as charge acceptor site. We expect these compounds to offer much greater TPA properties if suitable alternative methods of protecting the free amine from oxidation or replacing the acetoxy group are found (e.g. with perhaps using alkyl or aryl groups).

References Cited:

1. Cordes, D.B.; Lickiss, P.D.; Rataboul, F. "Recent Developments in the Chemistry of Cubic Polyhedral Oligosilsesquioxanes." *Chem. Rev*. **2010**, *10*, 2081-2173.
2. Lickiss, P.D.; Rataboul, F. "Fully Condensed Polyhedral Oligosilsesquioxanes (POSS): From Synthesis to Application." *Adv. Organomet. Chem*. **2008**, *57*, 1-116.
3. Laine, R.M.; Roll, M.F. "Polyhedral Phenylsilsesquioxanes." *Macromol*. **2011**, *44*, 1073-1109.
4. Chan, K.L.; Sonar, P.; Sellinger, A. "Cubic Silsesquioxanes for Use in Solution Processable Organic Light Emitting Diodes (OLED)." *J. Mater. Chem*. **2009**, *19*, 9103-9120.
5. Lin, W.-J.; Chen, W.-C.; Wu, W.-C.; Niu, Y.-H.; Jen, A.K.-Y. "Synthesis and Optoelectronic Properties of Starlike Polyfluorenes with a Silsesquioxane Core." *Macromol.* **2004**, *37*, 2335-2341.
6. Lee, J.; Cho, H.-J.; Jung, B.-J.; Cho, N.-S.; Shim, H.-K. "Stabilized Blue Luminescent Polyfluorenes: Introducing Polyhedral Oligomeric Silsesquioxane." *Macromol.* **2004**, *37*, 8523-8529.
7. Xiao, S.; Nguyen, M.; Gong, X.; Cao, Y.; Wu, H.; Moses, D.; Heeger, A.J. "Stabilization of Semiconducting Polymers with Silsesquioxane." *Adv. Funct. Mater*. **2003**, *13*, 25-29.
8. Chou, C.-H.; Hsu, S.-L.; Dinakaran, K.; Chiu, M.-Y.; Wei, K.-H. "Synthesis and Characterization of Luminescent Polyfluorenes Incorporating Side-Chain-Tethered Polyhedral Oligomeric Silsesquioxane Units." *Macromol.* **2005**, *38*, 745-751.
9. Sellinger, A.; Tamaki, R.; Laine, R.M.; Ueno, K.; Tanabe, H.; Williams, E.; Jabbour, G.E. "Heck Coupling of Haloaromatics with Octavinylsilsesquioxane: Solution Processable Nanocomposites for Application in Electroluminescent Devices." *Chem. Comm*. **2005**, 3700-3702.
10. Lo, M.Y.; Zhen, C.; Lauters, M.; Jabbour, G.E.; Sellinger, A. "Organic-Inorganic Hybrids Based on Pyrene Functionalized Octavinylsilsesquioxane Cores for Application in OLEDs." *J. Am. Chem. Soc*. **2007**, *129*, 5808-5809.
11. Sulaiman, S.; Bhaskar, A.; Zhang, J.; Guda, R.; Goodson III, T.; Laine, R.M. "Molecules with Perfect Cubic Symmetry as Nanobuilding Blocks for 3-D Assemblies. Elaboration of Octavinylsilsesquioxane. Unusual Luminescence Shifts May Indicate Extended Conjugation Involving the Silsesquioxane Core." *Chem. Mater*. **2008**, *20*, 5563-5573.
12. Laine, R.M.; Sulaiman, S.; Brick, C.; Roll, M.; Tamaki, R.; Asuncion, M.Z.; Neurock, M.; Filhol, J-S.; Lee, C-Y.; Zhang, J.; Goodson III, T.; Ronchi, M.; Pizzotti, M.; Rand, S.C.; Li, Y. "Synthesis and Photophysical Properties of Stilbeneoctasilsesquioxanes. Emission Behavior Coupled with Theoretical Modeling Studies Suggest a 3-D Excited State Involving the Silica Core." *J. Am. Chem. Soc*. **2010**, *132*, 3708-3722.

13. Asuncion, M.Z.; Laine, R.M. "Fluoride Rearrangement Reactions of Polyphenyl- and Polyvinylsilsesquioxanes as a Facile Route to Mixed Functional Phenyl, Vinyl T_{10} and T_{12} Silsesquioxanes." *J. Am. Chem. Soc*. **2010**, *132*, 3723-3736.

14. Yildirim, T.; Gehring, P.M.; Neumann, D.A.; Eaton, P.E.; Emrick, T. "Solid Cubane: A Brief Review." *Carbon* **1998**, *36*, 809-815.

15. Lee, J.; Hong, C.K.; Choe, S.; Shim, S.E. "Synthesis of Polystyrene/Silica Composite Particles by Soap-Free Emulsion Polymerization Using Positively Charged Colloidal Silica." *J. Colloid Interface Sci.* **2007**, *310*, 112-120.

16. Bachmann, S.; Wang, H.; Albert, K.; Partch, R. "Graft Polymerization of Styrene Initiated by Covalently Bonded Peroxide Groups on Silica." *J. Colloid Interface Sci.* **2007**, *309*, 169-175.

17. Kim, S.-G.; Sulaiman, S.; Fargier, D.; Laine, R.M. "Octaphenyloctasilsesquioxane and Polyphenylsilsesquioxane for Nanocomposite." In *Materials Syntheses. A Practical Guide*; Schubert, U., Hüsing, N., Laine, R., Eds.; Springer-Verlag: Wien, 2008; pp. 179-191.

18. Roll, M.; Asuncion, M.Z.; Kampf, J.; Laine, R.M. "*para*-Octaiodophenylsilsesquioxane, $[p\text{-}IC_6H_4SiO_{1.5}]_8$, a Nearly Perfect Nano-Building Block." *ACS Nano*, **2008**, *2*, 320-326.

19. Roll, M.F.; Mathur, P.; Takahashi, K.; Kampf, J. W.; Laine, R.M. "$[PhSiO_{1.5}]_8$ promotes self-bromination to produce $[o\text{-}BrPhSiO_{1.5}]_8$. Further bromination gives crystalline $[2,5\text{-}Br_2PhSiO_{1.5}]_8$ with a density of 2.38 g/cc and calculated refractive index of 1.7 (RI of sapphire is 1.76) or the tetraisocosa bromo compound $[Br_3PhSiO_{1.5}]_8$." *J. Matl. Chem*. 2011, 21, 11167-11176.

20. Roll, M.F.; "Symmetric Functionalization of Polyhedral Phenylsilsesquioxanes as a Route to Nano-Building Blocks." PhD dissertation, University of Michigan, **2010**. Molecular diameters were calculated based on single crystal x-ray data for silsesquioxane molecules with similar structures [$Styr_8$OPS and $(PhC{\equiv}C)_8$OPS] assuming cubic unit cells.

21. Nanjwade, B.K.; Bechra, H.M.; Derkar, G.K.; Manvi, F.V.; Nanjwade, V.K. "Dendrimers: Emerging polymers for drug-delivery systems." *Eur. J. Pharm. Sci*., **2009**, *38*, 185-196.

22. Brick, C.M; Tamaki, R.; Kim, S-G.; Asuncion, M.Z.; Roll, M.; Nemoto, T.; Laine, R.M. "Spherical, Polyfunctional Molecules Using Polybromooctaphenylsilsesquioxanes as Nanoconstruction Sites," *Macromol*. **2005**, *38*, 4655-4660.

23. Letant, S.E.; Herberg, J.; Dinh, L.N.; Maxwell, R.S.; Simpson, R.L.; Saab, A.P. "Structure and Catalytic Activity of POSS-Stabilized Pd Nanoparticles." *Catal. Comm.* **2007**, *8*, 2137-2142.

24. Garrett, C.E.; Prasad, K. "The Art of Meeting Palladium Specifications in Active Pharmaceutical Ingredients Produced by Pd-Catalyzed Reactions." *Adv. Synth. Catal*. **2004**, *346*, 889-900.

25. Samsonova, L.G.; Kopylova, T.N.; Svetlichnaya, N.N.; Andrienko,O.S. "The Photo-transformation of *trans*-Stilbene and Its Derivatives on Laser Excitation." *High Energy Chemistry,* **2002**, 36, 276-279.

26. Meier, H. "The Photochemistry of Stilbenoid Compounds and Their Role in Materials Technology." *Angew. Chem. Int. Ed. Engl.* **1992***, 31*, 1399-1540.

27. Malkes, L.Ya.; Boronenko, T.P. "Ultraviolet Absorption Spectra of ω-Triaryl-Substituted 1,2,4-Trivinylbenzenes." *Zhurnal Prikladnoi Spektroskopii,* **1974**, *21*, 172-175.

28. Meier, H.; Zertani, R.; Noller, K.; Oelkrug, D.; Krabichler, G. "Investigations on the Fluorescence of Styryl-substituted Benzenes." *Chem. Ber*. **1986**, *119***,** 1716-1724.

29. Anderson, S.E.; Bodzin, D.J.; Haddad, T.S.; Boatz, J.A.; Mabry, J.M.; Mitchell, C.; Bowers, M.T. "Structural Investigation of Encapsulated Fluoride in Polyhedral Oligomeric Silsesquioxane Cages Using Ion Mobility Mass Spectrometry and Molecular Mechanics." *Chem. Mater.*, **2008**, *20*, 4299-4309.

30. Feher, F.J.; Budzichowski, T.A. "Syntheses of Highly-Functionalized Polyhedral Oligosilsesquioxanes." *J. Organomet. Chem*. **1989**, *379*, 33-40.

31. Gregorius, H.; Baumgarten, M.; Reuter, R.; Tyutyulkov, N.; Müllen, K. "meta-Phenylene Units as Conjugation Barriers in Phenylenevinylene Chains." *Angew. Chem. Int. Ed. Engl.* **1992**, *31*, 1653-1655.

32. Hogen-Esch, T.E. "Synthesis and Characterization of Macrocyclic Vinyl Aromatic Polymers." *J. Poly. Sci. Part A: Polymer Chem.*, **2006**, *44*, 2139-2155.

33. Takahashi, K.; Sulaiman, S.; Katzenstein, J.M.; Snoblen, S.; Laine, R.M. "New Aminophenylsilsesquioxanes – Synthesis, Properties, and Epoxy Nanocomposites." *Australian J. Chem*. **2006**, *59*, 564-570.

34. Ramakrishna, G.; Bhaskar, A.; Goodson III, T. "Ultrafast Excited State Relaxation Dynamics of Branched Donor-π-Acceptor Chromophore: Evidence of a Charge-Delocalized State." *J. Phys. Chem. B*, **2006**, *110*, 20872-20878.

35. Ramakrishna, G.; Goodson III, T. "Excited-State Deactivation of Branched Two-Photon Absorbing Chromophores: A Femtoseond Transient Absorption Investigation." *J. Phys. Chem. A*, **2007**, *111*, 993-1000.

36. Albota, M.; Beljonne, D; Bredas, J-L.; Ehrlich. J.E.; Fu, J.Y.; Heikal, A.A; Hess, S.E.; Kogej, T.; Levin, M.D.; Marder, S.R.; Maughon, D.M.; Perry, J.W.; Rockel, H.; Rumi, M.; Subramaniam, G.; Webb, W.W.; Wu, X-L.; Xu, C. "Design of Organic Molecules with Large Two-Photon Absorption Cross Sections." *Science*, **1998**, 281, 1653-1656.

37. Zhang, J.; Goodson III, T. unpublished work.

38. Hong, B.; Thoms, T.P.S.; Murfee, H.J.; Lebrun, M.J. "Highly Branched Dendritic Macromolecules with Core Polyhedral Silsesquioxane Functionalities." *Inorg. Chem*., **1997**, *36*, 6146-6147.

39. Feher, F.J.; Wyndham, K.D. “Amine and Ester-Substituted Silsesquioxanes: Synthesis, Characterization and Use as a Core for Starburst Dendrimers.” *Chem. Comm*. **1998**, 323-324.

40. Dvornic, P.R.; Hartmann-Thompson, C.; Keinath, S.E.; Hill, E.J. “Organic-Inorganic Polyamidoamine (PAMAM) Dendrimer-Polyhedral Oligosilsesquioxane (POSS) Nanohybrids.” *Macromol.* **2004**, *37*, 7818-7831.

Chapter 5

Fluoride-Catalyzed Rearrangements of Polysilsesquioxanes. Mixed Methyl,Vinyl-T_8, -T_{10} and -T_{12} Cages.

Published in Applied Organometallic Chemistry vol. 24, pp. 551-557, 2010.

With contributions from Dr. Marco Ronchi (Dipartimento di Chimica Inorganica Metallorganica e Analitica dell'Universita` di Milano)

Abstract

Insoluble mixtures of polyvinylsilsesquioxane, -(vinyl$SiO_{1.5})_n$- PVSQ, and polymethylsilsesquioxanes, -(Me$SiO_{1.5})_n$- PMSQ, in tetrahydrofuran at ambient when treated with catalytic amounts (1-5 mole %) of fluoride ion introduced as tetrabutylammonium fluoride (n-Bu_4NF, TBAF) will depolymerize and dissolve. The resulting soluble species consist of [methyl$_x$vinyl$_{8-x}$($SiO_{1.5}$)]$_8$, [methyl$_x$vinyl$_{10-x}$($SiO_{1.5}$)]$_{10}$, and [methyl$_x$vinyl$_{12-x}$ ($SiO_{1.5}$)]$_{12}$. 1:1 ratio of PVSQ:PMSQ greatly favor formation of vinyl rich cages. Only at ratio of 1:5 are the proportions of methyl and vinyl groups in the cages approximately equal. Of the T_8, T_{10} and T_{12} species produced, all conditions tried including changing the solvent to ethanol or toluene or at reflux favor the formation of the larger cages sometimes completely excluding formation of the T_8 materials. Efforts to isolate the cage compounds by removal of solvent regenerates polysilsesquioxanes albeit those containing mixtures of methyl and vinyl groups. Introduction of $CaCl_2$ sufficient to form CaF_2 prior to workup prevents repolymerization allowing recovery of the mixed cage systems. The approach developed here provides a novel way to form mixed functional group silsesquioxane cages. The fact that T_{10} and T_{12} cage formation is favored appears to suggest that these cages are more stable than the traditionally produced T_8 cages.

5.1 Introduction

Polymer properties are dictated by a combination of monomer structure, chain length and processing. Monomer structure can often determine how the polymer coils, crystallizes, forms electrostatic or hydrogen bonds, and of course melts and/or dissolves. If the monomer unit provides extended conjugation along the polymer backbone, the polymer may offer conducting, semiconducting, emissive, or light absorptive properties of use in organic electronic and photonic applications. Rigid monomers lead to polymers with excellent mechanical properties and/or liquid crystallinity. Finally monomer structure can also dictate miscibility with other polymers.

Chain length can dictate T_g's, diffusion rates, viscosities, coefficients of thermal expansion (CTEs), extents of mechanical crosslinking and for short chains, the melt temperature. Processing provides control of chain-chain interactions on a molecular scale as a means of controlling global properties through control of molecular alignment providing for example, toughness, transparency, conductivity etc.

Given that specific polymer properties arise from specific types of monomers, degrees of polymerization and processing one can state: "One size does not fit all." We would like to suggest to the reader that there are certain types of polymer (oligomer) systems that may offer much more tailorability than others such that "One size fits many." One such system, encompasses the family of compounds called silsesquioxanes as illustrated in Figure **5.1**.[1-10]

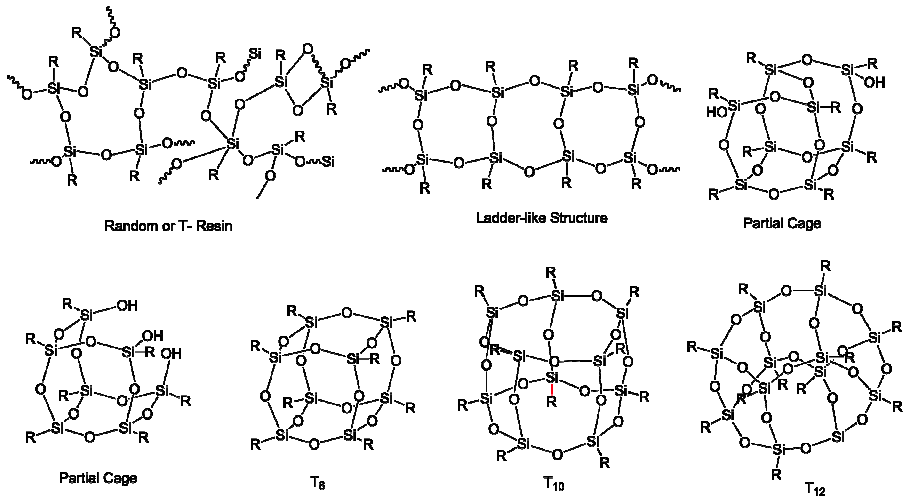

Figure 5.1. Types of silsesquioxanes.[1-14] Only oligomeric rather than polymeric ladders have been made to date.[6]

Because of the breadth of their properties, silsesquioxanes are of considerable interest to both the academic and industrial communities. This interest is such that, they have been the subject of 14 reviews in the last 25 years.[1-14] Furthermore, the R groups can and have been as varied as there are types of aliphatic and aromatic functional groups, offering considerable potential to control the properties of any oligomeric, polymeric, and/or organic/inorganic hybrid nanocomposites that could be made from them.[15] One drawback to the partial cages and oligomeric species is that they usually are not stable to further condensation of residual Si-OH groups, leading to the production of both H_2O and highly crosslinked materials. The resulting H_2O may affect the stability of the final product whereas further crosslinking may cause formation of insoluble materials that will precipitate or phase separate during processing, leading to unwanted properties, e.g. reduced transparency.

Here we describe a new approach to all of these materials (except ladder structures) that allows us to catalytically and selectively interconvert between many of the above structures at ambient temperatures (RT). In particular, the work reported here, representing baseline studies for a much greater set of studies, focuses on the conversion of mixtures of polymethylsilsesquioxane (PMSQ) and polyvinylsilsesquioxane (PVSQ) to mixed functional group T_{10} and T_{12} structures, Scheme **5.1**.

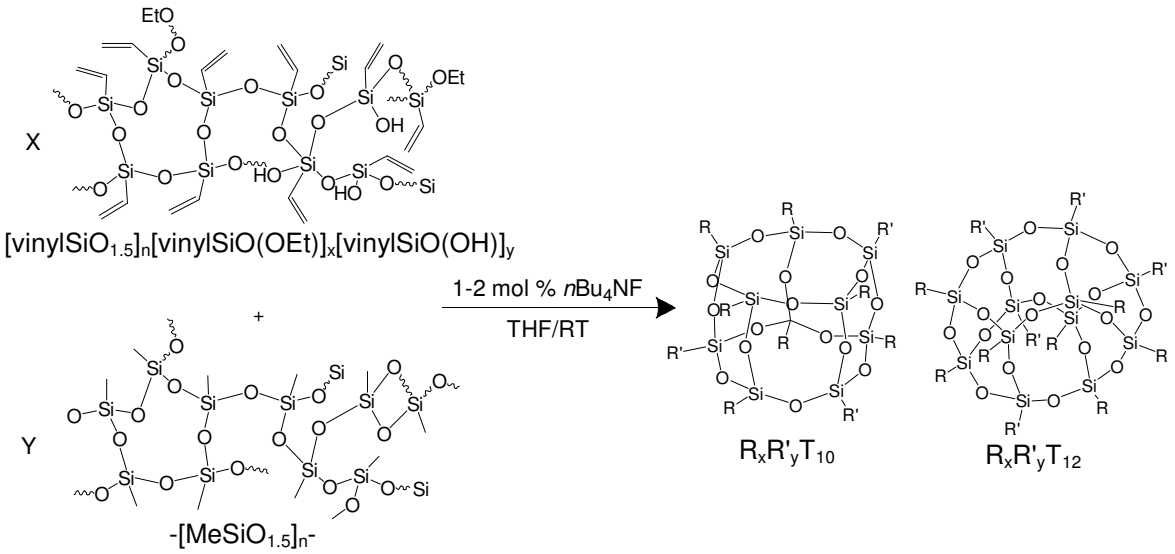

Scheme 5.1. General concept of fluoride catalyzed rearrangement of polysilsesquioxanes to mixed T_{10} and T_{12} isomers with varying vinyl and methyl contents. Note that some T_8 isomers are seen.

5.2 Experimental Procedures

The synthetic methods and characterization techniques are described in Chapter 2, along with more detailed experimental data.

5.3 Results and Discussion

It is pertinent to provide some background discussion to allow the reader to understand the motivation for the work presented here. Random structured silsesquioxanes are often called T resins and offer a number of useful properties centered about their excellent adhesion and high temperature stability. In one form, with R = H, methyl they are used as interlayer dielectrics processed either by spin-on or vapor deposition methods.[16-20] They are also called organic silicates.[21-24] In other forms they are used to form molds, as clear coats for a wide variety of substrates and for example are a major component of silicone-based caulks.[25] In other studies, they have been touted as potentially novel nanobuilding blocks for the construction of organic/inorganic hybrids with control of properties at nanometer length scales, and are also noted for having unusual properties in their own right.[27-38]

The work reported here extends work by Bassindale et al.[39-41] targeting the synthesis of $[RSiO_{1.5}]_8$ compounds from alkoxysilanes, see Scheme **5.2**, using 50 mol% nBu$_4$NF (tetrabutylammonium fluoride). Table **5.1** illustrates the yields for selected R groups. Of particular interest to us was the fact that no methyl cages were observed to form in these studies.

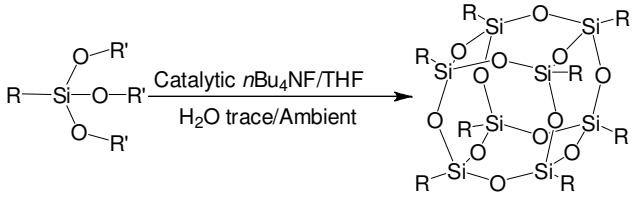

Scheme 5.2. Synthesis of $[RSiO_{1.5}]_8$ cages from alkoxysilanes.[39]

Table 5.1. Synthesis of cage compounds from the alkoxysilanes using nBu$_4$NF.[41a]

R	% T_8 yield	Other cages	R	% T_8 yield	Other cages
Phenyl	49	T_{12}	Hexyl	44	T_{10}
Methyl	0	--	Octyl	65	T_{10}
Vinyl	1	T_{10}, T_{12}	Isobutyl	26	T_{10}
Allyl	1	T_{10}, T_{12}	Cyclopentyl	95	--
			Cyclohexyl	84	--

Bassindale et al. coincidentally discovered that the use of 50 mol% nBu$_4$NF led to formation of fluoride encapsulated compounds as shown in the forward direction in Scheme **5.3**.[40,41] Most recently, Bowers et al. reported that the same products could be isolated directly from the cage by reaction of equimolar quantities of the tetramethylammonium fluoride, Me$_4$NF, as suggested in Scheme **5.3** going from right to left.[42]

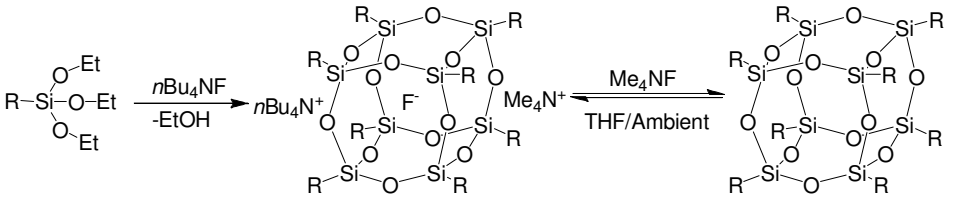

Scheme 5.3. Synthesis of fluoride ion encapsulation within silsesquioxane cages.[40-42]

In general, both groups found that F$^-$ encapsulation requires that the R groups be at least partially electron withdrawing, limiting the types of F$^-$@[RSiO$_{1.5}$]$_8$ (@ refers to encapsulated F$^-$) to R = aryl, vinyl and partially fluorinated alkyls. Of particular note was the discovery by Bowers et al. that reaction of [iBu$_7$(styrene)T$_8$] with stoichiometric Me$_4$NF gave a mixture of products (Scheme **5.4**) with F$^-$@[iBu$_7$(styrene)T$_8$]Me$_4$N$^+$ being a minor component. A second set of studies, shown in Schemes **5.5** and **5.6**, provides additional information.

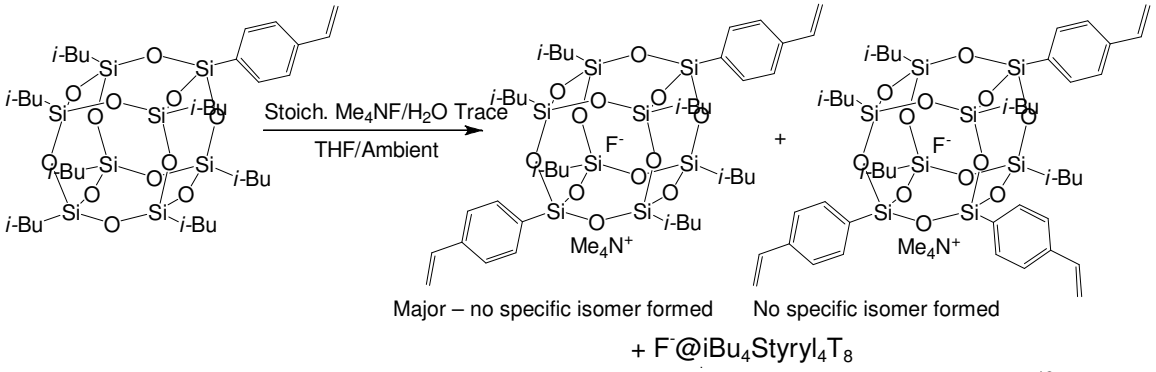

Scheme 5.4. Treatment of [iBu$_7$(styrene)T$_8$] with stoichiometric Me$_4$NF.[42]

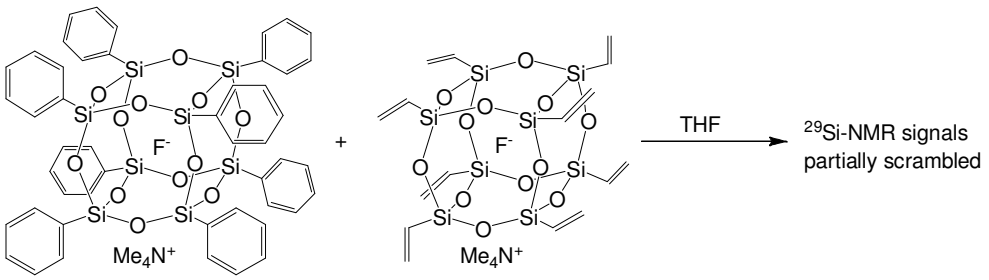

Scheme 5.5. Treatment of equimolar $F^-@[PhSiO_{1.5}]_8$ and $F^-@[ViSiO_{1.5}]_8$.[42]

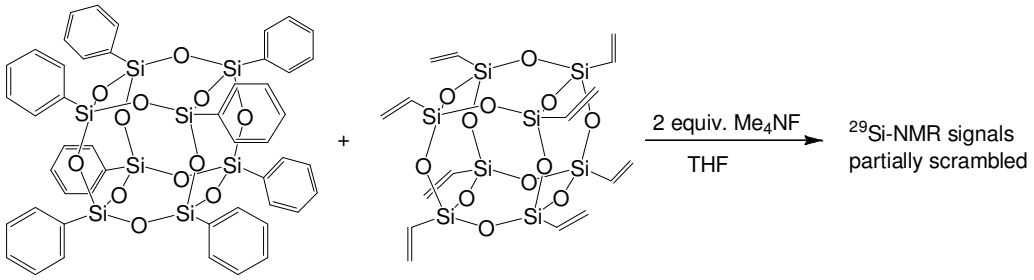

Scheme 5.6. Treatment of equimolar $[PhSiO_{1.5}]_8$ and $[ViSiO_{1.5}]_8$ with 2 equivalent Me_4NF.[42]

The reactions illustrated in Schemes **5.4**-**5.6** indicate that these cage systems are not truly stable at ambient in solution. They also suggest that the isolated F^- ion-encapsulated cage systems are actually kinetic products and they fall apart in solution. This suggested to us that such reactions might actually be promoted by only catalytic amounts of F^-. We have now done extensive studies on these systems and report here one single aspect of this work, the depolymerization of PVSQ and PMSQ mixtures to form cage structures.

The synthesis of octavinylsilsesquioxane, $[vinylSiO_{1.5}]_8$ from hydrolysis of $vinylSiCl_3$ in aqueous EtOH provides yields of 35-45% depending on the scale of the reaction.[43] The remaining material recovered from solution consists of a mixed polymer suggested by: $[vinylSiO_{1.5}]_n$,$[vinylSiO(OEt)]_x[vinylSiO(OH)]_y$. On removal of solvent, this material generates a completely insoluble and heretofore useless byproduct.

We were therefore surprised to find that treating this insoluble polymer with ≈ 2 mol% nBu$_4$NF in THF/ambient/24 h causes it to dissolve into solution (see Scheme **5.7**). MALDI-ToF of the solution shows a mixture of cages as seen in Figure **5.2**. However, efforts to isolate the cages led only to regenerated polymer, which however remained THF soluble.

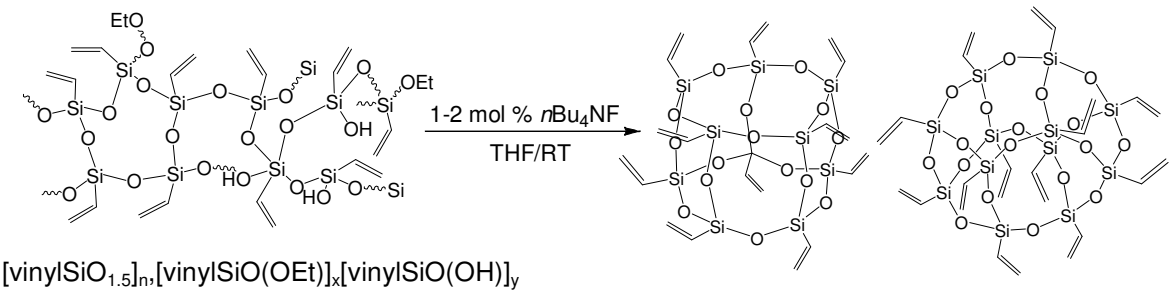

$[vinylSiO_{1.5}]_n$,$[vinylSiO(OEt)]_x[vinylSiO(OH)]_y$

Scheme 5.7. Treatment of PVSQ with catalytic *n*Bu_4NF.

The simplest explanation for repolymerization is as mentioned above: the cages are very labile in solution with the presence of F^- ion, and while easily formed, they revert to a soluble polymeric form upon concentration. Consequently, we decided to trap the F^- ion by adding small amounts of $CaCl_2$ to form the insoluble CaF_2 allowing the recovery of the cage compounds, Figure **5.2**. Recognizing that the original PVS is insoluble, Figure **5.3** illustrates the various processes observed by GPC.

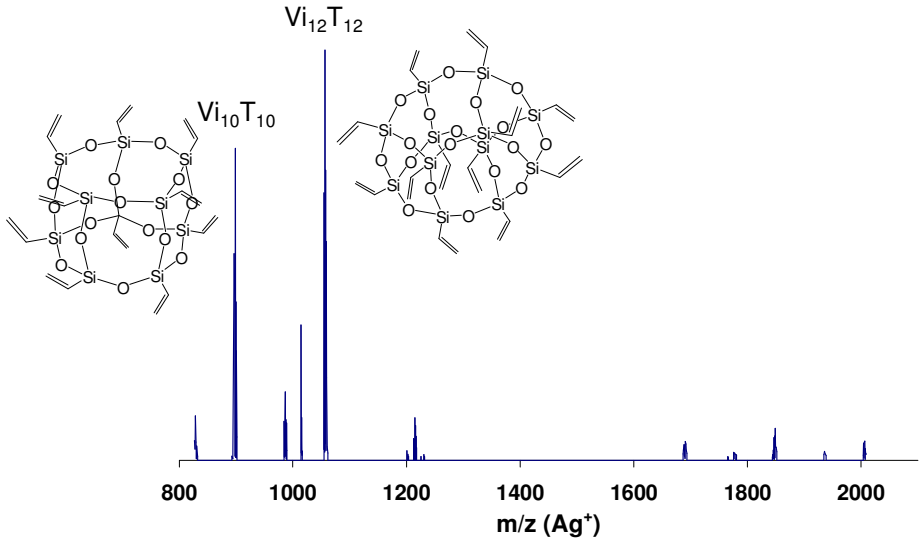

Figure 5.2. MALDI-TOF spectrum of *n*Bu_4NF-catalyzed PVSQ dissolution quenched with $CaCl_2$.

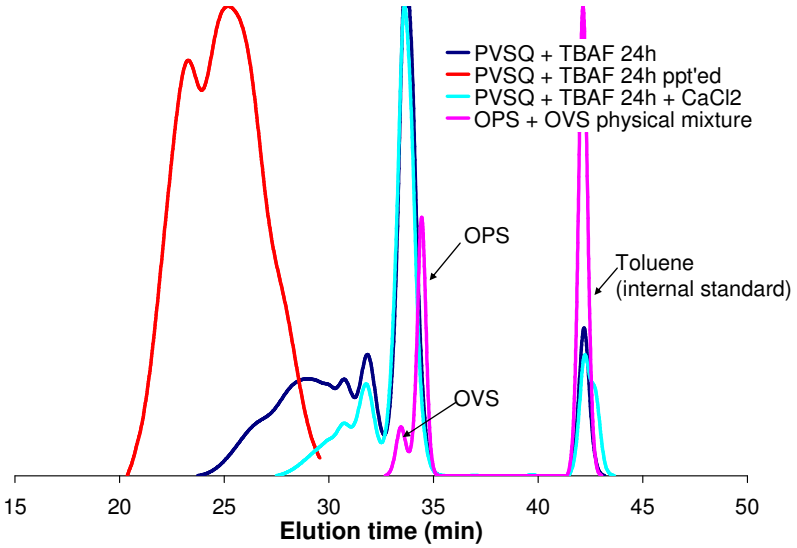

Figure 5.3. GPC analysis of ambient *n*Bu_4NF-catalyzed PVSQ dissolution. Note that on precipitation it returns to a high MW albeit soluble polymer. OPS is $[PhSiO_{1.5}]_8$ used as an internal standard, TBAF = *n*Bu_4NF.

It is important to point out that the major products seen by MALDI-ToF are the T_{10} and T_{12} cages. We see only small amounts of the T_8 materials. Thus, it could be argued that among the polyhedral silsesquioxane systems, the T_{10} and T_{12} cages are more stable than the T_8 cages.

One possible reason that T_8 compounds are most often recovered is that they are the least soluble of the cage systems and basically precipitate from solution first, as discussed by Brown et al.[44] Therefore, one might assume from these results that the T_8 systems are most stable cages. Clearly more work needs to be done; nonetheless the results reported here suggest whole new areas of research on the higher member cages.

We also conducted similar studies with PMSQ, which was insoluble in THF. The addition of ≈ 2 mol% *n*Bu_4NF solubilized approximately 25% of this polymer. The isolated product gives peaks in the MALDI-ToF spectrum that can be assigned to the $Me_{10}T_{10}$ cage and what appears to be an incomplete cage, $Me_9T_9(OH)_3$, missing one vertex. It is important to add that MALDI-ToF only sees species volatile under the analytical conditions. The GPC data suggest the presence of small amounts of oligomers not seen in the MALDI-ToF that may be partial cage species.

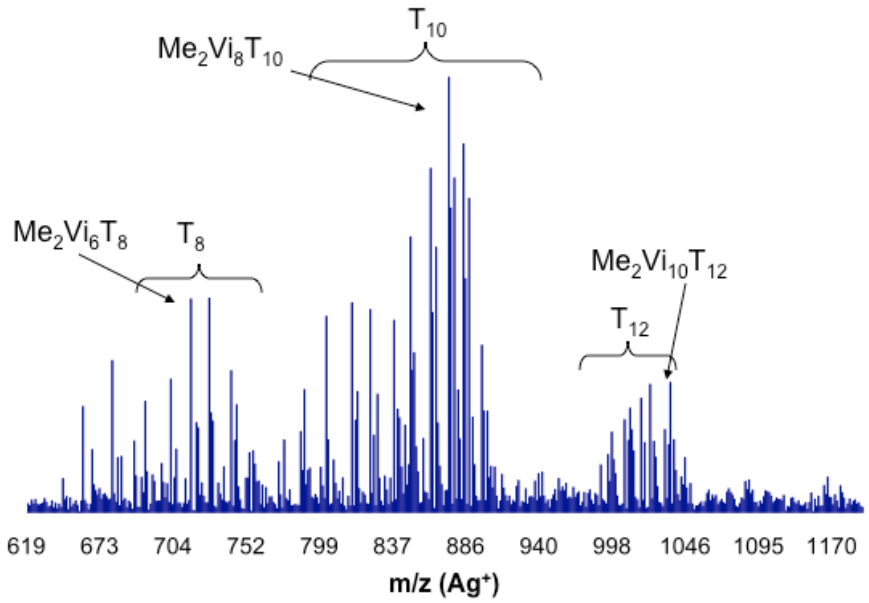

Figure 5.4. Room temperature *n*Bu$_4$NF-catalyzed dissolution of 1:1 PMSQ:PVSQ.

Given the apparent difficulty observed by Bassindale in producing methyl cages, we attempted to convert PMSQ and PVSQ to mixed cages per Scheme **5.1**. As seen in Figure **5.4**, at a 1:1 mole ratio, very few methyl groups are incorporated into the cages arguing for lower PMSQ reactivity. Thus, increasing the ratio to 5:1 provided better methyl:vinyl ratios in the soluble products as seen in Figure **5.5**.

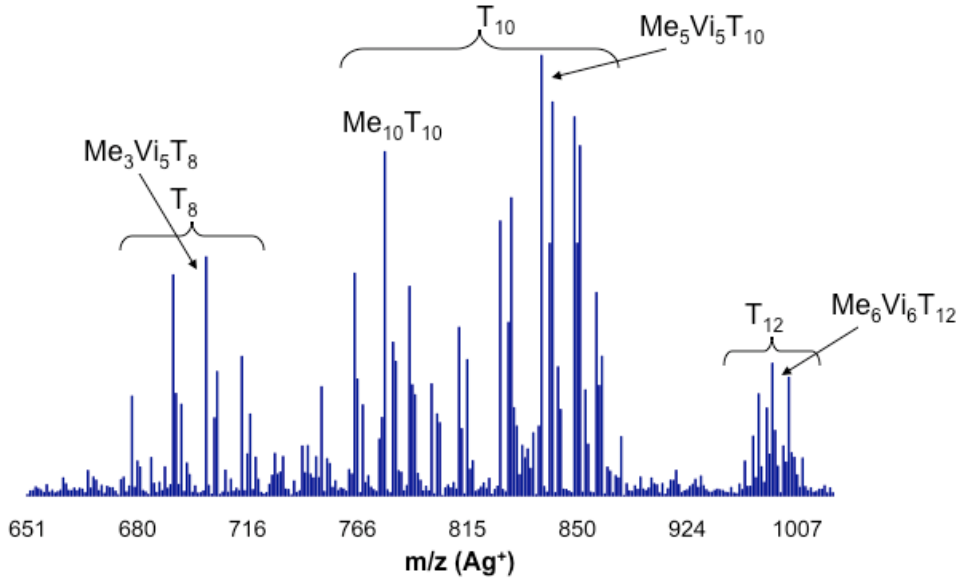

Figure 5.5. Room temperature *n*Bu$_4$NF-catalyzed dissolution of 5:1 PMSQ:PVSQ.

Other efforts to affect the ratios of methyl and vinyl groups in the resulting mixed cages led to solvent studies using toluene and EtOH. Unfortunately, only the PVSQ converts to cage compounds in toluene or EtOH at ambient (RT) with PMSQ remaining mostly unreactive. Also, at THF reflux it was possible to isolate small amounts of mixed-

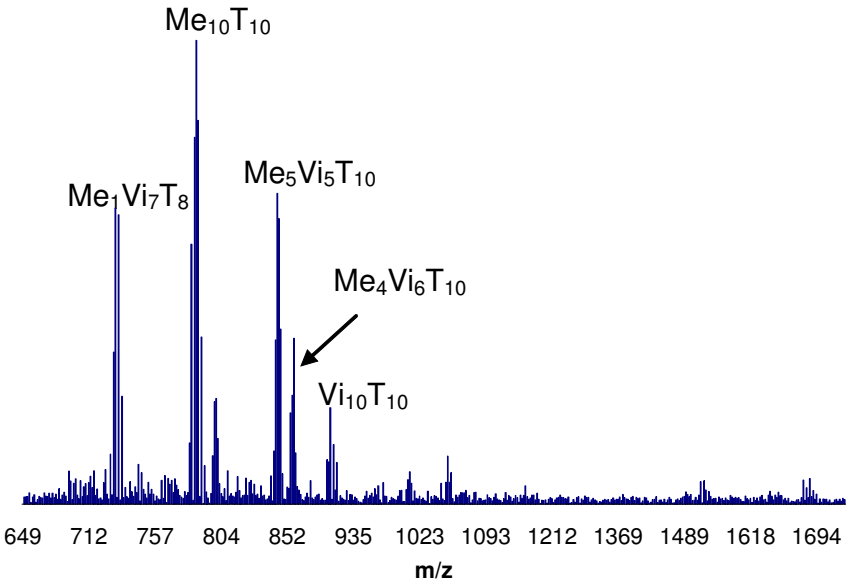

Figure 5.6. *n*Bu$_4$NF-catalyzed dissolution of 5:1 PMSQ:PVSQ in THF at reflux.

group systems per Figure **5.6**. Note that fluoride ion is known to cleave Si-C bonds on heating suggesting this route is not useful from a synthetic standpoint.[45]

The results obtained in these two papers differ from those observed here where the T_{10} and T_{12} cages are the major products. The *n*Bu$_4$NF concentrations used in our work were typically 1-3 mol% or 1:100 to 1:33 F^-:reactant ratios, contrasting with the 0.5:1 to 1:1 F^-:reactant ratios used in the work done by Bassindale et al. Although their two papers discuss the use of *n*Bu$_4$NF as a base in catalytic amounts, in reality they actually use 0.5:1 to 1:1 F^-:reactant molar ratios[42] where the fluoride may act simply as a base.

Clearly more work needs to be done on this system, especially the use of ^{29}Si- and ^{19}F- NMR to identify the active intermediates. However, there is sufficient information available from the above studies to make several general observations.

Given that the Si-O bond is 110-120 kcal/mol and the Si-F bond is even stronger at 120-140 kcal/mol for tetravalent silicon compounds,[46] the rapid exchange seen here catalyzed by F^- at concentrations of as little as 1 mol% of the silsesquioxane points to very

unusual processes. First, it is well recognized that F^- will act as a nucleophile reacting with Si-complexes to form highly fluxional pentacoordinate compounds where rapid exchange of the F^- ligand at silicon has been postulated even at subzero temperatures.[47,48] We assume that such a mechanism is occurring here, but with some differences, as the attack of F^- must lead to rapid fragmentation of polymeric and/or cage silsesquioxanes leading to species that can recombine to form primarily the T_{10} and T_{12} cages.

As noted above, the formation of $F^-@R_8T_8$ requires some electron withdrawing groups on the cage. It can be assumed that electron-withdrawing groups promote fragmentation as a first step in F^- encapsulation. The inability to form $F^-@R_8T_8$ where R = simple alkyl would suggest therefore that F^- cannot cause fragmentation of the Si-O bonds in these types of cages or in PMSQ. However F^- can promote fragmentation when R = vinyl, which in turn apparently can react with PMSQ to form mixed methyl,vinyl-silsesquioxane cages. This implies that the species generated, likely some type of $(vinylSi)_xO_yF^-$, is able to break Si-O bonds in PMSQ leading to at least partial fragmentation of PMSQ Si-O bonds. It may even be that double fluorides are actually the responsible species, e.g. $(vinylSi)_xO_yF^-_2$.[49]

The exact mechanisms and kinetics of this reaction are beyond the scope of this dissertation. In future papers and dissertations, our group will demonstrate methods of making multiple different types of mixed-functional group cages, beads-on-a-chain oligomers and methods of recycling T-resins.

5.4 Conclusions

Treatment of insoluble PMSQ and PVSQ with catalytic amount of nBu$_4$NF in tetrahydrofuran at ambient yield mixed methyl- and vinyl-functionalized T_8, T_{10}, and T_{12} cages after trapping of the F^- ion with $CaCl_2$. Higher ratios of PMSQ to PVSQ are required to introduce equal proportions of methyl and vinyl groups in the resulting SQ cages. Formation of T_{10} and T_{12} cages is greatly favored, suggesting that these cages are thermodynamic products, whereas T_8 cages are kinetic product.

References Cited:

1. Voronkov, M.G.; Lavrent'yev, V.I. "Polyhedral Oligosilsesquioxanes and Their

Homo Derivatives." *Top. Curr. Chem.* **1982**, *102*, 199-236.

2. Baney, R.H.; Itoh, M.; Sakakibara, A.; Suzuki, T. "Silsesquioxanes." *Chem. Rev*. **1995**, *95*, 1409-1430.
3. Lichtenhan, J. "Silsesquioxane-based Polymers." In *Polymeric Materials Encyc.*; Salmone, J.C., Ed.; CRC Press: N.Y., 1996; Vol. 10; pp. 7768-7777.
4. Provatas, A.; Matisons, J.G. "Silsesquioxanes: Synthesis and Applications." *Trends Polym. Sci*. **1997**, *5*, 327-333.
5. Duchateau, R. "Half-Sandwich Titanium Complexes Stabilized by a Novel Silsesquioxane Ligand: Soluble Model Systems for Silica-Grafted Olefin Polymerization Catalysts." *Chem. Rev*. **2002**, *102*, 3525-3542.
6. Abe, Y.; Gunji, T. "Oligo- and Polysiloxanes." *Prog. Poly. Sci*. **2004**, *29*, 149-182.
7. Phillips, S.H.; Haddad, T.S.; Tomczak, S.J. "Developments in Nanoscience: Polyhedral Oligomeric Silsesquioxane (POSS)-Polymers." *Current Opinion in Solid State and Mater. Sci*. **2004**, *8*, 21-29.
8. Laine, R.M. "Nanobuilding Blocks Based on the $[OSiO_{1.5}]_x$ (x = 6, 8, 10) Octasilsesquioxanes." *J. Mater. Chem*. **2005**, *15*, 3725-3744.
9. Lickiss, P.D.; Rataboul, F. "Fully Condensed Polyhedral Oligosilsesquioxanes (POSS): From Synthesis to Application." *Adv. Organomet. Chem*. **2008**, *57*, 1-116.
10. Loy, D.A.; Shea, K.J.; "Bridged Polysilsesquioxanes. Highly Porous Hybrid Organic-Inorganic Materials." *Chem. Rev*. **1995**, *95*, 1431-1442.
11. Calzaferri, G. "Octasilsesquioxanes." In *Tailor-Made Silicon-Oxygen Compounds, from Molecules to Materials*; Corriu, R. and Jutzi, P., Eds.; Friedr. Vieweg & Sohn mbH: Braunschweig/Wiesbaden, Germany, 1996; pp. 149-169.
12. Li, G.; Wang, L.; Ni, H.; Pittman, C.U. "Polyhedral Oligomeric Silsesquioxane (POSS) Polymers and Copolymers: A Review." *J. Inorg. and Organomet. Polymers,* **2001**, *11,* 123-151
13. Chan, K.L.; Sonar, P.; Sellinger, A. "Cubic silsesquioxanes for use in solution processable organic light emitting diodes (OLED)." *J. Mater. Chem.* **2009**, *19*, 9103-9120.
14. Cordes, D.B.; Lickiss, P.D.; Rataboul, F. "Recent Developments in the Chemistry of Cubic Polyhedral Oligosilsesquioxanes," *Chem. Rev.* **2010**, *10*, 2081–2173
15. For examples see: (a) *Organic/Inorganic Hybrid Materials*; Laine, R.M., Sanchez, C., Brinker, C.J., Giannelis, E., Eds.; MRS Symp. Ser. Vol. 519; Materials Research Society: Warrendale, PA, 1998. (b) *Organic/Inorganic Hybrid Materials*; Laine, R.M., Sanchez, C., Brinker, C.J., Giannelis, E., Eds.; MRS Symp. Ser. Vol. 628; Materials Research Society: Warrendale, PA, 2000. (c) *Organic/Inorganic Hybrid Materials 2004*; Laine, R.M., Schubert, U., Chujo, Y., Eds.; MRS Symp. Ser. Vol. 847; Materials Research Society: Warrendale, PA, 2005. (d) *Organic/Inorganic Hybrid Materials 2007*; Barbé, R., Laine, R.M., Sanchez, C., Schubert, U., Eds.; MRS Symp. Ser. Vol. 1007; Materials Research Society: Warrendale, PA, 2008.
16. Chen, Y.; Kang, E-T. "New Approach to Nanocomposites of Polyimides Containing

Polyhedral Oligomeric Silsesquioxane for Dielectric Applications." *Mater. Lett*. **2004**, *58*, 3716-3719.

17. Lee, J-K.; Char, K.; Rhee, H-W.; Ro, H-K.; Yoon, D.Y. "Synthetic Control of Molecular Weight and Microstructure of Processible Poly(methylsilsesquioxane)s for Low-Dielectric Thin Film Applications." *Polymer* **2001**, *42*, 9085-9089.
18. Mikoshiba, S.; Hayase, S. "Preparation of Low Density Poly(methylsilsesquioxane)s for LSI Interlayer Dielectrics with Low Dielectric Constant. Fabrication of Angstrom Size Pores Prepared by Baking Trifluoropropylsilyl Copolymers." *J. Mater. Chem*. **1999**, *9*, 591-598.
19. Mirau, P.A.; Yang, S. "Solid-State Proton NMR Characterization of Ethylene Oxide and Propylene Oxide Random and Block Copolymer Composites with Poly(methylsilsesquioxanes)." *Chem. Mater*. **2002**, *14*, 249-255.
20. Nguyen, C.V.; Carter, K.R.; Hawker, C.J.; Hedrick, J.L.; Jaffe, R.L.; Miller, R.D.; Remenar, J.F.; Rhee, H-W.; Rice, P.M.; Toney, M.F.; Trollsås, M.; Yoon, D.Y. "Low-Dielectric, Nanoporous Organosilicate Films Prepared via Inorganic/Organic Polymer Hybrid Templates." *Chem. Mater.* **1999,** *11,* 3080-3085.
21. Ro, H.W.; Char, K.; Jeon, E-C.; Kim, H-J.; Kwon, K.; Lee, H-J.; Lee, J-K.; Rhee, H-W; Soles, C.L.; Yoon, D.Y. "High-Modulus Spin-On Organosilicate Glasses for Nanoporous Applications." *Adv. Mater*. **2007**, *19*, 705-710.
22. Ro, H.W.; Jones, R.L.; Peng, H.; Hines, D.R.; Lee, H.-J.; Lin, E.K.; Karim, A.; Yoon, D.Y.; Gidley, D.W.; Soles, C.L. "The Direct Patterning of Nanoporous Interlayer Dielectric Insulator Films by Nanoimprint Lithography." *Adv. Mater.* **2007**, *19,* 2919-2924.
23. Kim, H.-C.; Wallraff, G.; Kreller, C.R.; Angelos, S.; Lee, V.Y.; Volksen, W.; Miller, R.D. "Photopatterned Nanoporous Media." *Nano Lett.* **2004**, *4*, 1169-1174.
24. Oh, W.; Ree, M. "Anisotropic Thermal Expansion Behavior of Thin Films of Polymethylsilsesquioxane, a Spin-on Glass Dielectric for High-Performance Integrated Circuits." *Langmuir* **2004**, *20*, 6932-6939.
25. Arkles, B. "Commercial Applications of Sol-Gel-Derived Hybrid Materials." *MRS Bulletin* May **2001**, 402-408.
26. Lichtenhan, J.D.; Vu, N.Q.; Carter, J.A.; Gilman, J.W.; Feher, F.J. "Silsesquioxane-Siloxane Copolymers from Polyhedral Silsesquioxanes." *Macromol.* **1993**, *26*, 2141-2142.
27. Wright, M.E.; Schorzman, D.A.; Feher, F.J.; Jin, R.-Z. "Synthesis and Thermal Curing of Aryl-Ethynyl-Terminated *co*POSS Imide Oligomers: New Inorganic/Organic Hybrid Resins." *Chem. Mater.* **2003**, *15*, 264-268.
28. Laine, R.M.; Choi, J.; Lee, I. "Organic/Inorganic Nanocomposites with Completely Defined Interfacial Interactions." *Adv. Mater*. **2001**, *13*, 800-803.
29. Roll, M.F.; Asuncion, M.Z.; Kampf, J.; Laine, R.M. "para-Octaiodophenylsilsesquioxane, $[p\text{-}IC_6H_4SiO_{1.5}]_8$, a Nearly Perfect Nano-Building Block." *ACS Nano* **2008**, *2*, 320-326.

30. Tamaki, R.; Tanaka, Y.; Asuncion, M.Z.; Choi, J.; Laine, R.M. "Octa(aminophenyl)-silsesquioxane as a Nanoconstruction Site." *J. Am. Chem. Soc*. **2001**, *123*, 12416-12417.

31. Tamaki, R.; Choi, J.; Laine, R.M. "A Polyimide Nanocomposite from Octa(aminophenyl)silsesquioxane." *Chem. Mater*. **2003**, *15*, 793-797.

32. Sulaiman, S.; Brick, C.M.; De Sana, C.M.; Katzenstein, J.M.; Laine, R.M.; Basheer, R.A. "Tailoring the Global Properties of Nanocomposites. Epoxy Resins with Low Coefficients of Thermal Expansion." *Macromol*. **2006**, *39*, 5167-5169.

33. Choi, J.; Harcup, J.; Yee, A.F.; Zhu, Q.; Laine, R.M. "Organic/Inorganic Hybrid Composites from Cubic Silsesquioxanes." *J. Am. Chem. Soc*. **2001**, *123*, 11420-11430.

34. Choi, J.; Tamaki, R.; Kim, S.G.; Laine, R.M. "Organic/Inorganic Imide Nanocomposites from Aminophenylsilsesquioxanes." *Chem. Mater*. **2003**, *15*, 3365-3375.

35. Laine, R.M.; Roll, M.; Asuncion, M.; Sulaiman, S.; Popova, V.; Bartz, D.; Krug, D.J.; Mutin, P.H. "Perfect and Nearly Perfect Silsesquioxane (SQs) Nanoconstruction Sites and Janus SQs." *J. Sol-Gel Sci. and Tech*. **2008**, *46*, 335-347.

36. Sulaiman, S.; Brick, C.; Roll, M.; Bhaskar, A.; Goodson III, T.; Zhang, J.; Laine, R.M. " Molecules with Perfect Cubic Symmetry as Nanobuilding Blocks for 3-D Assemblies. Elaboration of Octavinylsilsesquioxane. Unusual Luminescence Shifts May Indicate Extended Conjugation Involving the Silsesquioxane Core." *Chem Mater*. **2008**, *20*, 5563-5573.

37. Brick, C.M.; Tamaki, R.; Kim, S-G.; Asuncion, M.Z.; Roll, M.; Nemoto, T.; Laine, R.M. "Spherical, Polyfunctional Molecules Using Poly(bromophenylsilsesquioxane)s as Nanoconstruction Sites." *Macromol.* **2005**, *38*, 4655-4660.

38. Asuncion, M.Z.; Roll, M.F.; Laine, R.M. "Octaalkynylsilsesquioxanes, Nano Sea Urchin Molecular Building Blocks for 3-D Nanostructures." *Macromol.* **2008**, *41*, 8047-8052.

39. Bassindale, A.R.; Pourny, M.; Taylor, P.G.; Hursthouse, M.B.; Light, M.E. "Fluoride-Ion Encapsulation within a Silsesquioxane Cage." *Angew. Chem. Int. Ed.* **2003**, *42*, 3488-3490.

40. (a) Bassindale, A.R.; Chen, H.; Liu, Z.; MacKinnon, I.A.; Parker, D.J.; Taylor, P.G.; Yang, Y.; Light, M.E. "A Higher Yielding Route to Octasilsesquioxane Cages using Tetrabutylammonium Fluoride, Part 2: Further Synthetic Advances, Mechanistic Investigations and X-ray Crystal Structure Studies into the Factors that Determine Cage Geometry in the Solid State." *J. Organomet. Chem.* **2004**, *689*, 3287-3300. (b) Bassindale, A.R.; Parker, D.J.; Pourny, M.; Taylor, P.G.; Horton, P.N.; Hursthouse, M.B. "Fluoride Ion Entrapment in Octasilsesquioxane Cages as Models for Ion Entrapment in Zeolites. Further Examples, X-ray Crystal Structure Studies, and Investigations into How and Why They May Be Formed." *Organomet.* **2004***, 23*, 4400-4405.

41. (a) Bassindale, A.R.; Liu, Z.; MacKinnon, I.A.; Taylor, P.G.; Yang, Y.; Light, M.E.; Horton, P.N.; Hursthouse, M.B. "A Higher Yielding Route for T_8 Silsesquioxane Cages and X-ray Crystal Structures of Some Novel Spherosilicates." *Dalton Trans*.

2003, 2945-2949. (b) Liu, Z.; Bassindale, A.R.; Taylor, P.G. "Synthesis of Silsesquioxane Cages from Phenyl-*cis*-tetrol, 1,3-Divinyltetraethoxydisiloxane and Cyclopentyl Resins." *Chem. Res. Chinese U.* **2004**, *20*, 433-436.

42. Anderson, S.E.; Bodzin, D.J.; Haddad, T.S.; Boatz, J.A.; Mabry, J.M.; Mitchell, C.; Bowers, M.T. "Structural Investigation of Encapsulated Fluoride in Polyhedral Oligomeric Silsesquioxane Cages Using Ion Mobility Mass Spectrometry and Molecular Mechanics." *Chem. Mater*. **2008**, *20*, 4299-4309.
43. Harrison, P.G.; Hall, C. "Preparation and Characterization of Octasilsesquioxane Cage Monomers." *Main Group Met. Chem.* **1997**, *20*, 515-529.
44. Brown Jr., J.F.; Vogt Jr., L.H.; Prescott, P.I. "Preparation and Characterization of the Lower Equilibrated Phenylsilsesquioxanes." *J. Am. Chem. Soc*. **1964**, *86*, 1120-1125.
45. (a) Jones, G.R.; Landais, Y. "The Oxidation of the Carbon-Silicon Bond." *Tetrahedro*n, **1996**, 52, 7599-7662. (b) Itami, K.; Mitsudo, K.; Yoshida, J. "Directed Intermolecular Carbomagnesation across Vinylsilanes: 2-PyMe_2Si Group as a Removable Directing Group." *Angew. Chem.*, **2001**, *113*, 2399-2401.
46. Brook, M.A. *Silicon in Organic, Organometallic, and Polymer Chemistry*; Wiley: New York, 2000, pp. 29.
47. Farnham, W.B.; Harlow, R.L. "Stereomutation at Pentacoordinate Silicon by Intramolecular Ligand Exchange." *J. Am. Chem. Soc.* **1981**, *103*, 4608-4610.
48. Penso, M.; Albanese, D.; Landini, D.; Lupi, V. "Biaryl Formation: Palladium Catalyzed Cross-Coupling Reactions between Hypervalent Silicon Reagents and Aryl Halides." *J. Mol. Cat. A: Chemical* **2003**, *204-205*, 177-185.
49. Kost, D.; Kalikhman I. "Hypervalent Silicon Compounds." In *The Chemistry of Organic Silicon Compounds*; Rappoport, Z., Apeloig, Y., Eds.; John Wiley & Sons: Chichester, England, 1998; Vol. 2, pp. 1339-1436.

Chapter 6
Silsesquioxane-based Epoxy Resins with Very Low Coefficients of Thermal Expansion

Published in Macromolecules vol. 39, pp. 5167-5169, 2006.

Abstract

The cubic symmetry of octameric silsesquioxanes places reactive functionality in each octant in Cartesian space at a nanometer length scale. In principle, the coupling of these functional groups should permit covalent assembly of these novel organic/inorganic hybrids thereby providing mechanisms for tailoring global properties in the resulting nanocomposites at the finest length scales. We now find, building on earlier work, that it is possible to use the $[NH_2PhSiO_{1.5}]_8$ OAPS nanobuilding block with a variety of liquid polyfunctional epoxies to produce low viscosity (1000 MPa-sec), easily cured epoxy resin systems wherein the coefficient of thermal expansion (CTE) can be tailored over an order of magnitude. In particular, it is now possible to obtain CTEs near 25 ppm/°C in an unfilled epoxy resin, much lower than possible with traditional epoxy resins. This has significant implications for applications ranging from corrosion resistant coatings on aircraft fuselages to interlayer dielectrics and underfills in chip manufacture.

6.1 Introduction

Cubic silsesquioxanes are unique molecules that combine three-dimensional cubic symmetry with single nanometer diameters and a core that is the smallest single crystal of silica. Symmetry places a functional group on each vertex in a different octant in Cartesian space, providing the opportunity to form covalent bonds accordingly, such that the potential exists to construct materials in 1-, 2- or 3-dimensions nanometer by nanometer. In principle this permits manipulation of global properties by tailoring structures at

nanometer length scales allowing the finest control possible. It also provides access to materials with highly reproducible properties and the potential to predict and design them for specific applications.[1-10]

We recently began exploring the chemistries and properties of epoxy resins and polyimides made with octa(aminophenyl)silsesquioxane, $[NH_2PhSiO_{1.5}]_8$, OAPS (*m:p:o* ≈ 65:20:15).[11-14] In early studies, we demonstrated that global silsesquioxane nanocomposite properties can be tailored by controlling the structure of the organic tether linking cube vertices, at nanometer length scales.[15-19] We further demonstrated that control of the reaction chemistry during curing leads to the majority of epoxy groups forming a single type of tether. We were also able to identify, through modeling studies, how tether structure and flexibility control specific global properties.[15] Furthermore, by developing an understanding of the failure mechanisms of these materials and recognizing that these nanocomposites consist of single nanometer domain components, we developed a "nano-nano" composite using 100 nm core-shell rubber particles to greatly improve the fracture toughness of the most brittle system.[19]

We report here efforts to develop single-phase materials that offer control of the coefficients of thermal expansion (CTE) of silsesquioxane epoxy resins over an order of magnitude. Control of CTE is of considerable importance in multiple materials applications including coatings that offer resistance to abrasion, corrosion, photooxidation, hydrophobicity, staining, etc; where the polymer coating is applied to a glass, ceramic or metal substrates with quite dissimilar CTEs. In such instances, thermal cycling often leads to loss of adhesion followed by coating failure via chemical and/or mechanical mechanisms.[20]

CTE mismatches are also quite problematic in electronic applications for example in interlayer dielectrics and flip-chip underfills.[21] In the latter case, the underfill epoxy must match the CTEs of silicon based ICs (2-3 μm/^{o}C) and substrates (20-40 μm/°C) to ensure good thermal management. Current epoxy materials require silica fillers to adjust CTEs to ≈ 20 μm/^{o}C. Such CTEs are intermediate between substrates and silicon to minimize fatigue at solder joints. These fillers raise the viscosity to levels near 50,000 mPa-sec, making processing very difficult. Likewise, corrosion resistant epoxy resin coatings on aluminum alloys for aircraft bodies must minimize environmental corrosion, offer good

abrasion resistance and curing temperatures below 50°C, but also have CTEs close to those of the alloys (typically ≈ 22-24 μm/^{o}C), values heretofore unknown for simple epoxy systems and especially for primer coats on aircraft fuselages that are typically materials based on DGEBA/DDM (diglycidyl ether of bisphenol A / dimethyl diamino methane) systems.[22]

6.2 Experimental Procedures

The synthetic methods and characterization techniques are described in Chapter 2, along with more detailed experimental data.

6.3 Results and Discussions

We now find that it is possible to produce epoxy resin thermosets with a very wide range of CTEs from a series of epoxy resins (see Table **6.1** and Figure **6.1**) formulated using OAPS as the curing agent. The formulations chosen were made according to our original model systems, wherein the ratio of NH_2:epoxy groups was either 0.5 or 1.0. The first composition is that typically used for commercial resins, examples of which are given in Table **6.2**. The second composition was chosen because our original studies found that resins cured with this composition led to better control of the tether structures (linear tethers between cube vertices) and generally better tensile strengths and fracture toughness.[17-18]

Indeed, the same composition used here also offers better CTEs than those found for N = 0.5. To our knowledge, a CTE of 25 ppm/°C has not previously been reported for an "unfilled" liquid epoxy resin system cured under similar conditions. We believe it reflects the nature of our "nanofilled" system. However, there are other considerations here because on addition of 10 wt % nano-δ-alumina particles, the CTE drops only another 2-3 ppm (≈10 %). Note that the incorporation of nano fillers can introduce pores (even micro pores) and therefore, may not produce the expected decreases in CTE.

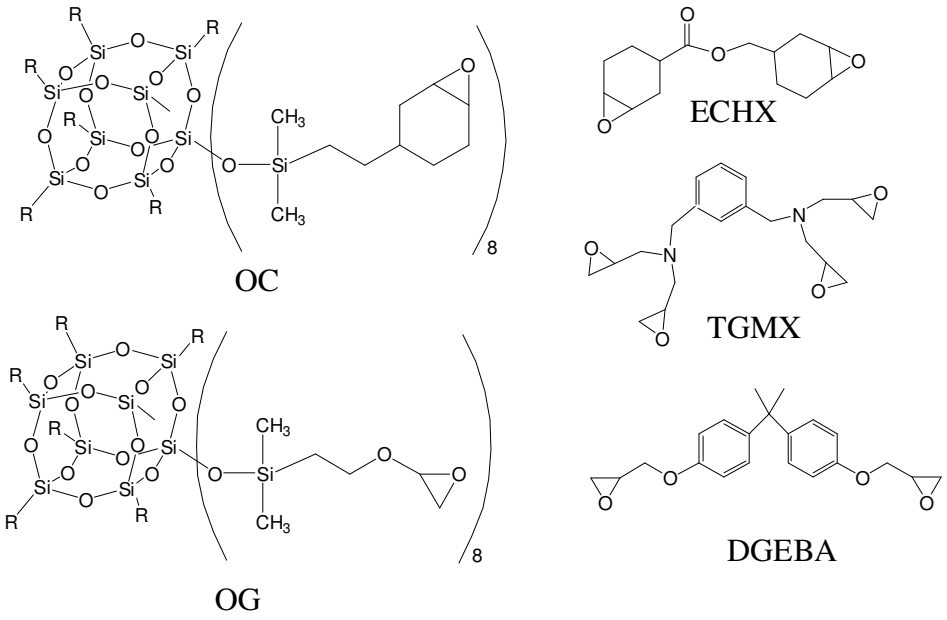

Figure 6.1. Sets of epoxies tested in OAPS resins.

Table 6.1. CTEs of selected epoxy resins where N = number of NH_2s/epoxy group.*

Epoxy	Molar Ratio N	CTE (ppm/°C) below	†Inflection point	CTE (ppm/°C) above
TGMX	0.5	55	120	103
TGMX	1	25 ± 2	110	46
TGMX	10 wt % Al_2O_3	22 ± 2	125	33
ECHX	0.5	91	110	191
ECHX	1	55	110	92
DGEBA	0.5	80	95	176
DGEBA	1	72	115	145
OG	0.5	196	100	179
OG	1	141	100	162
OC	0.5	185	120	240
OC	1	220 ± 10	100	329

*All samples cured 20 h/200°C/N_2. †No true T_gs were observed for any of the above resins by TMA or DSC. Inflection points were observed and measured as the intersection of slopes on the extreme ends of TMA plots.

Table 6.2. Published CTEs of selected epoxy resins where N = NH_2s/epoxy group = 0.5.

Epoxy	Curing Agent	Time/Max. Cure Temp. (°C)	CTE (ppm/^{o}C)	Ref.
4,4'-Bis(2,3-epoxypropoxy)-α-methylstilbene	Sulfanilamide	4 h/200	53	23
DGEBA	Polyamide	1 h/100	78	24
DGEBA	4,4-diaminodiphenylmethane	4 h/150	82	25
DGEBA	Diaminodiphenylsulfone	2 h/250	68	26
4,4'-Di(2,3-epoxypropyloxy)-biphenyl	4-aminoacetophenone azine	160	96	27
4,4'-Di(2,3-epoxypropyloxy)-biphenyl	Diaminodiphenylsulfone	4 h/220	64	28
ECHX	Methylhexahydrophthalic anhydride	15 min/250	87	29
DGEBA	Triethylenetetramine	100 ^{o}C	107	30
DGEBA	Phenol Formaldehyde	2 h/165	75	31
DGEBA	Cresol Formaldehyde	2 h/165	87	31
Triglycidyl *p*-aminophenol	Phenol Formaldehyde	2 h/165	63	31
Naphtalene diepoxide	Phenol formaldehyde	2 h/165	63	31

Our rationale for the observed behavior is twofold. First, due to steric effects in the silsesquioxane cage system, fewer amine hydrogens are available for reaction at the N = 0.5 stoichiometry. Once the silsesquioxane cage is locked into the epoxy network early in the reaction, the accessibility of the remaining unreacted amine hydrogens diminishes leading to incomplete curing of the resin and to high CTE values for the cured material. Second, in the system where N = 1, many more amine hydrogens are available for reaction than in the N = 0.5 composition, leading to higher crosslink density or more complete curing. Furthermore, at N = 1, the mole fraction of the "nanofiller" silsesquioxane cage in the cured material is twice as high as in the N = 0.5 system, hence the lower CTE. Finally, it is likely that the N = 1 stoichiometry also provides lower viscosities that in turn should lead to higher degrees of curing. Indeed the viscosities of all of the coating resin systems are less than about 1000 MPa-sec as determined using a parallel plate Rheometric RDS II E system at 10/s shear rate and 1 mm gap.

6.4 Conclusions

Cubic silsesquioxanes offer the potential to tailor global properties in nanocomposite systems nanometer by nanometer because such control occurs at the finest length scales possible. Building on previous work with epoxy resins, we demonstrate here that judicious choice of short chain, polyfunctional epoxies combined with non-traditional resin stoichiometries, it is possible to control epoxy resin CTEs over an order of magnitude. An additional important point is that we can obtain these very low CTEs starting from a low viscosity resin system.

References Cited:

1. Reviews: (a) Voronkov, M.G.; Lavrent'yev, V.I. "Polyhedral Oligosilsesquioxanes and Their Homo Derivatives." *Top. Curr. Chem.* **1982**, *102*, 199-236. (b) Baney, R.H.; Itoh, M.; Sakakibara, A.; Suzuki, T. "Silsesquioxane." *Chem. Rev*. **1995**, *95*, 1409-1430. (c) Provatas, A.; Matisons, J.G. "Silsesquioxanes: Synthesis and Applications." *Trends Polym. Sci*. **1997**, *5*, 327-333. (d) Loy, D.A.; Shea, K.J. "Bridged Polysilsesquioxanes. Highly Porous Hybrid Organic-Inorganic Materials." *Chem. Rev.* **1995**, *95*, 1431-1442. (e) Lichtenhan, J. "Silsesquioxane-based Polymers." In *Polymeric Materials Encyc.*; Salmone, J.C., Ed.; CRC Press: N.Y., 1996; Vol. 10; pp. 7768-7777.

2. (a) Gilman, J.W.; Schlitzere, D.S.; Lichtenhan, J.D. "Low Earth Orbit Resistant Siloxane Copolymers." *J. Appl. Poylm. Sci.* **1996**, *60*, 591-596. (b) Lichtenhan, J.D.; Gilman, J.W.; Feher, F.J. "Process for preparation of polyhedral oligomeric silsesquioxanes and synthesis of polymers containing polyhedral oligomeric silsesquioxane group segments", U.S. Patent 5,484,867, **1997**. (c) Gonzalez, R.I.; Phillips, S.H.; Hoflund, G.B. "In Situ Oxygen-Atom Erosion Study of Polyhedral Oligomeric Silsesquioxane-Siloxane Copolymer." *J. Spacecraft and Rockets* **2000**, *37*, 463-467. (d) Phillips, S.H.; Haddad, T.S.; Tomczak, S.J. "Developments in Nanoscience: Polyhedral Oligomeric Silsesquioxane (POSS)-Polymers." *Curr. Opin. Solid State Mater. Sci.* **2004**, *8*, 21-29. (e) Brunsvold, A.L.; Minton, T.K.; Gouzman, I.; Grossman, E.; Gonzalez, R.I. "An Investigation of the Resistance of Polyhedral Oligomeric Silsesquioxane Polyimide to Atomic-Oxygen Attack." *High Perform. Polym*. **2004**, *16*, 303-318. (f) Gonzalez, R.I.; Tomczak, S.J.; Minton, T.K.; Brunsvold, A.L.; Hoflund, G.B. "Synthesis and Atomic Oxygen Erosion Testing of Space-Survivable POSS (Polyhedral Oligomeric Silsesquioxane) Polyimides." *Proc. 9th Internat. Symp. Mater Space Environment*, Noordwijk, the Netherlands, **2003**, 113-120.

3. (a) Waddon, A.J.; Coughlin, E.B. "Crystal Structure of Polyhedral Oligomeric Silsesquioxane (POSS) Nano-materials: A Study by X-ray Diffraction and Electron Microscopy." *Chem. Mater.* **2003**, *15*, 4555-4561. (b) Gromilov, S.A.; Basova, T.V.; Emel'yanov, D. Yu.; Kuzmin, A.V.; Prokhorova, S.A. "Layer Arrangement in the Structure of Octakis-(trimethylsiloxy)octasilsesquioxane and Dodecakis-(trimethylsiloxy)cyclohexasiloxane." *J. Structural Chem*. **2004**, *45*, 471-475.

4. (a) Feher, F.J.; Newman, D.A.; Walzer, J.F. "Silsesquioxanes as Models for Silica Surfaces." *J. Am. Chem. Soc.* **1989**, *111*, 1741-1748. (b) Feher, F.J.; Budzichowski, T.A.; Blanski, R.L.; Weller, K.J.; Ziller, J.W. "Facile Syntheses of New Incompletely Condensed Polyhedral Oligosilsesquioxanes: $[(c\text{-}C_5H_9)_7Si_7O_9(OH)_3]$, $[(c\text{-}C_7H_{13})_7Si_7O_9(OH)_3]$, and $[(c\text{-}C_7H_{13})_6Si_6O_7(OH)_4]$." *Organomet.* **1991**, *10*, 2526-2528. (c) Maschmeyer, T.; Klunduk, M.C.; Martin, C.M.; Shephard, D.S.; Johnson, B.F.G.; Thomas, J.M. "Modelling the Active Sites of Heterogeneous Titanium-Centred Epoxidation Catalysts with Soluble Silsesquioxane Analogues." *Chem. Comm.* **1997**, *19*, 1847-1848.

5. (a) Feher, F.J.; Blanski, R.L. "Olefin Polymerization by Vanadium-Containing Silsesquioxanes: Synthesis of a Dialkyl-Oxo-Vanadium (V) Complex that Initiates Ethylene Polymerization." *J. Am. Chem. Soc.* **1992***, 114*, 5886-5887. (b) Feher, F.J.; Soulivong, D.; Eklud, A.G.; Wyndham, K.D. "Cross-Metathesis of Alkenes with Vinyl-Substituted Silsesquioxanes and Spherosilicates: A New Method for Synthesizing Highly-Functionalized Si/O Frameworks." *Chem. Comm.* **1997**, *13*, 1185-1186. (c) Severn, J.R.; Duchateau, R.; van Santen, R.A.; Ellis, D.D.; Spek, A.L. "Homogeneous Models for Chemically Tethered Silica-Supported Olefin Polymerization Catalysts." *Organomet*. **2002**, *21*, 4-6. (d) Duchateau, R.; Abbenhuis, H.C.L.; van Santen, R.A.; Meetsma, A.; Thiele, S.K.-H.; van Tol, M.F.H. "Half-Sandwich Titanium Complexes Stabilized by a Novel Silsesquioxane Ligand: Soluble Model Systems for Silica-Grafted Olefin Polymerization Catalysts." *Organomet.* **1998**, *17*, 5222-5224.

6. Maxim, N.; Magusin, P.C.M.M.; Kooyman, P.J.; van Wolput, J.H.M.C.; van Santen, R.A.; Abbenhuis, H.C.L. "Synthesis and Characterization of Microporous Fe-Si-O Materials with Tailored Iron Content from Silsesquioxane Precursors." *J. Phys. Chem. B*. **2002**, *106*, 2203-2209.

7. Bonhomme, C.; Toledano, P.; Maquet, J.; Livage, J.; Bonhomme-Coury, L. "Studies of Octameric Vinylsilsesquioxane by Carbon-13 and Silicon-29 Cross Polarization Magic Angle Spinning and Inversion Recovery Cross Polarization Nuclear Magnetic Resonance Spectroscopy." *J. Chem. Soc. Dalton Trans*. **1997**, *9*, 1617-1626.

8. (a) Bassindale, A.R.; Pourny, M.; Taylor, P.G.; Hursthouse, M.B.; Light**,** M.E. "Fluoride-Ion Encapsulation within a Silsesquioxane Cage." *Angew. Chem. Inter. Ed*. **2003**, *42*, 3488-3490. (b) Bassindale, A.R.; Parker, D.J.; Pourny, M.; Taylor, P.G.; Horton, P.N.; Hursthouse, M.B. "Fluoride Ion Entrapment in Octasilsesquioxane Cages as Models for Ion Entrapment in Zeolites. Further Examples, X-ray Crystal Structure Studies, and Investigations into How and Why They May Be Formed." *Organomet.* **2004**, *23*, 4400-4405.

9. Asuncion, M.Z.; Hasegawa, I.; Kampf, J.W.; Laine, R.M. "The Selective Dissolution of Rice Hull Ash to Form $[OSiO_{1.5}]_8[R_4N]_8$ (R = Me, CH_2CH_2OH) Octasilicates. Basic Nanobuilding Blocks and Possible Models of Intermediates Formed during Biosilicification Process." *J. Mater. Chem.* **2005**, *15*, 2114-2121.

10. Laine, R.M. "Nanobuilding Blocks Based on the $[OSiO_{1.5}]_x$ (x = 6, 8, 10) Octasilsesquioxanes." *J. Mater. Chem*. **2005**, *15*, 3725-3744.

11. Tamaki, R.; Tanaka, Y.; Asuncion, M.Z.; Choi, J.; Laine, R.M. "Octa(aminophenyl) silsesquioxane as a Nanoconstruction Site." *J. Am. Chem. Soc.* **2001**, *123*, 12416-12417.

12. Tamaki, R.; Choi, J.; Laine R.M. "A Polyimide Nanocomposite from Octa(aminophenyl)silsesquioxane." *Chem. Mater.* **2003**, *15*, 793-797.

13. Choi, J.; Tamaki, R.; Kim, S.G.; Laine, R.M. "Organic/Inorganic Imide Nanocomposites from Aminophenylsilsesquioxanes." *Chem. Mater*. **2003**, *15*, 3365-3375.

14. Choi, J.; Kim S.G.; Laine, R.M. "Organic/Inorganic Hybrid Epoxy Nanocomposites from Aminophenylsilsesquioxanes." *Macromol*. **2004**, *37*, 99-109.

15. Laine, R. M.; Choi, J.; Lee, I. "Organic-Inorganic Nanocomposites with Completely Defined Interfacial Interactions." *Adv. Mater*. **2001**, *13*, 800-803.

16. Laine, R.M.; Zhang, C.; Sellinger, A.; Viculis, L. "Polyfunctional Cubic Silsesquioxanes as Building Blocks for Organic/Inorganic Hybrids." *Appl. Organometal. Chem*. **1998**, *12*, 715-723.

17. Choi, J.; Harcup, J.; Yee, A.F.; Zhu, Q.; Laine, R.M. "Organic/Inorganic Hybrid Composites from Cubic Silsesquioxanes." *J. Am. Chem. Soc*. **2001**, *123*, 11420-11430.

18. Choi, J.; Yee, A.F.; Laine, R.M. "Organic/Inorganic Hybrid Composites from Cubic Silsesquioxanes. Epoxy Resins of Octa(dimethylsiloxyethylcyclohexylepoxide) Silsesquioxane." *Macromol.* **2003**, *36*, 5666-5682.

19. Choi, J.; Yee, A.F.; Laine, R.M. "Toughening of Cubic Silsesquioxane Epoxy Nanocomposites Using Core-Shell Rubber Particles: A Three-Component Hybrid System." *Macromol*. **2004**, *37*, 3267-3276.

20. (a) Lee, D.G.; Kim, B.C. "Investigation of Coating Failure on the Surface of a Water Ballast Tank of an Oil Tanker." *J. Adhes. Sci. Tech.* **2005**, *19*, 879-908. (b) Minami, F.; Takahara, W.; Nakamura, T. "Interface Strength Evaluation of LSI Devices Using the Weibull Stress." *J. ASTM. Int.* **2004**, *1*, 1-10

21. (a) Okura, J.H.; Shetty, S.; Ramakrishnan, B.; Dasgupta, A.; Caers, J. F. J. M.; Reinikainen T. "Guidelines to Select Underfills for Flip Chip On Board Assemblies and Compliant Interposers for Chip Scale Package Assemblies." *Microelect. Reliab*. **2000**, *40*, 1173-11880. (b) Palaniappan, P.; Baldwin, D.F.; Selman, P.J.; Wu, J.; Wong, C.P. "Correlation of Flip Chip Underfill Process Parameters and Materials Properties." *IEEE Trans. Electr. Packag. Manufa.* **1999,** *22*, 53-62. (c) Nysaether, J.B.; Lundstrom, P.; Liu, J. "Measurement of Solder Bump Lifetime as a Function of Underfill Material Properties." *IEEE Trans. Pack. Manufa. Tech., Part A,* **1998**, *21*, 281-287.

22. (a) Chattopadhyay, A.K.; Zentner, M.R. *"Aerospace and Aircraft Coatings."* Fed. of Soc. for Coatings Tech.: Philadelphia, PA., 1990; pp 16-19. (b) Wicks, Jr., Z.W.; Jones, F.N.; Pappas, S.P. *Organic Coatings: Science and Technology.* 2nd ed.; Wiley-Interscience: New York, 1999.

23. Benicewicz, B.C.; Smith, M.E.; Earls, J.D.; Duran, R.S.; Setz, S. M.; Douglas, P. "Magnetic Field Orientation of Liquid Crystalline Epoxy Thermosets." *Macromol.* **1998**, *31*, 4730-4738.

24. Tsuchida K.; Bell, J.P. "A New Epoxy/Episulfide Resin System for Coating Applications: Curing Mechanism and Properties." *Inter. J. Adhes. Adhes*. **2000**, *20*, 449-456.

25. Farren, C.; Akatsuka, M.; Takezawa, Y.; Itoh, Y. "Thermal and Mechanical Properties of Liquid Crystalline Epoxy Resins as a Function of Mesogen Concentration." *Polymer* **2001**, *42*, 1507-1514.

26. Su, W-F.A. "Thermoplastic and Thermoset Main Chain Liquid Crystal Polymers Prepared from Biphenyl Mesogen." *J.Poly. Sci.: Poly. Chem*. **1993**, *31*, 3251-3256.

27. Carfagna, C.; Amendola, E.; Giamberini, M.; D'Amore, A.; Priola, A.; Malucelli, G. "The Effect of Prepolymer Composition of Amino-Hardened Liquid Crystalline Epoxy Resins on Physical Properties of Cured Thermoset." *Macromol. Symp*. **1999**, *148*, 197-209.

28. Lee, J.Y.; Jang, J.; Hwang, S.S.; Hong, S.M.; Kim, K.U. "Synthesis and Curing of Liquid Crystalline Epoxy Resins Based on 4,4'-Biphenol." *Polymer* **1998**, *39*, 6121-6126.

29. Wong, C.P.; Vincent, M.B.; Shi, S. "Fast-Flow Underfill Encapsulant: Flow Rate and Coefficient of Thermal Expansion." *IEEE Trans. Comp. Pack. Manufa. Tech. Part A* **1998**, *21*, 360-364.

30. (a) Katz, H.S. "*Handbook of Fillers for Plastics*", Van Nostrand Reinhold: New York, 1987. (b) Miyagawa, H.; Rich, M.J.; Drzal, L.T. "Amine-Cured Epoxy/Clay Nanocomposites. II. The Effect of the Nanoclay Aspect Ratio." *J.Poly. Sci.: Poly. Phy,* **2004**, *42*, 4391-4400.

31. Zhang, Z.; Fan, L. "Development of Environmental Friendly Non-Anhydride No-Flow Underfills." *IEEE Trans. Comp. Pack. Tech.* **2002**, *25*, 140-147.

32. Asuncion, M.Z.; Laine, R.M. "Silsesquioxane Barrier Materials." *Macromol*. **2007**, *40*, 555-562.

Chapter 7
Future Work

In this dissertation, we have demonstrated new routes for the syntheses and functionalizations of octa-, deca-, and dodecameric silsesquioxanes and investigated their properties. In Chapter **3**, functionalization of octavinylsilsesquioxane (OVS) via cross-metathesis and Heck coupling reactions produced three series ("generations") of molecules with unique thermal (RStyrenylOS) and photophysical properties (R'VinylStilbeneOS), as well as branching points for the formation of star molecules (R"$_2$benzamideOS). Chapter **4** detailed our work on the synthesis and characterization of luminescent silsesquioxane molecules from 8-, 16-, and 24-brominated octaphenylsilsesquioxane (OPS). These molecules show novel photophysical properties indicating unique interactions between the organic tethers with the silsesquioxane cage. In Chapter **5** we discussed the rearrangement reactions of polyvinylsilsesquioxane (PVSQ) to form deca- and dodecavinylsilsesquioxane using catalytic amount of F^- ion in the form of nBu$_4$F. Using this method, we also synthesized mixed methyl- and vinyl-functionalized deca- and dodecasilsesquioxane molecules from polymethylsilsesquioxane (PMSQ) and PVSQ. Chapter **6** described our work on SQ-based epoxy composites with coefficients of thermal expansion (CTE) as low as 25 ppm/^{o}C without ceramic fillers.

Our work on luminescent R'VinylStilbeneOS and RStyr$_x$OPS have provided more evidence to support the idea of electron delocalization from the conjugated organic tethers to the octameric silsesquioxane cage. The unique solvatochromism of NH$_2$VinylStilbeneOS and its large two-photon absorption (TPA) cross-section (~100 GM/moiety) indicates charge transfer (CT) from the amine groups to the strongly electrophilic molecular orbital (MO) inside the silsesquioxane cage (Chapter **3**). The blue shift in the *o*-RStyr$_8$OPS compared to *p*-RStyr$_8$OPS suggests that the RStyrenyl groups of *o*-RStyr$_8$OPS sit over the electrophilic silsesquioxane cage face (Chapter **4**). On the other

hand, the emission spectra of *o*-RStyr$_8$OPS are similar to *p*-RStyr$_8$OPS, suggesting that the excited state of *o*-RStyr$_8$OPS involves conjugation through the silsesquioxane cage MO. The blue-shift in the absorption spectra of RStyr$_{24}$OPS compared to RStyr$_{16}$OPS indicates that the third RStyrenyl group on each phenyl ring causes overcrowding around the silsesquioxane cage corner and some RStyrenyl groups are forced to approach the silsesquioxane cage face, similar to the interaction seen in *o*-RStyr$_8$OPS. However, the red-shifts in the structureless emission spectra along with the lower quantum yields and higher TPA cross-section values indicate that the excited states of RStyr$_{24}$OPS involves the silsesquioxane cage MO and that there are two pathways for the excited-to-ground state transition: CT and normal radiative emission from a π^* state.

Most of the work published to date on the unique photoluminescence of silsesquioxane molecules involving electron delocalization to the silsesquioxane cage focuses on octameric or cubic molecules (T_8).[1-4] This, of course, introduces the question of how the photoluminescence of these molecules, and the extent of electron delocalization to the silsesquioxane cage, would be affected if the cage is of a different geometry such as the decameric (T_{10}) or dodecameric (T_{12}) structure.

DFT calculations of the electronic properties of several polyhedral H-silsesquioxanes (T_4-T_{18})[5] suggest that the HOMOs in both $H_{10}T_{10}$ and $H_{12}T_{12}$ consist mostly of the atomic orbitals of the oxygen atoms' lone-pair electrons with some contributions from the silicon atoms. The LUMOs for both molecules are combinations of the atomic orbitals of silicon, oxygen, and hydrogen atoms, with slightly different proportions from each type of atom for different molecules. The authors[5] also report a slight decrease in the HOMO-LUMO gap as the size of the silsesquioxane cage increases, from 7.4 eV for H_6T_6 to 6.2 eV for $H_{16}T_{16}$ (~7.0 eV calculated[4] for H_8T_8 vs. 4.4 eV measured[6]). Based on these findings, it should be reasonable to suggest that the photoluminescence of T_{10} and T_{12} molecules will be similar to that of T_8 molecules.

As mentioned in the Chapter **1**, amongst the different polyhedral silsesquioxane molecules, octameric silsesquioxanes have received the most attention from the research community because they are the most easily accessible polyhedral silsesquioxane molecules due to their tendency to preferentially form the more stable Si_4O_4 rings and their high insolubility.[7] With some exceptions,[8,9] most T_{10} and T_{12} molecules are collected as

byproducts from the synthesis of T_8 molecules and require extensive purification processes, such as recrystallization or HPLC, to obtain small yields (< 20%).[10-12] Fragmentation/rearrangement reactions of lower alkyl (C_2-C_4)-T_8 with K_2CO_3 or NaOH in acetone produce a mixture of T_{10} molecules in moderate yields (up to 50%) with the rest being unreacted T_8 precursor and traces of T_{12}.[13]

Fluoride ion-catalyzed rearrangement reactions of polymeric and cage silsesquioxanes as discussed in Chapter **5** provide a simpler method for the synthesis of T_{10} and T_{12} silsesquioxane molecules with high yields (80-90%). The ability to use polymeric silsesquioxanes, a byproduct in the synthesis of cage silsesquioxanes, as starting materials is an additional benefit, especially with PVSQ being the majority of the product in the synthesis of octavinylsilsesquioxane (OVS). Furthermore, this process provides the opportunity to make cage silsesquioxane molecules having mixed functional groups, with some control over the numbers of each functional group in the final product by changing the composition of the starting materials. However, an area that requires improvement is purification of the reaction products, as they are a mixture of molecules with similar structures and chemical properties, and therefore multiple separation processes, such as recrystallization and HPLC, are required if pure, single component product is desired.

On the other hand, if a mixture of products can be tolerated, i.e. treating these molecules as one would polymer chains having a range of molecular weights, then these separation steps can be omitted, using the products as synthesized. Keeping this in mind, members of our groups have already started work on synthesizing the T_{10} and T_{12} versions of BrStyrenylOS and R'VinylStilbeneOS, starting from $Vi_{10}T_{10}$ and $Vi_{12}T_{12}$. The synthetic procedures developed for these compounds can be applied to the T_{10} and T_{12} derivatives without any modifications.[14,15] Comparisons of the photophysical properties, including two-photon absorption (TPA) cross-section values, of these molecules will allow investigations into how the different silsesquioxane cage structures affect the electron delocalization process from the conjugated organic tethers into the silsesquioxane cages.

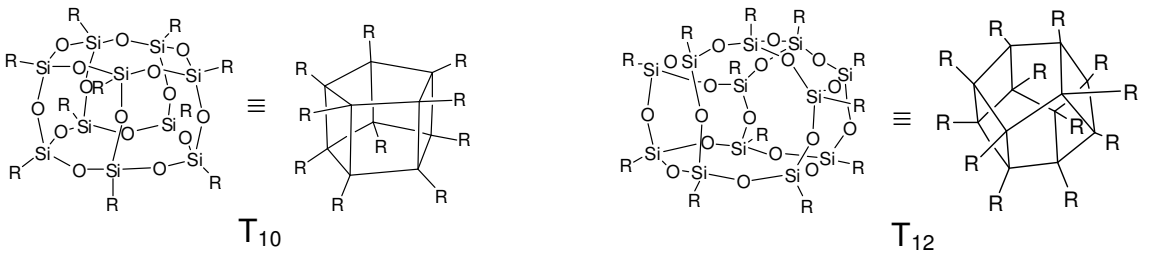

Figure 7.1. Simplified structures of T_{10} and T_{12} molecules.

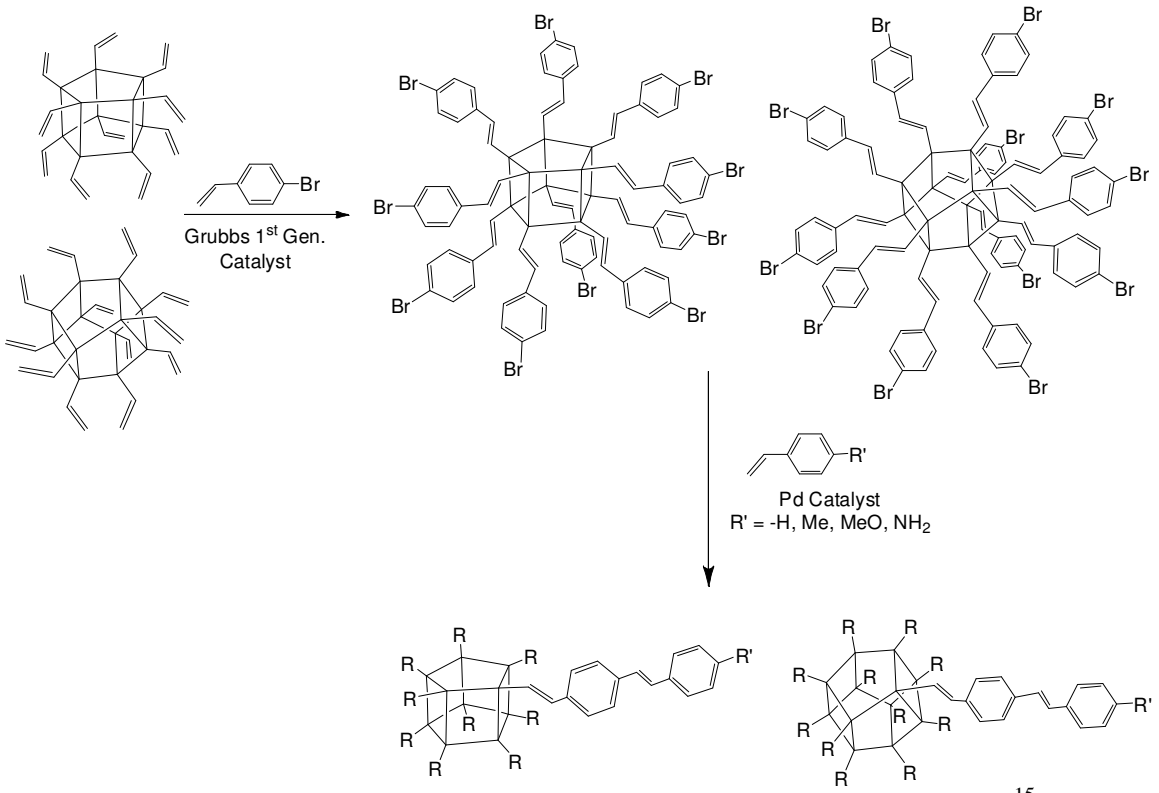

Scheme 7.1. Synthesis of BrStyrenyl$T_{10,12}$ and R'VinylStilbene$T_{10\text{-}12}$.[15]

The incorporations of silsesquioxane cages into linear polymeric materials to date have been limited to pendants[16,17] and end-caps[16,17] (Figure **7.2a**) due to the wide availability of the incompletely condensed trisilanol cubic silsesquioxane [$R_7T_7(OH)_3$]. On the other end of the spectrum, the highly crosslinked silsesquioxane-based networks from octa-functionalized cubic silsesquioxanes (Figure **7.2b**) have also been widely investigated.[11,18] The ability to synthesize silsesquioxane cages with an average two reactive groups from the fluoride ion-catalyzed rearrangement reactions of two different silsesquioxane polymers and/or cages has opened up another area of research: silsesquioxane-based beads-on-a-chain (BoC) polymers with silsesquioxane cages in the backbones of

the polymer chains (Scheme **7.2**). This new class of silsesquioxane-based polymers has considerable potential because it combines the thermal stability and mechanical properties of silsesquioxanes with ease of processing due to their superior solubility.

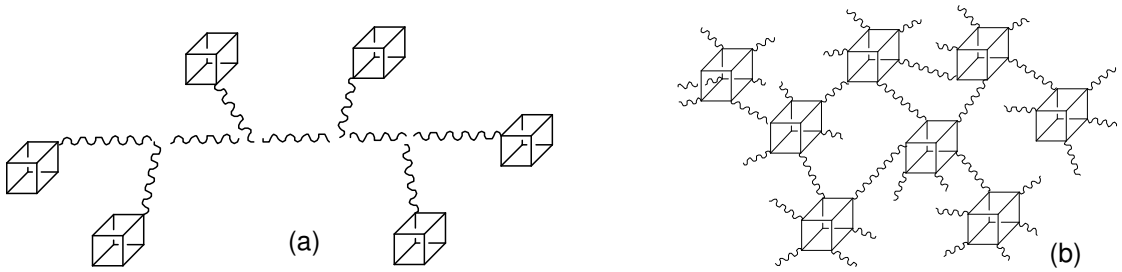

Figure 7.2. Schematic drawings of current silsesquioxane-based polymer materials.

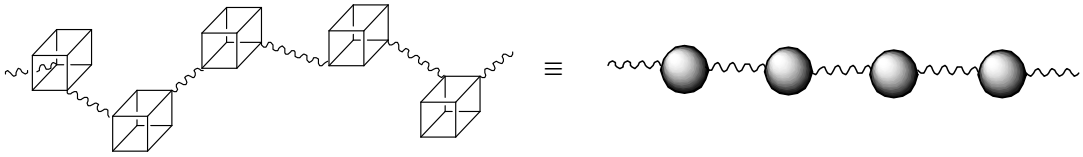

Figure 7.3. Silsesquioxane-based beads-on-a-chain (BoC) polymer.

Our group has published a paper on some preliminary work on the synthesis of BoC silsesquioxane polymer chains to investigate their photophysical properties.[14] However, the length of the polymer chains are limited to trimers and tetramers; presumable harsher reaction conditions or the use of different organic linkers can increase the polymer chain lengths. Altering the structures and lengths of the organic linkers should also give us the ability to tailor the properties of the resulting polymers, thereby giving access to multiple possible applications for this new set of materials.

Several examples of different organic linkers for silsesquioxane-based BoC polymers are shown in Schemes **7.3** and **7.5** below. In Scheme **7.3**, flexible disilane can be reacted with $Vi_2Ph_{8,10}T_{10,12}$ via hydrosilylation reaction. We expect the products to be thermally stable low-melting solids due to the flexibility of the polymer chains, making them suitable for applications such as high temperature lubrications.

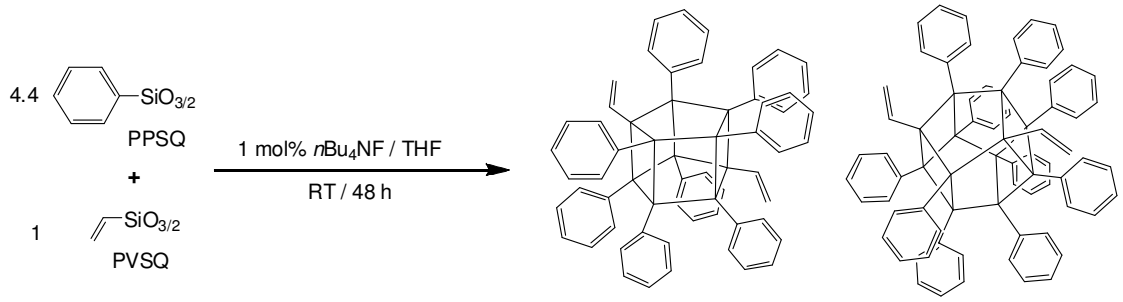

Scheme 7.2. Synthesis of $Vi_2Ph_{8,10}T_{10,12}$ from polyphenylsilsesquioxane (PPSQ) and polyvinylsilsesquioxane (PVSQ).[14]

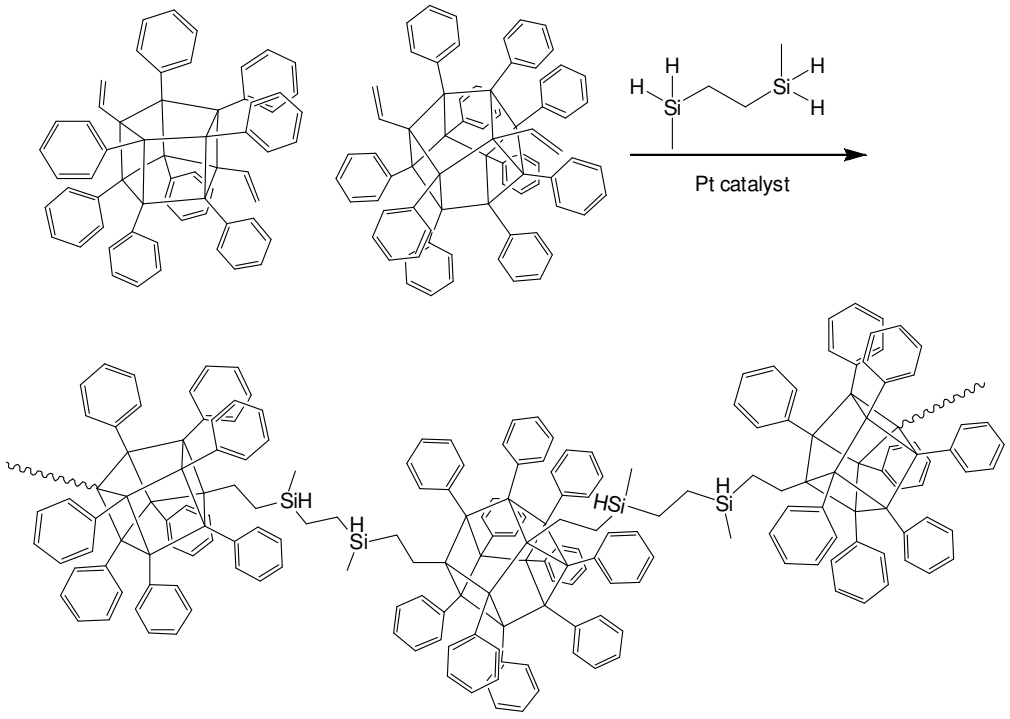

Scheme 7.3. Hydrosilylation of $Vi_2Ph_{8,10}T_{10,12}$ with 1,2-ethanediylbis(methylsilane) to form silsesquioxane-based BoC polymer with flexible organic linkers.

Our group has also succeeded in synthesizing $(NH_2Ph)_xPh_yT_{10,12}$ molecules from the fluoride ion-catalyzed rearrangement reactions of octa(aminophenyl)silsesquioxane (OAPS) and octaphenylsilsesquioxane (OPS). Scheme **7.5** shows rigid linker geometry for silsesquioxane-based BoC polymers from the reaction of $(NH_2Ph)_2Ph_{8,10}T_{10,12}$ with diglycidyl ether of bisphenol-A (DGEBA). We expect the product to be thermally stable up to 350^oC[19], making them suitable for a variety of high temperature applications.

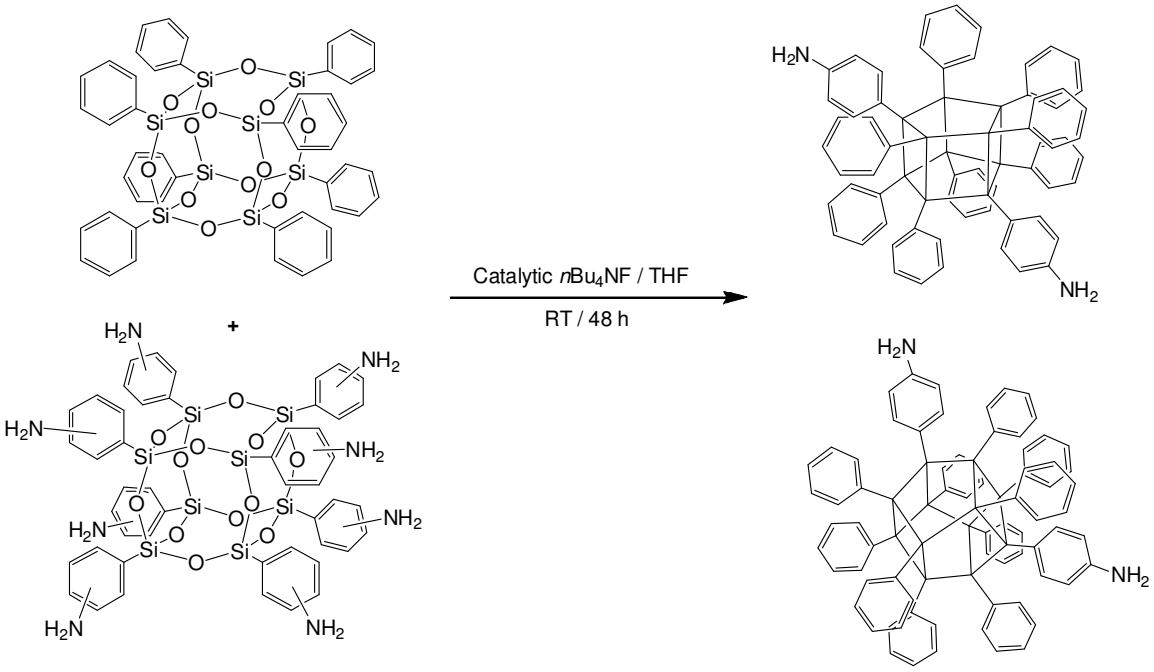

Scheme 7.4. Synthesis of $(NH_2Ph)_2Ph_{8,10}T_{10,12}$ from octaphenylsilsesquioxane (OPS) and octa(aminophenyl)silsesquioxane (OAPS).[20]

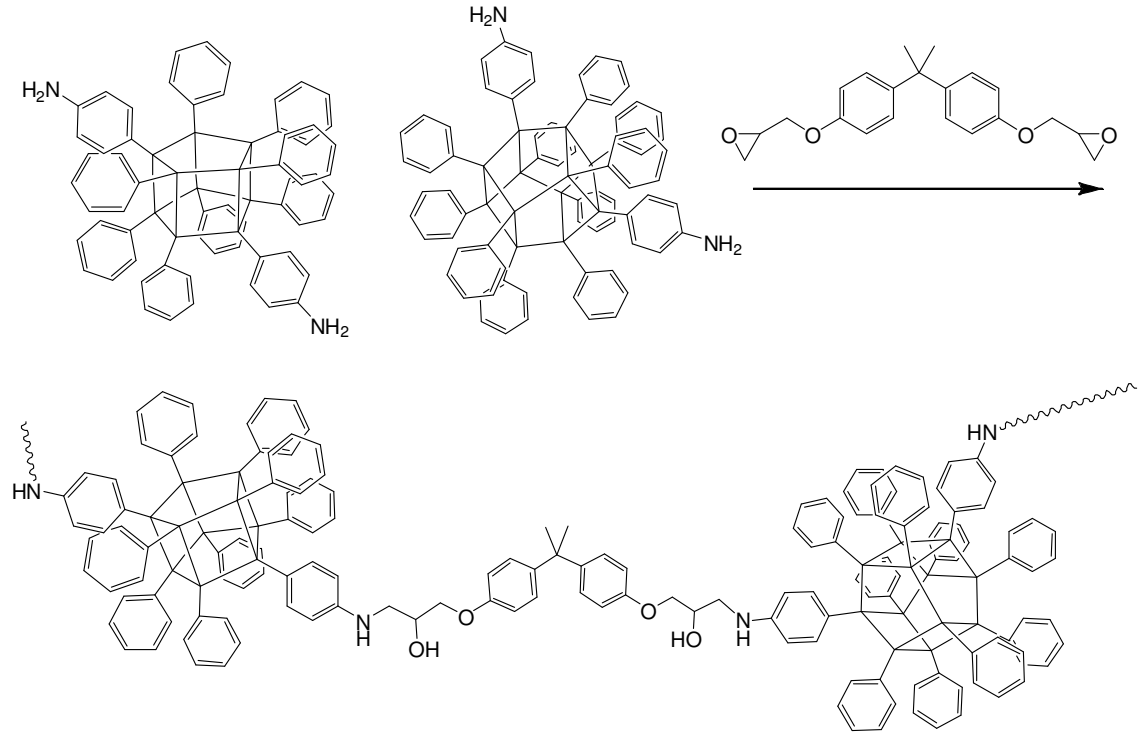

Scheme 7.5. Reaction of $(NH_2Ph)_2Ph_{8,10}T_{10,12}$ with DGEBA to form silsesquioxane-based BoC polymer with rigid organic linkers.

Even though our group has successfully applied the fluoride-ion rearrangement reactions to multiple silsesquioxane polymers and cage compounds, the exact reaction mechanisms are still not clear. In Chapter **5**, we offer an explanation based on general observations on the suspected active species in the reactions and possible reaction mechanisms. However, detailed ^{19}F- and ^{29}Si-NMR studies are required to correctly identify the active intermediates and the reaction mechanisms.

Furthermore, only one source of fluoride ions was used in Chapter **5**: tetra-*n*-butylammonium fluoride (TBAF). It is unclear what role, if any, the counter ion plays in these reactions. Other sources of fluoride ions that have been used by other groups for the synthesis of empty or fluoride-encapsulated silsesquioxane cages include tetramethylammonium fluoride[21] and potassium fluoride.[22] A careful and detailed study on the effects of different cations on the reaction will also contribute to the study of the reaction mechanisms.

References Cited:

1. André, P.; Cheng, G.; Ruseckas, A.; van Mourik, T.; Früchtl, H.; Crayston, J.A.; Morris, R.E.; Cole-Hamilton, D.; Samuel, I.D.W. "Hybrid Dendritic Molecule with Confined Chromophore Architecture to Tune Fluorescence Efficiency." *J. Phys. Chem. B* **2008**, *112*, 16382-16392.
2. Vautravers, N.R.; André, P.; Cole-Hamilton, D. "Fluorescence Activation of a Polyhedral Oligomeric Silsesquioxane in the Presence of Reducing Agents." *J. Mater. Chem.* **2009**, *19*, 4545-4550.
3. Zhen, C.-G.; Becker, U.; Kieffer, J. "Tuning Electronic Properties of Functionalized Polyhedral Oligomeric Silsesquioxanes: A DFT and TDDFT Study." *J. Phys. Chem. A* **2009**, *113*, 9707-9714.
4. Laine, R.M.; Sulaiman, S.; Brick, C.; Roll, M.; Tamaki, R.; Asuncion, M.Z.; Neurock, M.; Filhol, J.-S.; Lee, C.-Y.; Zhang, J.; Goodson III, T.; Ronchi, M.; Pizzotti, M.; Rand, S.C.; Li, Y. "Synthesis and Photophysical Properties of Stilbeneoctasilsesquioxanes. Emission Behavior Coupled with Theoretical Modeling Studies Suggest a 3-D Excited State Involving the Silica Core." *J. Am. Chem. Soc.* **2010**, *132*, 3708-3722.
5. Xiang, K.H.; Pandey, R.; Pernisz, U.C.; Freeman, C. "Theoretical Study of Structural and Electronic Properties of H-Solsesquioxanes." *J. Phys. Chem. B* **1998**, *102*, 8704-8711.
6. Azinović, D.; Cai, J.; Eggs, C.; König, H.; Marsmann, H.C.; Vepřek, S. "Photoluminescence from Silsesquioxanes $R_8(SiO_{1.5})_8$." *J. Luminescence* **2002**, *97*, 40-50.

7. Lickiss, P.D.; Rataboul, F. "Fully Condensed Polyhedral Oligosilsesquioxanes (POSS): From Synthesis to Application." *Adv. Organomet. Chem*. **2008**, *57*, 1-116.

8. Brown Jr., J.F.; Vogt, L.H.; Prescott, P.I. "Preparation and Characterization of the Lower Equilibrated Phenylsilsesquioxanes." *J. Am. Chem. Soc*. **1964**, *86*, 1120-1125.

9. Takahashi, K.; Sulaiman, S.; Katzenstein, J.M.; Snoblen, S.; Laine, R.M. "New Aminophenylsilsesquioxanes – Synthesis, Properties, and Epoxy Nanocomposites." *Aust. J. Chem*. **2006**, *59*, 564-570.

10. Agaskar, P.A.; Klemperer, W.G. "The Higher Hydridospherosiloxanes: Synthesis and Structures of $H_nSi_nO_{1.5n}$ (n = 12, 14, 16, 18)." *Inorg. Chim. Acta* **1995**, *229*, 355-364.

11. Laine, R.M.; Roll, M.F. "Polyhedral Phenylsilsesquioxanes." *Macromol*. **2011**, *44*, 1073-1109.

12. Liu, Z.H.; Bassindale, A.R.; Taylor, P.G. "Synthesis of Silsesquioxane Cages from Phenyl-*cis*-tetrol, 1,3-Divinyltetraethoxydisiloxane, and Cyclopentyl Resins." *Chem. Res. Chin. Univ*. **2004**, *20*, 433-436.

13. Rikowski, E.; Marsmann, H.C. "Cage-Rearrangement of Silsesquioxanes." *Polyhedron* **1997**, *16*, 3357-3361.

14. Asuncion, M.Z.; Laine, R.M. "Fluoride Rearrangement Reactions of Polyphenyl- and Polyvinylsilsesquioxanes as a Facile Route to Mixed Functional Phenyl, Vinyl T_{10} and T_{12} Silsesquioxanes." *J. Am. Chem. Soc*. **2010**, *132*, 3723-3736.

15. Jung, J.H.; Furgal, J.C.; Laine, R.M. Unpublished results.

16. Li, G.; Wang, L.; Ni, H.; Pittman Jr., C.U. "Polyhedral Oligomeric Silsesquioxane (POSS) Polymers and Copolymers: A Review." *J. Inorg. Organomet. Chem*. **2001**, *11*, 123-151.

17. Chan, K.L.; Sonar, P.; Sellinger, A. "Cubic Silsesquioxanes for Use in Solution Processable Organic Light Emitting Diodes (OLED)." *J. Mater. Chem*. **2009**, *19*, 9103-9120.

18. Laine, R.M. "Nano-Building Blocks Based on the $[OSiO_{1.5}]_8$ Silsesquioxanes." *J. Mater. Chem*. **2005**, *15*, 3725-3744.

19. Choi, J.; Kim, S.G.; Laine, R.M. "Organic/Inorganic Hybrid Epoxy Nanocomposites from Aminophenylsilsesquioxanes." *Macromol*. **2004**, *37*, 99-109.

20. Jung, J.H.; Laine, R.M. In press.

21. Anderson, S.E.; Bodzin, D.J.; Haddad, T.S.; Boatz, J.A.; Mabry, J.M.; Mitchell, C.; Bowers, M.T. "Structural Investigation of Encapsulated Fluoride in Polyhedral Oligomeric Silsesquioxane Cages Using Ion Mobility Mass Spectrometry and Molecular Mechanics." *Chem. Mater*. **2008**, *20*, 4299-4309.

22. Koželj, M.; Orel, B. "Synthesis of Polyhedral Phenylsilsesquioxanes with KF as the Source of the Fluoride Ion." *Dalton Trans*. **2008**, 5072-5075.

Appendix 1

Characterization Data of RStyrenylOS, R'VinylStilbeneOS, and R"$_2$BenzamideOS

Table A1.1. ^{1}H-NMR peaks and melting points of RStyrenylOS

Compound	^{1}H-NMR peaks (ppm)	Melting point (^{o}C)	Yield (%)
HStyrenylOS	6.32 (d, *J* = 19.4Hz, 8H, =C*H*-Si); 7.28-7.42 (m, 8H, =C*H*-Ph, 24H, Ph); 7.50 (d, *J* = 6.6Hz, 16H, Ph)	270	82.4
MeStyrenylOS	2.35 (s, 24H, -CH_3); 6.24 (d, *J* = 19.1Hz, 8H, =C*H*-Si); 7.14, (d, *J* = 8.1Hz, 16H, Ph); 7.28 (d, *J* = 19.8Hz, 8H, =C*H*-Ph); 7.33 (d, *J* = 8.1Hz, 16H, Ph)	315	74.7
MeOStyrenylOS	3.83 (s, 24H, -OCH_3); 6.14 (d, *J* = 19.1Hz, 8H, =C*H*-Si); 6.87, (d, *J* = 8.8Hz, 16H, Ph); 7.30 (d, *J* = 19.1Hz, 8H, =C*H*-Ph); 7.43 (d, *J* = 8.2Hz, 16H, Ph)	345	83.5
ClStyrenylOS	6.21 (d, *J* = 19.4Hz, 8H, =C*H*-Si); 7.25 (d, *J* = 19Hz, 8H, =C*H*-Ph); 7.28 (d, *J* = 8.8Hz, 16H, Ph); 7.35 (d, *J* = 8.8Hz, 16H, Ph)	310	76.1
BrStyrenylOS	6.27 (d, *J* = 19.1Hz, 8H, =C*H*-Si); 7.26 (d, *J* = 19Hz, 8H, =C*H*-Ph); 7.33 (d, *J* = 8.8Hz, 16H, Ph); 7.49 (d, *J* = 8.4Hz, 16H, Ph)	330	81.6
NO_2StyrenylOS	6.50 (d, *J* = 19.1Hz, 8H, =C*H*-Si); 7.43 (d, *J* = 19Hz, 8H, =C*H*-Ph); 7.58 (m, 8H, Ph); 7.82 (m, 8H, Ph); 8.20 (m, 8H, Ph); 8.37 (m, 8H, Ph)	n.a.	80.8

Table A1.2. ^{13}C-NMR peaks for selected RStyrenylOS

Compound	^{13}C-NMR peaks (ppm)
HStyrenylOS	117.3 (Si*C*H=CHPh), 126.7 (*o*-Ph), 128.6 (*m*-Ph), 128.9 (*p*-Ph), 137.3 (*ipso*-Ph), 149.2 (SiCH=*C*HPh)
MeOStyrenylOS	55.3 (-O*C*H_3), 113.9 (*m*-Ph), 114.8 (Si*C*H=CHPh), 128.3 (*o*-Ph), 130.4 (*ipso*-Ph), 148.4 (SiCH=*C*HPh), 160.1 (*C*-OCH_3)

Table A1.3. ^{29}Si-NMR peaks for selected (RStyrenyl)OS

Compound	^{29}Si-NMR peaks (ppm)
HStyrenylOS	78.23
BrStyrenylOS	78.45
NO_2StyrenylOS	78.96

Table A1.4. ^{1}H-NMR peaks of R'VinylStilbeneOS

Compound	^{1}H-NMR peaks (ppm)	Yield (%)
HVinylStilbeneOS	6.31 (d, *J* = 19.1Hz, 8H, =C*H*-Si); 7.09 (dd, 16H, Ph-C*H*=C*H*-Ph); 7.24-7.39 (m, 8H, Si-CH=C*H*-Ph, 24H, Ph); 7.48 (m, 48H, Ph)	79.4
MeVinylStilbeneOS	2.33 (s, 24H, -CH_3); 6.34 (d, *J* = 19.1Hz, 8H, =C*H*-Si); 7.09 (dd, 16H, Ph-C*H*=C*H*-Ph); 7.17, (d, *J* = 8.0Hz, 16H, Ph); 7.41 (m, 8H, Si-CH=C*H*-Ph, 16H, Ph); 7.49 (m, 32H, Ph)	74.2
MeOVinylStilbeneOS	3.83 (s, 24H, -OCH_3); 6.33 (d, *J* = 19.1Hz, 8H, =C*H*-Si); 6.90, (d, *J* = 8.8Hz, 16H, Ph); 7.03 (dd, 16H, Ph-C*H*=C*H*-Ph); 7.39 (d, *J* = 19.1Hz, 8H, Si-CH=C*H*-Ph); 7.47 (m, 48H, Ph)	81.3
NH_2VinylStilbeneOS	3.72 (s, 16H, -NH_2); 6.32 (d, *J* = 19 Hz, 8H, =C*H*-Si); 6.67 (d, *J* = 8.5Hz, 16H, Ph); 6.98 (dd, 16H, Ph-C*H*=C*H*-Ph); 7.34 (m, 8H, Si-CH=C*H*-Ph, 16H, Ph); 7.46 (m, 32H, Ph)	72.8

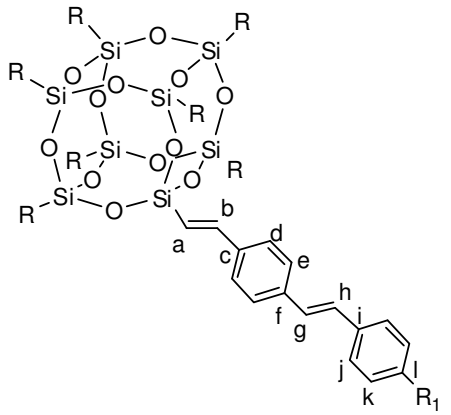

Table A1.5. ^{13}C-NMR peaks for selected R'VinylStilbeneOS

Compound	^{13}C-NMR peaks (ppm)
HVinylStilbeneOS	117.1 (a), 126.5 (d), 126.7 (e), 127.3 (j), 127.7 (h), 128.1 (g), 128.7 (k), 129.2 (l), 136.6 (c), 137.1 (f), 138.0 (i), 148.7 (b)
MeOVinylStilbeneOS	55.3 (m), 114.1 (k), 116.8 (a), 126.0 (h), 126.4 (e), 127.3 (d), 127.8 (j), 128.7 (g), 130.0 (i), 136.2 (c), 138.3 (f), 148.7 (b), 159.4 (l)

Table A1.6. ^{29}Si-NMR peaks for selected R'VinylStilbeneOS

Compound	^{29}Si-NMR peaks (ppm)
HVinylStilbeneOS	78.15
MeOVinylStilbeneOS	78.12
NH_2VinylStilbeneOS	78.06

Table A1.7. ^{1}H-NMR peaks for R"$_2$BenzamideOS

Compound	^{1}H-NMR peaks (ppm)	Yield (%)
$(NO_2)_2$BenzamideOS	6.55 (d, *J*=19.7Hz, 8H, SiC*H*=CHPh), 7.27 (d, *J*=18.7Hz, 16H, PhC*H*=C*H*Ph), 7.42 (d, *J*=19.4Hz, 8H, SiCH=C*H*Ph),7.65 (s, 16H, Ph), 7.82 (d, *J*=8.8Hz, 16H, Ph), 8.85 (dd, 32H, Ph), 8.99 (s, 8H, Ph), 9.16 (s, 16H, Ph), 10.9 (s, 8H, -N(*H*)C(=O)	90.5
Br_2BenzamideOS	6.50 (d, *J*=19.1Hz, 8H, SiC*H*=CHPh), 7.22 (d, *J*=19.3Hz, 16H, PhC*H*=C*H*Ph), 7.37 (d, *J*=19.2Hz, 8H, SiCH=C*H*Ph),7.57 (m, 24H, Ph), 7.73 (d, *J*=8.2Hz, 16H, Ph), 8.06 (m, 24H, Ph), 10.4 (s, 8H, -N(*H*)C(=O)	92.4

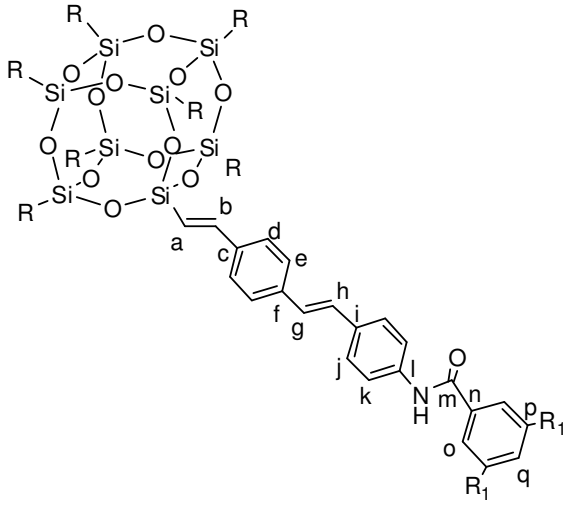

Table A1.8. ^{13}C-NMR peaks for R"$_2$BenzamideOS

Compound	^{13}C-NMR peaks (ppm)
$(NO_2)_2$BenzamideOS	117.0 (a), 119.9 (k), 121.1 (q), 127.1 (h), 127.4 (g), 128.0 (c,i), 128.4 (o), 128.9 (d,e,j), 133.5 (f), 136.1 (n), 137.8 (l), 148.2 (p), 148.5 (b), 164.9 (m)
Br_2BenzamideOS	116.9 (a), 120.9 (k), 123.0 (p), 127.1 (g,h), 127.2 (i), 127.4 (o), 128.0 (j), 129.2 (c), 130.1 (d,e), 133.2 (f), 136.0 (l), 138.7 (q,n), 149.3 (b), 162.8 (m)

Table A1.9. ^{29}Si-NMR peaks for R"$_2$BenzamideOS

Compound	^{29}Si-NMR peaks (ppm)
Br_2BenzamideOS	77.40

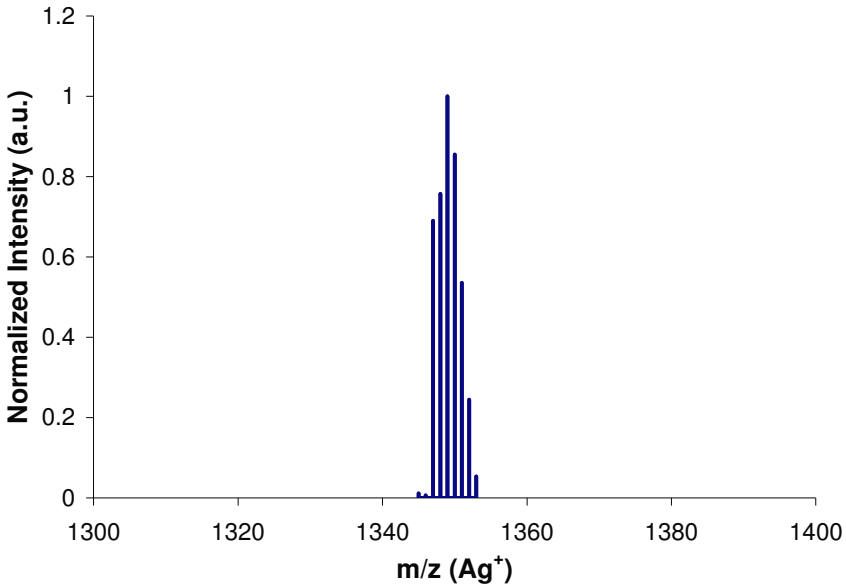

Figure A1.1. MALDI-ToF spectrum of HStyrenylOS.

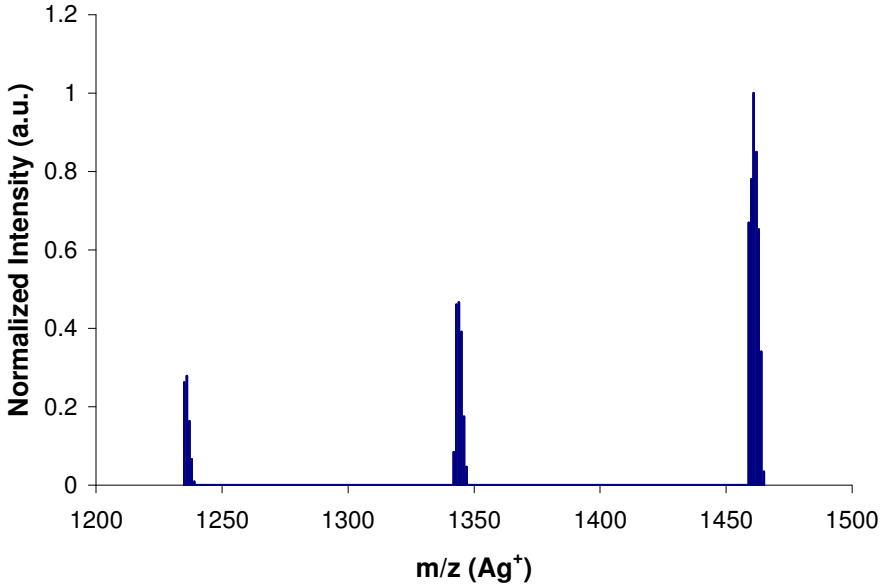

Figure A1.2. MALDI-ToF spectrum of MeStyrenylOS.

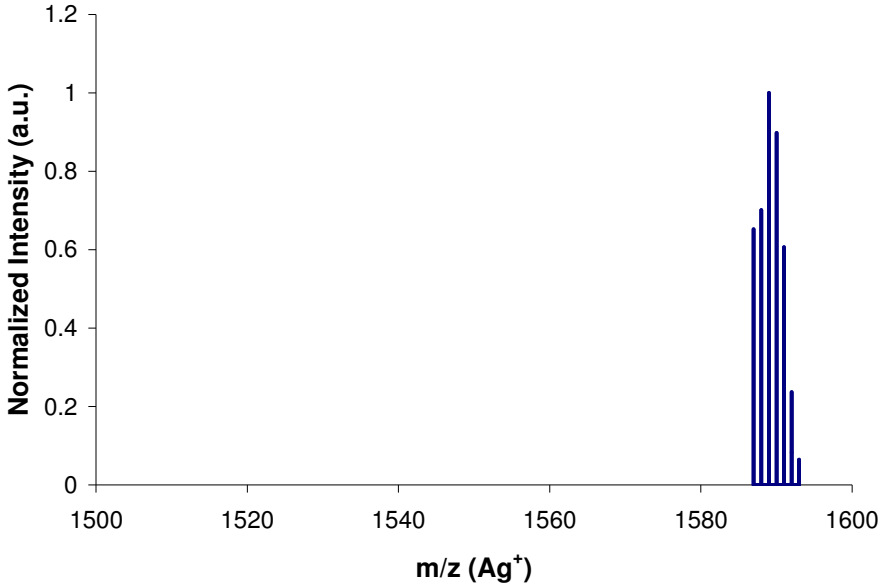

Figure A1.3. MALDI-ToF spectrum of MeOStyrenylOS.

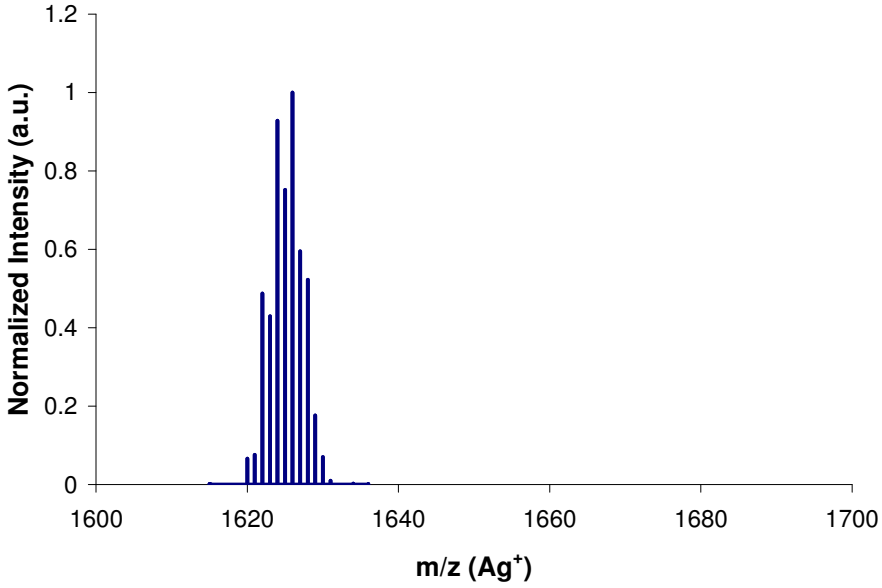

Figure A1.4. MALDI-ToF spectrum of ClStyrenylOS.

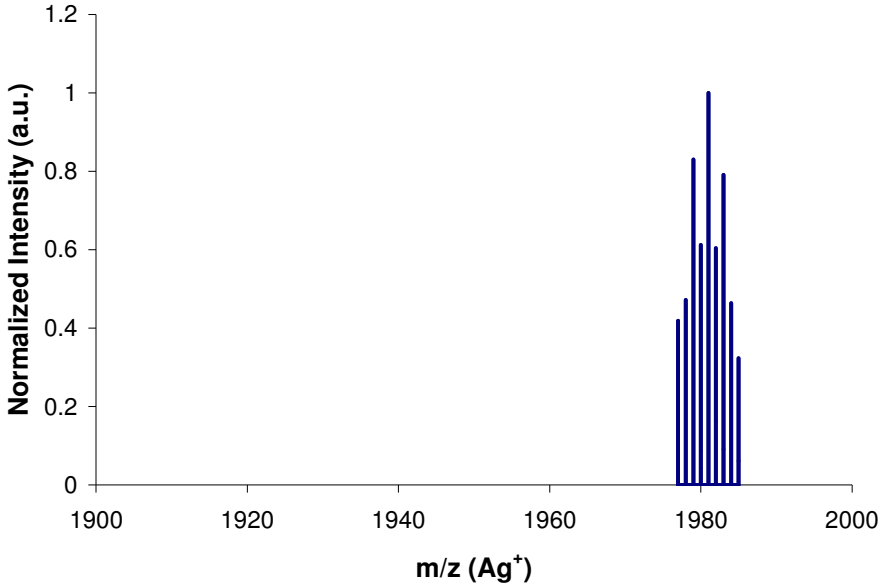

Figure A1.5. MALDI-ToF spectrum of BrStyrenylOS.

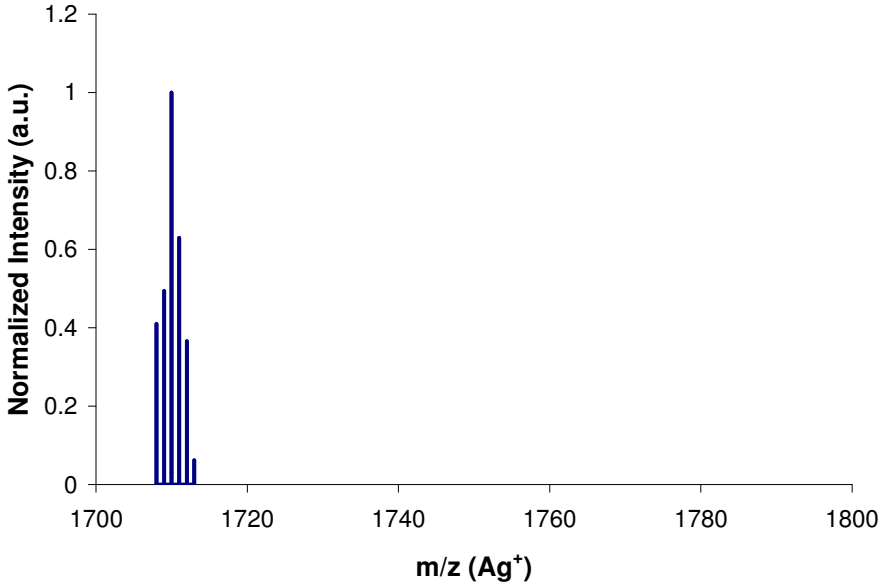

Figure A1.6. MALDI-ToF spectrum of NO_2StyrenylOS.

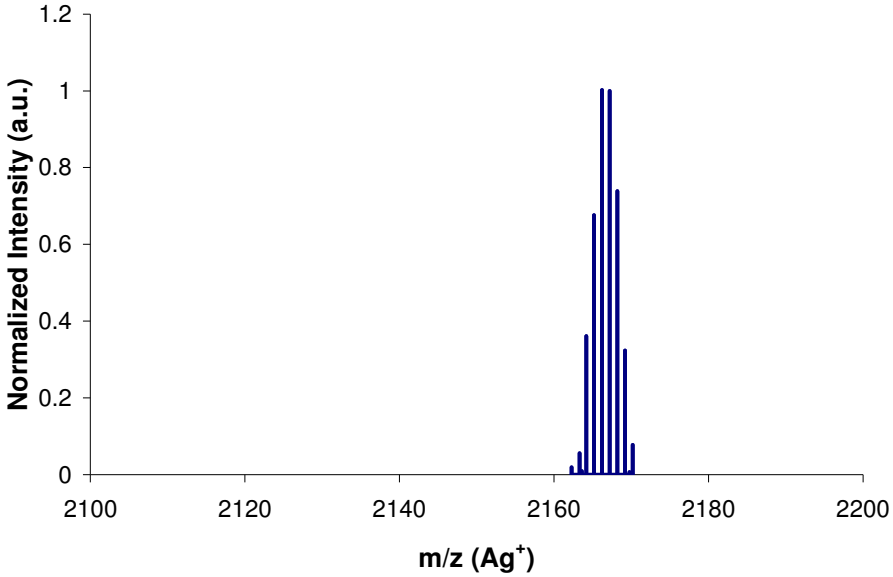

Figure A1.7. MALDI-ToF spectrum of HVinylStilbeneOS.

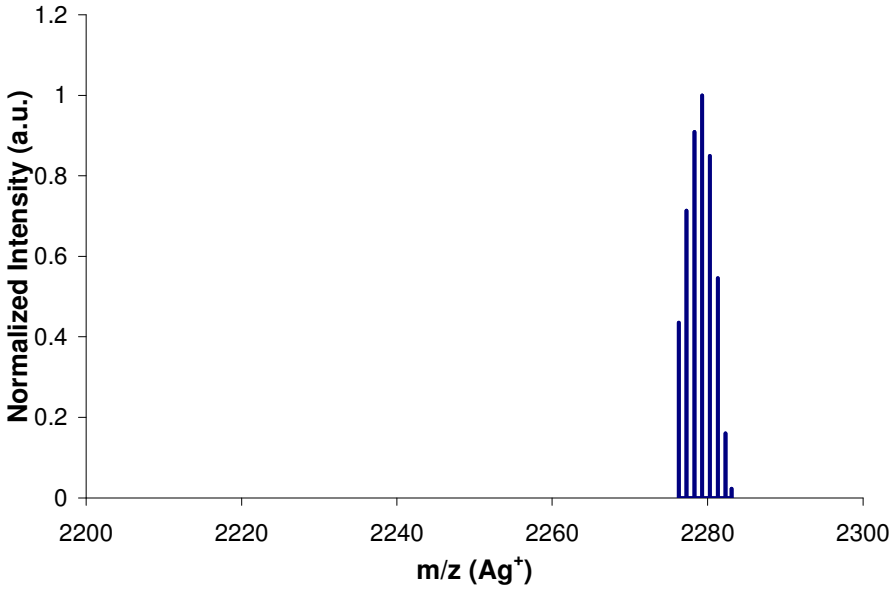

Figure A1.8. MALDI-ToF spectrum of MeVinylStilbeneOS.

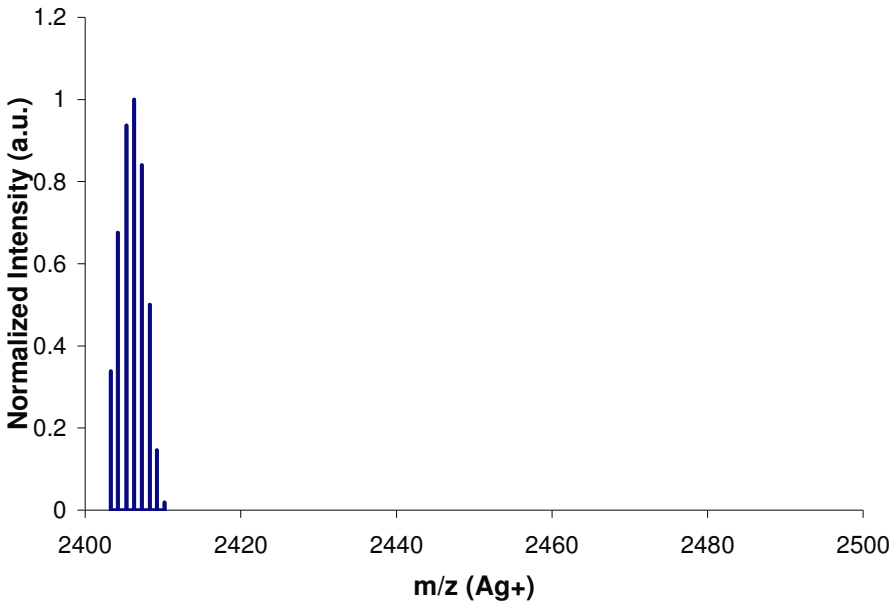

Figure A1.9. MALDI-ToF spectrum of MeOVinylStilbeneOS.

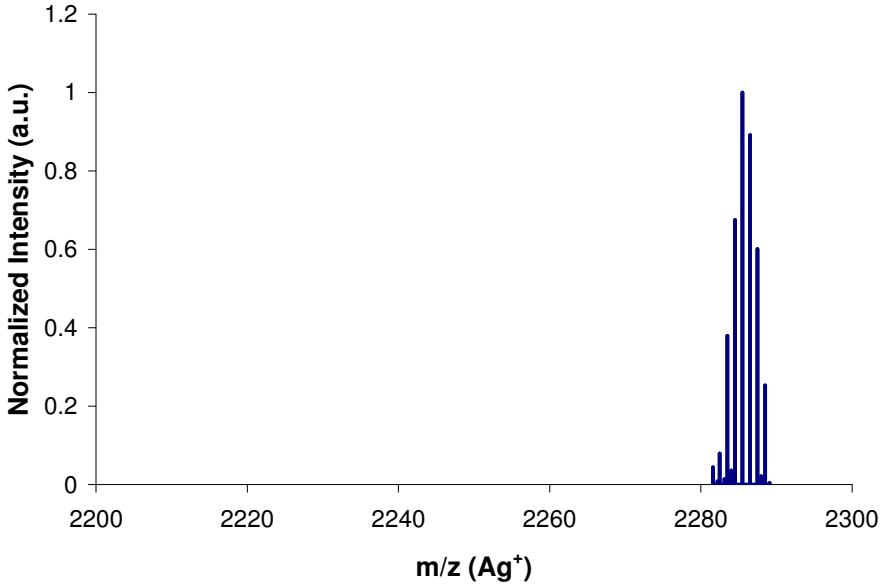

Figure A1.10. MALDI-ToF spectrum of NH_2VinylStilbeneOS.

Appendix 2

Characterization Data for [*o*-RPhSiO$_{1.5}$]$_8$, [2,5-R$_2$PhSiO$_{1.5}$]$_8$, and [R$_3$PhSiO$_{1.5}$]$_8$

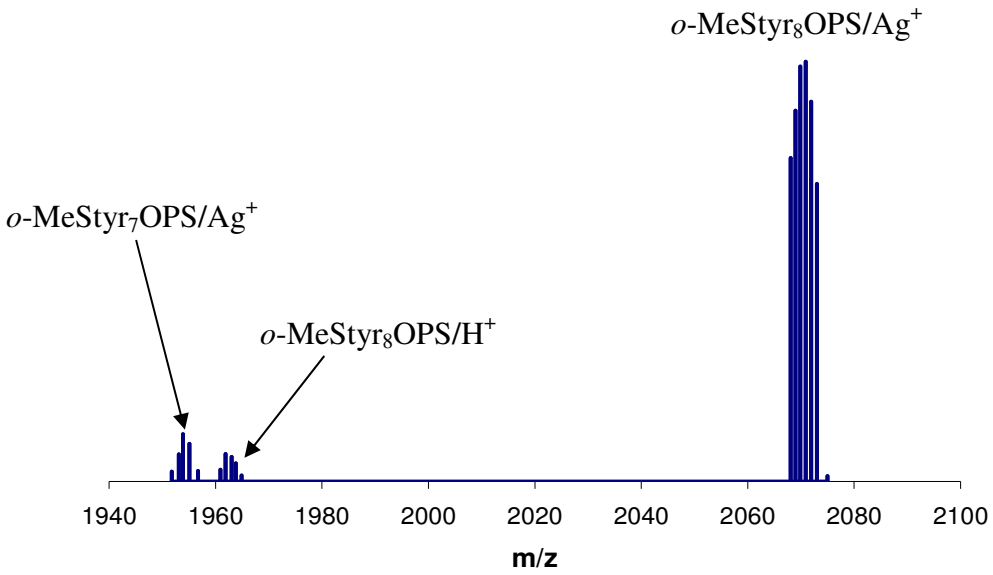

Figure A2.1. MALDI-ToF data of *o*-MeStyr$_8$OPS.

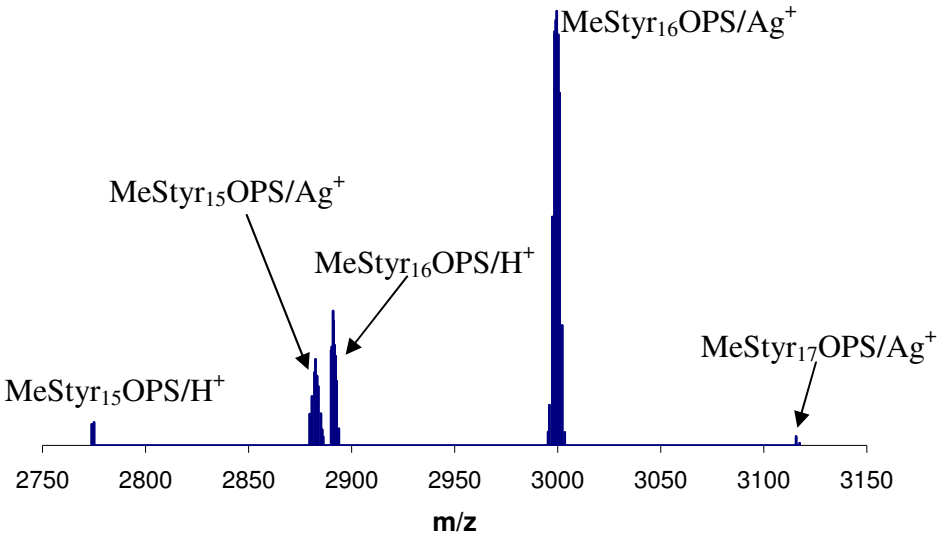

Figure A2.2. MALDI-ToF data of $MeStyr_{16}OPS$.

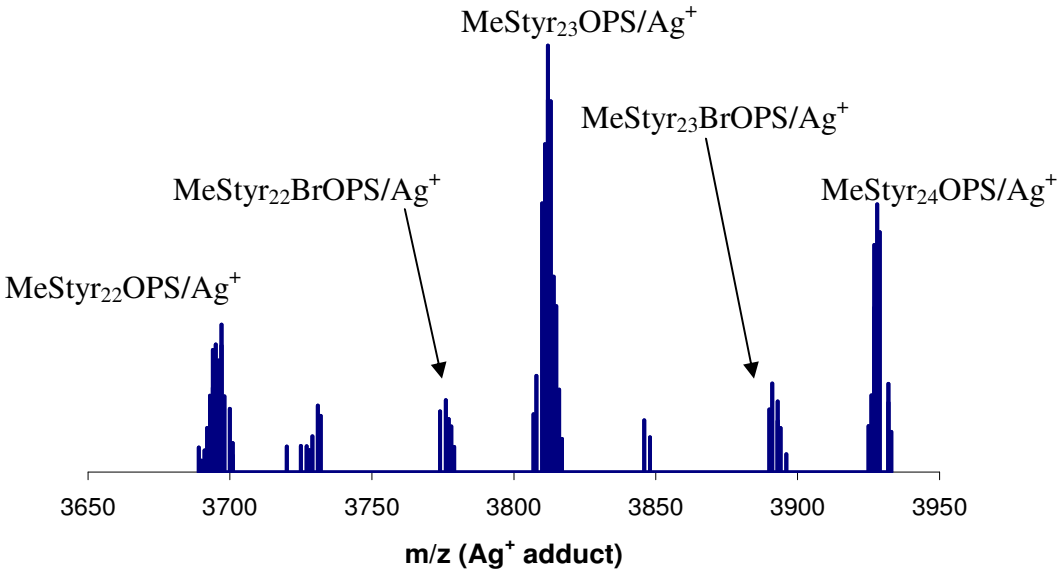

Figure A2.3. MALDI-ToF data of $MeStyr_{24}OPS$.

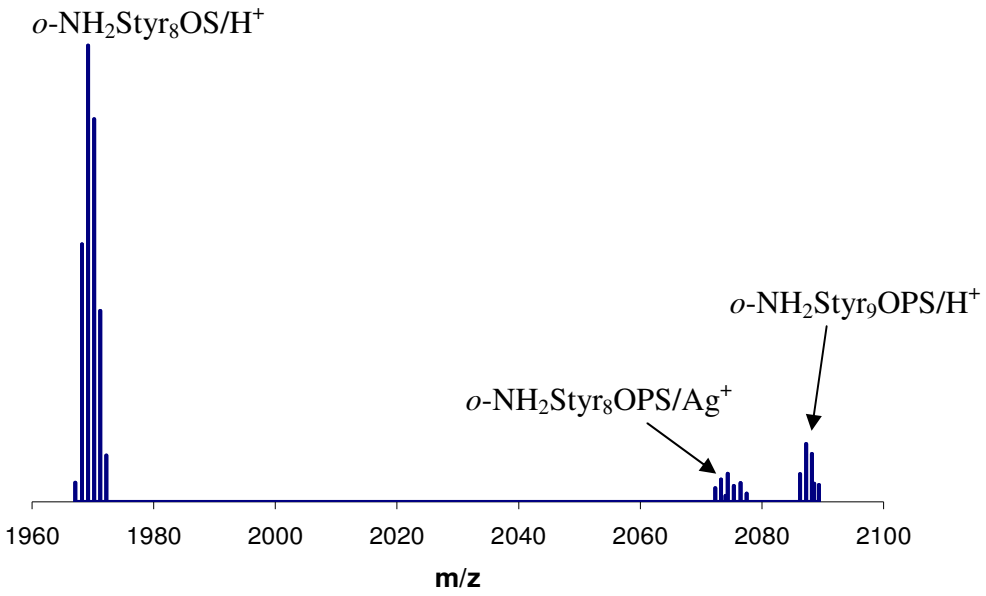

Figure A2.4. MALDI-ToF data of *o*-NH_2Styr_8OPS.

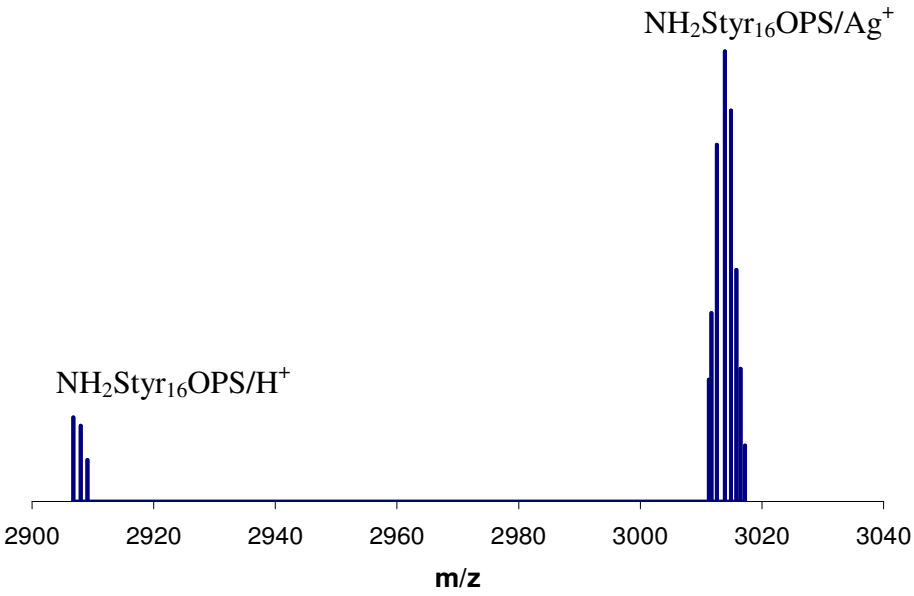

Figure A2.5. MALDI-ToF data of $NH_2Styr_{16}OPS$.

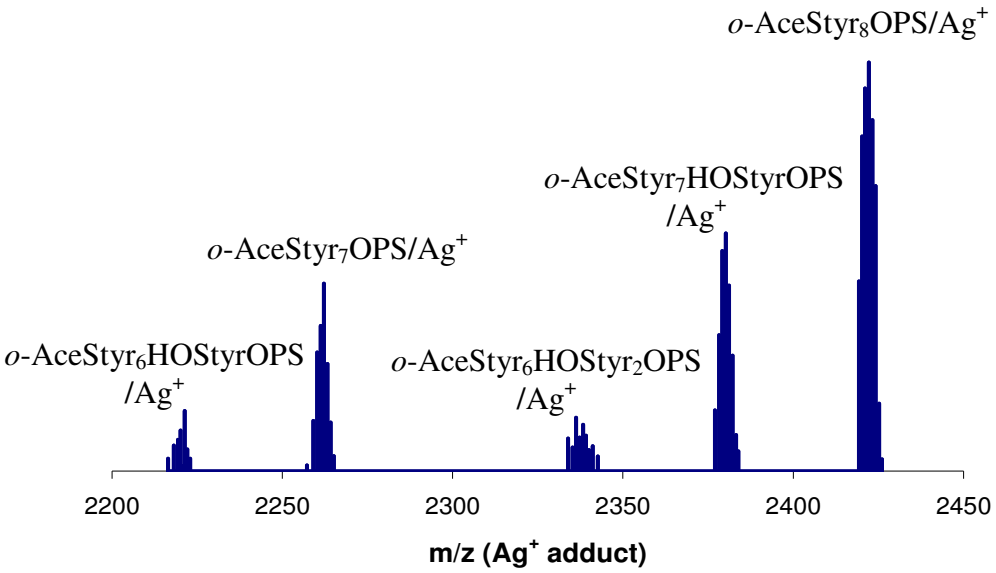

Figure A2.6. MALDI-ToF data of *o*-AceStyr$_8$OPS including partially deacylated groups as "HO."

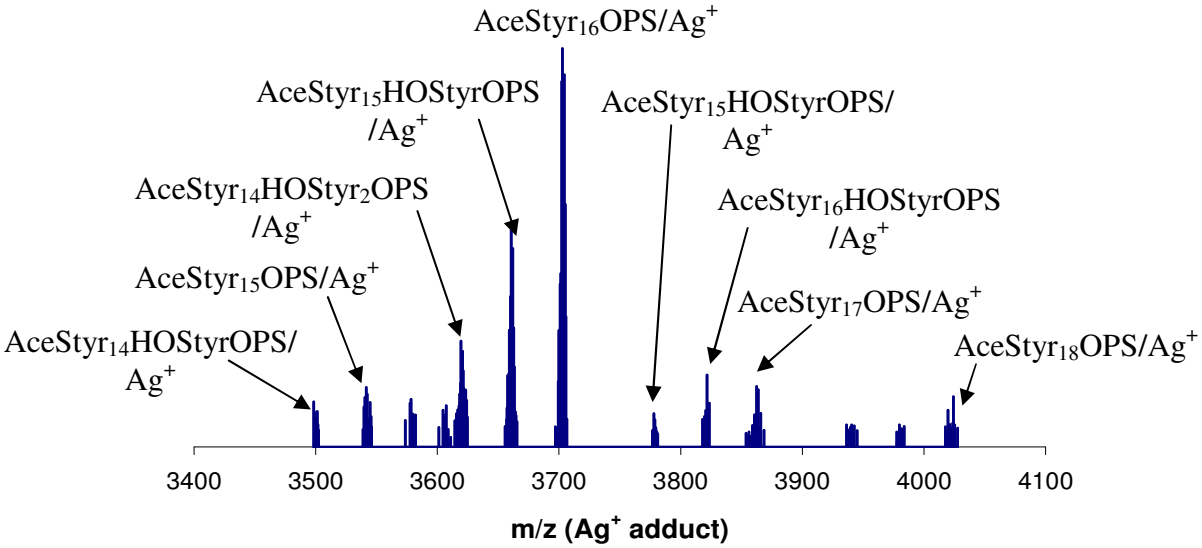

Figure A2.7. MALDI-ToF data of AceStyr$_{16}$OPS including partially deacylated groups as "HO."

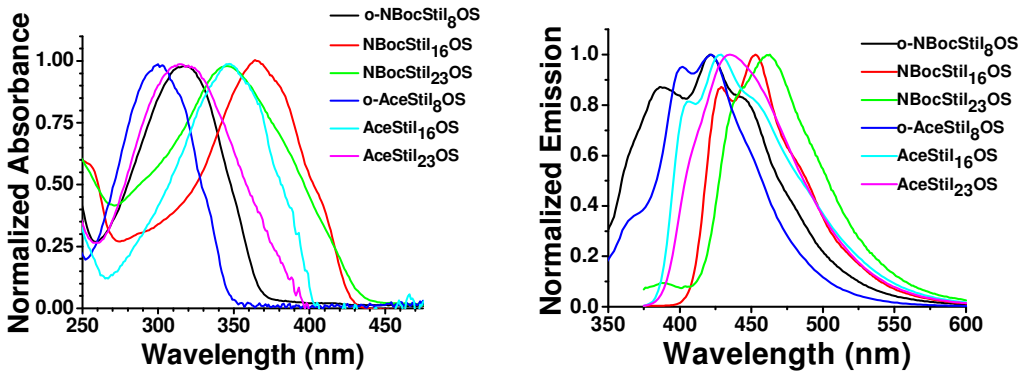

Figure A2.8. (a) Normalized optical absorption and (b) normalized steady-state fluorescence spectra of the investigated derivatives of silsesquioxane.

Appendix 3

MALDI-ToF Data for Mixed Methyl,Vinyl-T_8, -T_{10} and -T_{12} Cages

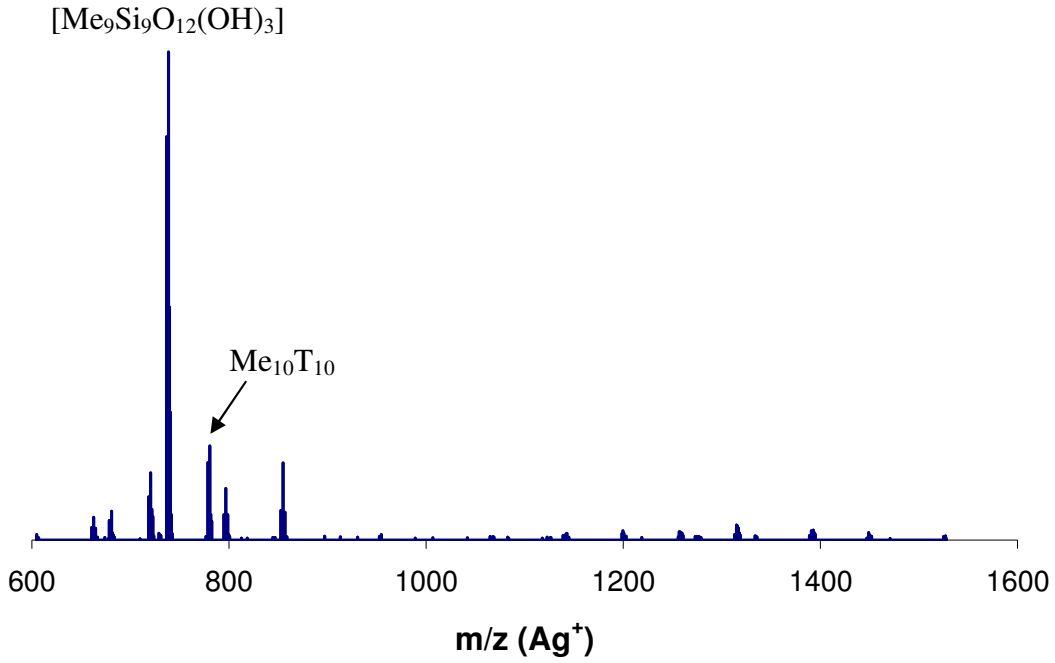

Figure A3.1. *n*Bu_4F-catalyzed dissolution of PMSQ in THF at room temperature

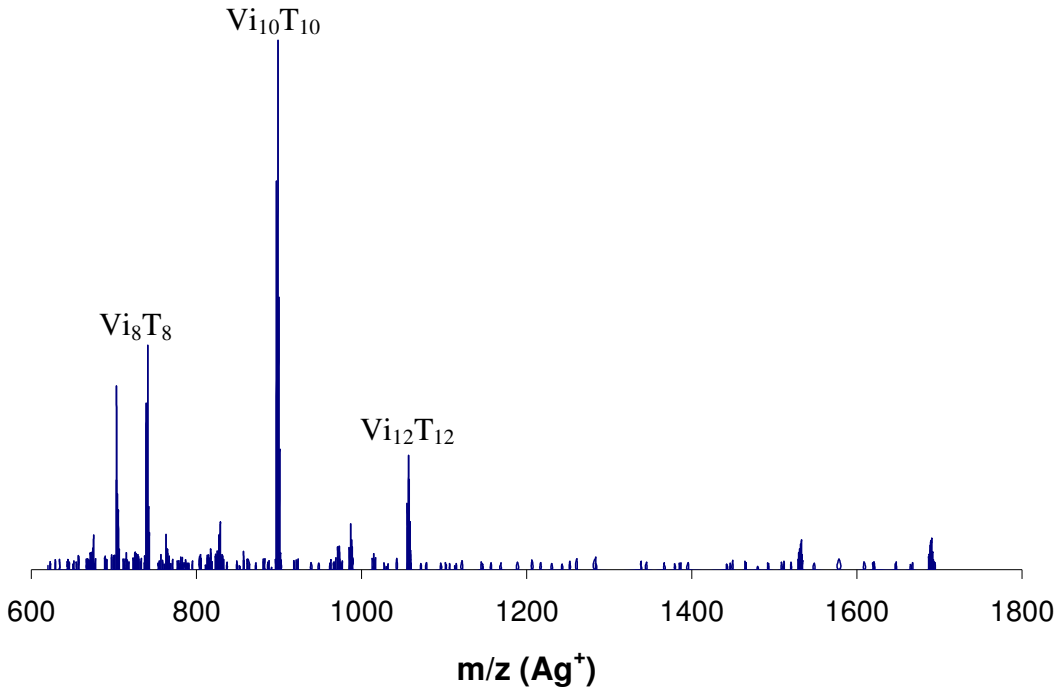

Figure A3.2. Room temperature *n*Bu$_4$F-catalyzed dissolution 5:1 PMSQ:PVSQ in toluene.

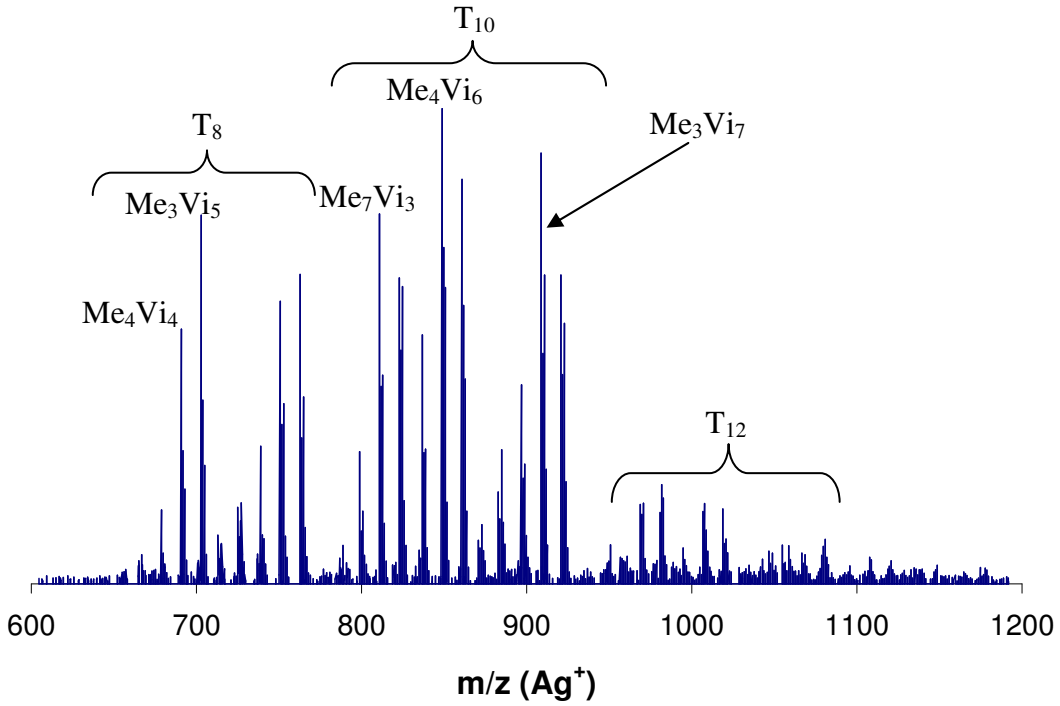

Figure A3.3. Room temperature *n*Bu$_4$F-catalyzed dissolution 2:1 PMSQ:PVSQ in 1:1 THF:EtOH.

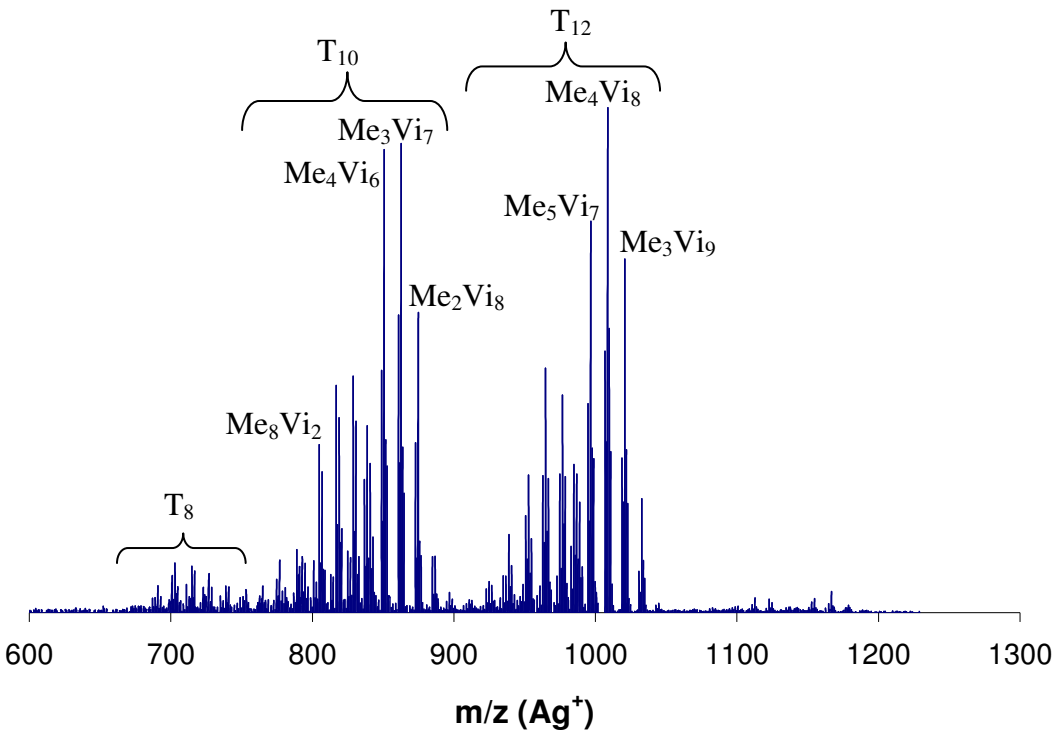

Figure A3.4. Room temperature *n*Bu$_4$F-catalyzed dissolution 2:1 PMSQ:PVSQ in 4:1 THF:EtOH.

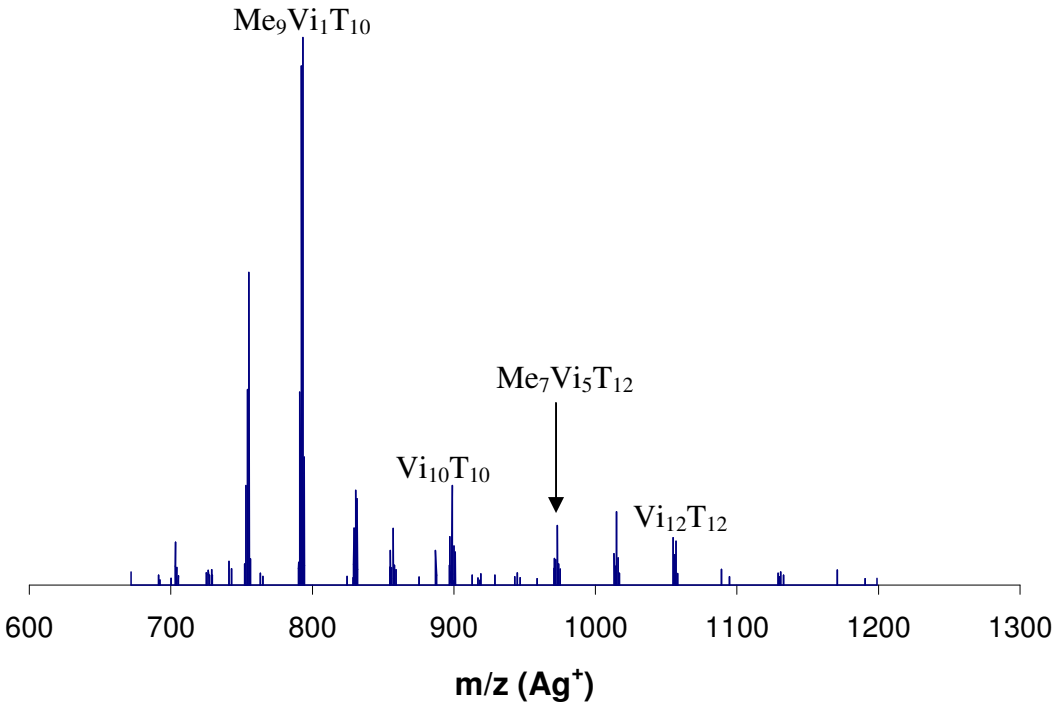

Figure A3.5. Room temperature *n*Bu$_4$F-catalyzed dissolution 2:1 PMSQ:PVSQ in 1:4 THF:EtOH.

Appendix 4
Synthesis and Hydrolysis of AceStyrenylOS

Experimental Section

Materials. Dichloromethane (CH_2Cl_2) was purchased from Fisher Scientific and distilled from CaH_2 under N_2 prior to use. Dioxane and THF were purchased from Fisher Scientific and distilled from Na/benzophenone under N_2 prior to use. Octavinylsilsesquioxane (OVS) and (*S*)-(+)-*O*-acetylmandelic acid were synthesized using previously reported methods.[1,2] All other chemicals were purchased from Sigma-Aldrich, Fisher Scientific, or Strem Chemicals, Inc., and used as received.

Analytical Methods

Gel Permeation Chromatography (GPC) analyses were done on a Waters 440 system equipped with Waters Styragel columns (7.8 x 300, HT 0.5, 2, 3, 4) with RI detection using Waters refractometer and THF as solvent. The system was calibrated using polystyrene standards and toluene as reference.

Nuclear Magnetic Resonance. All ^{1}H-NMR were performed in $CDCl_3$ or methanol-d_4 and recorded on a Varian INOVA 400 MHz spectrometer. ^{1}H-NMR spectra were collected at 400 MHz using a 6000Hz spectral width, a relaxation delay of 3.5 s, 30k data points, a pulse width of 38^o, and TMS (0.00 ppm) as the internal reference.

Thermogravimetric analyses were run on a SDT Q600 Simultaneous Differential DTA-TGA Instrument (TA Instruments, Inc., New Castle, DE). Samples (15-25 mg) were loaded in alumina pans and ramped at 10^{o}C/min to 1000^{o}C under dry air with a flow rate of 60 mL/min.

Matrix-Assisted Laser Desorption/Time-of-Flight Spectrometry. MALDI-TOF was done on a Micromass TofSpec-2E equipped with a 337 nm nitrogen laser in positive-ion reflectron mode using poly(ethylene glycol) as calibration standard, dithranol as matrix,

and $AgNO_3$ as ion source. Samples were prepared by mixing solutions of 5 parts matrix (10 mg/mL in THF), 5 parts sample (1 mg/mL in THF), and 1 part $AgNO_3$ (2.5 mg/mL in water) and blotting the mixture on target plate.

FTIR Spectra. Diffuse reflectance Fourier transform (DRIFT) spectra were recorded on a Nicolet 6700 FT-IR spectrometer (ThermoScientific, Waltham, MA). Optical grade, random cuttings of KBr (International Crystal Laboratories, Garfield, NJ) were ground, with 1.0 wt% of the sample to be analyzed. For DRIFT analysis, samples were packed firmly and leveled off at the upper edge to provide a smooth surface. The FTIR sample chamber was flushed continuously with N_2 prior (10 min) to data acquisition in the range 4000-400 cm^{-1}.

Synthesis of AcetoxyStyrenylOS.

To a dry 10 mL Schlenk flask under N_2 was added 0.40 g (5.1 mmol $–CH=CH_2$) of OVS and 21.0 mg (0.0265 mmol, 0.5 mol%) of 1st generation Grubbs catalyst. Dry CH_2Cl_2 (6 mL) was added by syringe followed by 0.20 mL (1.31 mmol) 4-acetoxystyrene. Additional 1.0 mL of 4-acetoxystyrene was added to the reaction mixture in 0.20 mL aliquots for the next 5 days (total = 1.20 mL, 7.84 mmol). The mixture was stirred at room temperature for an additional 2 days and then quenched by precipitation into 200 mL of methanol. The solution was then filtered and the product was further purified according to published procedure.[2] Yield = 91%; Conversion = 100%; MALDI-ToF (Ag^+): m/z = 1728.9 ($AceStyr_6HOStyr_2OS$, 9%), 1772.8 ($AceStyrl_7HOStyr_1OS$, 21%), 1813.8 ($AceStyr_8OS$, 70%), Calculated = 1814.0 ($AceStyr_8OS$); GPC: M_n = 2052, M_w = 2105, PDI = 1.03; TGA (air, 1000°C): Found = 27.5%, Calculated = 28.2%, $T_{d5\%}$ = 300°C; ^{1}H-NMR ($CDCl_3$): 2.29 (s, 24H, C(=O)C*H*$_3$), 6.23 (d, 8H, =C*H*-Si), 7.06 (d, 16H, Ph),7.31 (d, 8, =C*H*-Ph), 7.48 (d, 16H, Ph). FT-IR (KBr): ν_{C-H} = 3034, 3002, 2936 cm^{-1}, $\nu_{C=O}$ = 1763 cm^{-1}, $\nu_{C=C}$ =1603 cm^{-1}, ν_{Si-C} = 1206 cm^{-1}, $\nu_{Si-O-Si}$ 1124cm^{-1}.

Hydrolysis of AcetoxyStyrenylOS.

To a dry 50-mL Schlenk flask under N_2 was added 1.0 g (4.7 mmol –Ace) AcetoxyStyreneOS and 25 mL of THF. 37% HCl solution (0.2 mL, 2.4 mmol) and DI H_2O (1 mL, 55 mmol) were then added via syringe and the solution was stirred at room temperature.

The reaction was monitored by FT-IR, and when all the υC=O peak has disappeared, the reaction mixture was neutralized with saturated $NaHCO_3$ solution. The product was extracted with CH_2Cl_2 (3 x 10 mL). The combined organic layer was washed with DI H_2O (3 x 10 mL), dried over Na_2SO_4, and the solvent evaporated in vacuo to give white solid as product. Yield = 85%; Conversion = 100%; MALDI-ToF (Ag^+): m/z = 1477.2, Calculated = 1477.7; GPC: M_n = 1044, M_w = 1068, PDI = 1.02; TGA (air, 1000°C): Found = 38.8%, Calculated = 35.1%, $T_{d5\%}$ = 255°C; ^{1}H-NMR ($CDCl_3$): 6.12 (d, 8H, =C*H*-Si), 6.77 (d, 16H, Ph), 7.27 (d, 8H, =C*H*-Ph), 7.38 (d, 16H, Ph). FT-IR (KBr): ν_{O-H} = 3349 cm^{-1}, ν_{C-H} = 3027 cm^{-1}, $\nu_{C=C}$ = 1605 cm^{-1}, $\nu_{Si-O-Si}$ 1110 cm^{-1}.

Synthesis of (*S*)-*O*-AcetylMandelicStyrenylOS.

To a dry 50-mL round bottomed flask under N_2 was added 0.50 g (2.92 mmol -OH) HOStyrenylOS, 0.78 g (3.65 mmol) (*S*)-*O*-acetylmandelic acid, and 5 mL THF. The reaction solution was cooled to 0°C under stirring, and then a solution of 0.66 g (3.21 mmol) of DCC and 71 mg (0.6 mmol) of DMAP in 5 mL of THF was added via syringe. The reaction mixture was stirred at 0°C overnight and then quenched by filtering through celite. The filtrate was concentrated under reduced pressure and precipitated into 100 mL of methanol. The resulting white powder was filtered and dried in vacuo. Yield = 92%; Conversion = 100%; MALDI-ToF (Ag^+): m/z = 2886.6 Calculated = 2887.0; GPC: M_n = 3142, M_w = 3277, PDI = 1.04; TGA (air, 1000°C): Found = 17.7%, Calculated = 17.3%, $T_{d5\%}$ = 220°C; ^{1}H-NMR ($CDCl_3$): 2.22 (s, 24H, C(=O)C*H*$_3$), 6.11 (s, 8H, chiral *H*), 6.17 (d, 8H, =C*H*-Si), 6.98 (d, 16H, Ph), 7.24 (d, 8H, =C*H*-Ph), 7.39-7.44 (m, 40H, Ph), 7.57 (d, 16H, Ph).

Results and Discussions

As detailed in Chapter **3**, we have done work on the functionalization of OVS via cross-metathesis reaction with RStyrene, utilizing a variety of R groups to show the versatility of the reaction. In this work, we use 4-acetoxystyrene in the cross-metathesis reaction, realizing that it can be deprotected to form the free hydroxyl group, which gives us access to hydroxyl-functionalized SQ molecules in two simple synthetic steps.

In the following sections we discuss the synthetic methods and characterization of the three compounds synthesized in this work.

Synthetic Methods

The cross-metathesis reaction of OVS with 4-acetoxystyrene was carried out following the procedure developed in Chapter **3** with a slight modification. 4-acetoxystyrene was added into the reaction mixture in aliquots for several days instead of all at once at the beginning of the reaction as was done previously because we were not able to achieve complete octasubstitution using the old procedure. We suspect that the presence of excess 4-acetoxystyrene in the reaction mixture forms complexes with the ruthenium-based Grubbs catalyst, and thereby deactivating it. AceStyrenylOS is quite stable in ambient conditions and requires no special handling to prevent hydrolysis reaction.

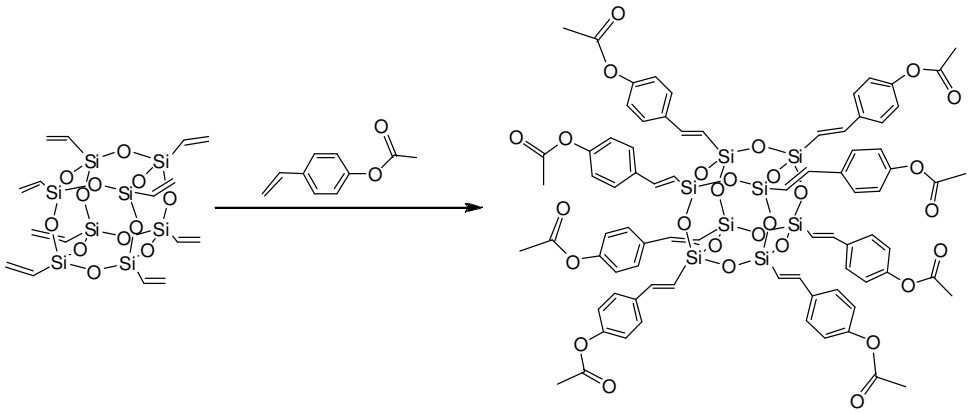

Scheme A4.1. Synthesis of AceStyrenylOS.

The synthesis of HOStyrenylOS was achieved by simple acid-catalyzed hydrolysis of AceStyrenylOS. The reaction was monitored by following the disappearance of $\nu_{C=O}$ peak in the FT-IR spectra of samples of the reaction mixture. Freshly synthesized HOStyrenylOS has to be kept away from ambient light to prevent degradation as evidenced by the change in color from white to pink.

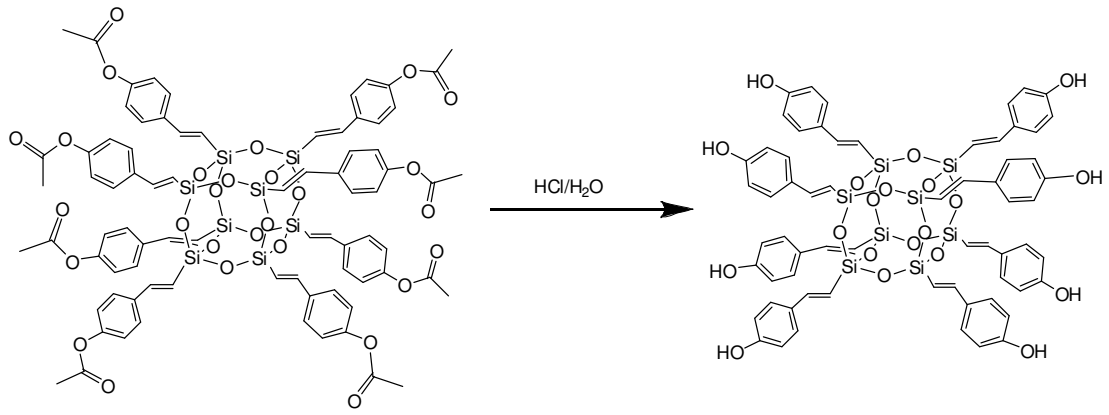

Scheme A4.2. Hydrolysis of AceStyrenylOS.

The coupling of HOStyrenylOS with (*S*)-(+)-(*O*)-acetylmandelic acid was accomplished following the well-known Steglich esterification procedure using N,N'-dicyclohexylcarbodiimide (DCC) as coupling agent with 4-dimethylaminopyridine (DMAP) as catalyst. The acetylation of (*S*)-(+)-mandelic acid was done to prevent their homo coupling during esterification reaction with HOStyrenylOS.

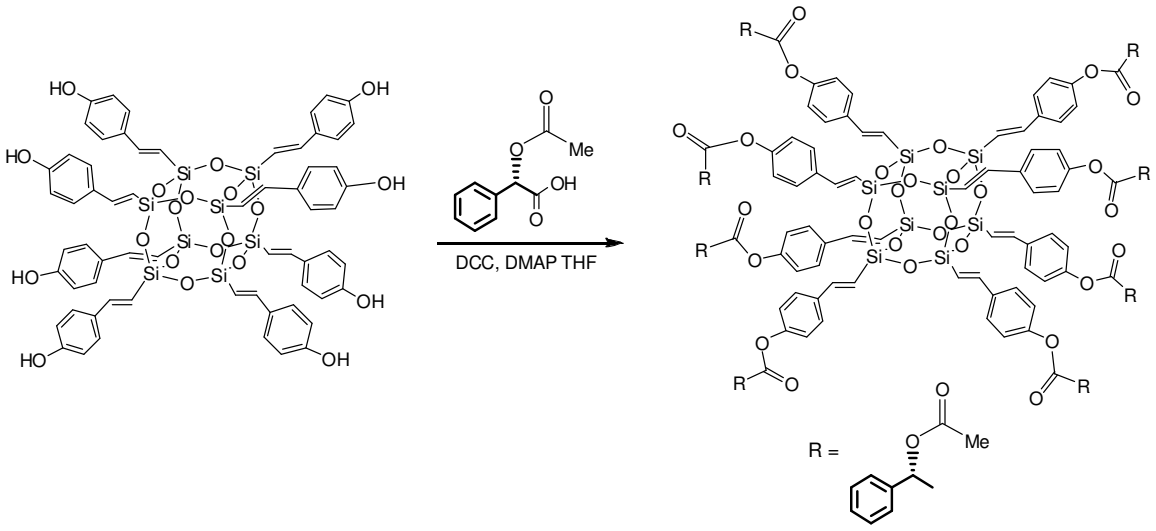

Scheme A4.3. Synthesis of MandeloylStyrenylOS.

Solubilities

All of the synthesized compounds are soluble in moderately polar organic solvents such as THF, 1,4-dioxane, and CH_2Cl_2. AceStyrenylOS and MandeloylStyrenylOS are

insoluble in highly polar solvents such as methanol, and in nonpolar solvents such as hexane. HOStyrenylOS are soluble in methanol.

Molecular Characterization

Table **A4.1** summarizes the molecular characterization data for AceStyrenylOS, HOStyrenylOS, and MandeloylStyrenylOS. ^{1}H-NMR and FT-IR data are listed in the Experimental section above. MALDI-Tof spectra of the three compounds are shown in Figures **A4.1-A4.3**. Complete octasubstitution was achieved for all three compounds. The MALDI-ToF spectrum of AceStyrenylOS (Figure **A4.1**) show some hydrolyzed acetoxy groups, which was not observed in the ^{1}H-NMR spectrum. We believe that the hydrolysis most likely occur due to cleavage of the acetyl group by the MALDI-ToF laser.

Table A4.1. Characterization data for RStyrenylOS.

R group	m/z (Ag^+ adduct)		GPC			
	MALDI-ToF	Calc.	M_n	M_w	FW	PDI
Ace	1813.8	1814.0	2052	2107	1706.1	1.03
HO	1477.2	1477.7	1044	1068	1369.8	1.02
Mandeloyl	2886.6	2887.0	3142	3277	2779.1	1.04

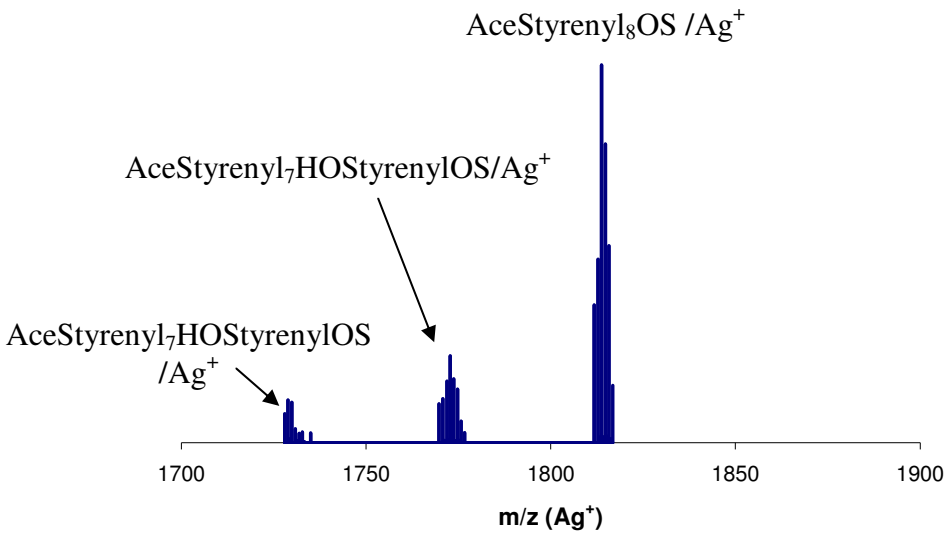

Figure A4.1. MALDI-ToF spectrum of AceStyrenylOS.

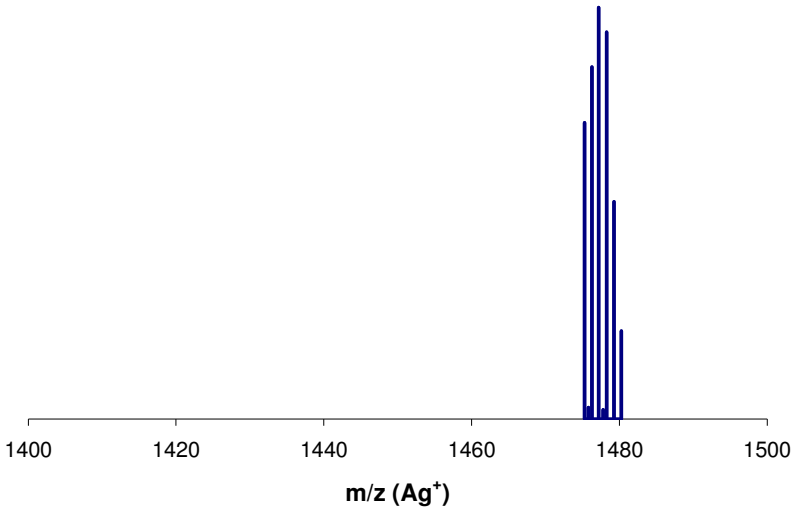

Figure A4.2. MALDI-ToF spectrum of HOStyrenylOS.

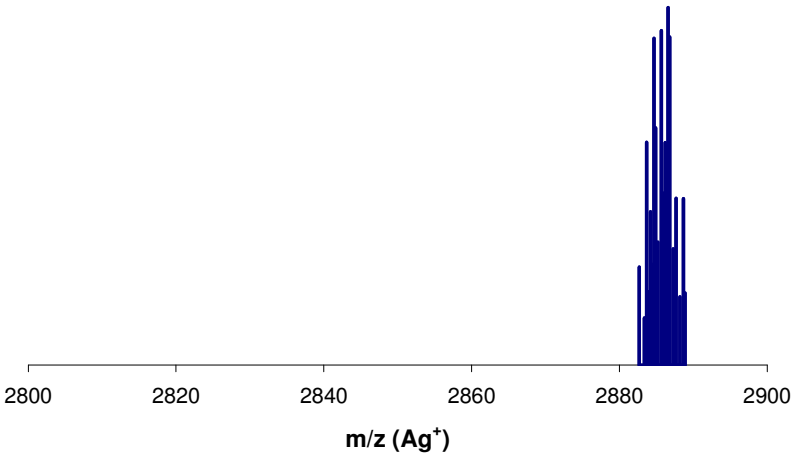

Figure A4.3. MALDI-ToF spectrum of MandeloylStyrenylOS.

GPC analyses of the three compounds (Table **A4.1**) show narrow molecular weight distributions, indicating that they retain their SQ cage structures. The values of M_n and M_w for HOStyrenylOS are lower than the calculated formula weight and the measured MALDI-ToF values. This is expected from GPC characterization of rigid and spherical molecules using flexible and linear standards.[3,4] However, the M_n and M_w values of AceStyrenylOS and MandeloylStyrenylOS are higher than the calculated formula weight and measured MALDI-ToF values. We believe that this is caused by the presence of the

rather flexible acetyl groups in both compounds, which increases the apparent size of the molecules in solution.

^{1}H-NMR data also corroborate the complete hydrolysis of AceStyrenylOS and the subsequent reaction of HOStyrenylOS with (*S*)-*O*-acetylmandelic acid. The ^{1}H-NMR spectrum of HOStyrenylOS shows the disappearance of the singlet acetyl-CH_3 groups of AceStyrenylOS at δ = 2.29 ppm. The phenol-OH groups do not appear in the ^{1}H-NMR spectrum of HOStyrenylOS as expected, due to the rapid hydrogen-deuterium exchange with the NMR solvent (methanol-d_4). The ^{1}H-NMR spectrum of MandeloylStyrenylOS shows the reappearance of the acetyl-CH_3 groups on the mandeloyl moiety at δ = 2.22 ppm, but the more significant change in the spectrum is the downfield shift of the aryl protons next to the phenoxy groups from δ = 6.77 ppm to δ = 6.98 ppm due to the electron-withdrawing character of the carbonyls attached to the phenoxy groups.

FT-IR spectra of AceStyrenylOS and HOStyrenylOS also confirm the complete hydrolysis of AceStyrenylOS. As mentioned earlier, the characteristic $\nu_{C=O}$ stretching peak of AceStyrenylOS at 1763 cm^{-1} is used to monitor the progress of the hydrolysis reactions. The ν_{O-H} stretching peak also appear at 3349 cm^{-1} in the FT-IR spectrum of HOStyrenylOS.

TGA data for all three compounds can be found in Table **A4.2** and Figure **A4.4**. MandeloylStyrenylOS shows the lowest onset temperature for its decomposition, most likely because of the presence of acetyl and benzylic groups. HOStyrenylOS also has lower mass-loss onset temperature than expected for a simple silsesquioxane structure, most likely because of oxidation of the hydroxyl groups. AceStyrenylOS shows good thermal stability considering that acetyl groups can thermally decompose fairly easily.[5]

Table A4.2. TGA data for RStyrenylOS.

R group	Ceramic yield (%)		$T_{d5\%}$ (^{o}C)
	Actual	Calc.	
Ace	27.5	28.2	298
HO	38.8	35.1	228
Mandeloyl	17.7	17.3	219

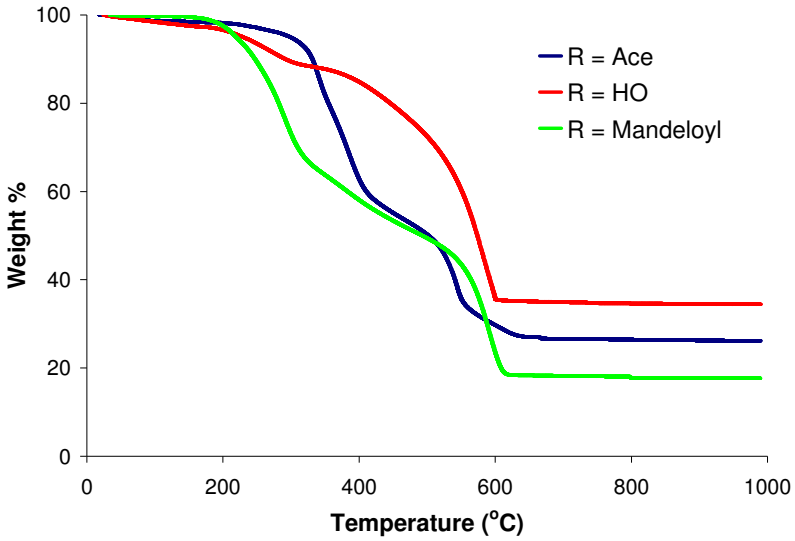

Figure A4.4. TGA data for RStyrenylOS.

References Cited:

1. Chatterjee, A.; Sasikumar, M.; Joshi, N.N. "Preparation of Enantiopure *trans*-1,2-Cyclohexanediol and *trans*-2-Aminocyclohexanol." *Synth. Commun*. **2003**, *37*, 1727-1733.
2. Garrett, C.E.; Prasad, K. "The Art of Meeting Palladium Specifications in Active Pharmaceutical Ingredients Produced by Pd-Catalyzed Reactions." *Adv. Synth. Catal*. **2004**, *346*, 889-900.
3. Sulaiman, S.; Bhaskar, A.; Zhang, J.; Guda, R.; Goodson III, T.; Laine, R.M. "Molecules with Perfect Cubic Symmetry as Nanobuilding Blocks for 3-D Assemblies. Elaboration of Octavinylsilsesquioxane. Unusual Luminescence Shifts May Indicate Extended Conjugation Involving the Silsesquioxane Core." *Chem. Mater*. **2008**, *20*, 5563-5573.
4. Laine, R.M.; Sulaiman, S.; Brick, C.; Roll, M.; Tamaki, R.; Asuncion, M.Z.; Neurock, M.; Filhol, J-S.; Lee, C-Y.; Zhang, J.; Goodson III, T.; Ronchi, M.; Pizzotti, M.; Rand, S.C.; Li, Y. "Synthesis and Photophysical Properties of Stilbeneoctasilsesquioxanes. Emission Behavior Coupled with Theoretical Modeling Studies Suggest a 3-D Excited State Involving the Silica Core." *J. Am. Chem. Soc*. **2010**, *132*, 3708-3722.
5. Košik, M.; Reiser, V.; Kováč, P. "Thermal Decomposition of Model Compounds Related to Branched 4-O-Methylglucuronoxylans." *Carbohydrate Research* **1979**, *70*, 199-207.